Mesoscale conductivity in argillic layers at SRS

by

Margaret F. Williamson

(Under the direction of C. Rhett Jackson)

Abstract

Observations from a grid of shallow, maximum-rise piezometers at the Savannah River Site, SC indicated that ground water perching on the argillic layer was common. However, flow measurements from an interflow-interception trench indicated that lateral flow was rare and most soil water percolated through the argillic layer. We hypothesized that the lack of frequent lateral flow was primarily due to penetration of pine tree roots through the argillic layer.

Ground penetrating radar (GPR) was used to map soil structure and anomalies, such as root holes, down to two meters depth at three 10x10-m plots. These maps were used to help place 1x10-m back-hoe excavated trenches and 1x10-m auger hole transects at each of the three plots. Depth from the surface to the argillic layer was measured using a tile probe, a knocking pole and then augering to the argillic layer. The results from these three techniques were compared to each other to determine statistical differences amongst the results. Compact constant-head permeameters (CCHPs) were used to measure in-situ hydraulic conductivities in the clay-loam matrix and visually apparent anomalies in the trenches and transects. Anomalies were visually investigated by excavating with a shovel. Photographs of soil wetness were taken with a multi-spectral camera.

We discovered that all anomalies found were represented on the GPR maps, but not all predicted anomalies on the GPR maps had high conductivities. We discovered that tree root

holes created anomalies, but that some conductivity anomalies were visually indistinguishable from low-conductivity soil.

Depth to clay layer was determined using a tile probe, knocking pole and an auger at 2x2-m spacing on each plot. Upon comparison, we discovered that augering was more accurate and less time-consuming, but more damaging to surrounding matrix then other techniques in these soils.

INDEX WORDS: Amoozemeter, argillic layer, auger, Bt horizon, bulk density, compact constant-head permeameter (CCHP), destructive sampling, ground penetrating radar (GPR), ground water, in-situ hydraulic conductivity, interflow, knocking pole, mesoscale conductivity, methylene blue dye, multi-spectral camera, percent pore space, Savannah River Site, shortwave-infrared light spectrum (SWIR), tile probe, pine tree tap roots, top soil, visible and near-infrared light spectrum (VNIR), water quality.

Mesoscale conductivity in argillic layers at SRS

by

Margaret F. Williamson

B.S., Louisiana State University, 2008

A Thesis Submitted to the Graduate Faculty

of The University of Georgia in Partial Fulfillment

of the

Requirements for the Degree

Master of Science

Athens, Georgia

2011

Mesoscale conductivity in argillic layers at SRS

by

Margaret F. Williamson

Approved:

Major Professor: C. Rhett Jackson

Committee: Lawrence A. Morris
John F. Dowd

Electronic Version Approved:

Maureen Grasso
Dean of the Graduate School
The University of Georgia
August 2011

Acknowledgments

This work was funded by a grant from the Department of Energy through the U.S. Forest Service Savannah River under Interagency Agreement DE-AI09-00SR22188. Many individuals helped make this thesis possible. Thank you to my thesis professor, Rhett Jackson and my committee members, John Dowd and Larry Morris for their expertise, helpful critique and positive attitudes. A big thanks to Todd Rasmussen for all of the LaTeX help and many many hours of decoding computer problems. Thanks to Michele Tobias from the University of California- Davis for her advice on multi-spectral cameras. Thank you to Vanessa Tobias and Amy Scaroni from Louisiana State University for their guidance and support.

Thank you to Shelley Robertson, Erin Harris and the other lab technicians/student workers from the Hydrology Lab at UGA. Thank you to Ben Morris, the hydrology technician at Savannah River Site. A special thanks to Damion Drover for all of his help with field work and GIS and for finally putting all those comic strips on our office door.

On a more personal note, thank you to my family for their unwavering emotional and (cough) financial support throughout the whole process. It means a lot to me that you guys have my back and think that what I do is pretty cool... or that you at least think it's cool that I think it's cool. Thank you to Fen for her love and affection.

Table of Contents

List of Tables

List of Figures

Chapter 1

Introduction

1.1 Problem Statment

Upland soils on Upper Coastal Plain hillslopes typically feature topsoils with high hydraulic conductivities and argillic layers with lower hydraulic conductivities. In this research, we investigated in-situ hydraulic conductivity of the argillic layers at the Savannah River Site (SRS) south of New Ellenton, SC. Previous research in the area by former graduate student James Greco suggests that the conductivity of the clay layer should be low enough to create relatively frequent interflow over the B horizon (Greco 2004), interflow being the lateral movement of water over a soil horizon of low conductivity. Maximum rise piezometers in the area showed that perching of saturated water above the clay is spatially and temporally common. However, trenches put in to detect lateral flow for the same experiment showed that significant interflow is rare and that most of the perched water percolates through the clay rather than flowing laterally over it. For the purposes of this research, we hypothesized that the growth, death and decay of deep tree roots may leave higher conductivity zones in the clay layer for water to move through.

The primary concern with increased rates of water percolation through argillic layers at SRS is understanding flow pathways of silvicultural chemicals such as nitrate fertilizer. The low hydraulic conductivities (Ksats) found by Greco 2004 in the argillic layers at SRS would suggest a fairly high frequency of lateral movement. Having higher Ksats in the argillic layers than previously accounted for could affect best management practices in the area, such as the proper use of silvicultural chemicals. This research is a small part of a larger project concerning the installation of high-intensity, short-rotation pine tree stands at SRS

for bioenergy supply, so it is important to properly understand infiltration trends in these soils and the potential role that old pine tree root holes play in these trends.

SRS is a Department of Energy facility in Aiken, SC that is currently primarily concerned with the handling and remediation of nuclear waste and the reduction of the facility's overall carbon footprint. The 310 mi^2 of land that make up SRS were previously farmland that was bought up by the Department of Energy during the height of Cold War tensions in 1950-1951. The combination of river bottoms and previously heavily managed farmland has made the soils at SRS heterogeneous (Figure 1.1).

The 3 most common soil map units present at SRS, according to the Natural Resources Conservation Service's national cooperative soil survey, are Dothan sand, Fuquay sand and Vaucluse-Ailey complex (Figure 1.2). Dothan sand forms in marine terraces and their parent material is loamy marine deposits. They are well drained soils with moderately high Ksats of 0.20 to 0.57 in/hr (0.0085 to 0.024 cm/min) found on 2 to 6% slopes. They do not flood or pond frequently and they have moderate available water holding capacity of $\approx$ 6.6 in (16.51 cm). The depth to their Bt horizon is more than 11 in (27.94 cm) at SRS and their depth to the seasonal high water table is $\approx$ 36 to 60 in (0.91 to 1.52 m) (National Cooperative Soil Survey 2009a).

Fuquay sand forms in marine terraces as well and their parent material is sandy and/or loamy marine deposits. They are well drained like Dothan sands, but they have moderately low to moderately high Ksats of 0.06 to 0.20 in/hr (0.0025 to 0.0085 cm/min), meaning that their limiting layer has a lower capacity to transmit water than the Dothan sands. They are found on 2 to 6% slopes and do not flood or pond. The depth to their Bt horizon is more than 21 in (53.34 cm) at SRS and their depth to the seasonal high water table is $\approx$ 48 to 72 in (1.22 to 1.83 m) (National Cooperative Soil Survey 2009b).

Vaucluse-Ailey complex forms in marine terraces. The parent material for Vaucluse is loamy marine deposits and the parent material for Ailey is sandy and/or loamy marine deposits. They are well drained and Vaucluse have very low to moderately high Ksats of

0.00 to 0.57 in/hr (0 to 0.024 cm/min) while Ailey have moderately low to moderately high Ksats of 0.06 to 0.20 in/hr (0.0025 to 0.0085 cm/min). They have no flooding or ponding frequency and they have a available water capacity of $\approx$ 4.4 in (11.17 cm) for Vaucluse and $\approx$ 4.1 in (10.41 cm) for Ailey. They are found on 6 to 15% slopes and their depth to a Bt horizon is more than 10 in (25.4 cm) at SRS. The depth to the seasonal high water table at SRS is more than 80 in (2.03 m) (National Cooperative Soil Survey 2009c).

Measured hydraulic conductivities in the soils of SRS showed that surface soils and mid soils (defined as being 0-60 cm in depth from the ground surface) have higher hydraulic conductivities than argillic soils (found at depths of 70 cm and deeper) (Greco 2004) (Figure 1.3). Typical profiles for each of these soils, along with more information, can be found in the appendices section of this thesis (Appendix A).

1.2 Research Questions, Related Hypotheses and Approaches

The primary question driving this research was: did any or all hydraulic conductivity anomalies in the argillic layer correspond with visible anomalies in the soils (such as old pine tree root holes)? The secondary research questions for this research included: 1. could we accurately pinpoint visible and hydraulic conductivity anomalies in the soil matrix using Ground Penetrating Radar, 2. could we, with the use of compact constant-head permeameters (CCHPs), locate hydraulic conductivity anomalies in the soil matrix (specifically in the argillic layer), 3. could methylene blue dye be used to accurately trace water movement through the soils at SRS, 4. could depth from the surface to the argillic layer be accurately measured with the use of a tile probe and/or a knocking pole and 5. could a multi-spectral camera be used to accurately take pictures of soil wetness in the soils of SRS?

In regards to the primary question, we hypothesized that any or all found hydraulic conductivity anomalies would respond with visible anomalies in the soil, such as old pine tree root holes. For the secondary research questions, we predicted that:

1. GPR could be used to accurately pinpoint visible and hydraulic conductivity anomalies in the soil matrix,

2. we would locate hydraulic conductivity anomalies in the argillic layer,

3. methylene blue dye would help show water movement through the soils at SRS,

4. the tile probe and/or the knocking pole would help determine accurate depths to the argillic layer from the surface and

5. the multi-spectral camera could accurately take pictures of soil wetness in the soils of SRS.

In order to test these hypotheses, we looked for potential old root holes and other anomalies in the soils of three different 10x10-m plots in the area with the help of Ground Penetrating Radar (GPR). Based on the three-dimensional diagrams created with the GPR data, we picked one 1x1.5-m square within each of the three 10x10-m plots to spray a ground water tracer, methylene blue dye, on in order to try and detect rainwater flow through the soils and, potentially, through any anomalies in the soils. The placement of each of these 1x1.5-m squares was decided based on areas of potential anomalies found with the GPR device. Then, we performed a destructive excavation of the soils at each of the 10x10-m plots with a back-hoe. At each plot, a 1x10-m strip containing the 1x1.5-m methylene blue square was dug down to 0.5m.

Amoozemeters were used to try to determine hydraulic conductivity of the soils within the .5-m digs. More 0.5-m digs were performed at each of the plots until either the amoozemeters could no longer take readings because we reached clay layers with undetectably low conductivities or until a total depth of 2m was reached. Throughout all of these processes, a multi-spectral camera was used to try to detect areas of higher soil moisture. Amoozemeter readings were also taken within the 10x10-m plots along 1x10-m transects outside of the trenches. Prior to the CCHP readings taken along the 1x10-m transects, depth from the surface to the argillic layer was recorded with the use of a tile probe, then a knocking pole

and then the actual depth was recorded with the use of an auger. The results from the former two tools were compared to the results from the auger.

1.3 Justification

The data from this research provides information on the variability of in-situ hydraulic conductivities in argillic layers of the Upper Coastal Plain. It is important to understand how water moves through these soils, specifically the argillic layer, and what controls the mesoscale conductivities of these layers. Since the characteristics of the argillic horizon strongly influence hillslope flow pathways, it was important to take a more in-depth look at the soils and their hydraulic properties.

By including scientific tools that are only recently employed in soils and hydrologic research, such as the GPR and the multi-spectral camera, we hoped to discover if their abilities proved useful to research in the field of ground water hydrology. GPR has been used in various fields of the earth sciences to illustrate stratigraphic profiles in soil (Naegeli et al. 1996), so it looked promising to use the device to try to detect potential anomalies in the argillic layer that could be letting water infiltrate the profile at higher rates.

Multi-spectral cameras have been used in various fields to detect wavelengths outside the immediate visible light spectrum. In the soils sciences, previous research showed that lower soil moisture reflects back more heavily in the visible and near-infrared light spectrum (VNIR) than in the short-wavelength infrared (SWIR), while higher soil moisture contents reflect back better with longer wavelengths (Lobell & Asner 2002). So, while using a multi-spectral camera to detect soil moisture was a given, it was important to see if the multi-spectral cameras with near-infrared abilities were as useful as those with greater infrared abilities since the former are more affordable and more easily available to the typical lab.

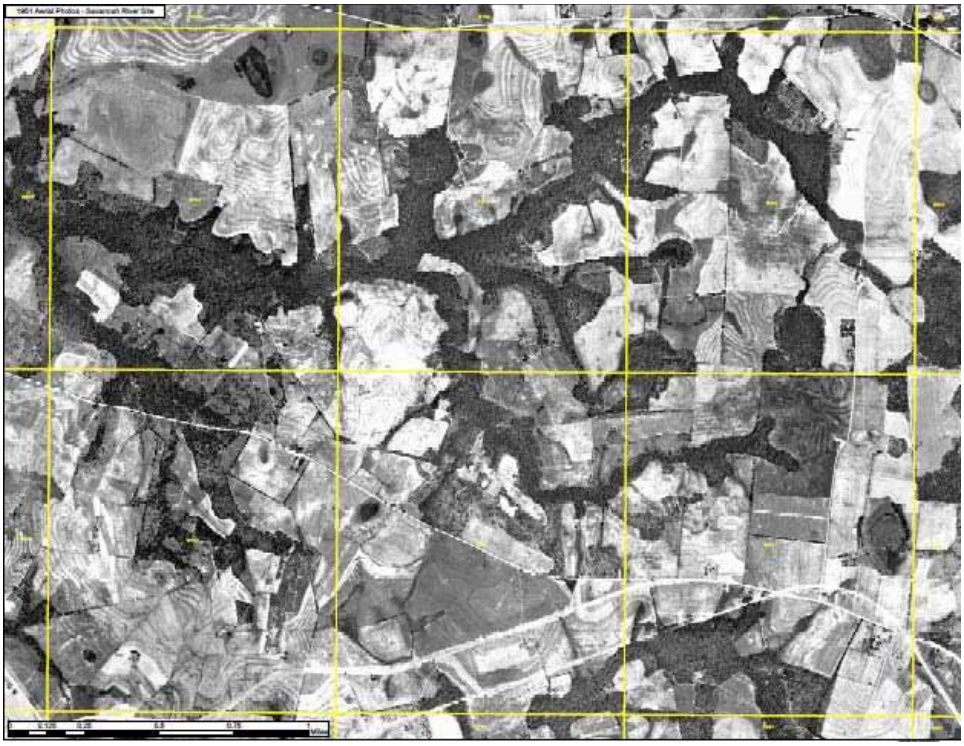

Figure 1.1: Aerial map of SRS in the 1950s.

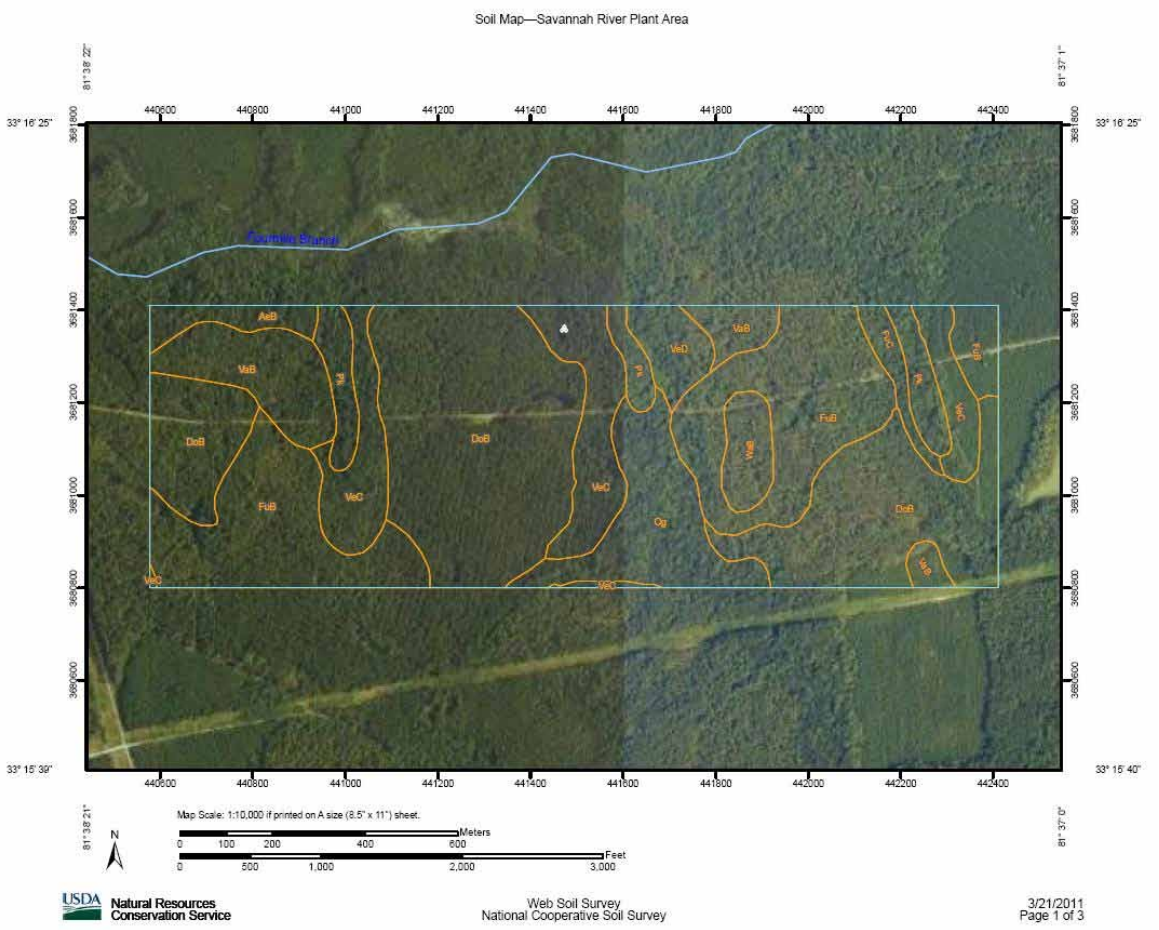

Figure 1.2: Soils map of SRS from the Natural Resources Conservation Service's web soil survey (www.websoilsurvey.nrcs.usda.gov).

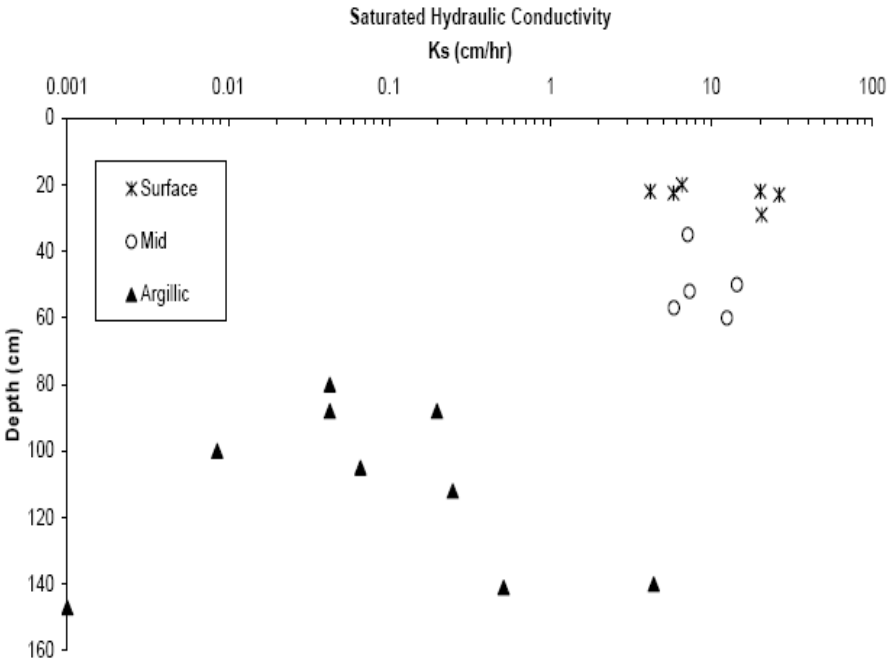

Figure 1.3: Ksats from various depths in SRS soils (Greco 2004.)

Chapter 2

Literature Review

The research questions explored in this thesis concern various areas (such as information on ground water hydrology, soil science and the use of several pieces of field equipment) that needed to be properly understood before accurate conclusions could be drawn from the results of this research. The purpose of this literature review is to provide an easy-to-read summary and synthesis of published literature relating to this thesis.

The papers reviewed in this section are organized into three main groups: 1. ground water hydrology (how water moves through the vadose zone, how slight hillslopes may affect water movement, how macropores in soils influence ground water infiltration and how these higher infiltration rates affect ground water quality), 2. soil morphology and hydraulics in the Coastal Plain (properties of soils, especially argillic layers, in the Coastal Plain and soil measurements such as bulk density) and 3. field equipment used in this research (GPR, Methylene Blue Dye, tile probe, knocking pole, auger, CCHPs and the multi-spectral camera), their background stories and their use in soils, hydrology and various other fields.

The organization for this section of the literature review is arranged first into these three groups and, within each group, organization precedes from broadest to most specific. The tools discussed in group 3 (Equipment), are listed in the chronological order in which they were used in the field.

2.1 Water Flow in Soils

Water flow through soils is determined by the homogeneity of a system and the potential affect of large macropores, such as old pine tree root holes, on water flow paths.

2.1.1 Flow in Homogeneous Systems (Darcy's Law)

The amount of flow in a ground water system can be predicted using Darcy's Law (Anderson and Burt 1978) with Q = discharge rate, K = hydraulic conductivity, A = cross-sectional area and $(\Delta h/\Delta L)$ = hydraulic gradient.

$$Q = -K\ A\ \frac{\Delta h}{\Delta L} \tag{2.1}$$

This rate of discharge (Q) can be into either a surficial system or it can be into an underground water system, such as an aquifer. When ground water quality of an aquifer is concerned, discharge rates are important because they indicate how much water is available to recharge an aquifer and they can have implications for how much and how fast constituents may enter the ground water supply (Fetter 2001).

Hydraulic conductivity (K) is a measurement of the properties of the media that the water is flowing through (texture, pore size, mineral composition, etc) and properties of the fluid itself (density, viscosity, etc) (Fetter 2001). Higher K rates indicate that fluids are moving through the soil matrix at a faster rate, which implies that there is a higher possibility for contaminants and constituents to make it through the soil matrix and into the ground water supply. A lower K rate would indicate that fluids move slower through the soil matrix and that there is more opportunity for those constituents and contaminants to be filtered out into the soil matrix before they get the chance to reach the ground water supply (Fetter 2001, McCarthy & Zachara 1989, McDowell-Boyer et al. 1986, McGechan & Lewis 2002).

In considering the ground water hydrology of a hillslope, Darcy's Law is useful for calculating the amount of outflow discharge at the bottom of a hillslope, which could also impact water quality in surficial systems such as streams, rivers and lakes (Anderson & Burt 1978, Meyles et al. 2003, Sidle 1984, Uchida et al. 2004, Uchida et al. 2005, Wilcox et al. 1997). When using Darcy's Law, one makes the assumptions that a system is both homogeneous

and isotropic (Fetter 2001), without allowing for the inclusion of such things as macropores, which would make the system heterogeneous. Understanding the relationship between soil wetting patterns in hillslopes and subsurface flow is important to adequately predict hillslope outflow. The fill-and-spill hypothesis by Tromp-van Meerveld & McDonnell 2006 predicts that significant subsurface flow occurs when the trench face at the bottom of a hillslope is connected to the subsurface saturated areas by the filling in of depressions in a hillslope and the spilling of water over topographic relief in the bedrock surface.

2.1.2 Flow in Non-Homogeneous Soils (Macropores)

Macropores affect the rate of ground water infiltration, are not well-accounted for in Darcy's equation models and should be considered when managing for ground water quality (Beven & Germann 1982, Selker 1992, Vervoort et al. 1999) since an increase in macropores could lead to higher infiltration rates, which would affect ground water quality (McCarthy & Zachara 1989, McDowell-Boyer et al. 1986, McGechan & Lewis 2002). Macropores are pore spaces in soils that are large enough to allow an increased amount of fluid through the soil matrix. Macropores can be created in soils by numerous processes: bioturbation from animals, root holes from plants, weathering processes and land management practices, just to name a few. Defining the actual size limitations of a macropore is harder then one might expect and many different papers have presented many different size ranges to define macropore classes (Beven & Germann 1982). Luxmoore 1981, for example, assigned three size classes: macro (>1000 μm), meso (10-1000 μm) and micro (<10 μm). In comparison, Bouma et al. 1977 defined macropores as $> 100\mu$m in diameter and Alaoui et al. 2011 defined macropores as >50 mum in diameter.

For the sake of simplification, this paper did not attempt to define macropore classes and instead focused on macropores that appeared as visually apparent anomalies in the soil (such as those created by old decayed tree roots) and how they influenced the Ksats in the argillic layers at SRS.

Surface soil layers have progressively lower conductivities with depth (Zaslavsky & Sinai 1981c) and the classification of conductivities as high or low varies from paper to paper and depends greatly on the soils, their history and the current management of the soils. High conductivities can be classified as (>10cm/hr) (Freeze 1972a, 1972b, Beven 1977), but we expected to find Ksats that were too high for the amoozemeters to measure at our soil anomalies.

2.2 Characteristics of Coastal Plain Soils

The SRS is located near the transition from the Piedmont geographic region to the Coastal Plain region (Figure 2.1) and the publication by Markewich et al. 1990 did an excellent job showing the comparisons and contrasts between the soils of the two regions. In this paper, Markewich et al. 1990 pointed out that soils typical of the Piedmont region tended to have low infiltration rates, more clay than Coastal Plain soils and had ponding and/or lateral water flow over the argillic layers, whereas Coastal Plain soils were typically thicker (2-8m), had high sand content and high infiltration rates (Figure 2.2).

Physical properties of soil contribute significantly to infiltration and runoff rates and, while the Piedmont and the Coastal Plain may have similar climatic histories and uplift rates, their soils come from different parent materials. As the soils mature over time, their interactions with water change and Markewich et al. 1990 said that this time variable and the parent material were the two most important factors in determining water-soil interactions, though, they argue, the parent material was the most important factor of the two.

2.2.1 Dominant Soil Series

The dominant soil order for both the Coastal Plain and the Piedmont are Ultisols, though the least developed Ultisols are found in the western Piedmont and eastern Coastal Plain, while the Fall Zone near the inner Coastal Plain primarily consists of deep soils with well-developed argillic horizons. Dothan sand (classification: thermic Plinthic Kandiudults), Fuquay sand

(classification: arenic Plinthic Kandiudults), two of the most common soil map units found at SRS, were originally classified as Paleudults, but have been re-classified as Kandiudults to meet the criteria of the Low Activity Clay Amendment to Soil Taxonomy. The third most common soil map unit at SRS, Vaucluse-Ailey complex (thermic Fragic Kanhapludults and thermic Arenic Kanhapludults, respectively) is also from the soil order Ultisols found commonly in the upper Coastal Plain.

Dothan sand forms in marine terraces and their parent material is loamy marine deposits. They are well drained soils with moderately high Ksats of 0.20 to 0.57 in/hr (0.0085 to 0.024 cm/min) found on 2 to 6% slopes. They do not flood or pond frequently and they have moderate available water capacity of ≈ 6.6 in (16.51 cm). The depth to the Bt horizon is more than 11 in (27.94 cm) at SRS and the depth to the water table is ≈ 36 to 60 in (0.91 to 1.52 m) (National Cooperative Soil Survey 2009a). They are classified as Kandiudults, thus, they have highly weathered, low activity clay soils.

Fuquay sand forms in marine terraces as well and their parent material is sandy and/or loamy marine deposits. They are well drained like Dothan sands, but they have moderately low to moderately high Ksats of 0.06 to 0.20 in/hr (0.0025 to 0.0085 cm/min), meaning that their limiting layer has a lower capacity to transmit water than the Dothan sands. They are found on 2 to 6% slopes and are not expected to pond or flood. The depth to the Bt horizon is more than 21 in (53.34 cm) at SRS and the depth to the water table is ≈ 48 to 72 in (1.22 to 1.83 m) (National Cooperative Soil Survey 2009b). They are also classified as Kandiudults and have highly weathered, low activity clay soils.

Vaucluse-Ailey complex forms in marine terraces. The parent material for Vaucluse is loamy marine deposits and the parent material for Ailey is sandy and/or loamy marine deposits. They are well drained and Vaucluse have very low to moderately high Ksats of 0.00 to 0.57 in/hr 0 to 0.024 cm/min) while Ailey have moderately low to moderately high Ksats of 0.06 to 0.20 in/hr (0.0025 to 0.0085 cm/min). They do not flood or pond and they have a low available water capacity of ≈ 4.4 in (11.17 cm) for Vaucluse and ≈ 4.1 in (10.41

cm) for Ailey). They are found on 6 to 15% slopes and the depth to a Bt horizon is more than 10 in (25.4 cm) at SRS. The depth to the water table at SRS is more than 80 in (2.03 m) (National Cooperative Soil Survey 2009c).

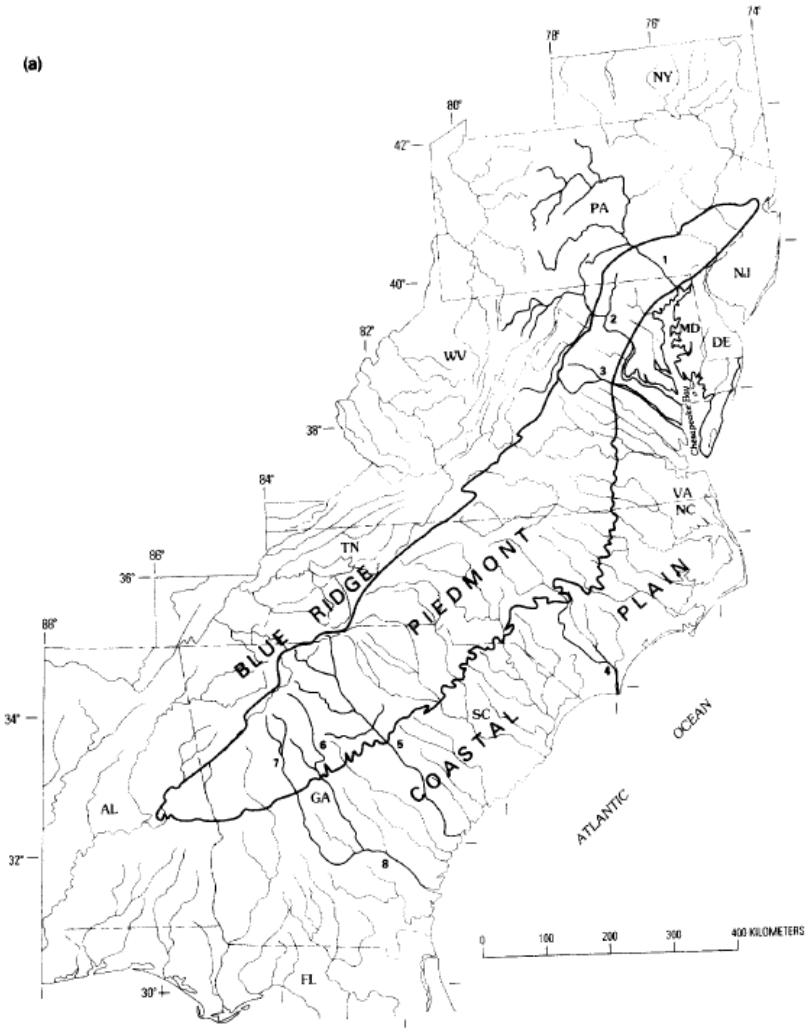

Figure 2.1: Map of the transition from the Piedmont geographic region to the Coastal Plain region (from Markewich et al. 1990).

2.3 Measurement of Spatial Variability of Argillic Horizons

The various pieces of equipment used in this research included GPR, methylene blue dye, a tile probe, a knocking pole, constant compact-head permeameters (CCHPs), and a multi-spectral camera. The GPR and the multi-spectral camera were non-invasive techniques for detecting potential soil anomalies and soil wetness, respectively. The methylene blue dye, tile probe, knocking pole, auger and CCHPs were direct-assessment techniques that each involved some sort of invasive measurements of the system.

2.3.1 Non-Invasive Measurements (GPR, Multi-spectral Camera)

GPR is commonly used to show stratigraphic profiles (Naegeli et al. 1996) as the changes in the dielectric for different stratigraphic layers creates GPR reflections, refractions or attenuation, which help make the difference visible. Though GPR is a device more typically used in geology and archeology than hydrology, the visibility of tree roots in archaeological surveys (Conyers & Cameron 1998) showed that it could prove a very useful device for this project as we were trying to detect vestigial taproots in the argillic layer that could be impacting the argillic layer's Ksat.

Soils found in the Coastal Plain where SRS is located should have worked well for mapping tree roots in the A and E horizons since they had a low dielectric and were highly electrically resistive (Butnor et al. 2001), but the clay-rich soil of the B horizon was not ideal for mapping tree root systems so we expected that there would be more trouble mapping the vestigial taproots in those soils. The differences between the dielectric of the taproots and the sandy soils would show stronger anomalies in the GPR maps than the differences between the dielectric of the taproots to the clay soils.

The final piece of equipment we used in this research and now address in this Literature Review was the multi-spectral camera. While it is more traditionally used in the arts, the multi-spectral camera is making an increased presence in the environmental sciences. Aleixos et al. 2002 used multi-spectral cameras with near-infrared capabilities to detect defects on

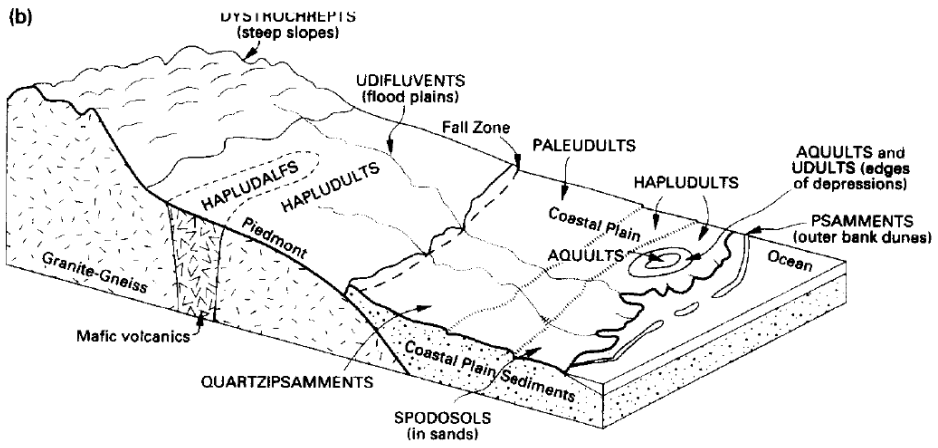

Figure 2.2: Figure of the soils of the Coastal Plain and Piedmont (from Markewich et al. 1990).

the skin surface of citrus crops in Spain in order to increase accuracy of machine vision fruit inspections. Zarco-Tejada et al. 2009 used an airborne multi-spectral camera with similar near-infrared capabilities (757.5 nm and 760.5 nm for Zarco-Tejada et al. 2009, 750 nm for Aleixos et al. 2002) to detect vegetation stress in olive, peach and orange orchards by imaging chlorophyll fluorescence.

Two papers concerning multi-spectral camera use in the earth sciences that were more relevant to the particular issues our research addressed were Hinkler et al. 2003 and Lobell & Asner 2002. Hinkler et al. 2003 used a low cost multi-spectral digital camera to detect changes in surface reflection at the arctic tundra at Ny-Ålesund, Svalbard and Lobell & Asner 2002 used multi-spectral cameras to detect the effects of moisture on soil reflectance. Lobell & Asner 2002 used multi-spectral cameras with visible, near-infrared and shortwave-infrared spectral ranges and discovered that soil reflectance was detectable at much lower soil moisture rates in the visible and near-infrared spectral ranges.

2.3.2 Direct-Assessment Techniques

Methylene blue dye is a commonly used ground water tracer. Gupte et al. 1996 used 1000:1 concentrations of deionized water to methylene blue dye powder for their experiments and they were able to detect ground water pathways in sandy soils in the Piedmont. Alaoui et al. 2011 used a similar ground water dye tracer, Brilliant Blue (BB), and were able to detect ground water pathways in forest soils, grassland soils and hillsloped areas in Kandergrund, Switzerland. While there are many other types of ground water tracers available for use out there (isotope markers, temperature markers, biological markers), dye tracers are easily detected and affordable (Davis et al. 2006).

Depth to the argillic layer can be estimated using soil penetration methods, such as the tile probe or the knocking pole. Depth to the argillic layer can tell us what sort of water storage potential a soil has - the greater the soil depth, the greater the potential for storing water (Lookingbill & Urban 2004).

In order to determine the depth from the surface to the argillic layer, soil penetration resistance can be measured. The logic behind soil penetration resistance is that argillic layers generally have more resistance to soil penetration than surface horizons and that the implementation of a sharp soil penetrating tool (such as a tile probe or a cone-tipped knocking pole) can help find the depth to the argillic layer faster and easier than thorough augering.

Soil penetration resistance varies with soil water content, bulk density, texture and organic matter (Busscher et al. 1997). Various equations can be used to help correct soil penetration resistance measurements for water contents, however multiple-equation corrections cannot guarantee that corrections being made to measurements are real and that they are not results from the correction differences (Busscher et al. 1997). Soil penetration resistance can also be affected by the management history of a soil (for example, the presence of a hardpan formed by previous tilling practices) and by the texture of a soil (for example, it is hard to penetrate well-graded sands to get to an argillic layer as the sand can move into and build on top of each other in pore spaces to make penetration more difficult). Increased amounts of organic matter on the surface can make it harder to penetrate the surface to get the argillic layer as well. Soil texture, structure and management history all influence a soil's bulk density. Bulk density is the density of intact, in-place soil and it has a highly variable range in soils (0.7-2.0 g/cm^3). Sands are denser with better structure and lower BD and a BD>1.6 g/cm^3 starts to inhibit root growth (Arya & Paris 1981, Rawls 1983).

The tile probe is commonly used in forest research to determine the depth of surface soils over a horizon more resistant to penetration (such as a Cr or R horizon) and can be used with relative accuracy within the top 50 cm of soil (Meyer et al. 2007, Nyquist et al. 2008). Meyer et al. 2007 measured soil depths with refraction seismic method (RSM) as well as with a tile probe and compared the different results each technique gave them to depths measured in a soil pit by their sites. For their tile probe measurements, they took five readings from randomly selected points within each of their grids and used the maximum value of the five

readings. Lookingbill & Urban 2004 relied solely on the tile probe method and recorded the average depth of three measurements for each of their 2x2-m plots.

The knocking pole is another tool used to measure soil thickness. It has a 3 cm diameter cone tip on the end of a metal rod, a slide-hammer weight of 5 kg on the top of the metal rod with a falling height of 50 cm for that weight (Yoshinaga & Ohnuki 1995).

CCHPs are designed to measure saturated hydraulic conductivity in the field. They work by maintaining a constant height of water (>5 cm) at the bottom of an augered hole in the unsaturated zone of a soil and measuring how much water and what rate of flow it takes to maintain that height (Amoozegar 1989). The CCHP is light weight, can hold 5 L of water, can be used on any landscape terrain and is easily transportable (Amoozegar 1989). The CCHP is easy to use and has been implemented by many people studying ground water hydrology, including some of the researchers previously cited in this Literature Review such as Price et al. 2010 and Greco 2004.

2.4 Conclusion/Recommendations

Based on our review of the literature, we believed that the equipment and techniques we hoped to utilize in this research were well supported by other previously published research. We felt that we had a good understanding of the hydrological processes involved in ground water flow at sites (and in soils) like those at SRS. We believed that the equipment we were using would provide us with adequate tools to explore the research questions we hoped to tackle and we believed that the research questions we hoped to tackle were of importance to the field of hydrology and to the proper management of the biofuel production site that would soon occupy our research areas at SRS.

Chapter 3

Materials and Methods

3.1 Study Area

Studied soil profiles were located in the Upper 4 Mile Branch Watershed within the SRS south of New Ellenton, South Carolina. Working through the Forest Service, Savannah River (USFS-SR), our research was conducted on three 10x10-m plots under regenerated pine stands along Old House Road (figures 3.1, 3.2). We chose our plots so that we had one ridgetop (Plot 1) and two backslopes (Plot 2 and Plot 3). We also chose our plots so that they were near road access, under managed pines in old fields and had few large trees to disrupt our GPR data.

Each of the three plots were assigned numbers: 1, 2 and 3. The 0,0 corner (the starting corner for the GPR maps and the origin on the 10x10m-grid we used to describe trench and methylene blue square locations) of Plot 1 was located at N33°16'3.4459789", W81°38'16.4748505". Plot 1 was above an old trench site and it was the plot located highest up on the hillslope. The 0,0 corner of Plot 2 was located at N33°16'3.8427944", W81°37'43.2279197". Plot 2 was below the old trench site and in the middle of the hillslope. The 0,0 corner of Plot 3 was located at N33°16'6.3235651", W81°37'27.7841308". Plot 3 was the furthest below the old trench site out of the three plots and it was at the bottom of the hillslope.

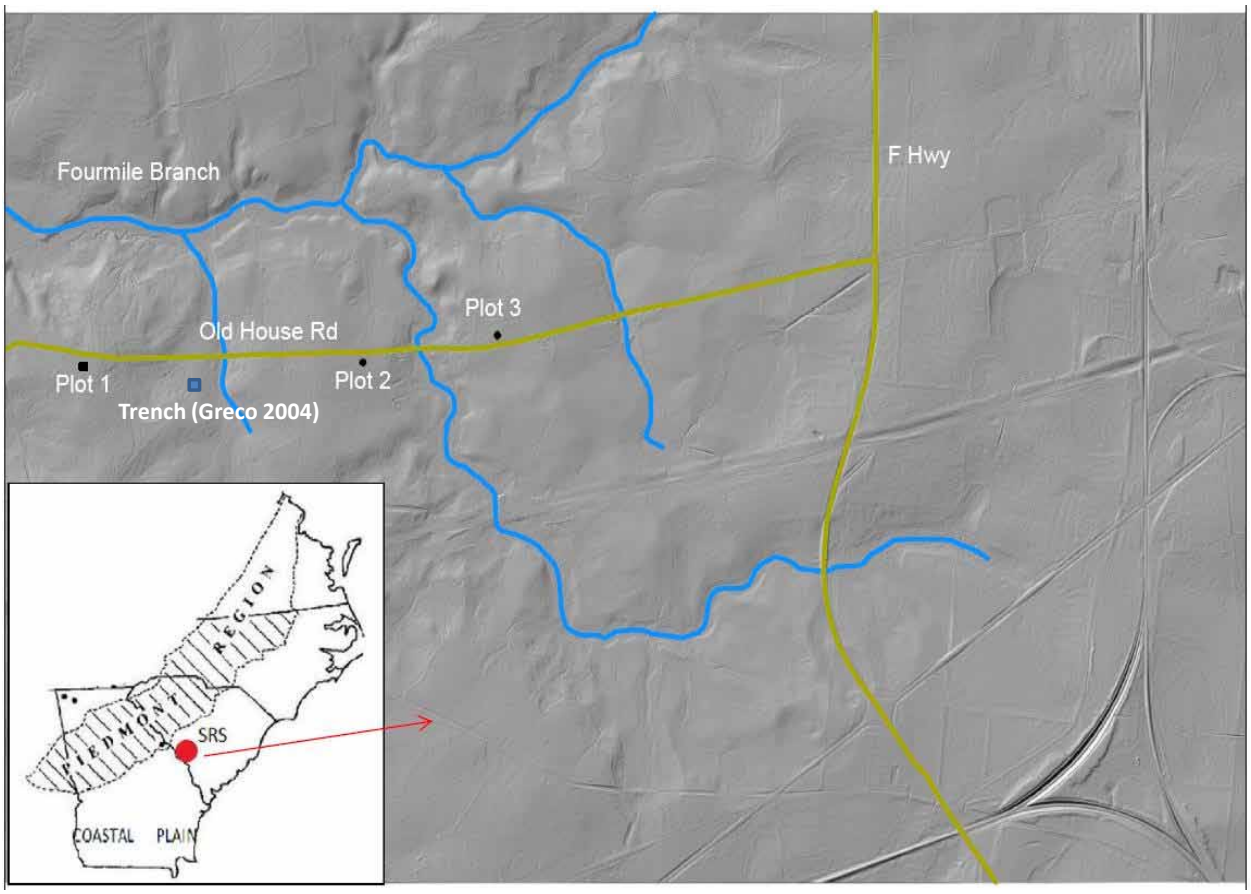

Figure 3.1: SRS, first with respect to the physiographic regions of Georgia and South Carolina and then a closeup map of our research Plots 1, 2 and 3 and the trench from Greco (2004) along Old House Rd in the Fourmile watershed within SRS.

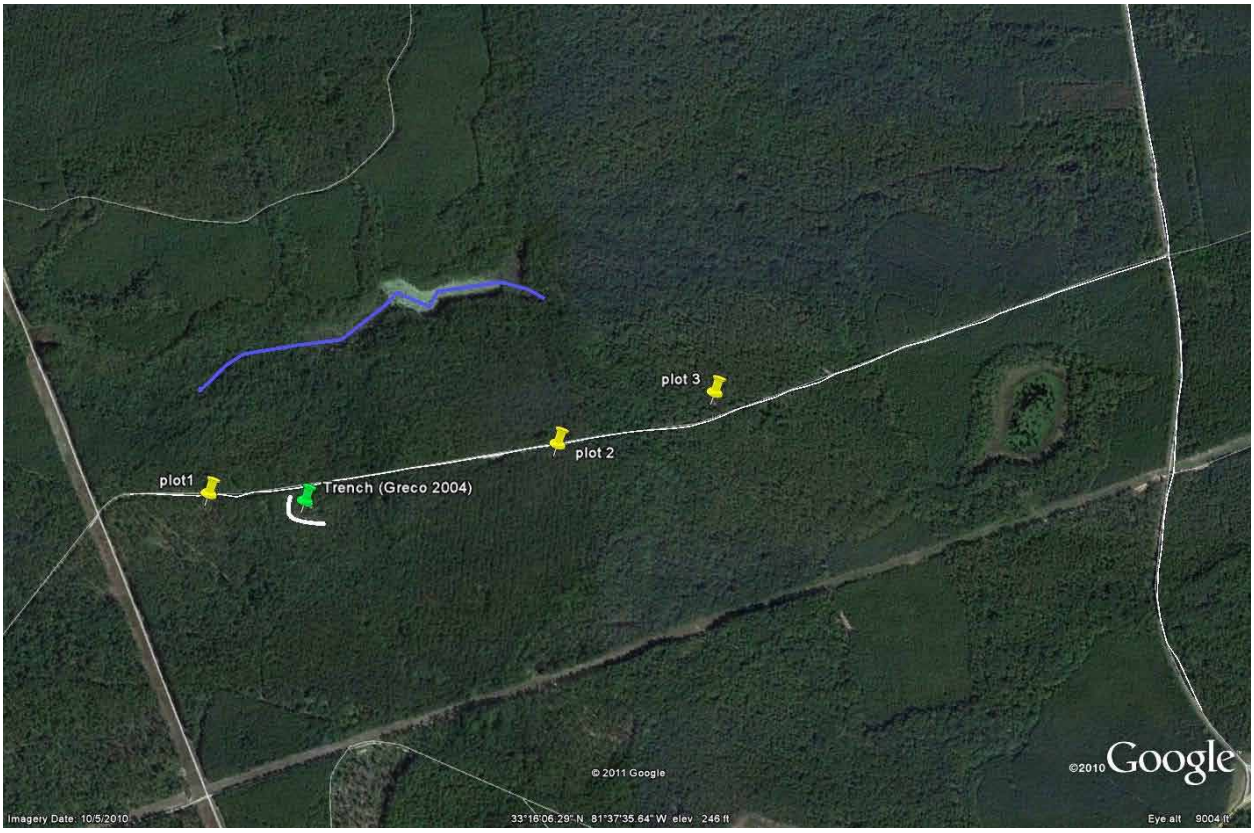

Figure 3.2: A closeup satellite image map of our research Plots 1, 2 and 3 and the trench from Greco (2004) along Old House Rd in the Fourmile watershed within SRS.

3.2 Field Methods

3.2.1 GPR

One 10x10-m plot was measured out on each of our three site locations. The plots were cleared of any debris (mostly twigs and branches) that could have negatively impacted the workability of the Ground Penetrating Radar (GPR). The three plots were scanned with the GPR unit on December 17, 2009 before any further field work was conducted in the plots. The GPR unit used for this study was a GSSI SIR-2000 with a 500 MHz antenna

Figure 3.3: SIR2000 GPR control unit with 500 MHz antenna connected to the survey wheel.

(Figure 3.3) and was run with the help of University of Georgia personnel from the Geology Department and the Warnell School of Forestry and Natural Resources (Figure 3.4). The maps created by the GPR surveys (Appendix B) showed areas of potential anomalies within each of the 10x10-m plots (figures 4.1, 4.3, 4.5) and allowed us to pick areas to be excavated, sprayed with ground water tracers and points to conduct conductivity measurements that would match up with where the GPR maps predicted there would be anomalies.

Figure 3.4: GPR surveying in action at Plot 1 with UGA personnel from the Geology Department and the Warnell School of Forestry and Natural Resources.

3.2.2 Methylene Blue Dye

Soil structure and preferential flow are highly related, but it is difficult to identify ground water pathways through soil (Vervoort et al. 1999). Methylene blue dye was used as an indicator of infiltration and percolation pathways at the three sample sites. A solution of deionized water and methylene blue dye powder was made at a concentration of 1000:1 (Gupte et al. 1996). Two 1x1.5-m methylene blue preliminary test plots, one with vegetation on it and one that was stripped bare of vegetation, were placed adjacent to each GPR plot. The purpose of the preliminary test plots was to estimate how much methylene blue was needed to track flow paths and to see if the O horizon affected the test. The preliminary test plots were sprayed with varying amounts of methylene blue dye and then dug up after enough rainfall had occurred to see how far down the dye traveled. The results of these preliminary test plots helped determine whether vegetation needed to be raked away on the 1x1.5-m methylene blue test plots inside each of the 10x10-m plots when it got closer to the excavation of the plot.

The two preliminary test plots by Plot 1 were sprayed with 6 L of methylene blue dye. The preliminary test plots by Plot 2 were sprayed with 4 L of methylene blue dye. The preliminary test plots at Plot 3 were sprayed with 2 L of methylene blue dye.

Each of the 1x1.5-m methylene blue test plots was sprayed with 4 L a week for 6 weeks (making for a total of 24 L of methylene blue dye on each of the squares) with the use of a pesticide back pack sprayer. For the last three weeks, the test plots were gently raked before spraying in order to remove any fallen leaves and/or pine needles to help ensure that the methylene blue dye was not getting caught up in the organic matter and had a fair chance of making it to the soil. All together, 12 L of the 24 L of methylene blue dye sprayed on each of the test plots was sprayed with raking first. All large vegetation in the test plots, such as vines, poison ivy and plant sprouts were left alone so as to limit the amount of disturbance to natural ground water flow into the soil as much as possible. Excavation of the 1x1.5-m

methylene blue test plots began on June 8, 2010 when 1x10-m strips were excavated down to 0.5 m at each of the three plots.

3.2.3 Multi-Spectral Camera

A multi-spectral camera was used to help identify anomalies by capturing pictures of soil moisture reflecting back at different wavelengths. Though multi-spectral cameras were one of the pieces of equipment that we used in this research that is not commonly used in the field of ground water hydrology, existing papers suggest that soil moisture contents above $\approx 20\%$ can be measured by reflectance of wavelengths in the visible and near infrared light spectrum (Lobell & Asner 2002). The multi-spectral camera used was a Canon PowerShot G10 digital camera modified to take picture in near infrared (NIR) and visible wavelengths. There were four filters for the multi-spectral camera: 1. a X-Nite 1000B - 2mm with the ability to capture pictures at 1000-1300 nm infrared, 2. a X-Nite 830 with the ability to capture pictures at 830-1200 nm infrared, 3. a X-Nite 715 with the ability to take pictures at 715-780 nm infrared, and 4. a X-Nite CC1 M58 which captured pictures while blocking out infrared.

3.2.4 Depth to Argillic

Depth to the argillic horizon was estimated three different ways: 1. with a tile probe, 2. with a knocking pole and 3. with an auger.

3.2.5 Tile Probe Method

A 1.5 m tile probe was used first at 0.5 m increments in each of the 10x10-m plots to determine depth from surface to the top argillic layer. A tile probe is a device that consists of a metal rod with a pointed tip on one end and a t-shaped handle on the other. The tile probe was driven into the ground until it would go no further and then the length of the tile probe that went into the ground was measured to determine depth to the argillic layer.

Depths were measured using this method at the 0.5 m increment at Plot 3, but the tile probe was not able to penetrate the surface at plots 1 or 2. The tile probe was used at 2 m increments for plots 1 and 2 in order to collect any possible depths from the device in a reasonable amount of time. After the tile probing, we switched to using a knocking pole. Then we used an auger to determine the actual depth to the argillic layer at all three plots at 2-m increments on all 10x10-m plots for both devices.

3.2.6 Knocking Pole Method

The knocking pole was designed according to the devices detailed in Shanley et al. 2003 and Yoshinaga & Ohnuki 1995. The knocking pole had a graduated 1-m section of metal pole with a cone-shaped end that attached to another 1-m section that housed a slide hammer. The slide hammer consisted of a weight that was lifted and dropped to drive the pointed end of the pole into the ground forcibly. The depth to argillic layer was determined when it took more than 5 slide hammer knocks to lower the knocking pole an additional 10 cm into the ground and the depth to argillic layer was then measured by determining where the ground level came in contact with the measured interval markings grooved into the knocking pole. An additional 1-m section of metal pole was provided in case the depth of the argillic layer was deeper than the first 1-m section. Knocking pole operators wore non-slip leather gloves and ear plugs for safety as the slide-hammer used to knock the pole into the ground was heavy and created a loud clanging sound at ear level to the operator.

3.2.7 Auger Method

After using the tile probe and the knocking pole, we augered holes at 2-m increments at each of the three 10x10-m plots until we reached the top of the clay layer. The depth of the hole was then measured and recorded. We alternated between using open bucket and closed bucket augers and we also alternated between the diameter sizes of the buckets we

used, depending on the soil texture (closed bucked for sandy, open bucket for clayey) and the availability of particular augers at the time of measuring.

As we augered each of the three plots at 2-m intervals within the 10x10-m plots, we recorded soil textural classes by feel and color (Appendix C) from two samples per line (equalling 12 recordings of soil texture and color from each plot).

3.2.8 In-Situ Hydraulic Conductivities

The first back-hoe excavation of the 1x10-m strips at each of the plots was done on June 8, 2010 down to 0.5 m at plots 1, 2 and 3. The back-hoe excavation was documented with the multi-spectral camera using primarily the unmodified camera filter, though pictures were taken of each of the freshly excavated 1x10-m strips with the four different modified camera filters to try to detect any areas of greater light reflectance where soil moisture was higher. Amoozemeter measurements were taken at any anomalies found inside the excavated 1x10-m strips with up to four anomaly readings per strip. When an amoozemeter measurement was found that was too fast to calculate, the amoozemeter water chambers had to be filled and emptied a total of four times (equal in volume to approximately 2 carboys full of water) still running at the too fast to calculate rate before the point could be determined an anomaly. The lower bound of these "too fast" readings were measured at >6.0 cm/min. Amoozemeter rates were determined when the water in the flow measuring reservoir dropped an equal distance over an equal time interval three times in a row.

In order to later calculate hydraulic conductivity rates from amoozemeter readings, the radius of the auger hole, depth from ground surface to the bottom of the auger hole, the distance from ground surface to the reference level of the amoozemeter flow measuring reservoir, total distance from the reference level to the bottom of the auger hole and the measured final depth from ground surface to the water level in the auger hole were all measured and recorded.

The second back-hoe excavation was done on June 23, 2010 down an additional 0.5 m to the first dig at Plot 1 and down an additional 1 ft (0.3048 m) at plots 2 and 3 due to an earlier then expected arrival at the clay layer for these last two plots. The same multi-spectral camera and amoozemeter reading methods were used on the second back-hoe excavation as were used on the first back-hoe excavation.

A third back-hoe excavation was not performed at any of the plots since all had reached clay layers of low hydraulic conductivities and Plot 1 could not be dug deeper without putting in trench walls for trench-wall stability and worker safety. Amoozemeter readings were also taken at 1x10-m transect lines (Appendix D), with up to four amoozemeter readings per transect, outside the 10x10-m plots on lines where the GPR maps showed high amounts of possible anomalies. When auger holes were too deep to see water level in the auger hole, a water level indicator was used to measure final depth from ground surface to the water level in the auger hole. When Ksat anomalies were detected in the 1x10-m transect lines, they were dug down to with a shovel in an attempt to visually verify the anomaly.

The equations we used to calculate hydraulic conductivity from amoozemeter measurements were:

$$i = \frac{Q}{\pi r^2} \tag{3.1}$$

$$G = \frac{1}{2\pi}\left[A_1 + A_2\left(\frac{H}{r}\right) + A_3\left(\frac{H}{r}\right)^2 + A_4\left(\frac{H}{r}\right)^3\right] \tag{3.2}$$

$$K = \frac{i}{1 + \frac{H\lambda_c}{G\pi r^2} + \frac{H^2}{G\pi r^2}} \tag{3.3}$$

The A values were given values from a soil texture/structure table (see table 3.1).

3.2.9 Soil Bulk Densities

To determine how soil densities might vary from each other in our soils, we took soil bulk density samples within anomalies and the soil horizons found in the trenches of all three plots. Two soil bulk density samples were collected at the visually apparent anomaly in Plot

Table 3.1: "A" values for soil texture/structure. Used in equation 3.2 to help calculate hydraulic conductivity from amoozemeter measurements.

Texture/Structure	**A1**	**A2**	**A3**	**A4**
Sand	0.079	0.516	-0.048	0.002
Structured Loams and Clays	0.083	0.514	-0.053	0.002
Unstructured Clays	0.094	0.489	-0.053	0.002

2 and the visually apparent anomaly in Plot 3. In Plot 1, three groups of samples were taken - the first was at location 6 m, 2.45 m and consisted of samples from the E and the Bt1 horizon, the second was at location 5 m, 4.17 m and consisted of samples from the Bt1 and the Bt2 horizon and the third was at location 5 m, 7.2 m and consisted of samples from the Bt1 and the Bt2 horizon. In Plot 2, three groups of samples were taken - the first was at 0 m, 2.7 m and consisted of samples from the E1 and the E2 horizon, the second was at 0 m, 3.4 m and consisted of samples from the E1 and the Bt horizon and the third was at 1 m, 7.4 m and consisted of samples from the E1 and the Bt horizon. In Plot 3, three groups of samples were taken - the first was at 4.5 m, 2.2 m and consisted of samples from the E1 and the Bt horizon, the second was at 4.5 m, 4.6 m and consisted of samples from the E1 and the E2 horizon and the third was at 5.5 m, 4.1 m and consisted of a sample from the E horizon.

To determine bulk density, we collected samples using a hammer-driven sampler with a core 7.5 cm long and 7.5 cm in diameter. Each of these samples was bagged, labeled and brought back to the lab to dry in a Fisher Scientific Isotemp Oven at 100-110°C for at least 48 hours (until constant weight). After each of the samples was thoroughly dry, its weight was measured and recorded and each sample's bulk density was calculated using an equation.

The mathematical equation used to calculate soil bulk density was:

$$\rho = \frac{m}{v} \tag{3.4}$$

with v being determined by the size of the sampling chamber, therefore:

$$v = \pi r^2 h = \pi \left(\frac{7.5}{2}\right)^2 7.5 \tag{3.5}$$

3.3 Statistical Methods

Descriptive statistics and regression analysis were used in this project to compare the depth to argillic layer results measured with the tile probe, the knocking pole and the auger. For our descriptive statistics, our null hypothesis was that $\mu_1 = \mu_o$ and $\mu_2 = \mu_o$, with $\mu_1 = tileprobe$, $\mu_2 = knockingpole$ and $\mu_o = auger$. Our alternative hypothesis was $\mu_1 \neq \mu_o$ and $\mu_2 \neq \mu_o$. For our regression analysis, we rejected R^2 values below 50%. The computer program Minitab 15.6 was used to run all statistical tests.

Chapter 4

Results and Discussion

4.1 GPR Results

The GPR device provided us with 3-D maps and surface maps at varying depths for each of the three plots we scanned. All potential anomalies showed up on the maps as shapes that were more elliptical than circular and were referred to as lenticular (blue-colored on the 3-D maps and red or orange-colored on the surface maps). For Plot 1, we had a 3-D map (Figure 4.1) and a surface map taken at 25 cm depth (Figure 4.2). For Plot 2, we had a 3-D map (Figure 4.3) and a surface map taken at 43 cm depth (Figure 4.4). For Plot 3, we had a 3-D map (Figure 4.5) and a surface map taken at 67 cm depth (Figure 4.6).

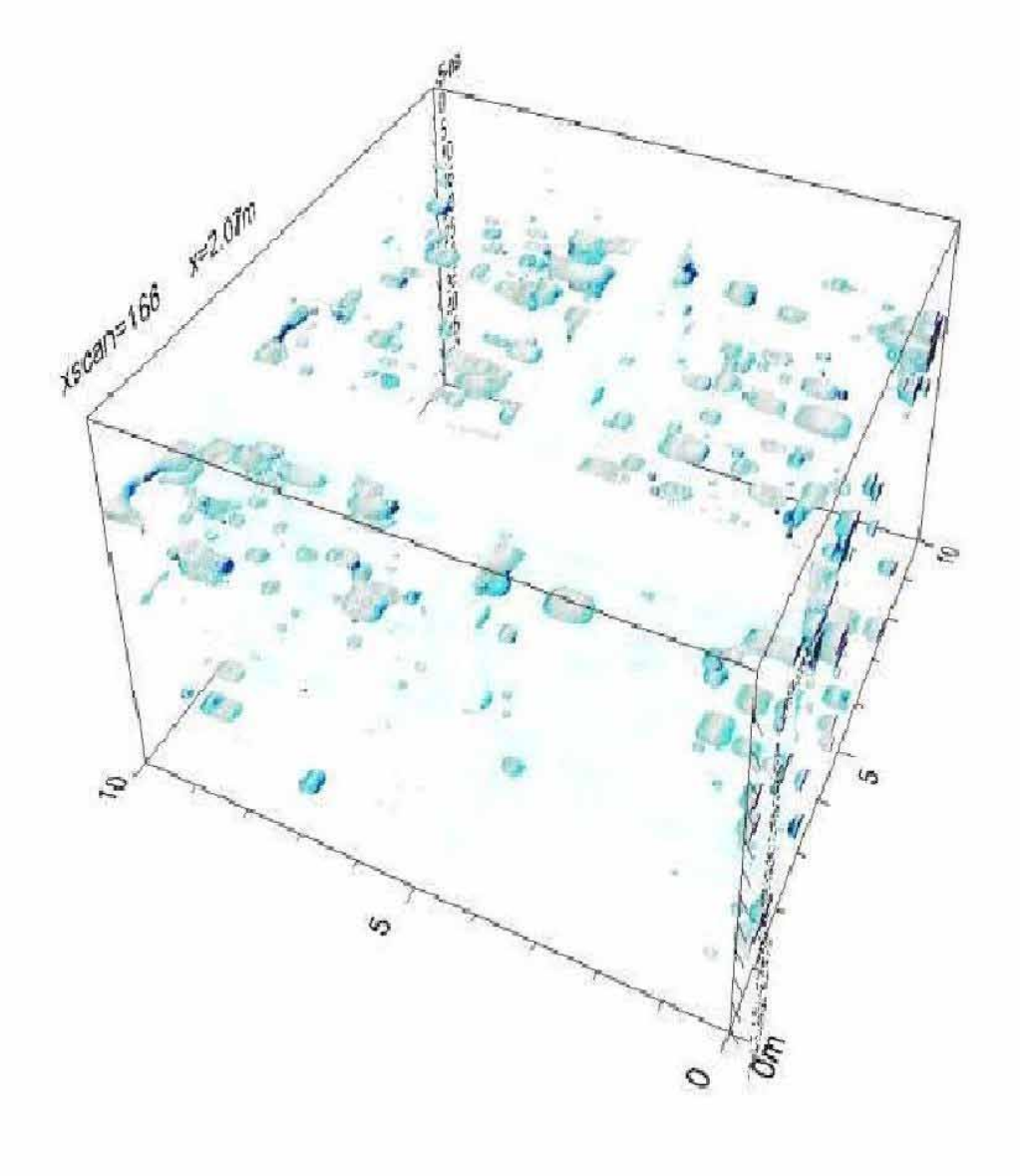

Figure 4.1: GPR map of Plot 1.

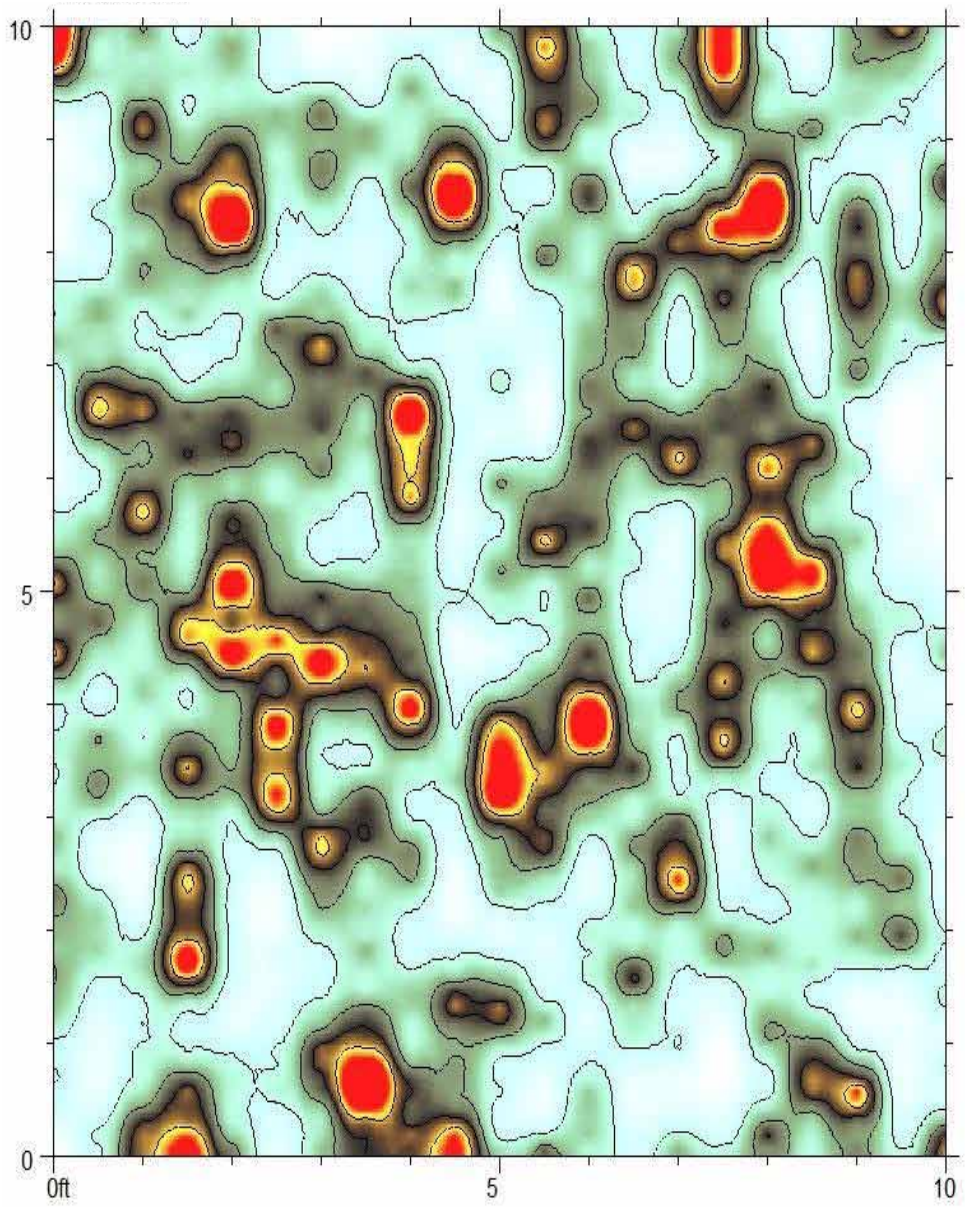

Figure 4.2: GPR map of Plot 1 at 25 cm depth (potential anomalies appear as lenticular-shaped red and yellow blobs).

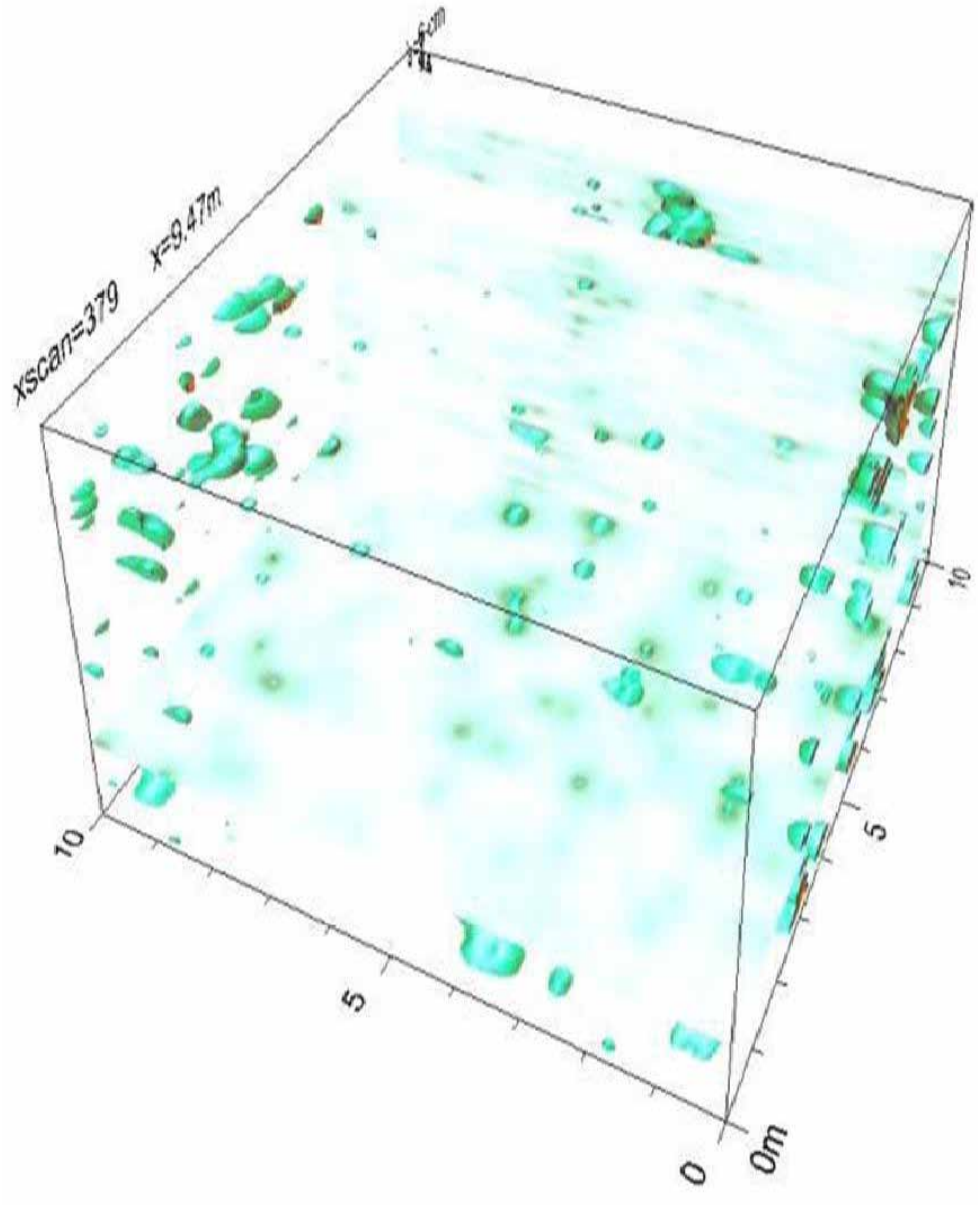

Figure 4.3: GPR map of Plot 2.

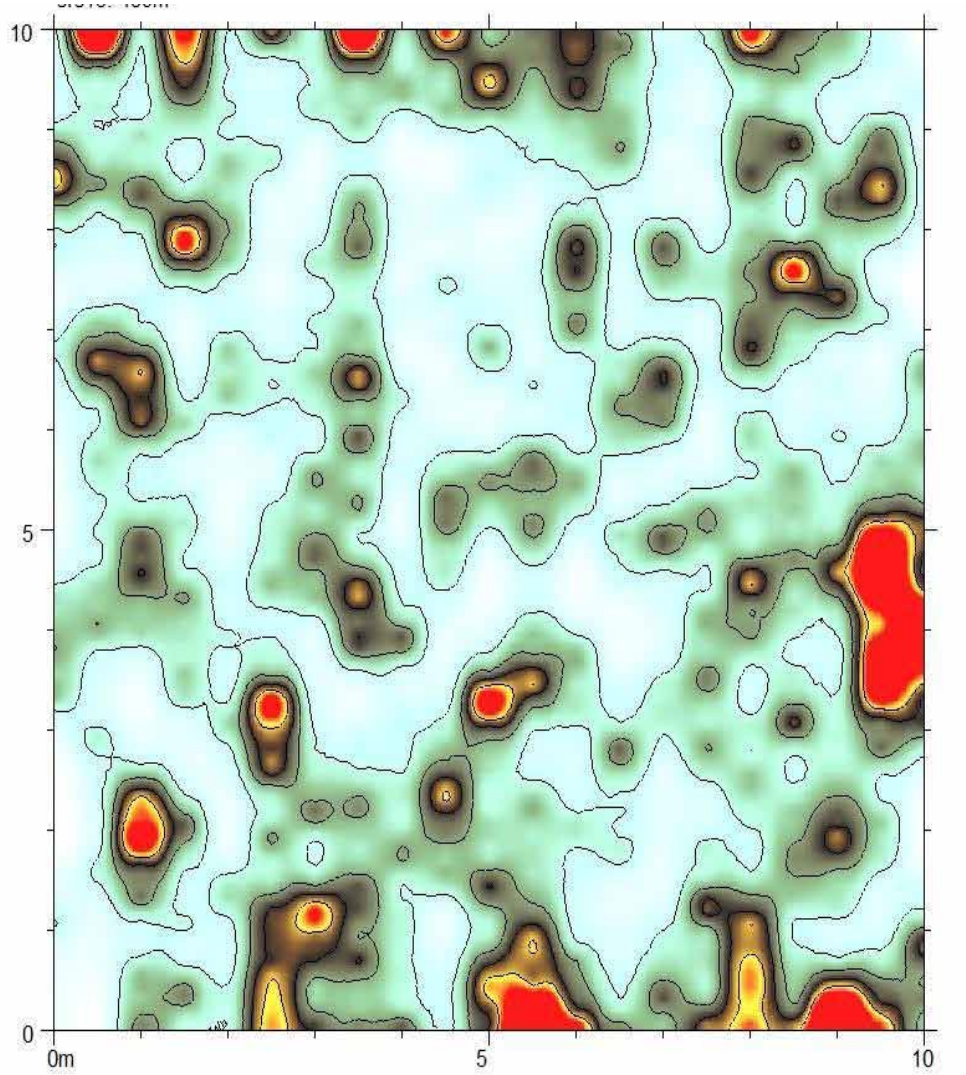

Figure 4.4: GPR map of Plot 2 at 43 cm depth (potential anomalies appear as lenticular-shaped red and yellow blobs).

4.2 Methylene Blue Dye Results/Multi-Spectral Camera Pictures

We used multi-spectral camera pictures to help record the results of the methylene blue dye ground water tracer tests. The two test spots by Plot 1 were sprayed with 6 L of methylene blue dye. When excavated, the test spot with no vegetative cover had more blue visible to the naked eye then the vegetated test spot. However, neither test spot had very much blue in the soil, even though the top soil was just skimmed off the top and the dig did not reach anywhere near 0.5 m (the first depth of excavation for the 10x10-m plots) (Figure 4.8). The test spots by Plot 2 were sprayed with 4 L of methylene blue dye. Upon excavation (once again, just a skimming off of the top soil), there was very little blue visible on either test spot, but there seemed to be more spots visible on the vegetated test spot then the bare test spot (though both had negligible amounts of blue on them) (Figure 4.9). The test spots at Plot 3 were sprayed with 2 L of methylene blue dye. Upon excavation (just a skimming off of the top soil), some dots of blue seemed visible to the naked eye on the vegetated plot upon removing the cover, but were damaged when further soil excavation took place (Figure 4.10).

None of the methylene blue dye squares within the 1x10-m strips in the plots showed traces of the blue dye to the first dig at 0.5 m deep (Figure 4.11).

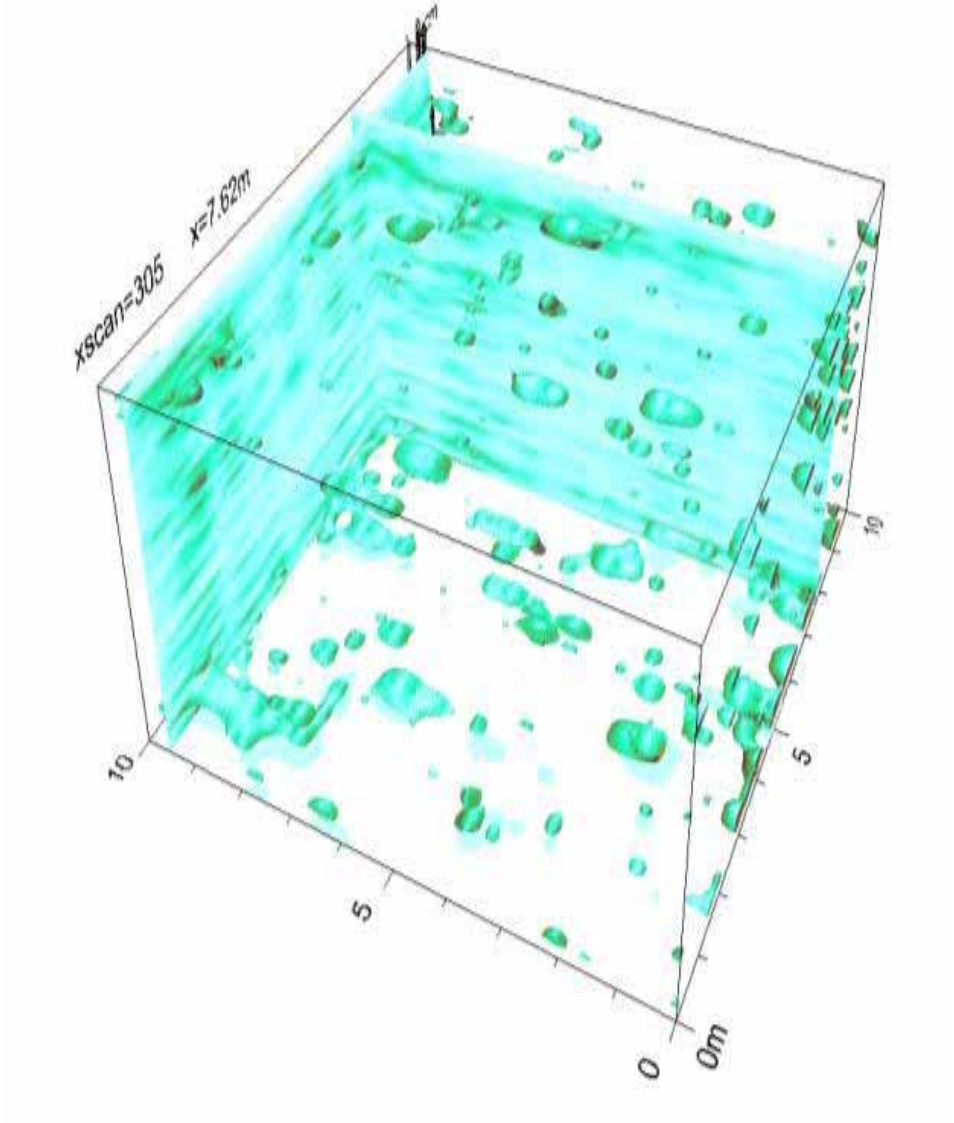

Figure 4.5: GPR map of Plot 3.

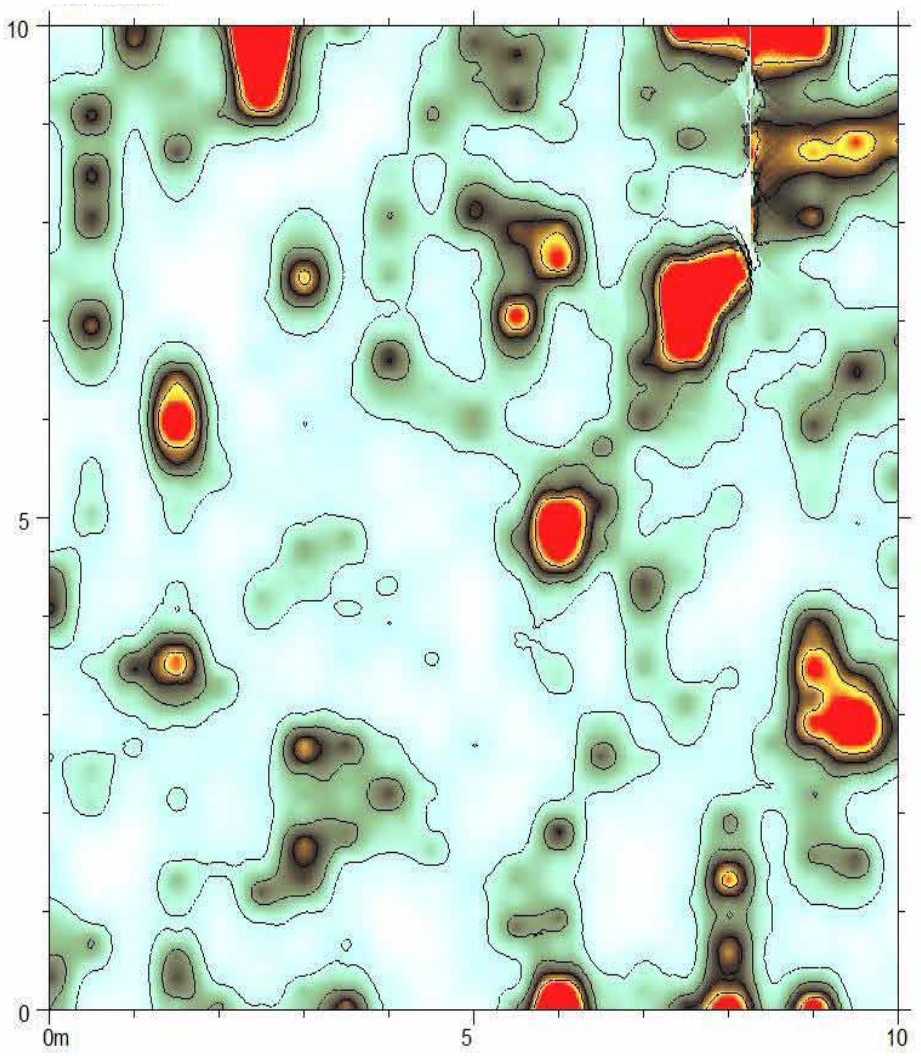

Figure 4.6: GPR map of Plot 3 at 67cm depth (potential anomalies appear as lenticular-shaped red and yellow blobs).

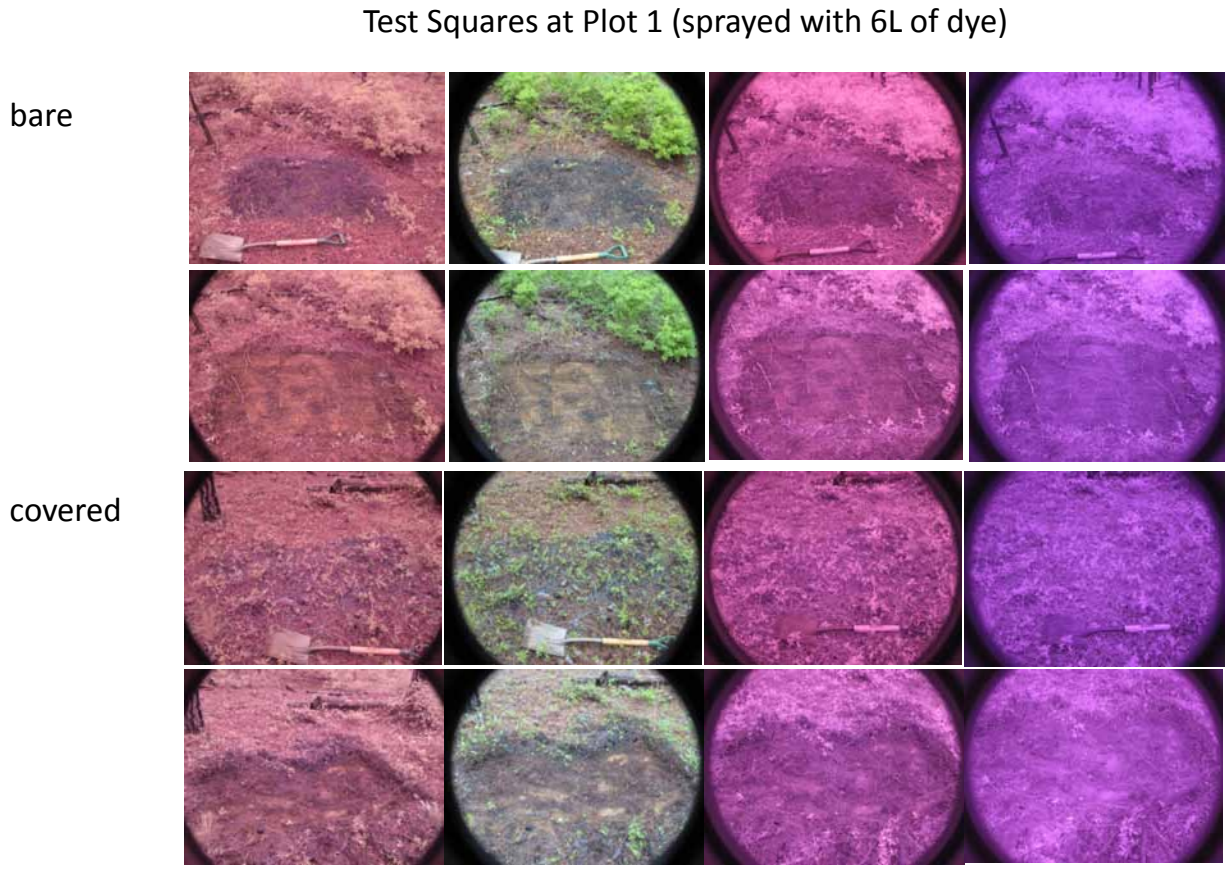

Figure 4.7: Multi-spectral camera pictures from methylene blue test squares at Plot 1, before and after excavation.

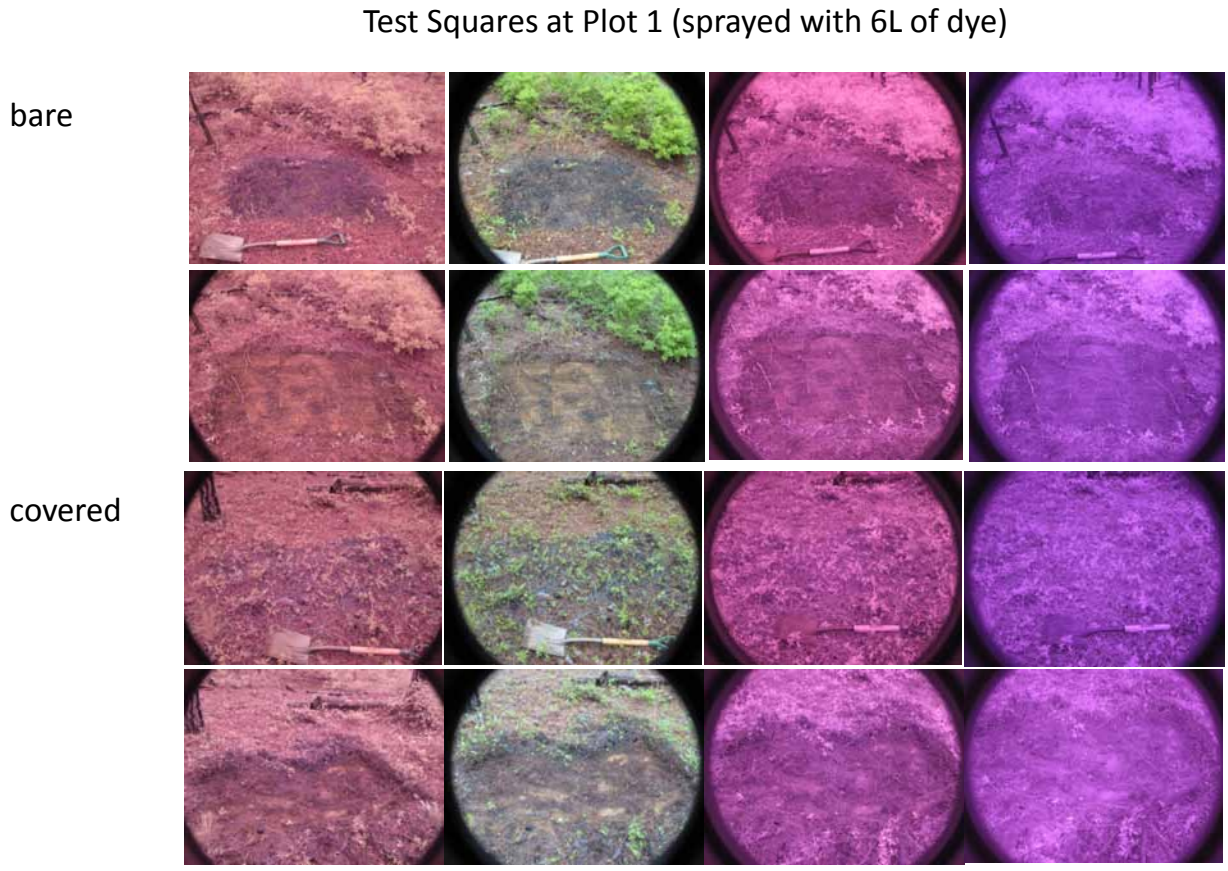

Figure 4.8: Multi-spectral camera pictures from methylene blue test squares at Plot 1, before and after excavation.

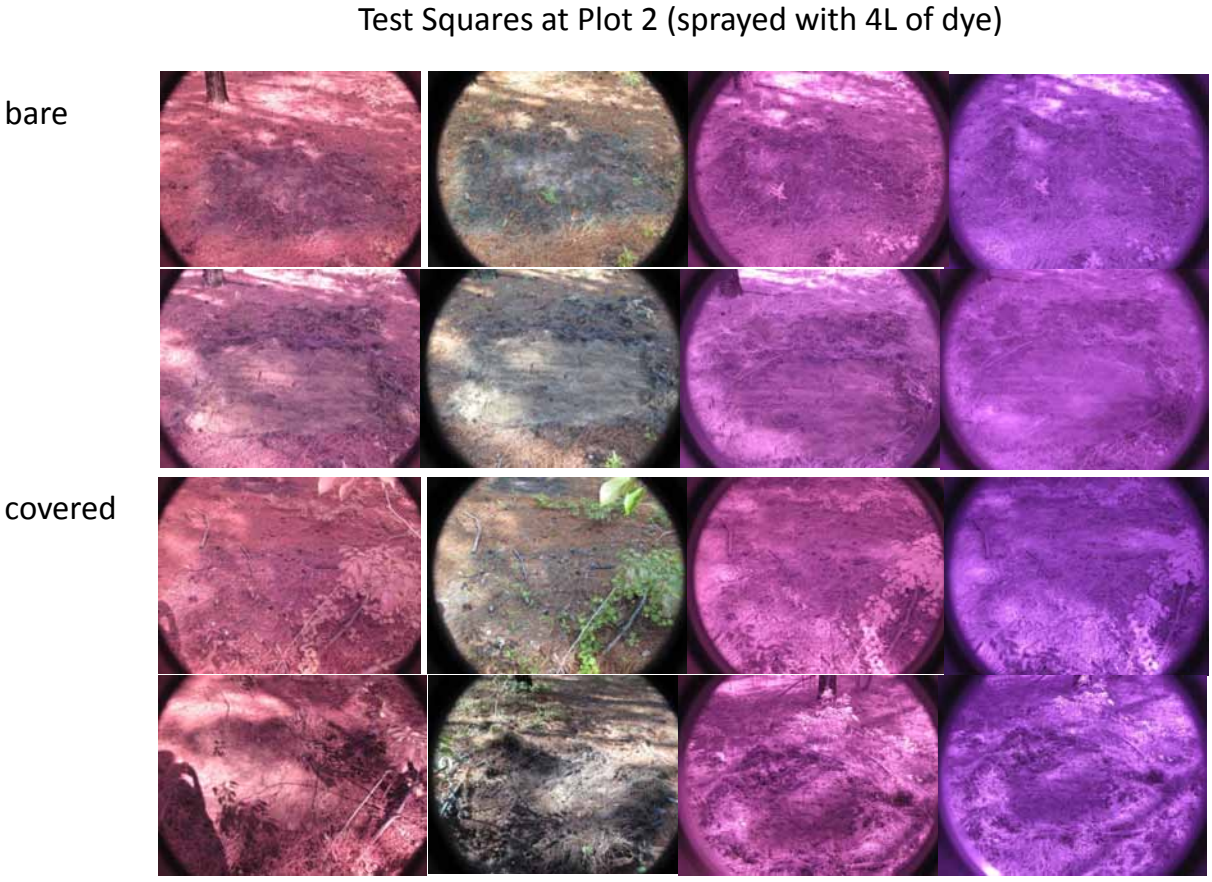

Figure 4.9: Multi-spectral camera pictures from methylene blue test squares at Plot 2, before and after excavation.

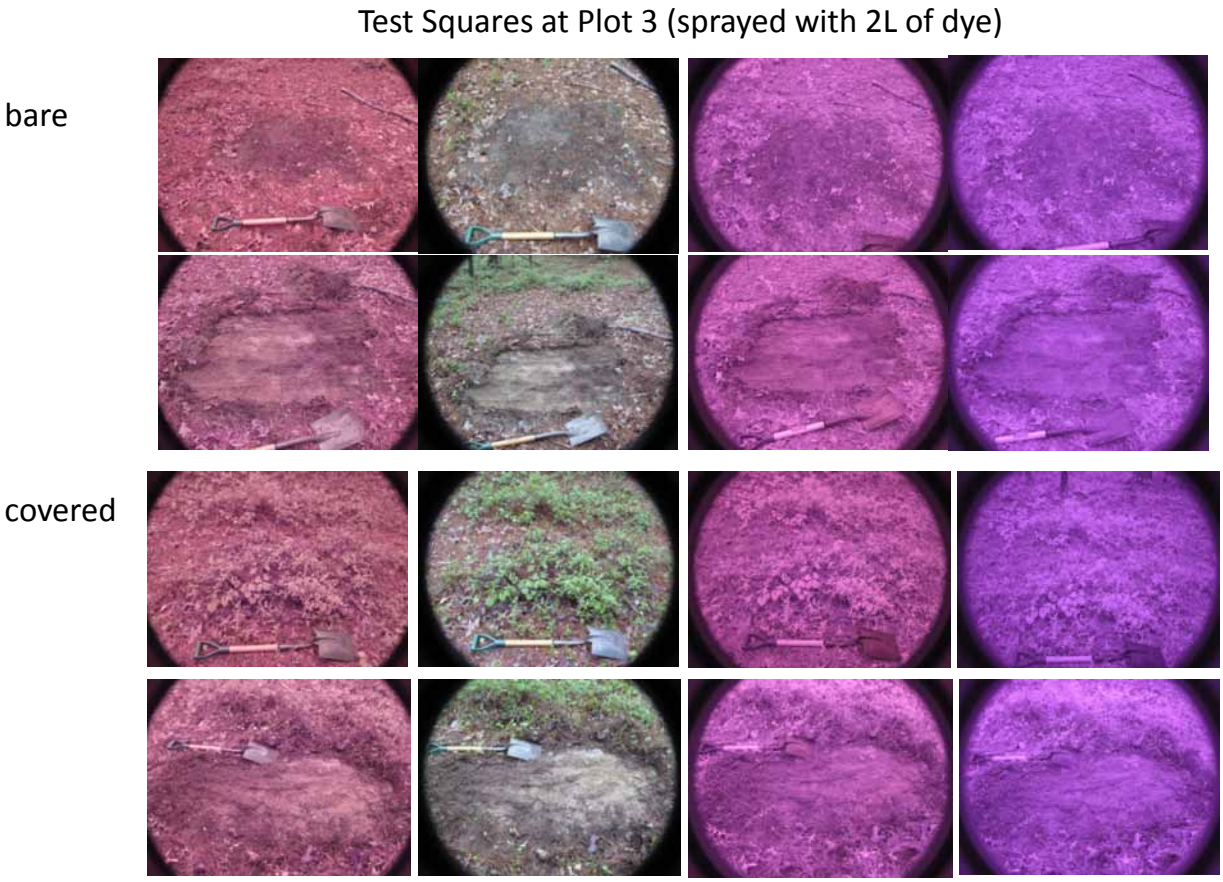

Figure 4.10: Multi-spectral camera pictures from methylene blue test squares at Plot 3, before and after excavation.

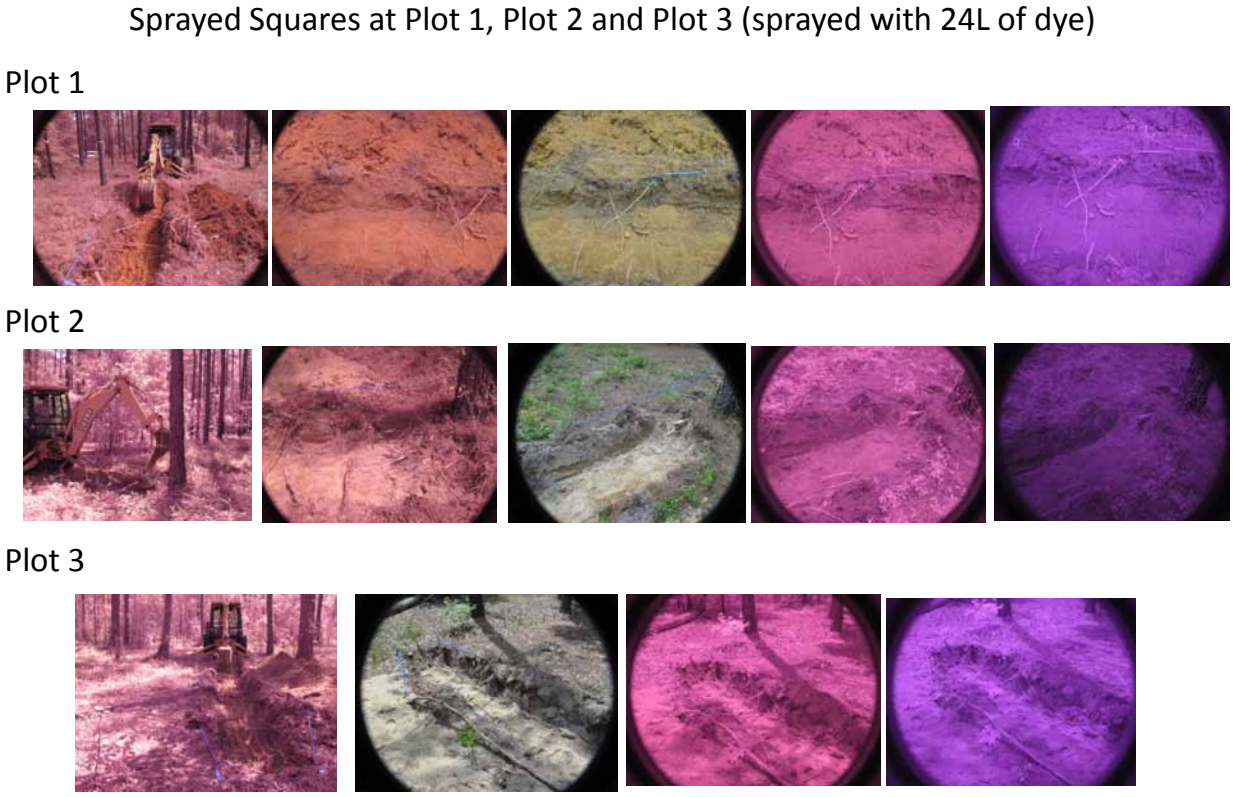

Figure 4.11: Multi-spectral camera pictures from methylene blue squares within Plots 1, 2 and 3, after excavation.

4.3 Tile Probe, Knocking Pole and Auger Results

Depth to the argillic layer was first estimated with a tile probe at each of the three plots at 2x2-m increments. We had difficulty getting the tile probe through some of the sandier soils at our plots, so we then estimated the depth to the argillic layer with a knocking pole. The slide-hammer at the top of the knocking pole allowed us to penetrate through the sandier soils with more force and measurements were taken at each plot at 2x2-m increments. Then, in order to determine actual depth to the argillic layer at all plots, we augered to the argillic

layer at each plot at 2x2-m increments. Using the data from the tile probe, knocking pole and auger measurements, we were able to compare the adequacy of both the tile probe and the knocking pole for determining accurate depth to the clay layer (aka, the depths recorded with the auger measurements) (figures 4.12, 4.13, 4.14, 4.15).

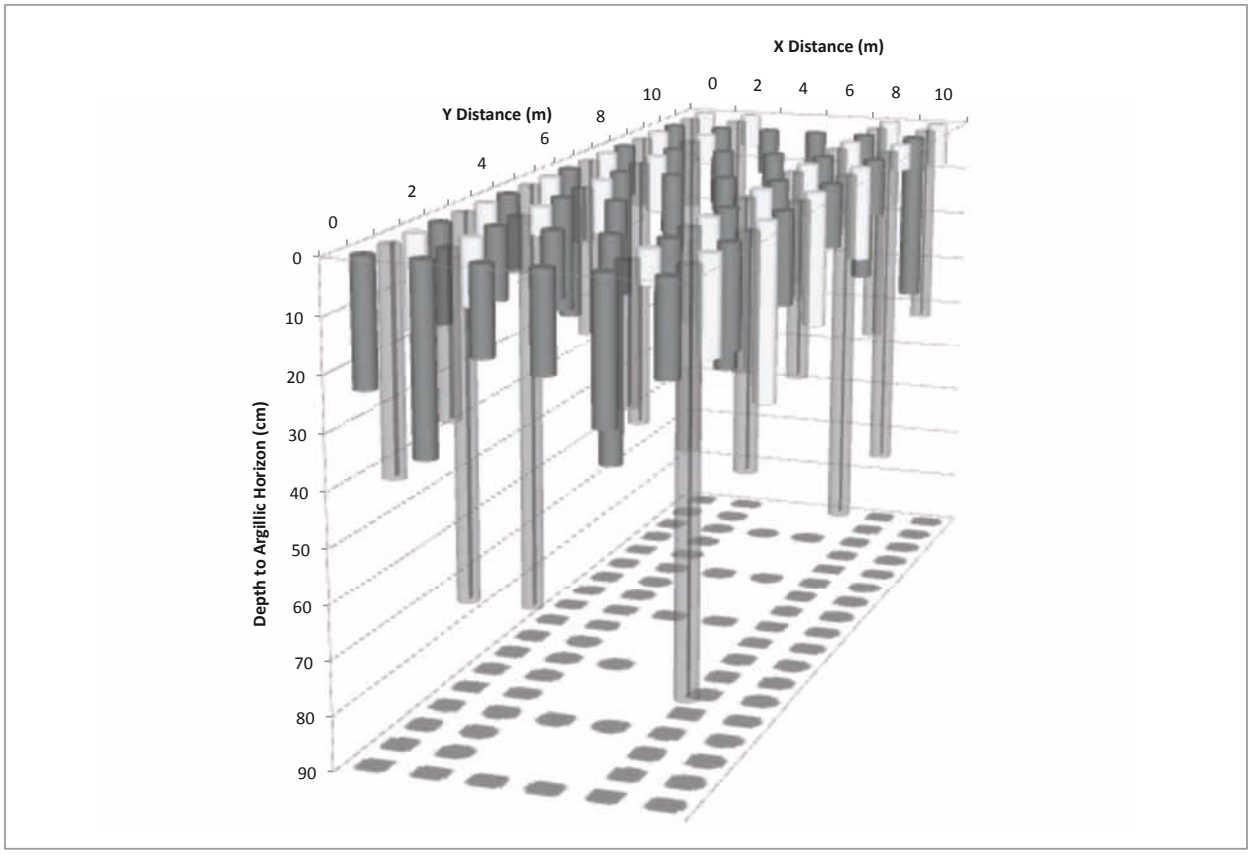

Figure 4.12: Tile Probe (transparent gray), Knocking Pole (dark gray) and Auger (white) Results for Plot 1.

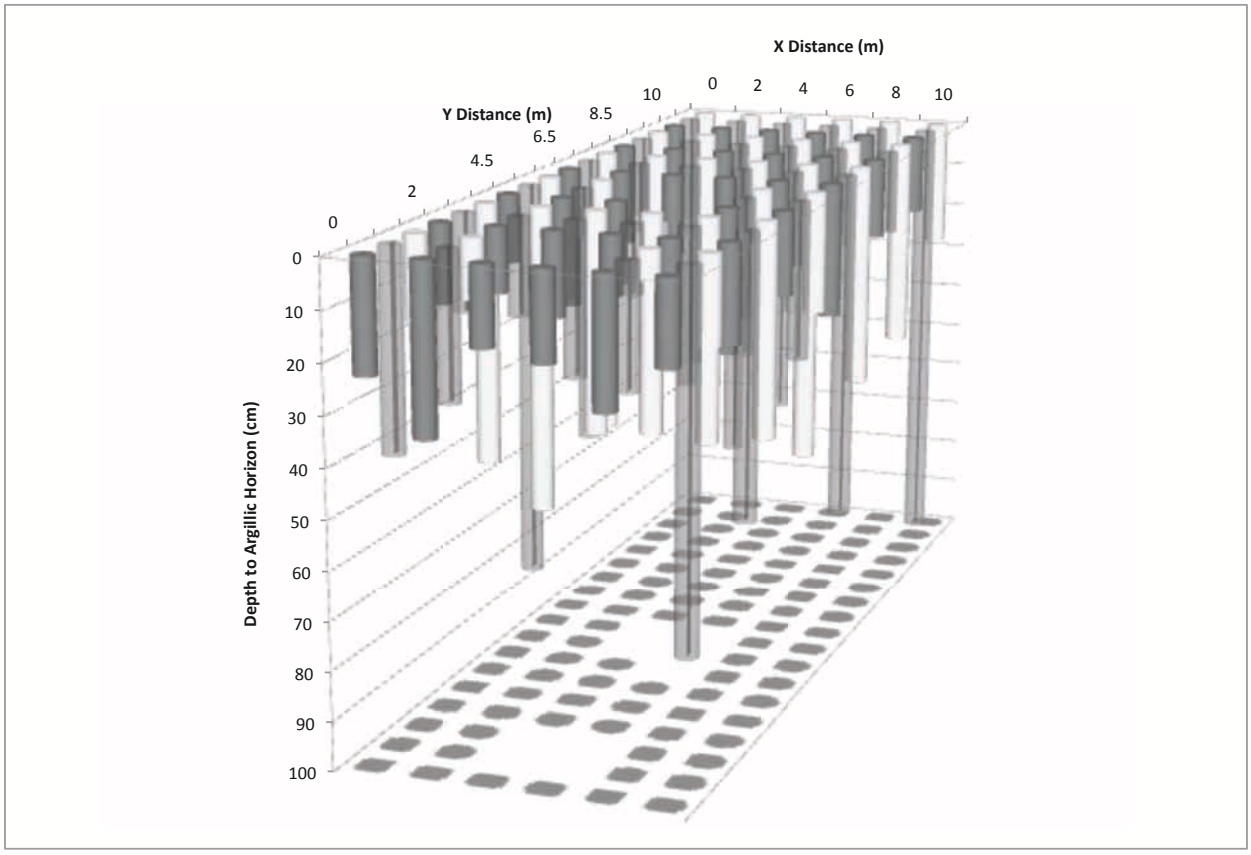

Figure 4.13: Tile Probe (transparent gray), Knocking Pole (dark gray) and Auger (white) Results for Plot 2.

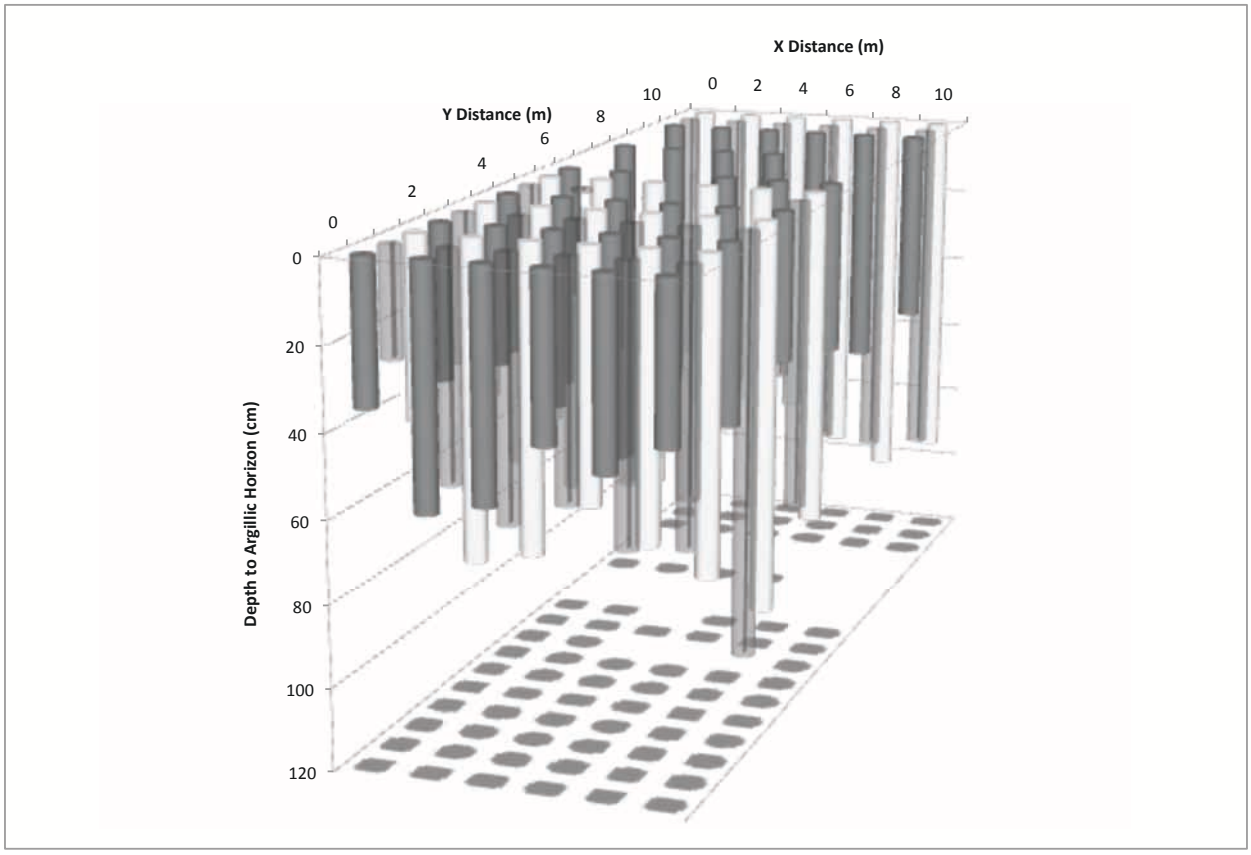

Figure 4.14: Tile Probe (transparent gray), Knocking Pole (dark gray) and Auger (white) Results for Plot 3.

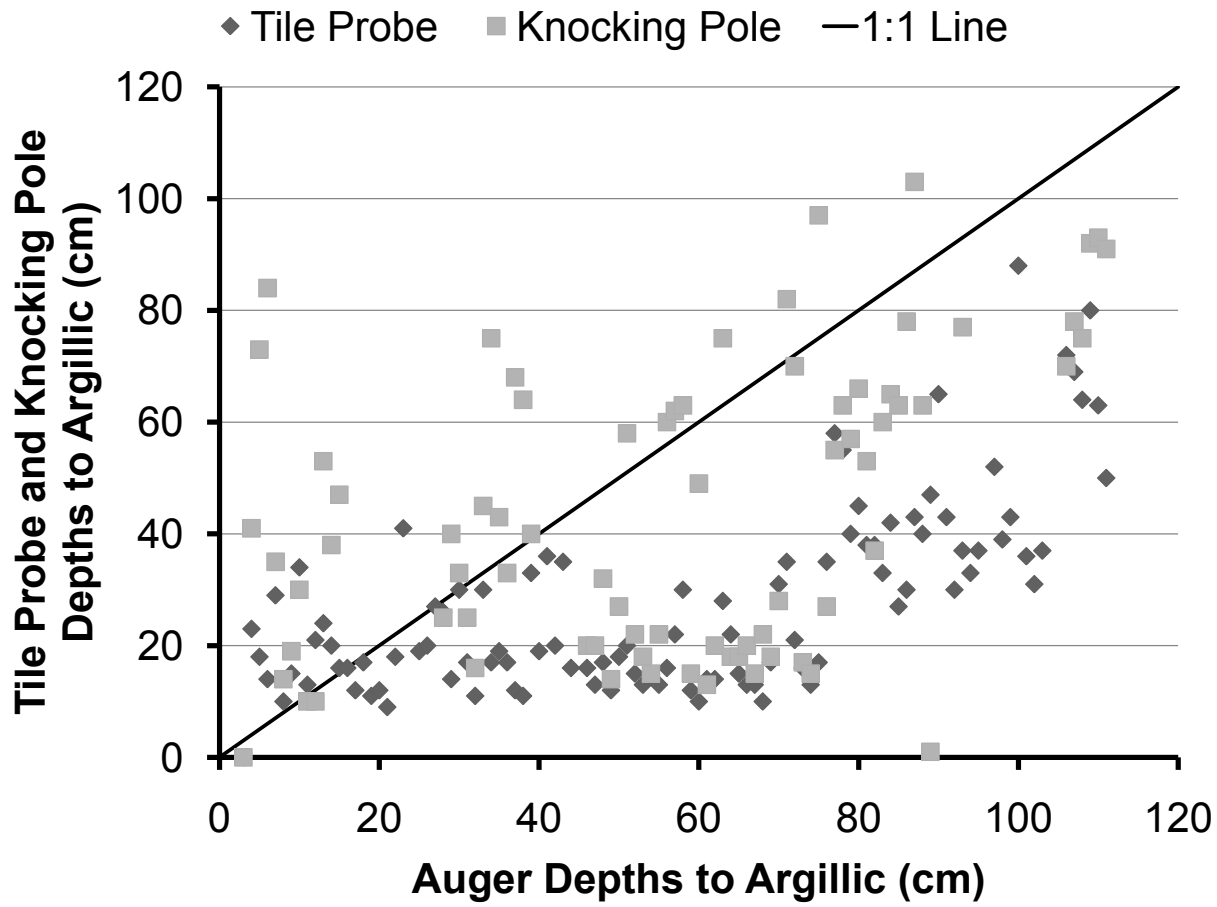

Figure 4.15: Tile probe, knocking pole and auger depth to argillic layer measurements, all plots.

4.4 Amoozemeter Results

Amoozemeter readings were taken in the trenches at all three plots in the argillic layer, at points where the GPR predicted potential anomalies and, when applicable, in visually apparent anomalies (Table 4.1, Figure 4.19). We then compared our in situ Ksat measurements for all plots with Ksat data from Greco 2004 to see if our Ksat results were comparable to the measurements he got in the soils of SRS (Table 4.2, Figure 4.20). Not all Ksat anoma-

lies found with the amoozemeters were visibly apparent soil anomalies (aka old tree root holes), but all Ksat anomalies were sited as potential anomalies in the GPR maps.

4.5 Soil Results

By looking at the depth to the argillic layer from the trench faces at Plot 2 and Plot 3, we were able to see that the depth to the argillic layer varied tremendously (Figure 4.21). Also from the trench faces at each of our plots, we were able to get an idea of what the average soil profile looked like for each plot and we were able to get bulk density measurements from the different horizons in each of the plots (Table 4.3).

The soil profiles for each of our three plots were: Plot 1: 0-6cm Ap, 6-40cm Bt1, 40+ cm Bt2 Plot 2: 0-11cm A, 11-25cm E1, 25-47cm E2, 47+ cm Bt Plot 3: 0-15cm Ap, 15-38cm E1, 38-70 E2, 70+ cm Bt

The profile at Plot 1 was different than the profiles at Plot 2 and Plot 3. At Plot 1, the argillic layer started very close to the surface and there were no E horizons. The Bt2 was looser and less firm than the Bt1 and there was presence of dropped out iron stone (Figure 4.22). In Plot 2, the A was very shallow and the E2 had some cementation (Figure 4.23). In Plot 3, the E1 was hard to dig through and firmly packed, but the E2 was very firmly packed and very hard to get through with the presence of cementation, iron stone and quartz (Figure 4.24).

The texture and % clay content were measured at three points in each plot. The % clay varied from as little as 20% to as much as 45-50%.

The various % clay contents and soil textures were as follows: Plot 1: 1. clay texture, 40% clay; 2. clay texture, 45-50% clay; 3. sandy-clay texture, 40% clay Plot 2: 1. sandy-clay-loam texture, 30% clay; 2. sandy-clay texture, 35-50% clay; 3. sandy-clay texture, 35-50% clay Plot 3: 1. sandy-loam texture, 25% clay, 2. sandy-clay-loam, 30% clay, 3. sandy-loam, 20% clay

For a look at soil texture and color samples taken in each plot, figures 4.16, 4.17, 4.18).

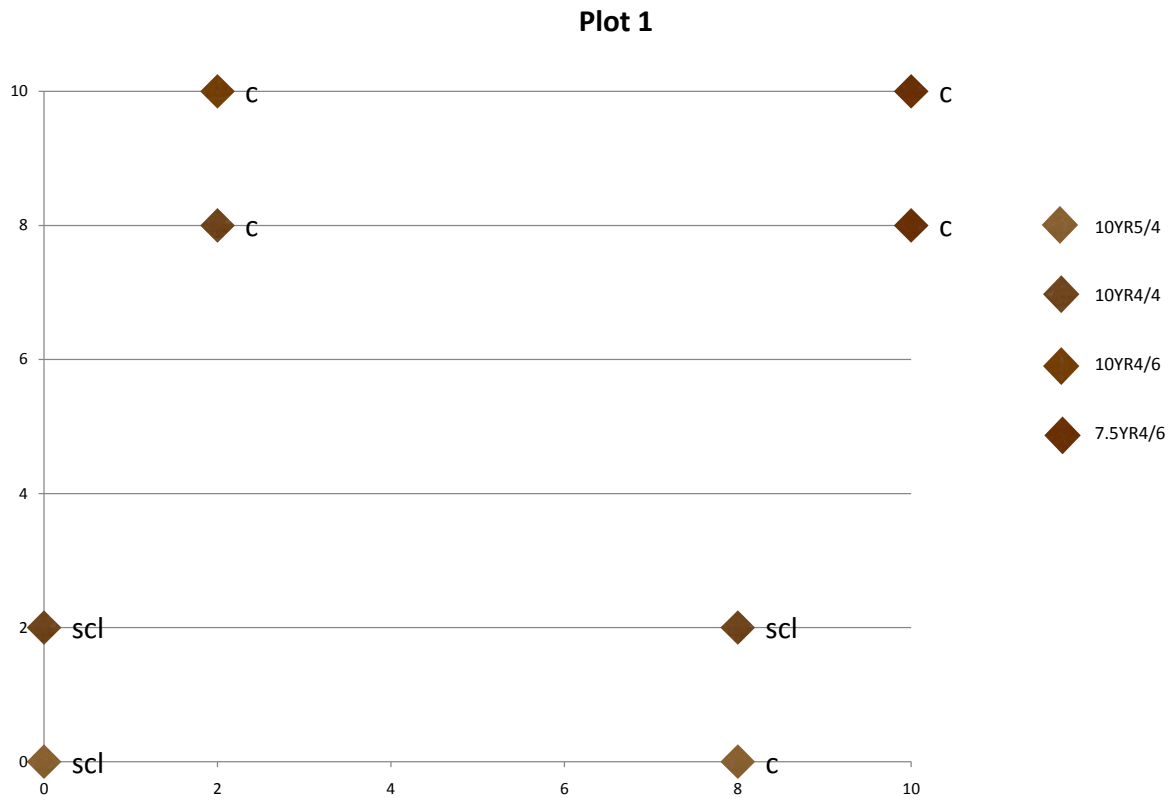

Figure 4.16: Soil texture and color samples taken at Plot 1. X and Y variables correspond with X and Y coordinates along the 10x10-m Plot.

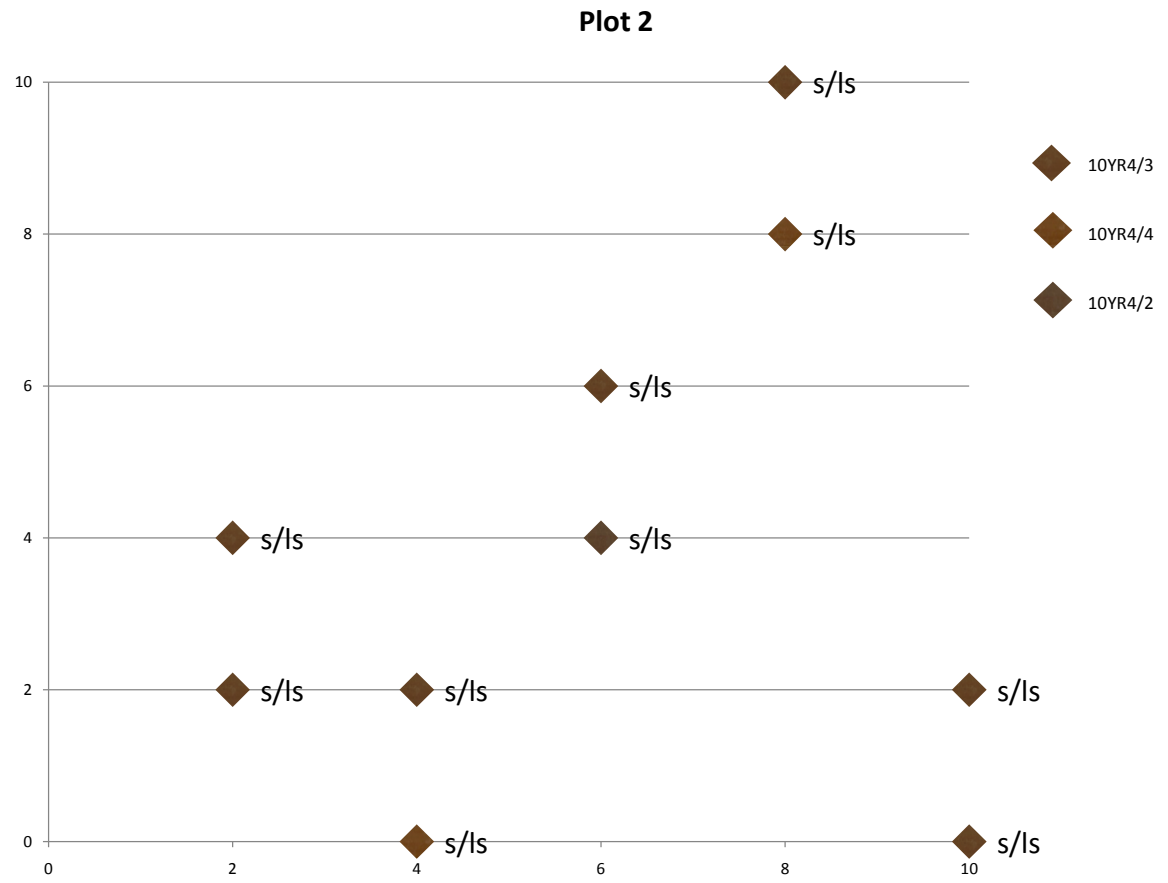

Figure 4.17: Soil texture and color samples taken at Plot 2. X and Y variables correspond with X and Y coordinates along the 10x10-m Plot.

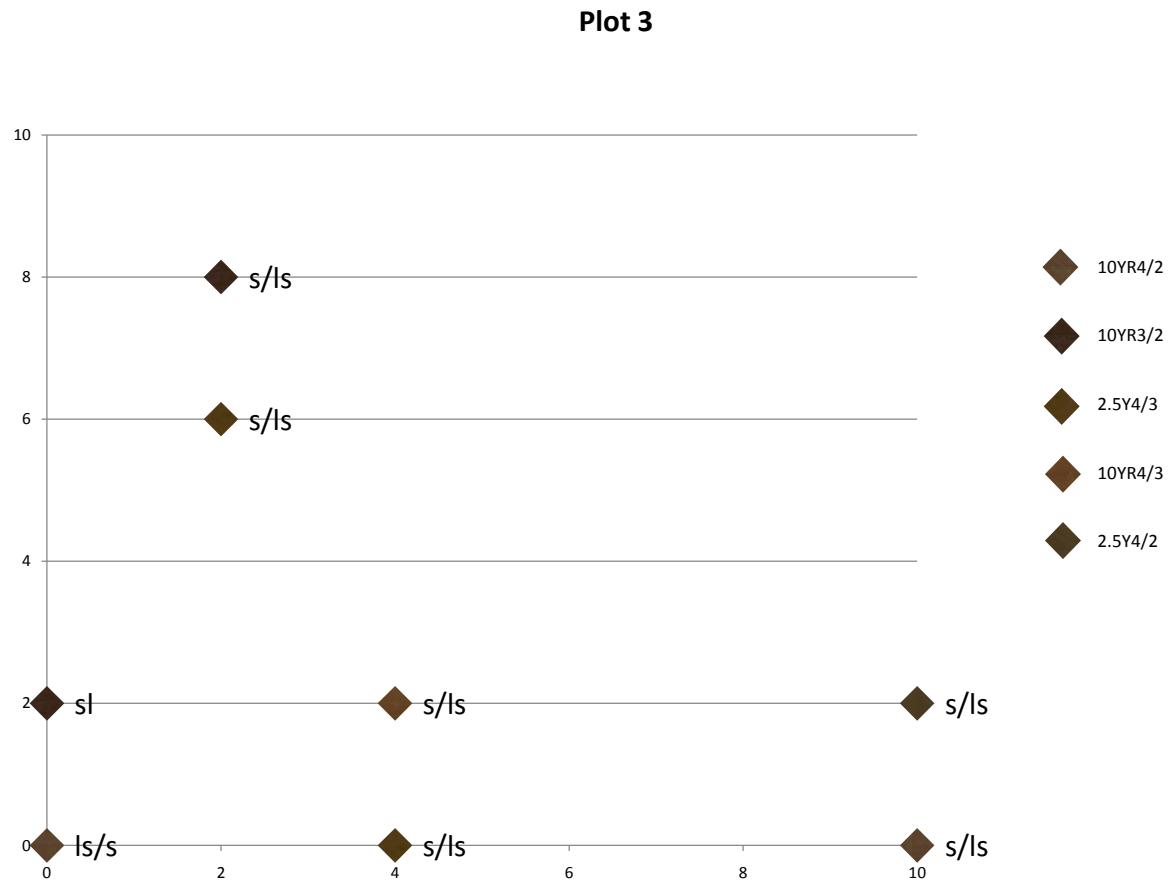

Figure 4.18: Soil texture and color samples taken at Plot 3. X and Y variables correspond with X and Y coordinates along the 10x10-m Plot.

Table 4.1: In situ Ksat measurements for all plots (in argillic layers in trench and soil matrix amoozemeter transects, at visually apparent anomalies (VAA) and at GPR predicted anomalies (GPR)).

Argillic Layers (neither GPR nor VAA).		Visually Apparent Anomalies.	
Location (Trench #, depth , x, y)	Ksat (cm/min)	Location (Trench #, depth, x, y)	Ksat (cm/min)
T1, .5m, 5.5, 5	0.015	T3, 1m, 5, 1.55	>6.0
T2, .5m, .5, 3.5	0.0059	T3, 1m, 5, 2.8	0.087
T2, .5m, .5, 9.2	0.0059	T3, 1m, 5, 3.8	0.022
T3, .5m, 5.5, 5.7	0.69	P3, .825m, .5, 7.5	>6.0
T3, .5m, 5.5, 8.5	1.6	P3, .73m, .5, 8	>6.0
3, 1m, 5.5, 1	0.017		
T3, 1m, 5.5, 6	0.015		
P1, .355m, 1.5, 1	>6.0		
P1, .355m, 1.5, 3	>6.0		
P2, .56m, 5.5, 4	>6.0		
P2, .59m, 5.5, 4.5	0.000078		
P3, .725m, .5, 7	0.0076		
P3, .76m, .5, 10	>6.0		
AVERAGE	2.03	AVERAGE	3.6
STDEV	2.8	STDEV	3.3
MEDIAN	0.015	MEDIAN	0.05
GEOMEAN	0.016	GEOMEAN	0.04
GPR Predicted Anomalies.			
Location (Trench #, depth, x, y)	Ksat (cm/min)	Location (Trench #, depth, x, y)	Ksat (cm/min)
T1, .5m, 5.5, 1.5	0.046	T3, .5m, 5.5, 3	0.69
T1, .8048m, 5.5, 3.1	0.016	T3, 1m, 5.5, 4	0.018
T1, .5m, 5.5, 3.5	0.029	T3, 1m, 5, 2	0.14
T1, .8048m, 5.5, 5.3	0.011	T3, 1m, 5, 3	0.092
T1, .8048m, 5.5, 6.5	0.0036	T3, 1m, 5, 4.3	0.0018
T1, .8048m, 5.5, 8.1	0.0094	P1, .37m, 1.5, 0	>6.0
T2, .5m, .5, 1	0.087	P1, .35m, 1.5, 1.5	0.000039
T2, .5m, .5, 8.5	0.0037	P2, .52m, 5.5, 3.5	>6.0
AVERAGE 0.082			
STDEV 2.03			
MEDIAN 0.018			
GEOMEAN 0.026			

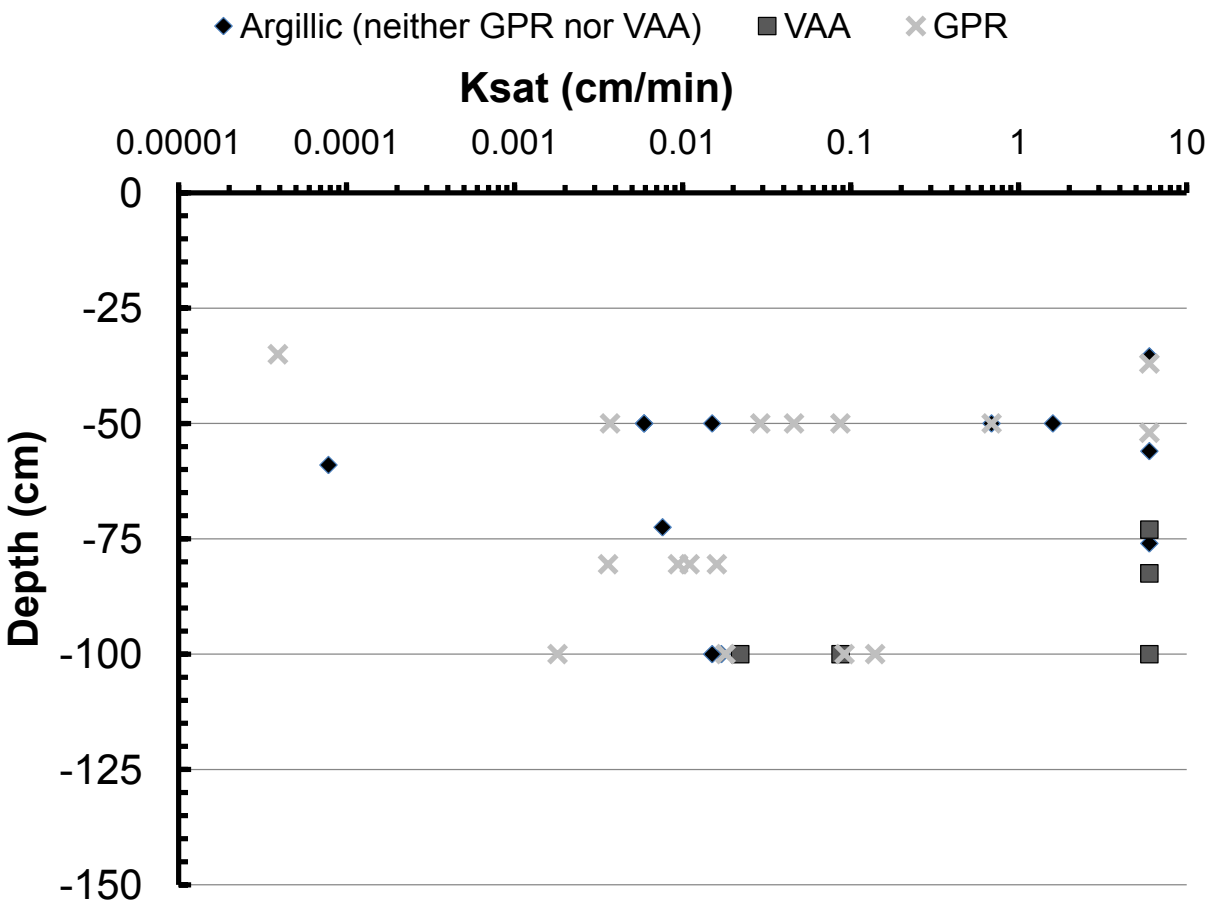

Figure 4.19: In situ Ksat measurements for all plots (in argillic layers in trench/soil matrix amoozemeter transects, at visually apparent anomalies (VAA) and at GPR predicted anomalies (GPR)) at various depths from the surface.

Table 4.2: In situ Ksat measurements for all plots (in argillic layers in trench/soil matrix amoozemeter transects and from Ksat data from Greco 2004, at visually apparent anomalies (VAA) and at GPR predicted anomalies (GPR)).

Argillic Layers (neither GPR nor VAA).		Visually Apparent Anomalies.	
Location (Trench #, depth , x, y)	Ksat (cm/min)	Location (Trench #, depth, x, y)	Ksat (cm/min)
T1, .5m, 5.5, 5	0.015	T3, 1m, 5, 1.55	>6.0
T2, .5m, .5, 3.5	0.0059	T3, 1m, 5, 2.8	0.088
T2, .5m, .5, 9.2	0.0059	T3, 1m, 5, 3.8	0.022
T3, .5m, 5.5, 5.7	0.69	P3, .825m, .5, 7.5	>6.0
T3, .5m, 5.5, 8.5	1.6	P3, .73m, .5, 8	>6.0
3, 1m, 5.5, 1	0.017		
T3, 1m, 5.5, 6	0.015		
P1, .355m, 1.5, 1	>6.0		
P1, .355m, 1.5, 3	>6.0		
P2, .56m, 5.5, 4	>6.0		
P2, .59m, 5.5, 4.5	0.000078		
P3, .725m, .5, 7	0.0076		
P3, .76m, .5, 10	>6.0		
Greco 2004, .8m	0.00072		
Greco 2004, .88m	0.00072		
Greco 2004, 1.4m	0.073		
Greco 2004, 1.05m	0.0011		
Greco 2004, 1.41m	0.0085		
Greco 2004, 1.12m	0.0041		
Greco 2004, 1m	0.00014		
Greco 2004, .88m	0.0033		
Greco 2004, 1.47m	<0.00014		
AVERAGE	1.2	AVERAGE	3.6
STDEV	2.3	STDEV	3.7
MEDIAN	0.008	MEDIAN	0.055
GEOMEAN	0.019	GEOMEAN	0.044
GPR Predicted Anomalies.			
Location (Trench #, depth , x, y)	Ksat (cm/min)	Location (Trench #, depth, x, y)	Ksat (cm/min)
T1, .5m, 5.5, 1.5	0.046	T3, .5m, 5.5, 3	0.69
T1, .8048m, 5.5, 3.1	0.016	T3, 1m, 5.5, 4	0.018
T1, .5m, 5.5, 3.5	0.029	T3, 1m, 5, 2	0.14
T1, .8048m, 5.5, 5.3	0.011	T3, 1m, 5, 3	0.092
T1, .8048m, 5.5, 6.5	0.0036	T3, 1m, 5, 4.3	0.0018
T1, .8048m, 5.5, 8.1	0.0094	P1, .37m, 1.5, 0	>6.0
T2, .5m, .5, 1	0.087	P1, .35m, 1.5, 1.5	0.000039
T2, .5m, .5, 8.5	0.0037	P2, .52m, 5.5, 3.5	>6.0
AVERAGE 0.082 STDEV 2.03 MEDIAN 0.017 GEOMEAN 0.015			

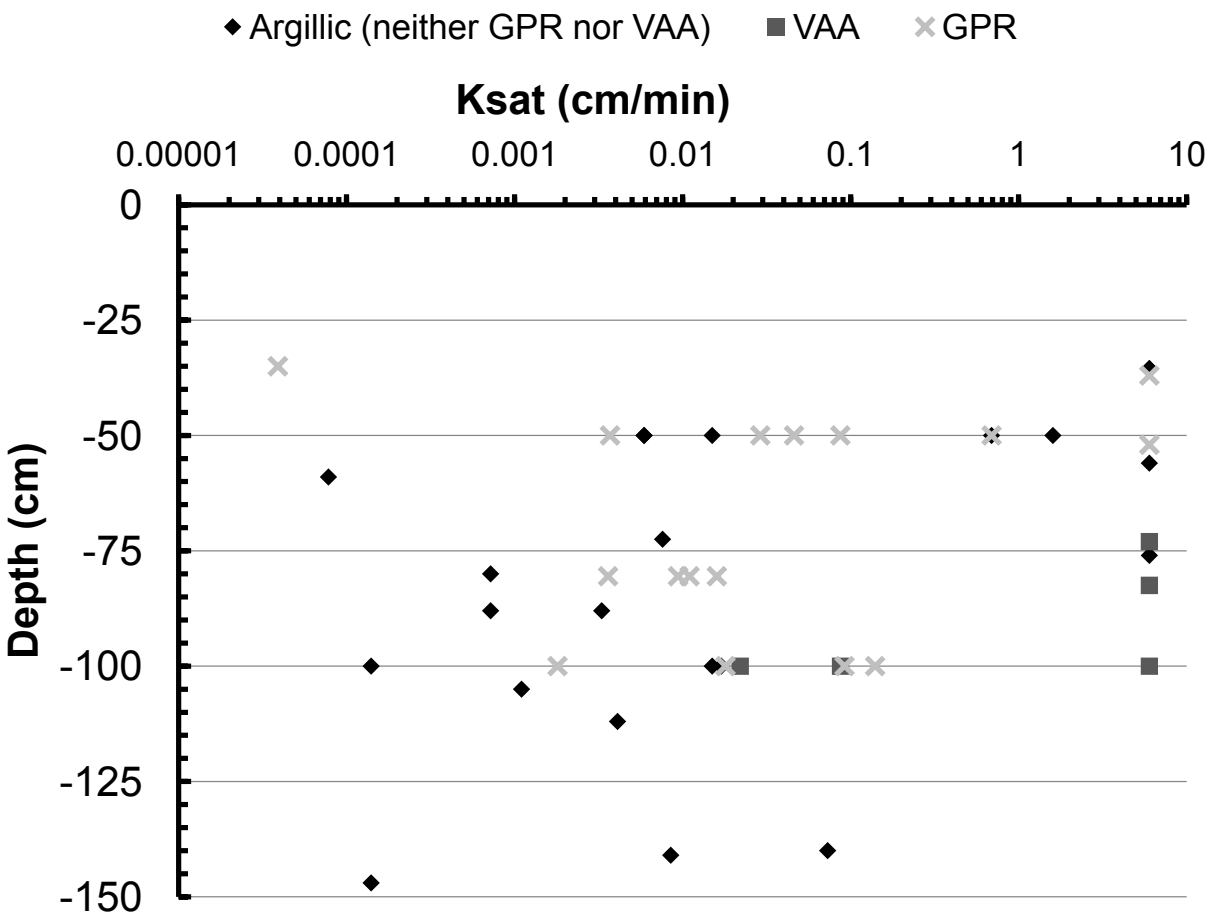

Figure 4.20: In situ Ksat measurements for all plots (in argillic layers in trench/soil matrix amoozemeter transects and from Ksat data from Greco 2004, at visually apparent anomalies (VAA) and at GPR predicted anomalies (GPR)) at various depths from the surface.

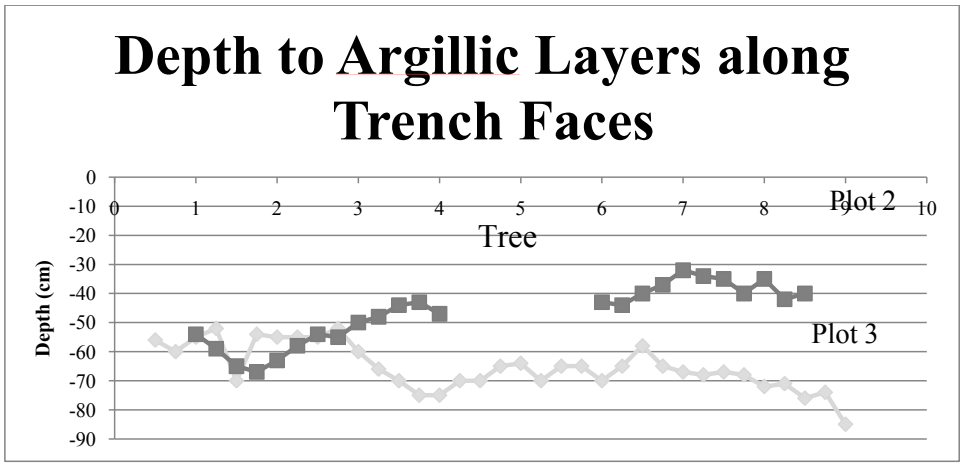

Figure 4.21: Depth to argillic layer along trench face at Plot 2 and Plot 3.

Table 4.3: Bulk density measurements of soil samples at all plots.

Soil Matrix Samples		Visually Apparent Anomalies	
Location (Plot #, X, Y, Soil Horizon)	Bulk Density (g/cm^3)	Location (Plot #)	Bulk Density (g/cm^3)
P1, 6, 2.45, E	1.71	P2	1.7154
P2, 0, 2.7, E1	1.43	P3	1.3668
P2, 0, 2.7, E2	1.77		
P2, 0, 3.4, E1	1.76		
P2, 1, 7.4, E1	1.73		
P3, 4.5, 2.2, E1	1.37		
P3, 4.5, 4.6, E1	1.75		
P3, 4.5, 4.6, E2	1.53		
P3, 5.5, 4.1, E	1.7		
MEDIAN	1.71		
AVERAGE	1.64		
STDEV	0.15		
P1, 6, 2.45, Bt1	1.58		
P1, 5, 4.17, Bt1	1.44		
P1, 5, 4.17, Bt2	1.63		
P1, 5, 7.2, Bt1	1.86		
P1, 5, 7.2, Bt2	1.53		
P2, 0, 3.4, Bt	1.69		
P2, 1, 7.4, Bt	1.69		
P3, 4.5, 2.2, Bt	1.63		
MEDIAN	1.63		
AVERAGE	1.63		
STDEV	0.12		

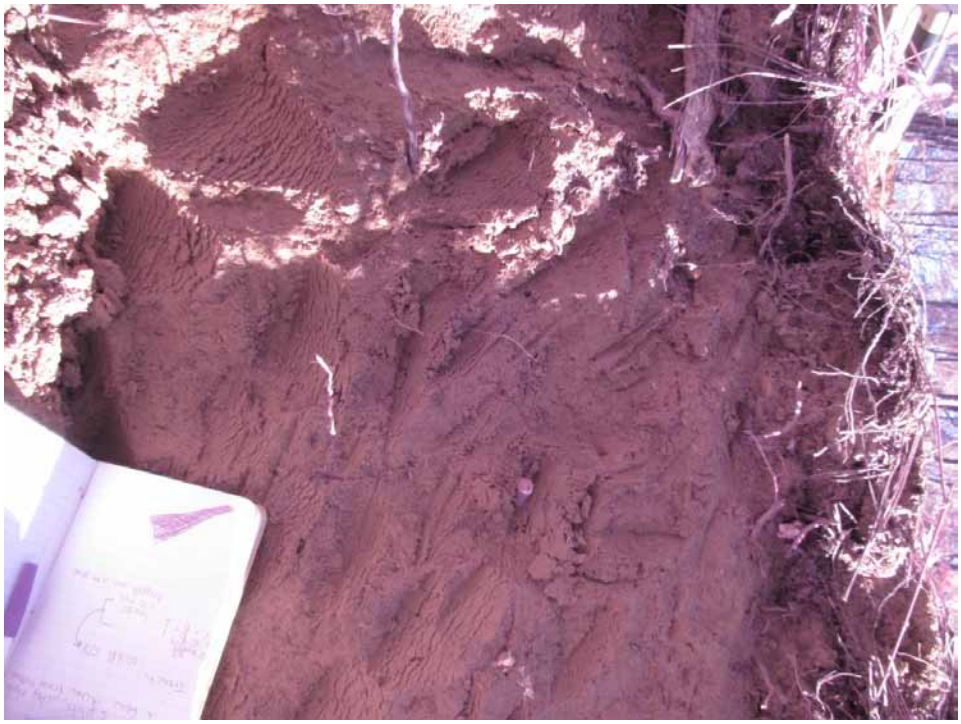

Figure 4.22: Soil profile at Plot 1.

Figure 4.23: Soil profile at Plot 2.

Figure 4.24: Soil profile at Plot 3.

4.6 Discussion

4.6.1 GPR

What the GPR showed us was the reflection changes from an interface with two contrasting dielectrics (Goodman 2011). The larger the dielectric changes, the stronger the reflection and the brighter the anomaly lenticular shapes on the GPR maps. The Z-values from the specific GPR slices used to make our GPR surface maps can be found at the back of our GPR report in Appendix B and there were large variations in Z-values, which would lead us

to infer that there were various types of interfaces (such as sand, clay, etc) reflecting back microwaves to the GPR unit from the ground in all of our plots. This could indicate that either there was less clay in the spots where the return was strongest (which were also spots that all of our Ksat anomalies corresponded with) or that there were at least more pores in those spots. The lack of clay could be created, for example, by old tree roots decaying and providing spaces for upper horizons to fill into previously clay horizons. However, since we found, more often than not, soils with high Ksats that looked comparable to clays with low Ksats, it might be possible that the clay areas with higher Ksats are more porous than the clays with low Ksats and this higher porosity could be created by a number of things, such as animal turbation, heterogeneity from vegetation or other biota, soil chemistry or previous management practices. Higher contrast between the dielectrics in our soils could also indicate that there was greater porosity in the brighter anomaly lenticular shapes as more porous materials can also have more void spaces (Goodman 2011). The equation used to determine the reflection for microwaves from Z-values is (Goodman et al. 2011):

$$R = \frac{Z_2 \; cos \; \Theta_1 - Z_1 \; cos \; \Theta_2}{Z_2 \; cos \; \Theta_1 + Z_1 \; cos \; \Theta_2} \tag{4.1}$$

The GPR maps proved somewhat effective for predicting anomalies in the soil. Though they provided us with many false positives (aka, predicted soil anomalies in spots where we could not visually verify them and/or there were no unusually high Ksats), there was not a single visually apparent soil anomaly found upon excavation that did not also show up on the GPR maps (Figure 4.25) and all ground surface anomalies (such as tree stumps or live trees) at each of the three plots also showed up on the GPR maps (figures 4.26, 4.27, 4.28).

The heterogeneity of the soil profiles at SRS might be the cause of some of the false positives found in the GPR maps. Since GPR detects dielectric differences between vestigial taproots and sandy soils better than dielectric differences between vestigial taproots and clay soils (Butnor et al. 2001), perhaps the large variability in depth from the surface to the argillic layer at the research plots (Figure 4.21) caused more GPR reflections, refractions and/or attenuations then there would have been in a more homogeneously sandy top soil.

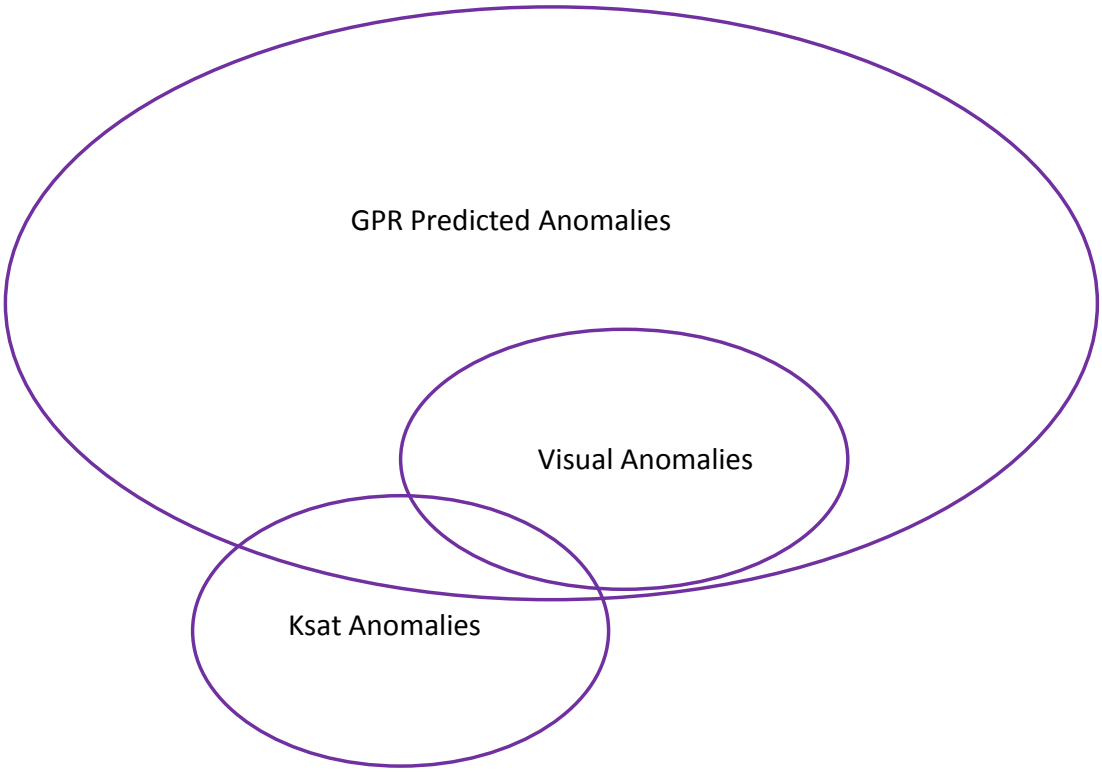

Figure 4.25: Venn diagram describing the relationships between Ksat anomalies, visually apparent anomalies and predicted anomalies on the GPR maps.

We only took one GPR reading at each of the plots with a 500 MHz antenna and all of the plots were scanned on the same day under the same soil moisture conditions. It might have been interesting to take GPR readings at each of the plots multiple times under different soil moisture conditions and with different antennae and then compare the different reflection maps.

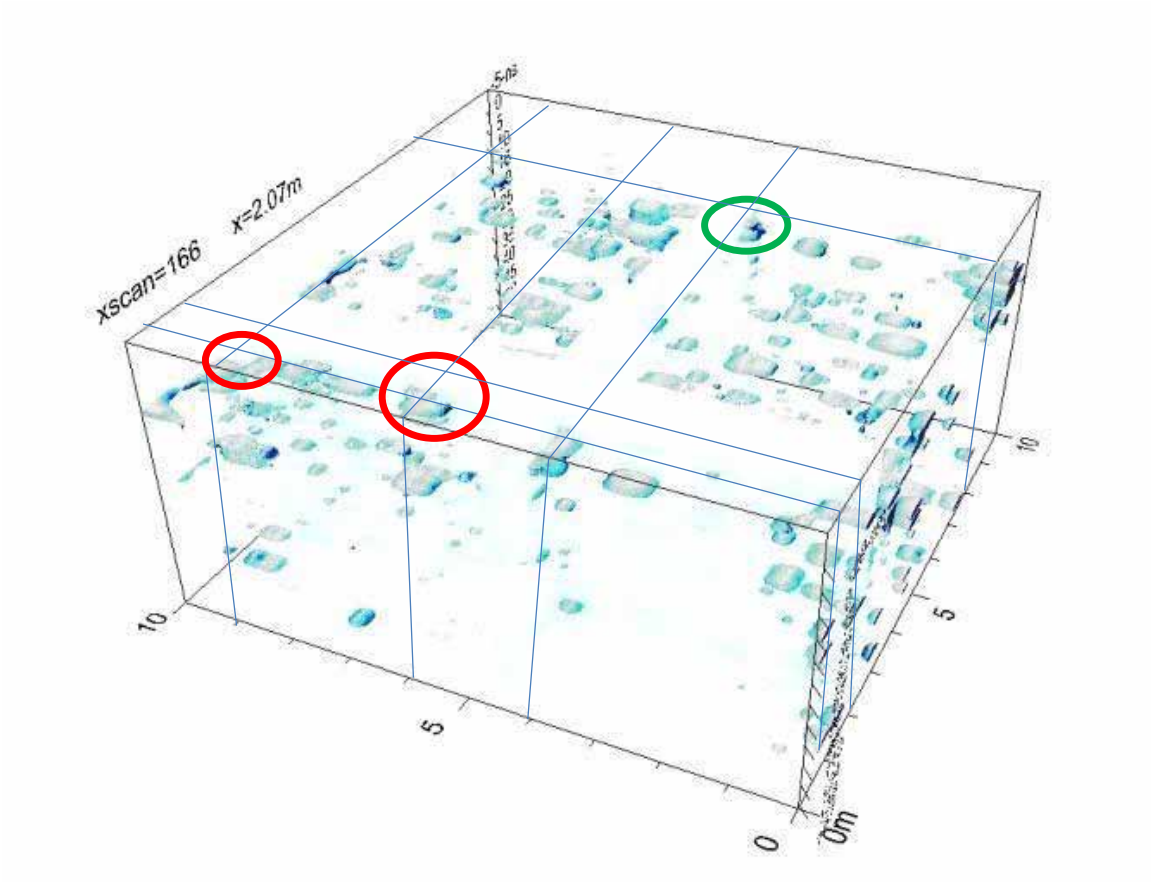

Figure 4.26: Map of all surface anomalies (stumps in red and trees in green) on Plot 1 overlain on GPR map of the same plot.

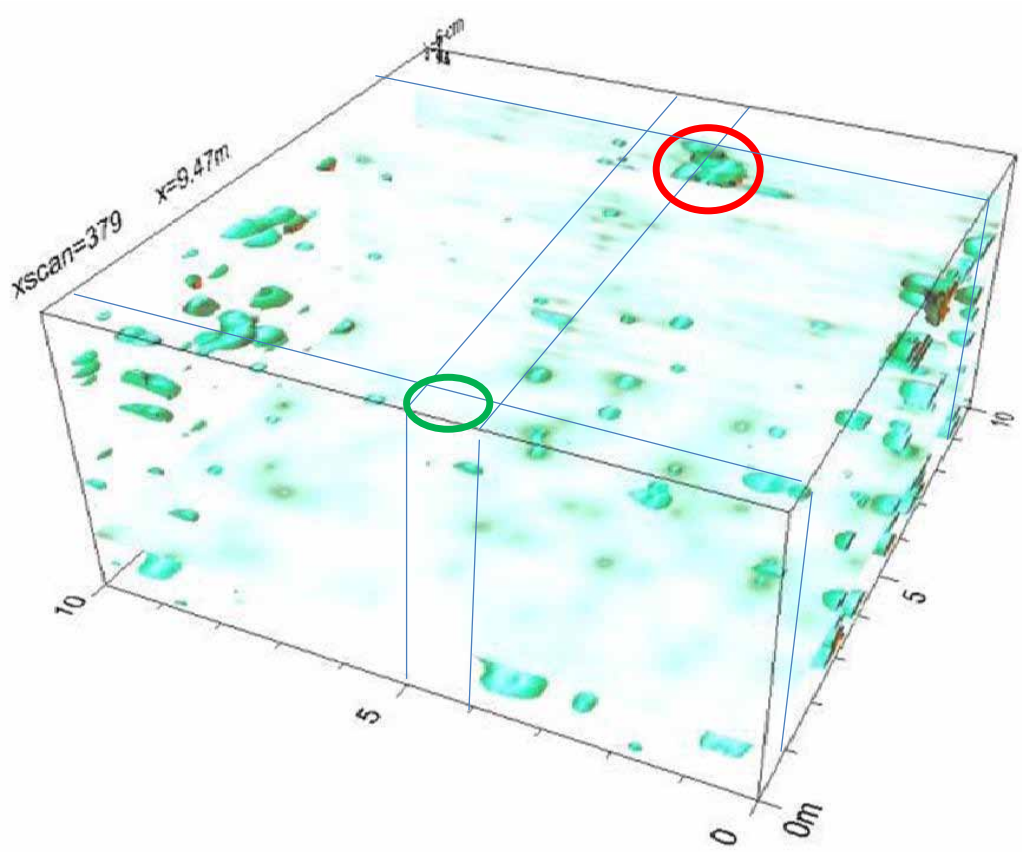

Figure 4.27: Map of all surface anomalies (stumps in red and trees in green) on Plot 2 overlain on GPR map of the same plot. Notice that the green circle is located at a gap in the GPR map where we had to stop and start the GPR unit to get around the large tree, so it shows up as a gap on the map instead of a lenticular-shaped anomaly.

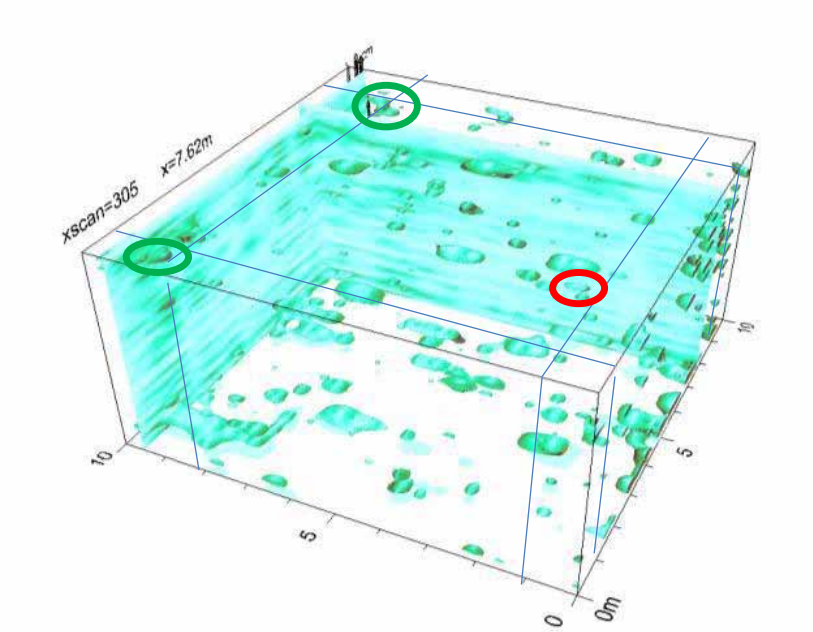

Figure 4.28: Map of all surface anomalies (stumps in red and trees in green) on Plot 3 overlain on GPR map of the same plot.

4.6.2 Methylene Blue Dye

Neither the test spots outside the plots nor the methylene blue squares within the 1x10-m strips in the plots showed traces of methylene blue dye once we dug below the surface. While methylene blue dye has been used successfully as a ground water tracer by other researchers, there were several factors in our experiment that could explain our lack of methylene blue results.

Price et al. 2010 stated that soils underlying forest trees should have, among other things, low bulk densities. The typical bulk densities of the SRS soils were high. Perhaps the management of our research plots as pine tree stands caused too much soil compaction and warranted them atypical forest soils. Perhaps high soil compaction could be the cause of our lack of methylene blue dye infiltration. Or perhaps it is not fair to compare the soil bulk densities from SRS to the bulk densities from Price et al. 2010's research in the southern Blue Ridge Mountains of North Carolina.

Alaoui et al. 2011 found success in their ground water tracer research using Brilliant Blue (BB) dye. BB does not strongly absorb to negatively charged soil matrixes, but even it is prone to adsorption in clay soils. The biggest difference, perhaps, between Alaoui et al.'s successful use of ground water tracers and this research's unsuccessful results would probably be the amount of dye used and the form of application. Alaoui et al. 2011 sprayed 100 L of BB dye on $1m^2$-plots at a constant intensity of 36 mm h^{-1} whereas we sprayed a 1x1.5-m square in the 1x10-m strips at each plot with 2 L of methylene blue dye at whatever low intensity a hand-pumped back-pack sprayer is capable of producing.

4.6.3 Tile Probe, Knocking Pole and Auger

The descriptive statistics we found from our tile probe, knocking pole and auger data lead us to reject the null hypotheses that the mean of each method was equal to the mean of the auger results (aka, true depth to the clay layer).

For Plot 1, we see that $\mu_1(19.31) \neq \mu_o(13.21)$ and that $\mu_2(40.04) \neq \mu_o(13.21)$.

For Plot 2, we see that $\mu_1(18.49) \neq \mu_o(47.21)$ and that $\mu_2(34.17) \neq \mu_o(47.21)$.

For Plot 3, we see that $\mu_1(46.67) \neq \mu_o(74.40)$ and that $\mu_2(65.10) \neq \mu_o(74.40)$.

For all plots combined, we see that $\mu_1(27.80) \neq \mu_o(45.00)$ and that $\mu_2(44.71) \neq \mu_o(45.00)$.

Running a regression analysis comparing tile probe measurements to auger measurements and knocking pole measurements to auger measurements for each plot individually and then for all plots combined, we found that neither the tile probe nor the knocking pole were

appropriate methods for predicting accurate depths to the clay layer at the soils in SRS (see appendix E).

For the tile probe to auger measurements for Plot 1, we got a R^2=0.5% and a P=0.741, telling us that the tile probe was not an appropriate method for indicating true depth to the clay layer. For Plot 2, we got a R^2=0.7% and a P=0.694. For Plot 3, we got a R^2=38.0% and a P=0.001. While this was better than the other R^2 values for tile probe measurements at plots 1 and 2, it was still small enough for us to determine that it was still not an appropriate method for determining accurate depth to clay at Plot 3. For all plots combined together, we got a R^2=45.6% and a P<0.001. Once again, while this R^2 was higher than the others we calculated for the tile probe method at each plot individually, it was still not high enough for us to accept that the tile probe was an accurate method for determining depth to clay at the soils in SRS.

For the knocking pole to auger measurements for Plot 1, we got a R^2=0.6% and a P=0.712, telling us that the knocking pole was not an appropriate method for indicating true depth to the clay layer. For Plot 2, we came to the same conclusions with a R^2=0.2% and a P=0.836. For Plot 3, we got a R^2=67.3% and a P<0.001, so we concluded that the knocking pole could be an adequate method for predicting depth to clay at this particular plot. For all plots combined together, we got a R^2=20.9% and a P<0.001. This R^2 was not high enough for us to accept that the knocking pole was an adequate method for predicting depth to clay at the soils in SRS.

Soil penetration resistance varies with soil water content, bulk density, texture and organic matter (Busscher et al. 1997). Various equations can be used to help correct soil penetration resistance measurements for water contents, however multiple-equation corrections cannot guarantee that corrections being made to measurements are real and that they are not results from the correction differences (Busscher et al. 1997).

We tried to take all tile probe and knocking pole measurements in dry conditions to help control for soil water content (as well as to reduce any safety hazards that could be brought

upon by standing in the woods with a large metal rod during a thunder storm or by using a heavy and slippery slide hammer), however it was not always possible to avoid the rain during the summer field season in South Carolina and varying levels of humidity could have impacted soil water content as well. No equations were implemented to try to correct for varying soil water contents as it seemed that soil texture was the most obvious cause of our inability to get accurate argillic depth readings with the tile probe and knocking pole and delving further into the various equations and models concerning soil water content and soil penetration resistance was beyond the scope of this project.

Meyer et al. 2007 had success with estimating soil depths using the tile probe, but their mineral soil depths were measured on top of Cr and R horizons. The tile probe was certainly not capable of penetrating through Cr or R horizons, but it seemed to not have too much trouble penetrating through the Bt horizons at SRS. The soils that Meyer et al. 2007 dealt with had very low clay content (<5%) and low water-holding capacity, which also could have made penetration easier. More interestingly than that, perhaps, was that the most difficulty we had with the tile probe was getting it to penetrate through the E1 and E2 horizons at Plot 2. Something about the texture of the sand made the soil very resistant to tile probe penetration and we ended up with very shallow tile probe predicted depths for what turned out to be 47+cm depths to the Bt.

The knocking pole was used to try and estimate accurate depth to the argillic layer after we realized that the tile probe was not giving us accurate readings. While the knocking pole was able to penetrate through the E1 and E2 horizons of Plot 2 more successfully than the tile probe, it slammed right through the Bt horizons at our plots and was not able to provide accurate depth to argillic layer readings either.

4.6.4 Amoozemeter

Amoozemeter readings were taken in the trenches at all three plots in the argillic layer, at points where the GPR predicted potential anomalies and, when applicable, in visually

apparent anomalies (Table 4.1). Not all Ksat anomalies found with the amoozemeters were visibly apparent soil anomalies (aka old tree root holes), but all Ksat anomalies were sited as potential anomalies in the GPR maps.

4.6.5 Multi-spectral Camera

Though previous research has shown that near-infrared multi-spectral capabilities were adequate enough to reflect back soil moisture (Lobell & Asner 2002), we were not able to capture pictures of ground water pathways after the use of amoozemeters. We attempted to capture soil moisture in this way when we came across Ksat anomalies that were not visibly apparent soil anomalies, but the multi-spectral cameras could not capture it. This could have been due to the fast draining nature of the soils where we found Ksat anomalies, the extremely high heat at SRS during the summer time, the direct sunlight on many of these plots that could impede the ability of the multi-spectral camera to take adequate pictures or it could have just been an overstretching of the ability of the tool. Lobell & Asner 2002 also captured their soil moisture contents in a lab setting with more controlled light exposure than was capable in the field. Moisture on vegetation surfaces did show up in our multi-spectral camera pictures, however, and a camera with larger infra-red capabilities could potentially be able to capture more soil moisture in the field.

4.6.6 Soil

The transition from the Piedmont geographic region to the Coastal Plain region happens around the area of SRS (Figure 2.1), resulting in the presence of a blend of soil characteristics typical in both the Piedmont and the Coastal Plain. The soils of the Coastal Plain are usually thicker than Piedmont soils (2-8 m and <1 m, respectively) and have higher sand content and infiltration rates than the Piedmont soils (Markewich et al. 1990) (Figure 2.2)

Bulk density measurements were taken at anomalies found in the trenches at all plots and in the different soil horizons found in the trenches in all three plots (Table 4.3). The

bulk densities taken at the anomalies and within the different soil horizons were all relatively high (1.36-1.85) and would infer that root growth was inhibited in the soils found: 1. at the anomaly in Plot 2, 2. in Plot 1 at the E in the first group of samples and the Bt1 from the third group of samples, 3. in Plot 2 at the E2 in the first group of samples and the E1 in both the second group of samples and the third group of samples, and 4. in Plot 3 in the E1 in the second group of samples.

The range in bulk densities here are comparable to the range of bulk densities Whipkey 1965 found in their research in Ohio for the soil textural classes of sandy loam ($\approx$ 1.33 and 1.41), loam ($\approx$ 1.78) and clay loam ($\approx$ 1.80). The anomaly bulk densities in our research were not significantly different from our bulk density measurements in non-anomaly soils in all three plots, however, there were only two anomaly bulk densities and running statistics with a $n = 2$ was not appropriate. The anomaly bulk densities had a mean of 1.541 with a standard deviation of 0.247 while the non-anomaly bulk densities at Plot 1 had a mean of 1.62339 with a standard deviation of 0.1455, Plot 2 had a mean of 1.6779 with a standard deviation of 0.1262 and Plot 3 had a mean of 1.5947 with a standard deviation of 0.1506 (see appendix E).

Chapter 5

Conclusion

For our primary research question, we accepted the hypothesis that any or all found hydraulic conductivity anomalies corresponded with visible anomalies in the soil, such as old pine tree root holes. Overall, we found quite a lot of Ksat anomalies in the soils at SRS that would explain the increase in the amount of infiltration occurring and the lack of predicted lateral flow. Whenever we did find visible soil anomalies (aka old root holes), they did present Ksat anomalies, however, there is much more going on in these soils to cause the abundance of Ksat anomalies than what is visible to the naked eye. Further research into the cause of these Ksat anomalies in non-visible anomaly soils is recommended.

For our secondary research questions, we accepted the hypotheses that: 1. the GPR was useful for accurately pinpointing visible and hydraulic conductivity anomalies in the soil matrix and 2. we located hydraulic conductivity anomalies in the argillic layer. We believe that the GPR can be a useful tool in helping predict the heterogeneity of a soil, which in turn has implications for the presence of Ksat anomalies, and we were certainly able to locate hydraulic conductivity anomalies in the argillic layer with the use of amoozemeters.

We rejected the hypotheses that: 1. the methylene blue dye helped show water movement through the soils at SRS, 2. the tile probe and/or knocking pole were helpful for determining accurate depths to the argillic layer from the surface and 3. the multi-spectral camera accurately took pictures of soil wetness in the field in the soils of SRS. Methylene blue dye, a commonly used tool in soils and hydrology research, did not prove useful in these particular soils in the quantities we used. The tile probe and the knocking pole, while also commonly used in soils and hydrology research, were not adequate tools for predicting the depth to

the argillic layers in the soils at SRS. The use of an auger for determining argillic depths is more accurate for measuring depths in these soils, however any future research planning to implement this method must acknowledge the impact of large augering holes in the soil on infiltration trends and should plan accordingly. The multi-spectral camera did not prove useful to our research.

5.1 Recommendations for Further Research

This thesis was the 1st of a 3-part research project. As year zero of the project, we looked at in-situ hydraulic conductivities and the correlation of any anomalies in these conductivities with anomalies in the soils of SRS, specifically the argillic layer, prior to the installation of a biofuel production site of pine trees. Future research will look at how in-situ hydraulic conductivities are affected once the biofuel production site of pine trees has been installed and then there will be further follow-up research to see how in-situ hydraulic conductivities are affected after the trees have been harvested.

Since the presence of visibly apparent anomalies did not always coincide with the many hydraulic conductivity anomalies we found out in the field, a more in-depth look at the microbiology, chemistry and geologic history of the soils at these sites in SRS may prove interesting and useful.

We accepted the usefulness of GPR in our research and future research may find further help from the GPR by taking multiple readings with various antennaes and under varying soil wetness conditions.

Our research had no success in tracing ground water pathways in the soils at SRS with methylene blue dye, but an increase in the amount of dye used may prove useful for this task. Methylene blue dye could also be experimented with further to see if one could trace ground water flow with it by first avoiding the problem of the dye getting caught up in the surface organic matter. One could potentially experiment with this by digging a hole in the

ground, putting some methylene blue dye powder in the hole, re-covering the hole and, after enough rain has occurred, excavating the area to see if the dye traced ground water flow.

Further research into the use of tile probes and knocking poles in SRS soils for accurate depth to argillic layers could be carried out by varying the season in which the measurements are taken. Since soil moisture impacts soil resistivity, it might be possible to get more accurate depth readings by carrying out the measurements in the summer when the soil is more dry.

The multi-spectral camera might also prove more useful in future research if one can determine a way to better control light exposure. While our research did not have particular success with this piece of equipment, we believe it is a worthwhile tool to have around and could prove very useful under different conditions than our research presented.

Bibliography

Alaoui, A., U. Caduff, H. H. Gerke and R. Weingartner. 2011. Preferential flow effects on infiltration and runoff in grassland and forest soils. Vadose Zone Journal. 10:367-377.

Aleixos, N., J. Blasco, F. Navarrón and E. Moltó. 2002. Multispectral inspection of citrus in real-time using machine vision and digital signal processors. Computers and Electronics in Agriculture. 33(2):121-137.

Amoozegar, A. 1989. A compact constant-head permeameter for measuring saturated hydraulic conductivity of the vadose zone. Soil Science Society of America Journal. 53(5):1356-1361.

Anderson, M. G. and T. P. Burt. 1978. Role of topography in controlling throughflow generation. Earth Surface Processes. 3:331-344.

Arya, L. M. and J. F. Paris. 1981. A physicoempirical model to predict the soil moisture characteristic from particle-size distribution and bulk density data. Soil Science Society of America Journal. 45:1023-1030.

Beven, K. 1977. Hillslope hydrographs by the finite element method. Earth Surface Processes. 2:13-28.

Beven, K. and P. Germann. 1982. Macropores and water flow in soils. Water Resources Research. 18(5):1311-1325.

Bouma, J., A. Jongerius, O. Boersma, A. Jager and D. Schoonderbeek. 1977. The function of different types of macropores during saturated flow through four swelling soil horizons. Soil Science Society of America Journal. 41:945-950.

Busscher, W. J., P. J. Bauer, C. R. Camp and R. E. Sojka. 1997. Correction of cone index for soil water content differences in a coastal plain soil. Soil and Tillage Research. 43(3-4):205-217.

Butnor, J. R., J. A. Doolittle, L. Kress, S. Cohen and K. H. Johnsen. 2001. Use of ground-penetrating radar to study tree roots in the southeastern United States. Tree Physiology. 21(10).

Conyers, L. B. and C. M. Cameron. 1998. Ground-penetrating radar techniques and three-dimensional computer mapping in the American southwest. Journal of Field Archaeology. 25(14):417-430.

Davis, S. N., G. M. Thompson, H. W. Bentley and G. Stiles. 2006. Ground-water tracers - a short review. Ground Water. 18(1):14-23.

Fetter, C. W. 2001. Applied Hydrogeology. Prentice Hall.

Freeze, R. A. 1972a. Role of subsurface flow in generating surface runoff, 1, base flow contributions to channel flow. Water Resources Research. 8(3):609-623.

Freeze, R. A. 1972b. Role of subsurface flow in generating surface runoff, 2, upstream source areas. Water Resources Research. 8(5):1272-1283.

Goodman, D. (personal communication, July 7, 2011).

Goodman, D., P. Salvatore, A. Novo and G. Morelli. 2011. GPR Imaging in Archaeology. Submitted for publication.

Greco, J. 2004. Controls and occurrence of interflow over a restrictive argillic horizon in a low gradient hillslope. Masters Thesis. University of Georgia, Athens, Georgia, United States of America.

Gupte, S. M., D. E. Radcliffe, D. H. Franklin and L. T. West. 1996. Anion transport in a piedmont ultisol: II. Local-scale parameters. Soil Science Society of America Journal. 60:762-770.

Hinkler, J., J. B. Ørbæk and B. U. Hansen. 2003. Detection of spatial, temporal, and spectral surface changes in the Ny-Ålesund area 79°N, Svalbard, using a low cost multispectral camera in combination with spectroradiometer measurements. Physics and Chemistry of the Earth, Parts A/B/C. 28(28-32):1229-1239.

Jackson, C. R. 1992. Characterization of subsurface flow in shallow-soiled hillslopes. Doctoral Thesis. University of Washington, Seattle, Washington, United States of America.

Lobell, D. B. and G. P. Asner. 2002. Moisture effects on soil reflectance. Soil Science Society of America Journal. 66:722-727.

Lookingbill, T. and D. Urban. 2004. An empirical approach towards improved spatial estimates of soil moisture for vegetation analysis. Landscape Ecology. 19:417-433.

Luxmoore, R. J. 1981. Micro-, meso-, and macroporosity of soil. Soil Science Society of America Journal. 45:671.

Markewich, H. W., M. J. Pavich and G. R. Buell. 1990. Contrasting soils and landscapes of the Piedmont and Coastal Plain, eastern United States. Geomorphology. 3(3-4):417-447.

McCarthy, J. F. and J. M. Zachara. 1989. Subsurface transport of contaminants. Environmental Science and Technology. 23(5):496-502.

McDowell-Boyer, L. M., J. R. Hunt and N. Sitar. 1986. Particle transport through porous media. Water Resources Research. 22(13): 1901-1921.

McGechan, M. B. and D. R. Lewis. 2002. Transport of particulate and colloid-sorbed contaminants through soil, Part I: General Principles. Biosystems Engineering. 83(3): 255-273

Meyer, M. D., M. P. North, A. N. Gray and H. S. J. Zald. 2007. Influence of soil thickness on stand characteristics in a Sierra Nevada mixed-conifer forest. Plant and Soil. 294:113-123

Meyles, E., A. Williams, L. Ternan and J. Dowd. 2003. Runoff generation in relation to soil moisture patterns in a small Dartmoor catchment, Southwest England. Hydrological Processes. 17:251-264.

Naegeli, M. W., P. Huggenberger and U. Uehlinger. 1996. Ground penetrating radar for assessing sediment structures in the hyporheic zone of a prealpine river. Journal of the North American Benthological Society. 15(3):353-366.

National Cooperative Soil Survey. 2009a. Dothan sand. Map Unit Description. Natural Resources Conservation Service.

National Cooperative Soil Survey. 2009b. Fuquay sand. Map Unit Description. Natural Resources Conservation Service.

National Cooperative Soil Survey. 2009c. Vaucluse-Ailey complex. Map Unit Description. Natural Resources Conservation Service.

Nyquist, N. E., P. A. Freyer and L. Toran. 2008. Stream bottom resistivity tomography to map ground water discharge. Ground Water. 46(4):561-569

Price, K., C. R. Jackson and A. J. Parker. 2010. Variation of surficial soil hydraulic properties across land uses in the southern Blue Ridge Mountains, North Carolina, USA. Journal of Hydrology. 383:256-268.

Rawls, W. J. 1983. Estimating soil bulk density from particle size analysis and organic matter content. Soil Science. 135(2):123-125.

Selker, J. 1992. Fingered flow in two dimensions: 1. Measurement of matric potential. Water Resources Research. 28(9):2513-2521.

Shanley, J. B., K. N. Hjerdt, J. J. McDonnell and C. Kendall. 2003. Shallow water table fluctuations in relation to soil penetration resistance. Ground Water. 41(7):964-972.

Sidle, R. C. 1984. Shallow groundwater fluctuations in unstable hillslopes of coastal Alaska. Band 20.

Tromp-van Meerveld, H. J. and J. J. McDonnell. 2006. Threshold relations in subsurface stormflow: 2. The fill and spill hypothesis. Water Resources Research. 42.

Uchida, T., Y. Asano and T. Mizuyama. 2004. Water Resources Research. 40(W12401):1-13.

Uchida, T., I. T. Meerveld and J. J. McDonnell. 2005. The role of lateral pipe flow in hillslope runoff response: An intercomparison of non-linear hillslope response. Journal of Hydrology. 311:117-133.

Vervoort, R. W., D. E. Radcliffe and L. T. West. 1999. Soil structure development and preferential solute flow. Water Resources Research. 35(4):913-928.

Wilcox, B. P., B. D. Newman, D. Brandes, D. W. Davenport and K. Reid. 1997. Runoff from a semiarid ponderosa pine hillslope in New Mexico. Water Resources Research. 33(10):2301-2314.

Whipkey, R. Z. 1965. Subsurface stormflow from forested slopes. Bulletin of the International Society of Science and Hydrology. 10(2):74-85.

Yoshinaga, S. and Y. Ohnuki. 1995. Estimation of soil physical properties from a handy dynamic cone penetrometer test. Journal of the Japan Society of Erosion Control Engineering. 48(3):22-28.

Zarco-Tejada, P. J., J. a. J. Berni, L. Suárez, G. Sepulcre-Cantó, F. Morales and J. R. Miller. 2009. Imaging chlorophyll fluorescence with an airborne narrow-band multispectral camera for vegetation stress detection. Remote Sensing of Environment. 113(6):1262-1275.

Zaslavsky, D. and A. S. Rogowski. 1969. Hydrologic and morphologic implications of anisotropy and infiltration in soil profile development. Soil Science Society of America Proceedings. 33:594-599.

Zaslavsky, D. and G. Sinai. 1981a. Surface hydrology: I-Explanation of phenomena. American Society of Civil Engineers Journal of Hydraulics Division. 107:1-16.

Zaslavsky, D. and G. Sinai. 1981b. Surface hydrology: III-Causes of lateral flow. American Society of Civil Engineers Journal of Hydraulic Division. 107:37-52.

Zaslavsky, D. and G. Sinai. 1981c. Surface hydrology: IV-Flow in sloping, layered soils. American Society of Civil Engineers Journal of Hydraulics Division. 107:53-64.

Appendix A

SRS Soil Map and Descriptions

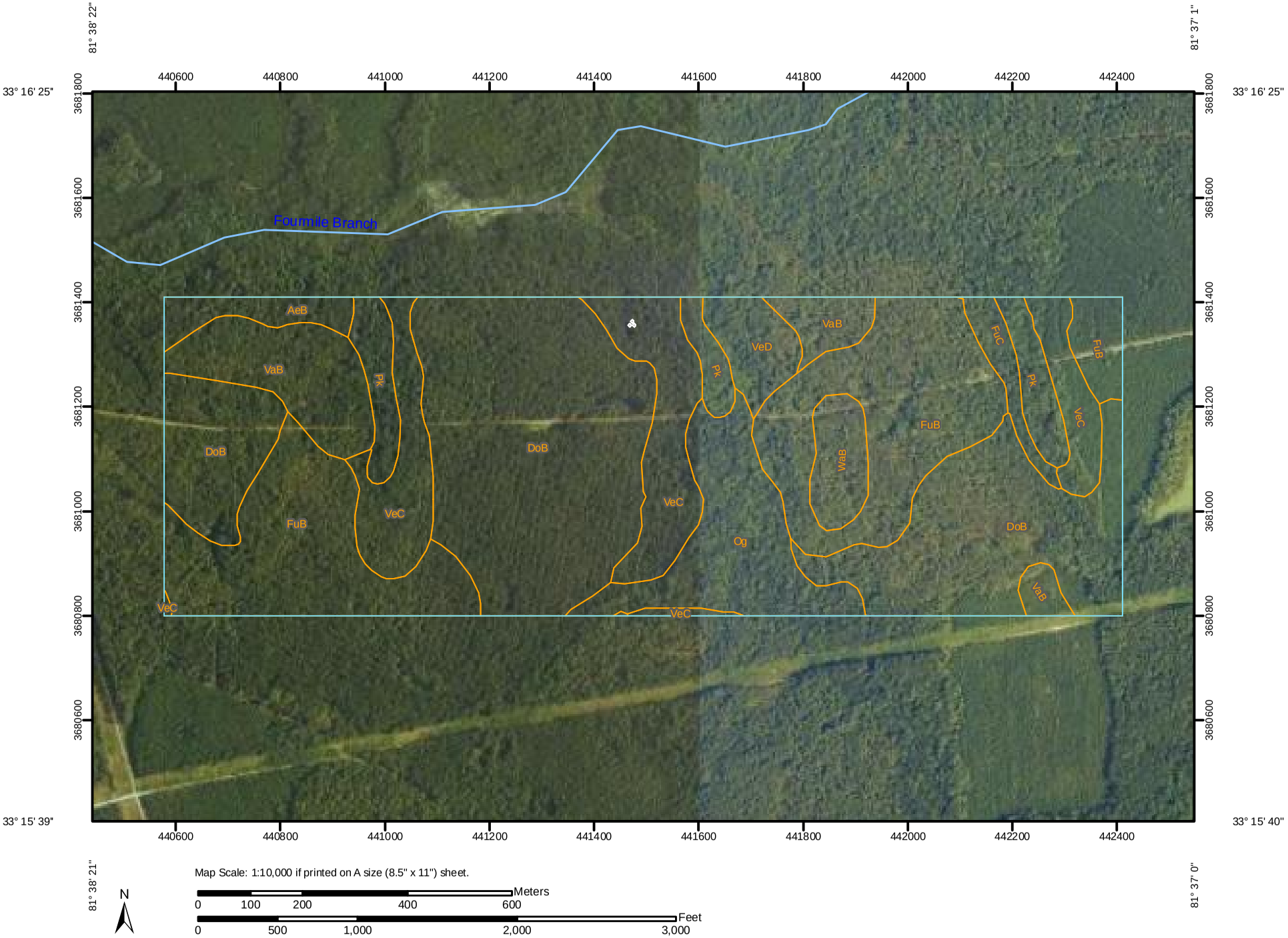
81° 38' 22"
81° 37' 1"
33° 16' 25"
33° 15' 39"
33° 15' 40"
81° 38' 21"
81° 37' 0"
440600
440800
441000
441200
441400
441600
441800
442000
442200
442400
3681800
3681600
3681400
3681200
3681000
3680800
3680600
Fourmile Branch
AeB
VaB
Pk
DoB
FuB
VeC
VeD
WaB
Og
FuC
Map Scale: 1:10,000 if printed on A size (8.5" x 11") sheet.
N
Meters
0 100 200 400 600
Feet
0 500 1,000 2,000 3,000

MAP LEGEND

Area of Interest (AOI)
- Area of Interest (AOI)

Soils
- Soil Map Units

Special Point Features
- Blowout
- Borrow Pit
- Clay Spot
- Closed Depression
- Gravel Pit
- Gravelly Spot
- Landfill
- Lava Flow
- Marsh or swamp
- Mine or Quarry
- Miscellaneous Water
- Perennial Water
- Rock Outcrop
- Saline Spot
- Sandy Spot
- Severely Eroded Spot
- Sinkhole
- Slide or Slip
- Sodic Spot
- Spoil Area
- Stony Spot
- Very Stony Spot
- Wet Spot
- Other

Special Line Features
- Gully
- Short Steep Slope
- Other

Political Features
- Cities

Water Features
- Oceans
- Streams and Canals

Transportation
- Rails
- Interstate Highways
- US Routes
- Major Roads
- Local Roads

MAP INFORMATION

Map Scale: 1:10,000 if printed on A size (8.5" × 11") sheet.

The soil surveys that comprise your AOI were mapped at 1:15,840.

Please rely on the bar scale on each map sheet for accurate map measurements.

Source of Map: Natural Resources Conservation Service
Web Soil Survey URL: http://websoilsurvey.nrcs.usda.gov
Coordinate System: UTM Zone 17N NAD83

This product is generated from the USDA-NRCS certified data as of the version date(s) listed below.

Soil Survey Area: Savannah River Plant Area
Survey Area Data: Version 9, Jul 20, 2009

Date(s) aerial images were photographed: 8/22/2005

The orthophoto or other base map on which the soil lines were compiled and digitized probably differs from the background imagery displayed on these maps. As a result, some minor shifting of map unit boundaries may be evident.

Map Unit Legend

Savannah River Plant Area (SC696)			
Map Unit Symbol	**Map Unit Name**	**Acres in AOI**	**Percent of AOI**
AeB	Ailey sand, 2 to 6 percent slopes, wet substratum	5.1	1.8%
DoB	Dothan sand, 2 to 6 percent slopes	103.5	37.4%
FuB	Fuquay sand, 2 to 6 percent slopes	64.5	23.3%
FuC	Fuquay sand, 6 to 10 percent slopes	3.8	1.4%
Og	Ogeechee sandy loam, ponded	21.4	7.7%
Pk	Pickney sand, frequently flooded	12.7	4.6%
VaB	Vaucluse sandy loam, 2 to 6 percent slopes	20.7	7.5%
VeC	Vaucluse-Ailey complex, 6 to 10 percent slopes	32.5	11.7%
VeD	Vaucluse-Ailey complex, 10 to 15 percent slopes	6.5	2.3%
WaB	Wagram sand, 2 to 6 percent slopes	6.0	2.2%
Totals for Area of Interest		**276.7**	**100.0%**

Savannah River Plant Area

DoB—Dothan sand, 2 to 6 percent slopes

Map Unit Setting

Elevation: 250 to 450 feet
Mean annual precipitation: 45 to 57 inches
Mean annual air temperature: 50 to 77 degrees F
Frost-free period: 210 to 243 days

Map Unit Composition

Dothan and similar soils: 100 percent

Description of Dothan

Setting

Landform: Marine terraces
Landform position (three-dimensional): Tread
Down-slope shape: Convex
Across-slope shape: Convex
Parent material: Loamy marine deposits

Properties and qualities

Slope: 2 to 6 percent
Depth to restrictive feature: More than 80 inches
Drainage class: Well drained
Capacity of the most limiting layer to transmit water (Ksat): Moderately high (0.20 to 0.57 in/hr)
Depth to water table: About 36 to 60 inches
Frequency of flooding: None
Frequency of ponding: None
Available water capacity: Moderate (about 6.6 inches)

Interpretive groups

Land capability (nonirrigated): 2e

Typical profile

0 to 8 inches: Loamy sand
8 to 11 inches: Loamy sand
11 to 31 inches: Sandy clay loam
31 to 80 inches: Sandy clay loam

Data Source Information

Soil Survey Area: Savannah River Plant Area
Survey Area Data: Version 9, Jul 20, 2009

Savannah River Plant Area

FuB—Fuquay sand, 2 to 6 percent slopes

Map Unit Setting

Elevation: 250 to 450 feet
Mean annual precipitation: 45 to 57 inches
Mean annual air temperature: 50 to 77 degrees F
Frost-free period: 210 to 243 days

Map Unit Composition

Fuquay and similar soils: 100 percent

Description of Fuquay

Setting

Landform: Marine terraces
Landform position (three-dimensional): Tread
Down-slope shape: Convex
Across-slope shape: Convex
Parent material: Sandy and/or loamy marine deposits

Properties and qualities

Slope: 2 to 6 percent
Depth to restrictive feature: More than 80 inches
Drainage class: Well drained
Capacity of the most limiting layer to transmit water (Ksat): Moderately low to moderately high (0.06 to 0.20 in/hr)
Depth to water table: About 48 to 72 inches
Frequency of flooding: None
Frequency of ponding: None
Available water capacity: Moderate (about 6.5 inches)

Interpretive groups

Land capability (nonirrigated): 2s

Typical profile

0 to 8 inches: Sand
8 to 21 inches: Loamy sand
21 to 35 inches: Sandy clay loam
35 to 70 inches: Sandy clay loam

Data Source Information

Soil Survey Area: Savannah River Plant Area
Survey Area Data: Version 9, Jul 20, 2009

Savannah River Plant Area

VeC—Vaucluse-Ailey complex, 6 to 10 percent slopes

Map Unit Setting

Elevation: 250 to 450 feet
Mean annual precipitation: 45 to 57 inches
Mean annual air temperature: 50 to 77 degrees F
Frost-free period: 210 to 243 days

Map Unit Composition

Vaucluse and similar soils: 55 percent
Ailey and similar soils: 45 percent

Description of Vaucluse

Setting

Landform: Marine terraces
Landform position (three-dimensional): Tread
Down-slope shape: Convex
Across-slope shape: Convex
Parent material: Loamy marine deposits

Properties and qualities

Slope: 6 to 15 percent
Depth to restrictive feature: More than 80 inches
Drainage class: Well drained
Capacity of the most limiting layer to transmit water (Ksat): Very low to moderately high (0.00 to 0.57 in/hr)
Depth to water table: More than 80 inches
Frequency of flooding: None
Frequency of ponding: None
Available water capacity: Low (about 4.4 inches)

Interpretive groups

Land capability (nonirrigated): 3e

Typical profile

0 to 3 inches: Loamy sand
3 to 10 inches: Loamy sand
10 to 22 inches: Sandy clay loam
22 to 60 inches: Sandy clay loam
60 to 74 inches: Loamy sand

Description of Ailey

Setting

Landform: Marine terraces
Landform position (three-dimensional): Tread
Down-slope shape: Convex
Across-slope shape: Convex
Parent material: Sandy and/or loamy marine deposits

Properties and qualities

Slope: 6 to 15 percent
Depth to restrictive feature: More than 80 inches
Drainage class: Well drained
Capacity of the most limiting layer to transmit water (Ksat): Moderately low to moderately high (0.06 to 0.20 in/hr)
Depth to water table: More than 80 inches
Frequency of flooding: None
Frequency of ponding: None
Available water capacity: Low (about 4.1 inches)

Interpretive groups

Land capability (nonirrigated): 3s

Typical profile

0 to 3 inches: Sand
3 to 23 inches: Sand
23 to 30 inches: Sandy clay loam
30 to 72 inches: Sandy clay loam

Data Source Information

Soil Survey Area: Savannah River Plant Area
Survey Area Data: Version 9, Jul 20, 2009

Appendix B

Ground Penetrating Radar Report

Preliminary Geophysical Survey Results for the Savannah River Site Study Area Aiken, South Carolina

Prepared for

The University of Georgia Warnell School of Forestry and Natural Resources

By

Jessica Cook Hale and Hillary Sletten
The University of Georgia Geology Department

February 4, 2010

Table of Contents

Index of Figures

Section I: Introduction

On December 17, 2009, University of Georgia (UGA) personnel conducted GPR surveys at three different areas within the Savannah River Site located near Aiken, South Carolina. The purpose of these surveys was to assist researchers in the UGA Warnell School of Forestry and Natural Resources in locating the remains of vestigial pine tree taps roots within the A and B soil horizons. The soil stratigraphy under investigation consists of an A horizon that is predominantly plow zone comprised of sandy loam, or a loamy sand, and a B horizon consisting of a typical Georgia Piedmont iron rich clay.

Previous hydrogeological research has found that water is penetrating into the B horizon and traveling down slope. This finding is of interest because the B horizon should in theory be more impervious to the groundwater that has passed through the A horizon easily. The current working hypothesis is that vestigial pine tree taproots may provide the mechanism for this transfer of groundwater as they penetrate into the B horizon; once the tree has died or been harvested, the tap root decomposes into organic materials that remain within the B horizon, theoretically allowing groundwater to percolate from the surface horizon into the clay.

The use of GPR is a common application to elucidate stratigraphic profiles (see (Markus W. Naegeli, et al., 1996). The difference in the dielectric for different stratigraphic layers allows the investigator to “see” the changes in stratigraphic horizon. We were therefore optimistic that we would see stratigraphic changes. With respect to seeing vestigial taproots from now-dead pine trees, the occurrence of tree roots in archaeological surveys suggests that tap roots should theoretically be visible in our surveys (Conyers and Cameron, 1998). The difference between our survey and the work documented in Conyers’ and Camerons’ study is that roots, and not archaeological features, are in fact the chosen target.

GPR has been successfully used as a method for mapping living deciduous tree root systems (Hruska, et al., 1997) (Schoor and Colvin, 2009) and borehole techniques have been applied with mixed results to mapping living taproot structures from standing coniferous trees (Butnor, et al., 2006a). The goal of this survey was to map taproot structures from trees that have been cut, eliminating the need to use the tomographic borehole techniques employed by Butnor. The identification of anomalies with possible vestigial taproot structures from harvested pine trees relies on the assumption that the decaying taproots will contain more organic matter and

sandy loam/loamy sand from the A horizon. It follows that these decaying taproots will also have a different potential for absorbing, retaining, and conducting moisture from the A horizon into the B horizon (Galagedara, et al., 2005) in addition to documented increases in carbon found in decaying taproot systems (Butnor, et al., 2006b) . Furthermore, Butnor, et al., concluded that the ideal soils for mapping tree roots have a low dielectric and are highly electrically resistive. Soils that have these characteristics include sandy soils such as those found on the Coastal Plain of the southeast U.S. where the Savannah River Site is located (Butnor, et al., 2001). Conversely, however, clay rich soil conditions were found to be poor sites for mapping tree root systems and so the B horizon at the Savannah River Site survey areas may be less than ideal for locating potential vestigial taproots once this horizon is reached.

The sum of all these factors is that decaying tap roots have a different composition from the surrounding soil horizons, chemically and hydrologically (among other things), and therefore should have a different dielectric than the surrounding soil horizons. The difference in dielectric between two materials is what creates GPR reflections, refractions, or attenuation, and so these differences ought to be visible. Within the clay rich horizons, we hoped to still see some differences in dielectric between the vestigial taproot systems and the surrounding clays, whereas the sandier A Horizon is expected to have much lower dielectric, thus showing stronger anomalies. Invesetigators used GPR processing software capable of rendering high resolution plan view maps, vertical profiles, and 3D volumes in this study, further heightening the ability to locate and highlight anomalies that potentially correlate to vestigial taproot systems.

These data are only maps of anomalies, however, and cannot be firmly tied to vestigial taproot systems until actual ground-truthing is performed. It is hoped that these GPR datasets can be compared to actual excavations of each survey area at various depths, and where anomalies are found to correlate to vestigial taproots, the GPR velocities and corresponding dielectric can be used to model future GPR work at this study area.

Section II: Methods: Ground Penetrating Radar

Ground Penetrating Radar (GPR) works along the same principles as standard radar: it sends out a pulse of electromagnetic (EM) energy in the microwave spectrum and then measures the two-way travel time of the return of that signal when it is reflected back to the antenna. This two-way travel time can be used to approximate distance to the target (whatever it was that reflected/refracting the energy), and therefore can be used to approximate depth. In comparison, it has some important differences from standard radar. Unlike standard radar, which travels through air, GPR microwaves must pass through the subsurface. Soil, rock, and other materials buried within the ground interact with the energy pulse differently. Firstly, the materials within the subsurface slow the pulse, and cause it to lose energy (attenuation), and secondly they can diffract the energy into lower angles prior to the wave completely losing all of its energy. If the wave is completely reflected back to the antenna, this is called a “hard reflection” and usually represents the presence of metal within the subsurface.

Data are collected in lines called transects on a grid and stored in the hard drive of a GPR unit. Upon collection, the data are displayed on the unit’s screen using a real-time image. The image is then stored as a data file. Both the raw image shown on the screen and the stored data file place the top of the soil at the top of the image, and the bottom of the image represents the lowest depth to which the GPR can “see”, or image. This is called a vertical profile. Within the vertical profile, one can often see parabolic shapes. These represent areas within the subsurface that are causing the GPR energy pulse to be deflected or diffracted into lower angles before they can penetrate deeper into the subsurface. Sometimes one can see a sharply defined column; this usually is a hard reflector and can be differentiated from non-metal materials by its shape, which is far more distinct than a lower angled parabola. Materials such as brick, which usually contain some iron that was originally part of the clay source used to make the brick, often create defined parabolas, or even something approaching the crisp shape of a hard reflector column. Ditches infilled with soil materials that contrast with those below it usually create “x” or checkerboard-like shapes due to the geometry of the microwaves as they reach deeper into the trench, and then travel out of it. Experienced GPR operators can interpret vertical profiles in the field, but for best interpretation the data must be processed using software suites that can render the vertical profiles into horizontal plan view maps defined by their respective depths. These horizontal plan view maps are called “slices” and it is using these “slices” that researchers make data

interpretations.

The GPR unit used in this study was a GSSI SIR-2000 using a 500 MHz antenna in all three survey areas (Figure 1). The frequency of a given antenna represents an average of the energy frequencies emitted by it. The range controls the depth of the microwave penetration into the soil. The lower the frequency, the deeper the antenna can image, because lower frequencies don't attenuate as easily within the subsurface. However, lower frequencies also have longer wavelengths, and so cannot resolve finer details. For finer resolution one needs a higher frequency antenna, but then one must forgo deep penetration. For the Savannah River Site survey areas, which have been categorized as Grid One, Grid Two and Grid Three according to the order they were surveyed, it was expected that the vestigial taproots remaining would be within 10 feet (3 meters) of the surface, if not shallower. Therefore 500 MHz is an appropriate choice, as it can image to approximately 1-3 meters deep. All of the instrument parameters such as gain and wave position were set by hand in the field. All three grids were 10 meters by 10 meters and all of them had slightly different slopes, reflecting their different locations within the watershed in this area. With the exception of the final grid, each transect was collected without significant obstacles and did not have to be broken into different data segments (Figure 2). In Grid Three, however, one line had to be shortened due to the presence of a large oak tree squarely in the middle of the path of the transect.

Figure 1

SIR2000 GPR control unit with 500 MHz antenna connected to the survey wheel.

Figure 2
Data collection in Grid One along the last transect.

After the data were collected, they were processed using GPR_Slice. The data were first background filtered and migrated, and then 50 horizontal time slices were generated from the vertical profiles. Depth calculations were done using a block model that assigned different dielectrics to different depths within the vertical profiles. These differing dielectrics create different velocities for the EM energy, and this creates variability in depth penetration according to variability in dielectric. These dielectrics were generated by curve-fitting a hyperbola at different time depths within the vertical profiles (Figure 3). The diameter of the hyperbolae widens as the velocity slows down and the dielectric increases, and narrows when the velocity increases and the dielectric decreases. Depth calculations generated by the block model for the velocities within the profile allow the software to assign more accurate depth ranges to individual time slices.

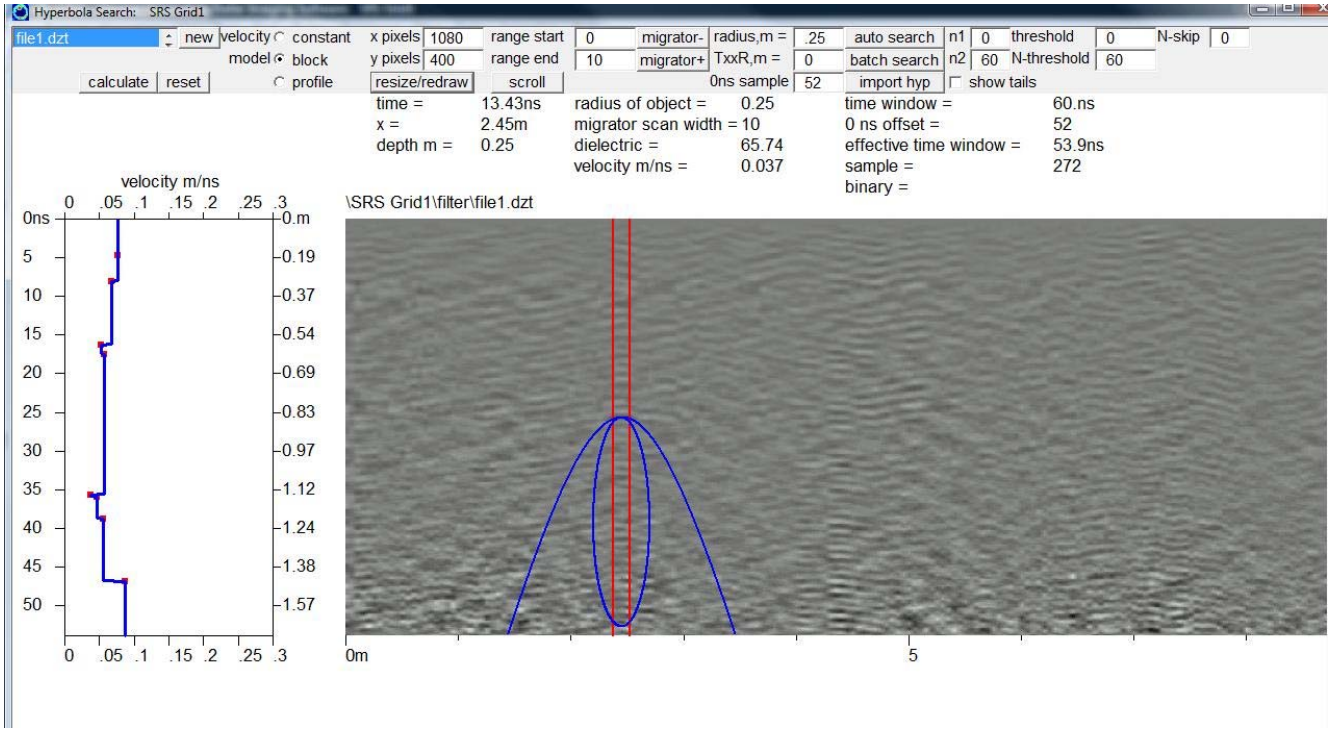

Figure 3
Hyperbola curve fitting showing the block velocity model.

It is important to note that the word “anomaly” will be used hereafter to describe areas where the data show differences from that which is expected within the subsurface, because absent actual ground-truthing of the data by excavation of the anomalous features, one can not say with any certainty what these patterns in the data actually represent. However, patterns within anomalies can be obvious to the trained eye, allowing for spatial analysis as well as more accurate placement of bucket auger coring and/or other methods of excavation.

Section III: Results

Figure 4, below, shows the grid plot for Grid One. This grid contained no line breaks. Grid One shows distinct anomalies from the surface to depth that are sub-angular and potentially consistent with vestigial taproots. Plan views of the data (Figure 5) show clearly that these sub angular anomalies range in size from approximately 25 cm to 1 meter at the largest, which is also consistent with the size of potential vestigial taproots. The color display of these velocities – yellow to bright red in Figure 3 – indicates high velocity returns. This is not consistent with a soil containing sandy loam, loamy sand, or even high concentrations of organic materials, but it is consistent with a material that contains more moisture than the surrounding soils or sediments. Figure 6 shows a 3D model rendered in GPR_Slice of Grid One, from the surface to the maximum depth of EM pulse penetration. The sub-angular anomalies are generally oval in shape, almost like lozenges. Again, these anomalies are representative of areas with higher velocity returns than the surrounding materials within the subsurface and may reflect areas with greater moisture concentration, or areas with greater electrical conductivity. Field notes for all three grids are included in Appendix A.

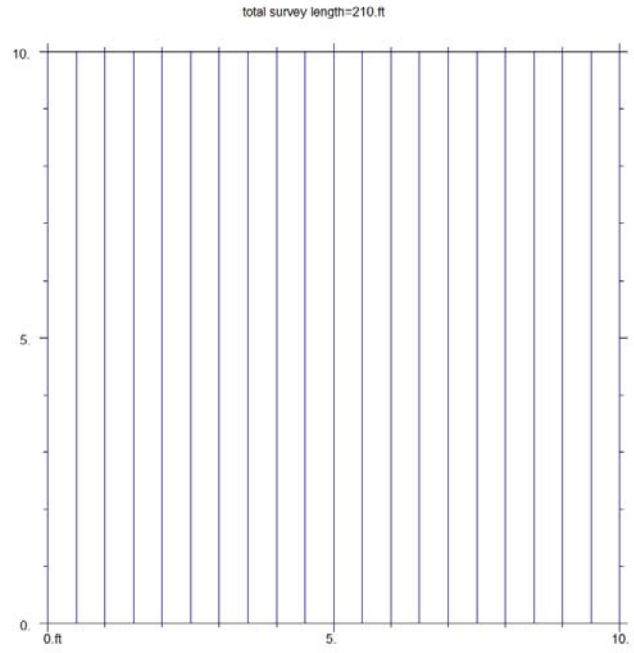

Figure 4
Plan view map of Grid One.

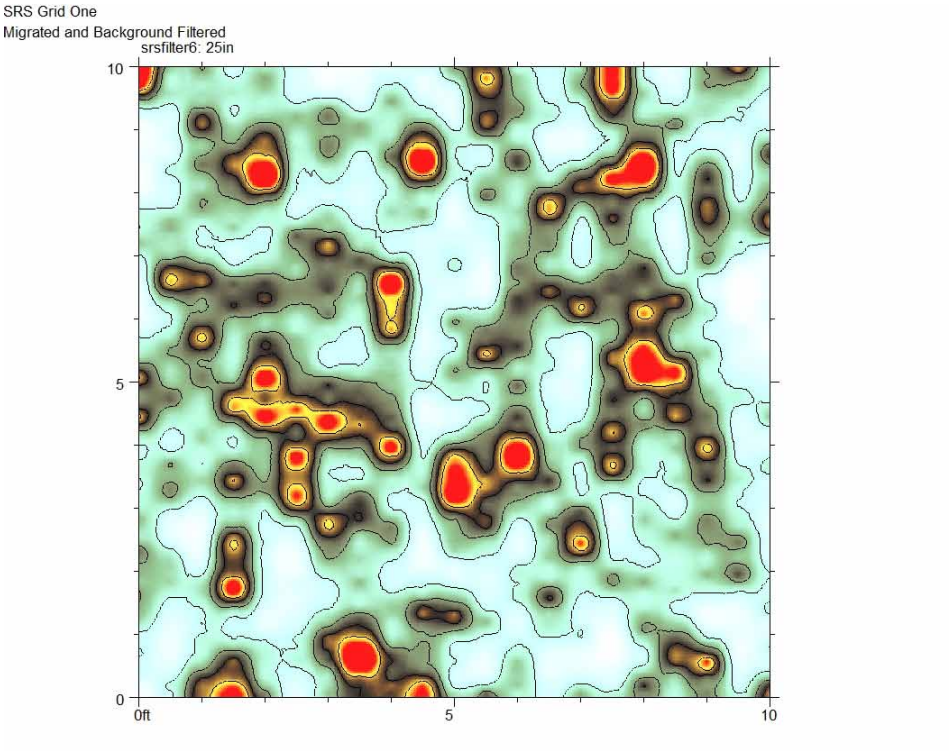

Figure 5
Grid One, 25 cm deep. Areas in red and yellow represent areas where higher velocity returns occur.

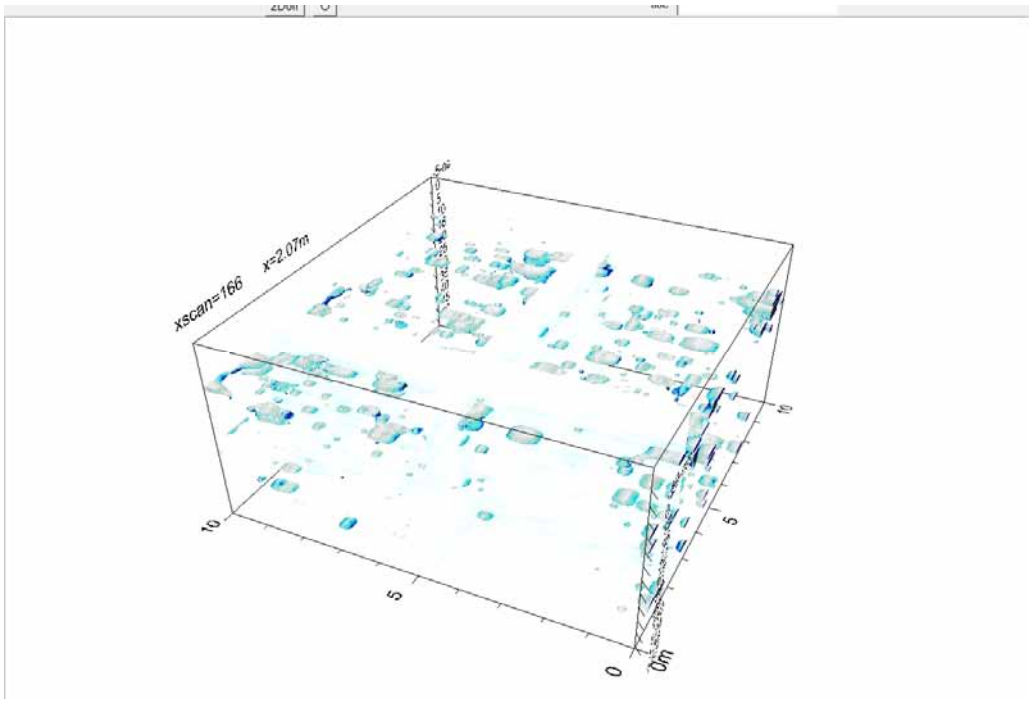

Figure 6
3D Model of Grid One showing sub-angular anomalies. Lozenge shapes represent areas of higher velocity return.

Grid Two showed a similar appearance. Figure 7, below, shows the grid plot, which like Grid One consisted of unbroken transects collected along the Y axis orientation. GPR time slice 13 (Figure 8) demonstrates that Grid Two has the same types of high velocity returns as Grid One. The 3D model (Figure 9) rendered for Grid Two, like that which displays the full volume for Grid One, has the same collection of oval-shaped, lozenge-like anomalies that correspond to the high velocity anomalies shown in yellow-red on the plan view time slices. These appear at all depths, from the surface to the bottom of the profiles.

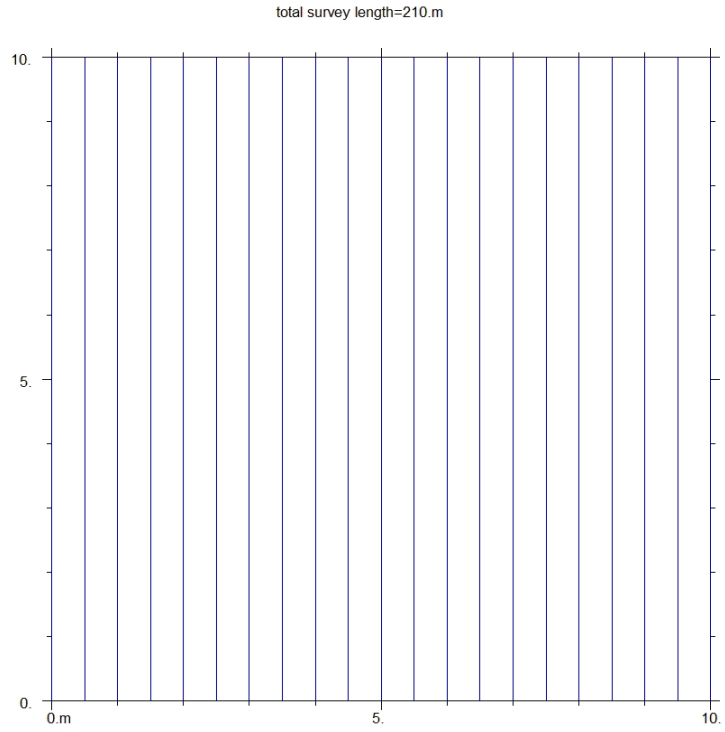

Figure 7
Grid plot for survey Grid Two.

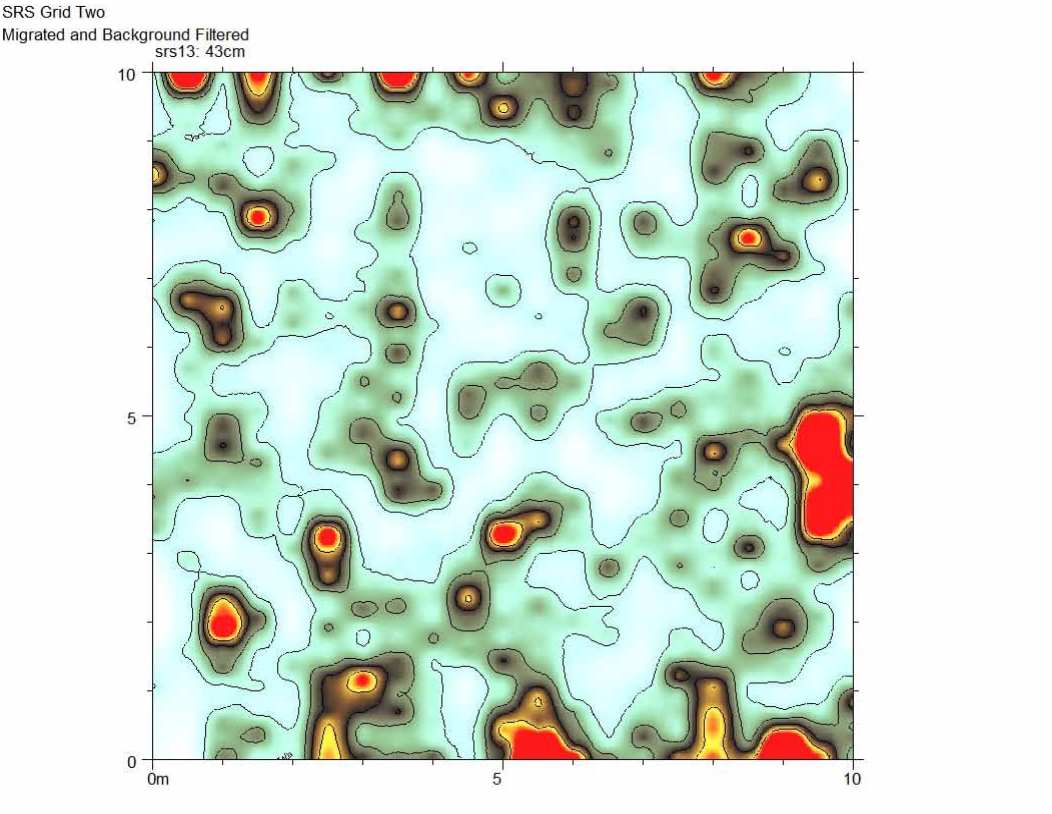

Figure 8
GPR time slice 13 for Grid Two at 43 cm deep. Coloration of anomalies is the same as above in Figure 5.

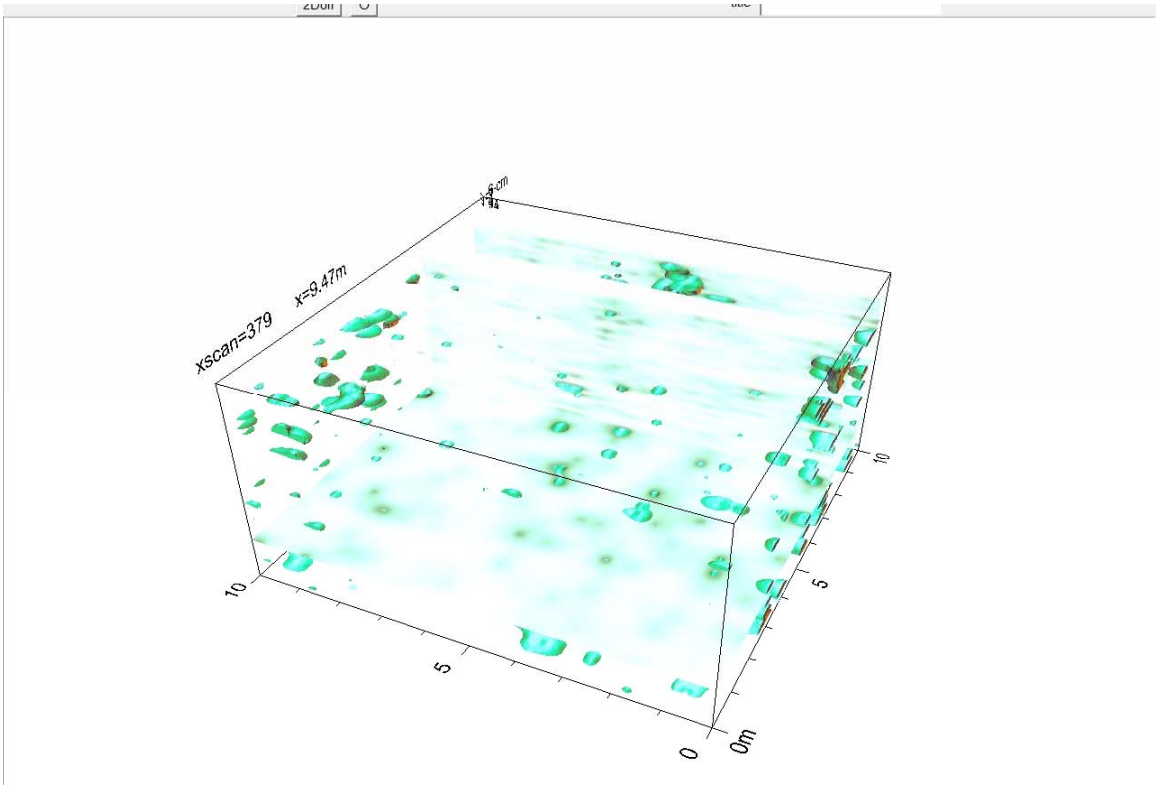

Figure 9
3D volume of GPR data for Grid Two. The lozenge shaped anomalies represent higher velocity returns as in Figure 6, above.

Grid Three contained two shortened lines due to the position of an oak tree directly within the path of the transect. The GPR survey line was truncated at 7 meters in length instead of the full 10 meters for the lines corresponding to the transects pulled at 7.5 meters on the X axis, and 8 meters on the X axis (Figure 10). During data processing, the search algorithm was set to interpolate between the missing data points, and so the final time slices as well as the 3D models show only a slender line of missing data. It is important to note that while the interpolation is considered reasonable and valid, the data display that results cannot be considered as reliable as other areas within the data displays, wherein interpolations for missing data were not done.

3D modeling and time slice 10 of Grid Three shows the same sort of sub-angular anomalies as the previous two grids (Figure 11, Figure 12). What is especially interesting is that at least one anomaly is found proximal to the shortened line. This shortened line, as noted above, had to be truncated due to the presence of a tree. It is reasonable to speculate that the anomaly associated with this area may correlate to the root system of the oak tree. This anomaly, located

from 8 to 10 meters on the Y axis and at 8 to 9 meters on the X axis, is a somewhat linear feature that certainly has a shape consistent with root structures seen in deciduous trees like the oak tree that caused the truncation of the transect.

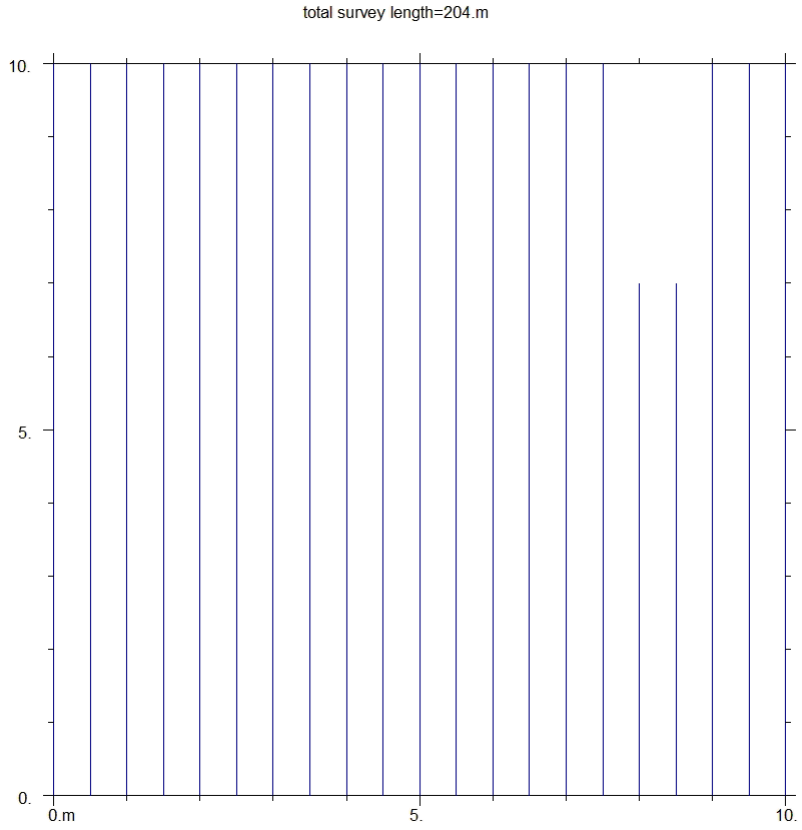

Figure 10
Grid Map for Grid Three showing two truncated lines at 8 and 8.5 m

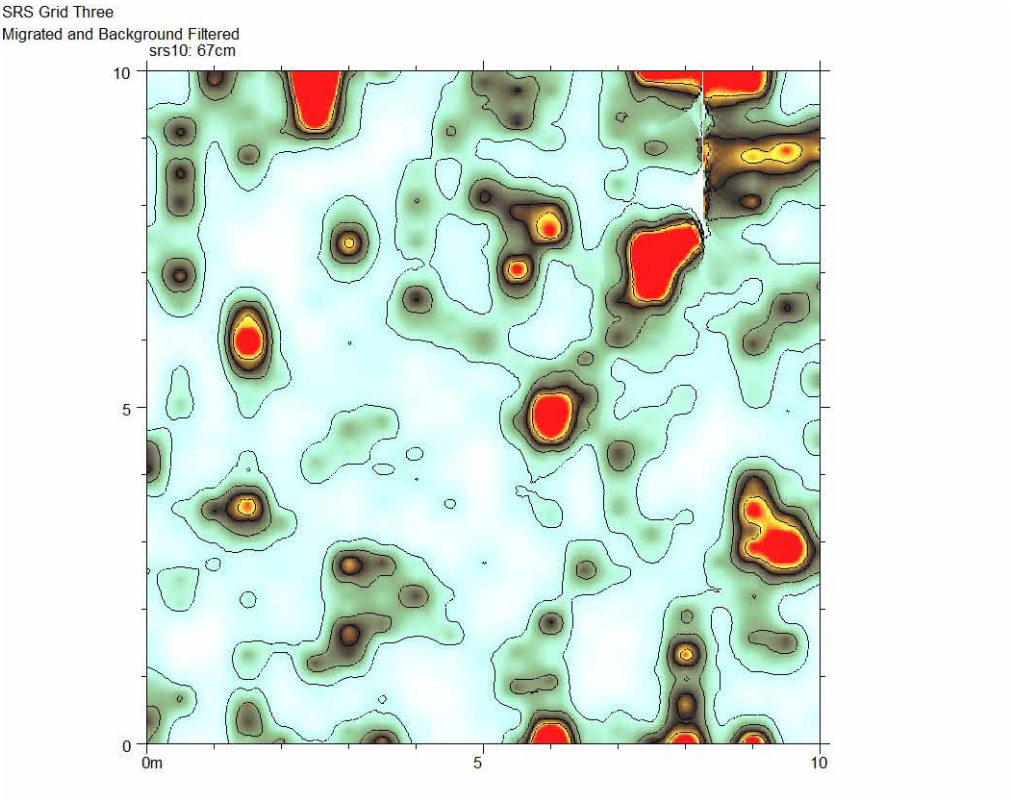

Figure 11
Time slice 10 of Grid Three at a depth of 67 cm. Coloration of anomalies is the same as Figures 5 and 8, representing higher velocity returns

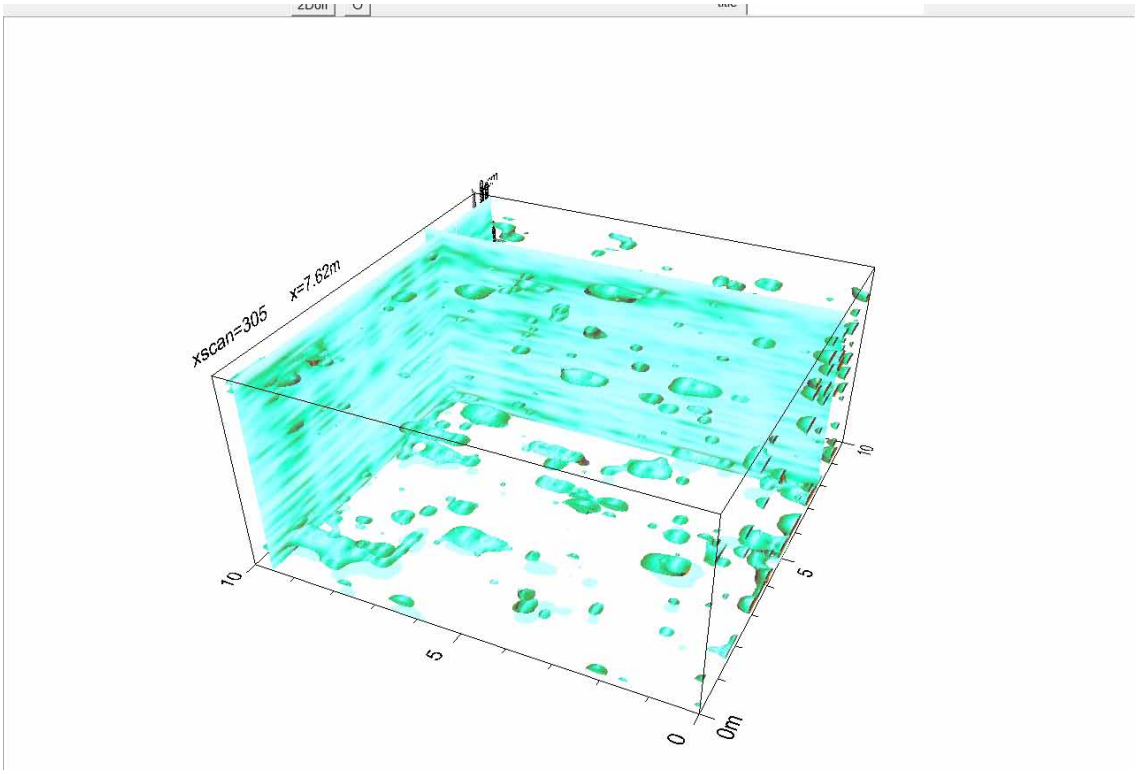

Figure 12
3D model of Grid Three. Lozenge shaped anomalies represent the same types of features as in Figures 9 and 6, above.

Section IV: Conclusions and Discussion

It is clear that the subsurface is more heterogeneous than one might think based merely upon the divisions into the A and B horizons as discussed in the introduction to this report. However given that this area of South Carolina was rural farmland prior to the creation of the Savannah River Site, the heterogeneous subsurface is understandable. For approximately a century, this land was under plow and subjected to significant disturbance.

This heterogeneity manifests as intermingled anomalies within the GPR data that exhibit different dielectrics from their surroundings. The higher velocities of return exhibited by these anomalies are not necessarily consistent with a sandy loam. In fact, what one would expect to see in a sandy loam is the opposite phenomenon, with the GPR EM pulses traveling deeper into the subsurface without being strongly reflected back to the antenna. Materials that are more saturated in water or soils and sediments that are more clay rich typically generate this kind of strong reflectivity. Without actually ground-truthing these data, it is impossible to determine which of these phenomenon, or any other phenomenon, is responsible for these anomalies.

A comparison of these data with Butnor's data from 2001 shows some similarities. Figure 13 shows a vertical profile from the 2001 study where the taproots show up as tight parabolas. The data collected for this study did not find clearly defined parabolas. Instead, the anomalies were columnar in shape (Figure 14). In the data collected for this survey, the anomalies go to depth, as well, unlike the anomalies seen in Butnor's data from 2001. The Butnor study employed a 400 MHz antenna, not a 500 MHz as in our study. Butnor noted that the 1.5 GHz antenna that was also used in their study provided higher resolution at shallower depth than the 400 MHz. This was not as much of an issue for this study because the targets sought were at greater depth, below approximately 25 cm. Also, the Butnor data are displayed using only red, blue, and white in the color display, whereas survey data for this project are shown using a full color spectrum. This visual difference has an effect on the way in which the viewer "sees" these anomalies. In the data collected for this survey, the full color spectrum used to display the vertical profiles renders a more columnar aspect than in the Butnor study.

When the horizons were detected within the GPR data from this study, and these profiles were compared to the Butnor profiles, a good correlation was found (Figure 13, Figure 14, Figure 15). This function within GPR_Slice used the amplitude of return to determine

where the horizons and/or anomalies within the subsurface lie. In theory, then, areas where taproots penetrate into the soil, or areas with greater water saturation, should show up as changes in the horizon.

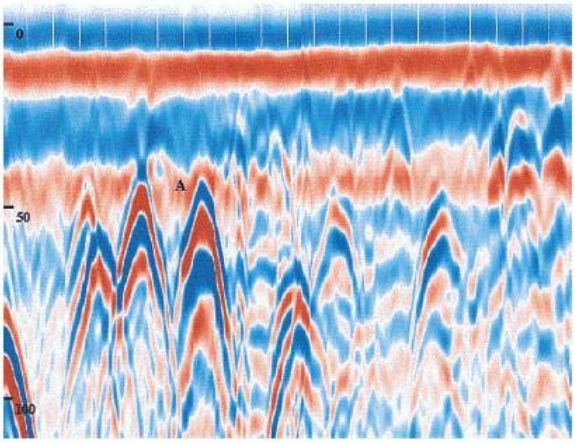

Figure 13
GPR vertical profile showing parabolic anomalies that correlate to loblolly pine taproots (Butnor, 2001).

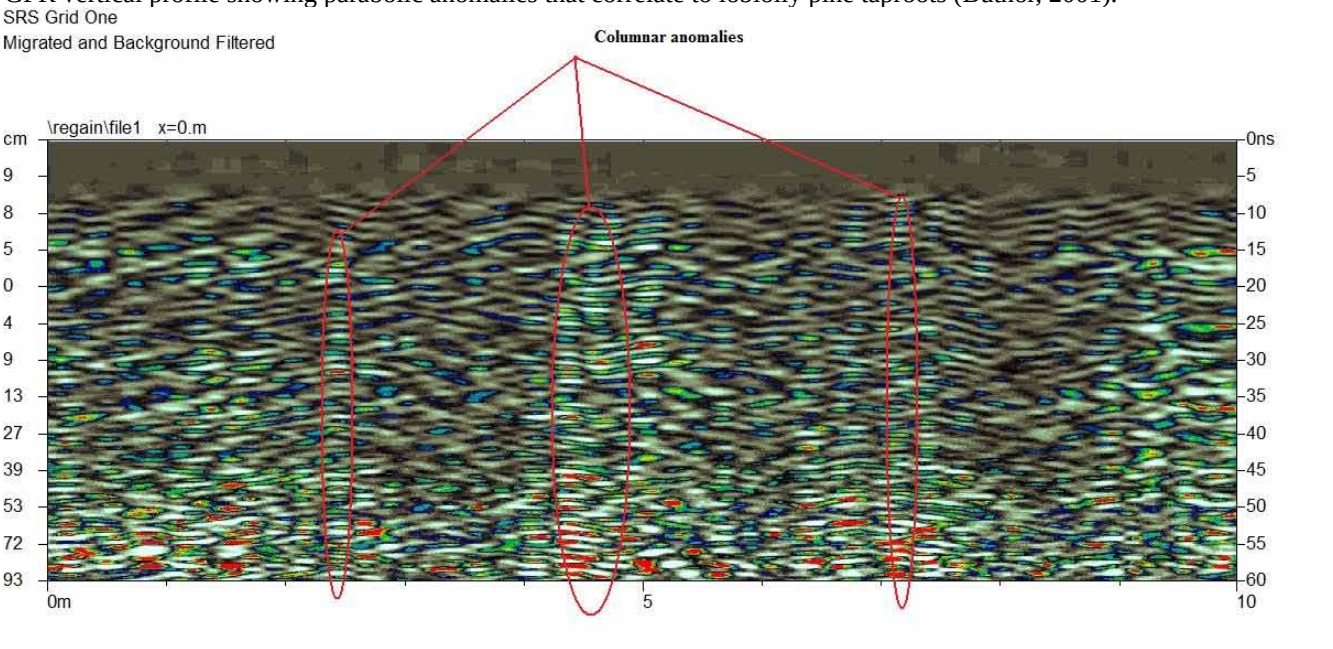

Figure 14
Vertical profile, Grid One, showing columnar anomalies.

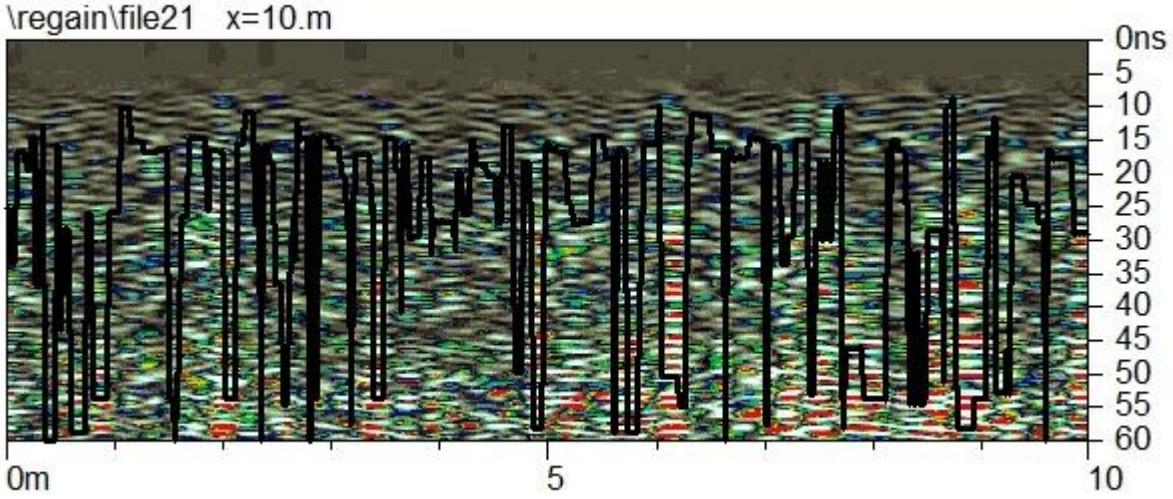

Figure 15
Vertical profile, Grid One, showing horizon detection based on amplitude of return. Note the apparent penetration into the subsurface of the columnar anomalies.

The initial purpose of these surveys was to look for GPR anomalies that correlate to vestigial tap roots left over when pine trees have died or been harvested. It is reasonable to assume that vestigial tap roots would perhaps retain a higher level of water saturation than a surrounding soil, particularly a sandy loam or loamy sand horizon that drains well. It is therefore reasonable to speculate that if these anomalies are caused by higher water saturation zones, it is possible that vestigial tap roots could be the source for this phenomenon. To verify this hypothesis, the next phase would be to ground-truth the survey grids.

Section V: References

Butnor, J.R., Doolittle, J.A., Kress, L., Cohen, S., Johnsen, K.H., 2001 *Use of ground-penetrating radar to study tree roots in the southeastern United States*, Tree Physiology 21, 10.

Butnor, J.R., Johnsen, K.H., Wikström, P., Lundmark, T., Linder, S., 2006a. *Imaging Tree Roots with Borehole Radar*, 11th International Conference on Ground Penetrating Radar, June 19-22, 2006, Columbus, Ohio, USA.

Butnor, J.R., Johnsen, K.H., Sanchez, F.G., 2006b. *Whole-tree and forest floor removal from a loblolly pine plantation have no effect on forest floor CO2 efflux 10 years after harvest*, Forest Ecology and Management 227, 6.

Conyers, L.B., Cameron, C.M., 1998. *Ground-Penetrating Radar Techniques and Three-Dimensional Computer Mapping in the American Southwest*, Journal of Field Archaeology 25, 14.

Galagedara, L.W., Parkin, G.W., Redman, J.D., Bertold, P.v., Endres, A.L., 2005. *Field studies of the GPR ground wave method for estimating soil water content during irrigation and drainage*, Journal of Hydrology 301, 16.

Hruska, J., Cermak, J., Sustek, S., 1997. *Mapping tree root systems with ground-penetrating radar*, Tree Physiology 19, 6.

Markus W. Naegeli, Huggenberger, P., Uehlinger, U., 1996. *Ground Penetrating Radar for Assessing Sediment Structures in the Hyporheic Zone of a Prealpine River*, Journal of the North American Benthological Society 15, 14.

Schoor, M.v., Colvin, C., 2009. *Tree root mapping with ground penetrating radar*, 11th SAGA Biennial Technical Meeting and Exhibition, Swaziland.

Appendix A: Field Notes

Savannah River Site

12/17/09

Grid One

Position 136.0

	1	2	3	4	5
Gain Points	7	41	46	50	58
File	X0	X1	Y0	Y1	Notes
1	0	0	0	10	
2	0.5	0.5	10	0	Off ground at 19.5m
3	1	1	0	10	Stump at 9.5m
4	1.5	1.5	10	0	Stump at 6.0m
5	2	2	0	10	Stump at 6.0m
6	2.5	2.5	10	0	
7	3	3	0	10	
8	3.5	3.5	10	0	
9	4	4	0	10	Stump at 7.5m
10	4.5	4.5	10	0	Stump at 2.5m
11	5	5	0	10	
12	5.5	5.5	10	0	Roots at 5.5m
13	6	6	0	10	Stump at 2.5-3.0m
14	6.5	6.5	10	0	
15	7	7	0	10	
16	7.5	7.5	10	0	Swerve at 3.0m
17	8	8	0	10	
18	8.5	8.5	10	0	Ditch at 5.5m
19	9	9	0	10	
20	9.5	9.5	10	0	
21	10	10	0	10	

Savannah River Site

12/17/09

Grid Two

Position 134.0

	1	2	3	4	5
Gain Points	-2	41	46	50	58
File	X0	X1	Y0	Y1	Notes
22	0	0	0	10	
23	0.5	0.5	10	0	
24	1	1	0	10	
25	1.5	1.5	10	0	
26	2	2	0	10	
27	2.5	2.5	10	0	
28	3	3	0	10	
29	3.5	3.5	10	0	
30	4	4	0	10	
31	4.5	4.5	10	0	
32	5	5	0	10	
33	5.5	5.5	10	0	
34	6	6	0	10	
35	6.5	6.5	10	0	
36	7	7	0	10	
37	7.5	7.5	10	0	
38	8	8	0	10	
39	8.5	8.5	10	0	
40	9	9	0	10	
41	9.5	9.5	10	0	Swerve at 4.0m
42	10	10	0	10	

Savannah River Site

12/17/09

Grid Three

Position 134.0

Gain	1	2	3	4	5
Points	-7	33	39	43	52

File	X0	X1	Y0	Y1	Notes
43	0	0	0	10	
44	0.5	0.5	10	0	
45	1	1	0	10	
46	1.5	1.5	10	0	
47	2	2	0	10	
48	2.5	2.5	10	0	
49	3	3	0	10	
50	3.5	3.5	10	0	
51	4	4	0	10	
52	4.5	4.5	10	0	
53	5	5	0	10	
54	5.5	5.5	10	0	
55	6	6	0	10	
56	6.5	6.5	10	0	
57	7	7	0	10	
58	7.5	7.5	10	0	
59	8	8	0	7	
60	8.5	8.5	7	0	
61	9	9	0	10	
62	9.5	9.5	10	0	
63	10	10	0	10	

P1 (srsfilter6)			P2 (srs13)			P3 (srs10)		
X	Y	Z	X	Y	Z	X	Y	Z
0	0.0625	3	0	0.0625	533	0	0.0625	253
0	0.1875	2	0	0.1875	675	0	0.1875	118
0	0.3125	23	0	0.3125	371	0	0.3125	567
0	0.4375	37	0	0.4375	586	0	0.4375	316
0	0.5625	4	0	0.5625	662	0	0.5625	171
0	0.6875	47	0	0.6875	676	0	0.6875	200
0	0.8125	29	0	0.8125	262	0	0.8125	185
0	0.9375	3	0	0.9375	615	0	0.9375	261
0	1.0625	20	0	1.0625	2446	0	1.0625	54
0	1.1875	46	0	1.1875	681	0	1.1875	141
0	1.3125	47	0	1.3125	895	0	1.3125	132
0	1.4375	43	0	1.4375	276	0	1.4375	70
0	1.5625	54	0	1.5625	1058	0	1.5625	261
0	1.6875	59	0	1.6875	241	0	1.6875	43
0	1.8125	6	0	1.8125	141	0	1.8125	18
0	1.9375	53	0	1.9375	138	0	1.9375	42
0	2.0625	32	0	2.0625	109	0	2.0625	79
0	2.1875	41	0	2.1875	618	0	2.1875	72
0	2.3125	104	0	2.3125	347	0	2.3125	95
0	2.4375	22	0	2.4375	257	0	2.4375	114
0	2.5625	3	0	2.5625	89	0	2.5625	193
0	2.6875	44	0	2.6875	45	0	2.6875	157
0	2.8125	67	0	2.8125	332	0	2.8125	9
0	2.9375	30	0	2.9375	322	0	2.9375	27
0	3.0625	8	0	3.0625	413	0	3.0625	28
0	3.1875	44	0	3.1875	278	0	3.1875	53
0	3.3125	10	0	3.3125	3444	0	3.3125	61
0	3.4375	3	0	3.4375	2407	0	3.4375	80
0	3.5625	47	0	3.5625	434	0	3.5625	75
0	3.6875	41	0	3.6875	2334	0	3.6875	55
0	3.8125	2	0	3.8125	2752	0	3.8125	168
0	3.9375	12	0	3.9375	1846	0	3.9375	279
0	4.0625	25	0	4.0625	1530	0	4.0625	743
0	4.1875	8	0	4.1875	729	0	4.1875	192
0	4.3125	64	0	4.3125	2613	0	4.3125	468
0	4.4375	195	0	4.4375	1117	0	4.4375	441
0	4.5625	40	0	4.5625	61	0	4.5625	103
0	4.6875	13	0	4.6875	258	0	4.6875	21
0	4.8125	11	0	4.8125	1112	0	4.8125	28
0	4.9375	52	0	4.9375	180	0	4.9375	12
0	5.0625	184	0	5.0625	85	0	5.0625	24
0	5.1875	51	0	5.1875	287	0	5.1875	8
0	5.3125	15	0	5.3125	762	0	5.3125	15
0	5.4375	20	0	5.4375	143	0	5.4375	31
0	5.5625	23	0	5.5625	77	0	5.5625	5

0	5.6875	43	0	5.6875	159	0	5.6875	8
0	5.8125	2	0	5.8125	757	0	5.8125	46
0	5.9375	7	0	5.9375	350	0	5.9375	30
0	6.0625	13	0	6.0625	789	0	6.0625	58
0	6.1875	6	0	6.1875	539	0	6.1875	10
0	6.3125	5	0	6.3125	384	0	6.3125	1
0	6.4375	1	0	6.4375	560	0	6.4375	72
0	6.5625	5	0	6.5625	153	0	6.5625	87
0	6.6875	9	0	6.6875	1085	0	6.6875	68
0	6.8125	1	0	6.8125	1770	0	6.8125	59
0	6.9375	5	0	6.9375	509	0	6.9375	87
0	7.0625	29	0	7.0625	815	0	7.0625	298
0	7.1875	76	0	7.1875	329	0	7.1875	44
0	7.3125	26	0	7.3125	198	0	7.3125	20
0	7.4375	3	0	7.4375	186	0	7.4375	246
0	7.5625	33	0	7.5625	485	0	7.5625	315
0	7.6875	46	0	7.6875	1314	0	7.6875	32
0	7.8125	6	0	7.8125	1809	0	7.8125	14
0	7.9375	19	0	7.9375	342	0	7.9375	104
0	8.0625	1	0	8.0625	516	0	8.0625	34
0	8.1875	2	0	8.1875	935	0	8.1875	26
0	8.3125	3	0	8.3125	1347	0	8.3125	31
0	8.4375	6	0	8.4375	8286	0	8.4375	9
0	8.5625	31	0	8.5625	6669	0	8.5625	62
0	8.6875	3	0	8.6875	836	0	8.6875	46
0	8.8125	16	0	8.8125	2846	0	8.8125	12
0	8.9375	6	0	8.9375	1514	0	8.9375	15
0	9.0625	0	0	9.0625	235	0	9.0625	148
0	9.1875	9	0	9.1875	233	0	9.1875	320
0	9.3125	12	0	9.3125	1160	0	9.3125	174
0	9.4375	7	0	9.4375	912	0	9.4375	26
0	9.5625	64	0	9.5625	194	0	9.5625	69
0	9.6875	192	0	9.6875	328	0	9.6875	202
0	9.8125	138	0	9.8125	359	0	9.8125	81
0	9.9375	139	0	9.9375	98	0	9.9375	32
0.5	0.0625	5	0.5	0.0625	194	0.5	0.0625	20
0.5	0.1875	51	0.5	0.1875	63	0.5	0.1875	13
0.5	0.3125	16	0.5	0.3125	167	0.5	0.3125	51
0.5	0.4375	3	0.5	0.4375	173	0.5	0.4375	55
0.5	0.5625	12	0.5	0.5625	318	0.5	0.5625	335
0.5	0.6875	8	0.5	0.6875	501	0.5	0.6875	531
0.5	0.8125	6	0.5	0.8125	728	0.5	0.8125	115
0.5	0.9375	11	0.5	0.9375	103	0.5	0.9375	24
0.5	1.0625	12	0.5	1.0625	650	0.5	1.0625	14
0.5	1.1875	10	0.5	1.1875	518	0.5	1.1875	15
0.5	1.3125	11	0.5	1.3125	170	0.5	1.3125	18
0.5	1.4375	20	0.5	1.4375	915	0.5	1.4375	5

0.5	1.5625	15	0.5	1.5625	1856	0.5	1.5625	7
0.5	1.6875	25	0.5	1.6875	1135	0.5	1.6875	10
0.5	1.8125	55	0.5	1.8125	37	0.5	1.8125	3
0.5	1.9375	27	0.5	1.9375	31	0.5	1.9375	101
0.5	2.0625	43	0.5	2.0625	97	0.5	2.0625	394
0.5	2.1875	46	0.5	2.1875	161	0.5	2.1875	115
0.5	2.3125	36	0.5	2.3125	781	0.5	2.3125	171
0.5	2.4375	6	0.5	2.4375	854	0.5	2.4375	302
0.5	2.5625	4	0.5	2.5625	621	0.5	2.5625	217
0.5	2.6875	11	0.5	2.6875	681	0.5	2.6875	14
0.5	2.8125	3	0.5	2.8125	1551	0.5	2.8125	14
0.5	2.9375	7	0.5	2.9375	3090	0.5	2.9375	19
0.5	3.0625	39	0.5	3.0625	573	0.5	3.0625	100
0.5	3.1875	69	0.5	3.1875	242	0.5	3.1875	138
0.5	3.3125	79	0.5	3.3125	775	0.5	3.3125	52
0.5	3.4375	32	0.5	3.4375	762	0.5	3.4375	215
0.5	3.5625	21	0.5	3.5625	743	0.5	3.5625	205
0.5	3.6875	103	0.5	3.6875	122	0.5	3.6875	19
0.5	3.8125	11	0.5	3.8125	346	0.5	3.8125	29
0.5	3.9375	13	0.5	3.9375	2562	0.5	3.9375	50
0.5	4.0625	3	0.5	4.0625	3577	0.5	4.0625	45
0.5	4.1875	7	0.5	4.1875	581	0.5	4.1875	10
0.5	4.3125	34	0.5	4.3125	1701	0.5	4.3125	32
0.5	4.4375	20	0.5	4.4375	2102	0.5	4.4375	129
0.5	4.5625	17	0.5	4.5625	933	0.5	4.5625	93
0.5	4.6875	99	0.5	4.6875	238	0.5	4.6875	128
0.5	4.8125	79	0.5	4.8125	269	0.5	4.8125	19
0.5	4.9375	5	0.5	4.9375	1778	0.5	4.9375	308
0.5	5.0625	28	0.5	5.0625	1026	0.5	5.0625	375
0.5	5.1875	10	0.5	5.1875	843	0.5	5.1875	51
0.5	5.3125	23	0.5	5.3125	892	0.5	5.3125	149
0.5	5.4375	71	0.5	5.4375	1309	0.5	5.4375	227
0.5	5.5625	54	0.5	5.5625	1415	0.5	5.5625	247
0.5	5.6875	16	0.5	5.6875	2854	0.5	5.6875	64
0.5	5.8125	19	0.5	5.8125	1140	0.5	5.8125	36
0.5	5.9375	14	0.5	5.9375	1226	0.5	5.9375	69
0.5	6.0625	15	0.5	6.0625	252	0.5	6.0625	10
0.5	6.1875	9	0.5	6.1875	74	0.5	6.1875	5
0.5	6.3125	35	0.5	6.3125	978	0.5	6.3125	83
0.5	6.4375	37	0.5	6.4375	1063	0.5	6.4375	336
0.5	6.5625	194	0.5	6.5625	3954	0.5	6.5625	288
0.5	6.6875	108	0.5	6.6875	7505	0.5	6.6875	45
0.5	6.8125	85	0.5	6.8125	2419	0.5	6.8125	404
0.5	6.9375	7	0.5	6.9375	433	0.5	6.9375	856
0.5	7.0625	11	0.5	7.0625	2659	0.5	7.0625	373
0.5	7.1875	36	0.5	7.1875	963	0.5	7.1875	196
0.5	7.3125	15	0.5	7.3125	378	0.5	7.3125	177

0.5	7.4375	76	0.5	7.4375	129	0.5	7.4375	58
0.5	7.5625	55	0.5	7.5625	454	0.5	7.5625	123
0.5	7.6875	20	0.5	7.6875	1296	0.5	7.6875	72
0.5	7.8125	4	0.5	7.8125	443	0.5	7.8125	228
0.5	7.9375	14	0.5	7.9375	1315	0.5	7.9375	490
0.5	8.0625	16	0.5	8.0625	300	0.5	8.0625	619
0.5	8.1875	7	0.5	8.1875	186	0.5	8.1875	141
0.5	8.3125	54	0.5	8.3125	1319	0.5	8.3125	194
0.5	8.4375	34	0.5	8.4375	4588	0.5	8.4375	752
0.5	8.5625	2	0.5	8.5625	941	0.5	8.5625	548
0.5	8.6875	3	0.5	8.6875	416	0.5	8.6875	14
0.5	8.8125	10	0.5	8.8125	993	0.5	8.8125	48
0.5	8.9375	30	0.5	8.9375	902	0.5	8.9375	249
0.5	9.0625	3	0.5	9.0625	409	0.5	9.0625	851
0.5	9.1875	5	0.5	9.1875	2821	0.5	9.1875	330
0.5	9.3125	6	0.5	9.3125	920	0.5	9.3125	242
0.5	9.4375	23	0.5	9.4375	126	0.5	9.4375	41
0.5	9.5625	55	0.5	9.5625	281	0.5	9.5625	6
0.5	9.6875	5	0.5	9.6875	487	0.5	9.6875	6
0.5	9.8125	8	0.5	9.8125	8849	0.5	9.8125	77
0.5	9.9375	38	0.5	9.9375	15861	0.5	9.9375	44
1	0.0625	70	1	0.0625	3141	1	0.0625	51
1	0.1875	99	1	0.1875	2062	1	0.1875	20
1	0.3125	84	1	0.3125	715	1	0.3125	46
1	0.4375	24	1	0.4375	2722	1	0.4375	35
1	0.5625	17	1	0.5625	3090	1	0.5625	15
1	0.6875	11	1	0.6875	625	1	0.6875	12
1	0.8125	29	1	0.8125	606	1	0.8125	80
1	0.9375	47	1	0.9375	390	1	0.9375	48
1	1.0625	10	1	1.0625	325	1	1.0625	36
1	1.1875	37	1	1.1875	663	1	1.1875	80
1	1.3125	14	1	1.3125	5511	1	1.3125	13
1	1.4375	14	1	1.4375	1922	1	1.4375	33
1	1.5625	27	1	1.5625	981	1	1.5625	26
1	1.6875	42	1	1.6875	382	1	1.6875	27
1	1.8125	35	1	1.8125	8358	1	1.8125	10
1	1.9375	8	1	1.9375	14476	1	1.9375	21
1	2.0625	0	1	2.0625	1177	1	2.0625	66
1	2.1875	2	1	2.1875	5977	1	2.1875	37
1	2.3125	1	1	2.3125	6910	1	2.3125	10
1	2.4375	3	1	2.4375	1714	1	2.4375	12
1	2.5625	1	1	2.5625	1327	1	2.5625	204
1	2.6875	3	1	2.6875	58	1	2.6875	262
1	2.8125	9	1	2.8125	167	1	2.8125	38
1	2.9375	10	1	2.9375	628	1	2.9375	42
1	3.0625	6	1	3.0625	276	1	3.0625	214
1	3.1875	21	1	3.1875	138	1	3.1875	45

1	3.3125	24	1	3.3125	191	1	3.3125	82
1	3.4375	58	1	3.4375	163	1	3.4375	740
1	3.5625	15	1	3.5625	410	1	3.5625	431
1	3.6875	8	1	3.6875	238	1	3.6875	16
1	3.8125	18	1	3.8125	238	1	3.8125	13
1	3.9375	16	1	3.9375	2751	1	3.9375	106
1	4.0625	66	1	4.0625	1741	1	4.0625	25
1	4.1875	50	1	4.1875	1117	1	4.1875	14
1	4.3125	15	1	4.3125	695	1	4.3125	25
1	4.4375	20	1	4.4375	3379	1	4.4375	133
1	4.5625	17	1	4.5625	5563	1	4.5625	77
1	4.6875	19	1	4.6875	923	1	4.6875	9
1	4.8125	12	1	4.8125	3742	1	4.8125	11
1	4.9375	62	1	4.9375	4776	1	4.9375	22
1	5.0625	78	1	5.0625	570	1	5.0625	19
1	5.1875	45	1	5.1875	1032	1	5.1875	3
1	5.3125	8	1	5.3125	536	1	5.3125	7
1	5.4375	45	1	5.4375	945	1	5.4375	10
1	5.5625	88	1	5.5625	928	1	5.5625	3
1	5.6875	176	1	5.6875	346	1	5.6875	2
1	5.8125	98	1	5.8125	356	1	5.8125	6
1	5.9375	26	1	5.9375	1080	1	5.9375	20
1	6.0625	35	1	6.0625	7152	1	6.0625	20
1	6.1875	28	1	6.1875	4168	1	6.1875	7
1	6.3125	22	1	6.3125	1059	1	6.3125	9
1	6.4375	12	1	6.4375	3733	1	6.4375	78
1	6.5625	157	1	6.5625	7010	1	6.5625	44
1	6.6875	88	1	6.6875	4192	1	6.6875	14
1	6.8125	45	1	6.8125	1240	1	6.8125	24
1	6.9375	15	1	6.9375	873	1	6.9375	29
1	7.0625	25	1	7.0625	214	1	7.0625	16
1	7.1875	4	1	7.1875	1320	1	7.1875	110
1	7.3125	30	1	7.3125	1786	1	7.3125	169
1	7.4375	7	1	7.4375	62	1	7.4375	66
1	7.5625	16	1	7.5625	61	1	7.5625	14
1	7.6875	65	1	7.6875	315	1	7.6875	80
1	7.8125	60	1	7.8125	366	1	7.8125	91
1	7.9375	59	1	7.9375	106	1	7.9375	48
1	8.0625	4	1	8.0625	1383	1	8.0625	77
1	8.1875	21	1	8.1875	991	1	8.1875	26
1	8.3125	40	1	8.3125	4845	1	8.3125	6
1	8.4375	98	1	8.4375	4290	1	8.4375	7
1	8.5625	41	1	8.5625	461	1	8.5625	10
1	8.6875	12	1	8.6875	603	1	8.6875	63
1	8.8125	6	1	8.8125	847	1	8.8125	77
1	8.9375	59	1	8.9375	3232	1	8.9375	105
1	9.0625	148	1	9.0625	749	1	9.0625	59

1	9.1875	116	1	9.1875	139	1	9.1875	138
1	9.3125	16	1	9.3125	867	1	9.3125	133
1	9.4375	14	1	9.4375	611	1	9.4375	170
1	9.5625	48	1	9.5625	189	1	9.5625	311
1	9.6875	7	1	9.6875	222	1	9.6875	122
1	9.8125	39	1	9.8125	142	1	9.8125	782
1	9.9375	66	1	9.9375	165	1	9.9375	335
1.5	0.0625	168	1.5	0.0625	194	1.5	0.0625	45
1.5	0.1875	112	1.5	0.1875	726	1.5	0.1875	335
1.5	0.3125	39	1.5	0.3125	4316	1.5	0.3125	519
1.5	0.4375	54	1.5	0.4375	3598	1.5	0.4375	295
1.5	0.5625	142	1.5	0.5625	921	1.5	0.5625	567
1.5	0.6875	53	1.5	0.6875	194	1.5	0.6875	71
1.5	0.8125	12	1.5	0.8125	34	1.5	0.8125	6
1.5	0.9375	14	1.5	0.9375	527	1.5	0.9375	127
1.5	1.0625	24	1.5	1.0625	2712	1.5	1.0625	127
1.5	1.1875	2	1.5	1.1875	654	1.5	1.1875	185
1.5	1.3125	5	1.5	1.3125	424	1.5	1.3125	472
1.5	1.4375	9	1.5	1.4375	445	1.5	1.4375	187
1.5	1.5625	63	1.5	1.5625	360	1.5	1.5625	5
1.5	1.6875	287	1.5	1.6875	1023	1.5	1.6875	64
1.5	1.8125	160	1.5	1.8125	334	1.5	1.8125	108
1.5	1.9375	19	1.5	1.9375	2934	1.5	1.9375	58
1.5	2.0625	58	1.5	2.0625	5033	1.5	2.0625	221
1.5	2.1875	64	1.5	2.1875	801	1.5	2.1875	319
1.5	2.3125	97	1.5	2.3125	524	1.5	2.3125	19
1.5	2.4375	158	1.5	2.4375	6	1.5	2.4375	74
1.5	2.5625	121	1.5	2.5625	646	1.5	2.5625	67
1.5	2.6875	3	1.5	2.6875	468	1.5	2.6875	53
1.5	2.8125	25	1.5	2.8125	407	1.5	2.8125	61
1.5	2.9375	9	1.5	2.9375	763	1.5	2.9375	35
1.5	3.0625	35	1.5	3.0625	119	1.5	3.0625	331
1.5	3.1875	13	1.5	3.1875	413	1.5	3.1875	280
1.5	3.3125	97	1.5	3.3125	2903	1.5	3.3125	54
1.5	3.4375	188	1.5	3.4375	1672	1.5	3.4375	951
1.5	3.5625	11	1.5	3.5625	3216	1.5	3.5625	1113
1.5	3.6875	88	1.5	3.6875	433	1.5	3.6875	244
1.5	3.8125	20	1.5	3.8125	1212	1.5	3.8125	215
1.5	3.9375	8	1.5	3.9375	1956	1.5	3.9375	36
1.5	4.0625	1	1.5	4.0625	814	1.5	4.0625	13
1.5	4.1875	5	1.5	4.1875	1405	1.5	4.1875	268
1.5	4.3125	22	1.5	4.3125	4634	1.5	4.3125	257
1.5	4.4375	16	1.5	4.4375	1316	1.5	4.4375	9
1.5	4.5625	198	1.5	4.5625	94	1.5	4.5625	10
1.5	4.6875	105	1.5	4.6875	549	1.5	4.6875	164
1.5	4.8125	93	1.5	4.8125	955	1.5	4.8125	145
1.5	4.9375	12	1.5	4.9375	709	1.5	4.9375	156

1.5	5.0625	7	1.5	5.0625	2687	1.5	5.0625	287
1.5	5.1875	16	1.5	5.1875	763	1.5	5.1875	116
1.5	5.3125	9	1.5	5.3125	1922	1.5	5.3125	48
1.5	5.4375	10	1.5	5.4375	435	1.5	5.4375	158
1.5	5.5625	22	1.5	5.5625	331	1.5	5.5625	643
1.5	5.6875	16	1.5	5.6875	262	1.5	5.6875	271
1.5	5.8125	28	1.5	5.8125	82	1.5	5.8125	627
1.5	5.9375	18	1.5	5.9375	1615	1.5	5.9375	1577
1.5	6.0625	21	1.5	6.0625	3137	1.5	6.0625	1086
1.5	6.1875	132	1.5	6.1875	594	1.5	6.1875	179
1.5	6.3125	47	1.5	6.3125	400	1.5	6.3125	735
1.5	6.4375	24	1.5	6.4375	445	1.5	6.4375	656
1.5	6.5625	107	1.5	6.5625	42	1.5	6.5625	59
1.5	6.6875	19	1.5	6.6875	117	1.5	6.6875	86
1.5	6.8125	9	1.5	6.8125	260	1.5	6.8125	172
1.5	6.9375	0	1.5	6.9375	299	1.5	6.9375	80
1.5	7.0625	9	1.5	7.0625	161	1.5	7.0625	11
1.5	7.1875	14	1.5	7.1875	593	1.5	7.1875	8
1.5	7.3125	29	1.5	7.3125	442	1.5	7.3125	38
1.5	7.4375	76	1.5	7.4375	590	1.5	7.4375	17
1.5	7.5625	11	1.5	7.5625	1076	1.5	7.5625	5
1.5	7.6875	38	1.5	7.6875	899	1.5	7.6875	39
1.5	7.8125	19	1.5	7.8125	10831	1.5	7.8125	109
1.5	7.9375	60	1.5	7.9375	9433	1.5	7.9375	124
1.5	8.0625	32	1.5	8.0625	917	1.5	8.0625	28
1.5	8.1875	31	1.5	8.1875	2940	1.5	8.1875	173
1.5	8.3125	67	1.5	8.3125	585	1.5	8.3125	201
1.5	8.4375	116	1.5	8.4375	252	1.5	8.4375	113
1.5	8.5625	88	1.5	8.5625	636	1.5	8.5625	97
1.5	8.6875	10	1.5	8.6875	50	1.5	8.6875	795
1.5	8.8125	27	1.5	8.8125	156	1.5	8.8125	219
1.5	8.9375	34	1.5	8.9375	1566	1.5	8.9375	187
1.5	9.0625	39	1.5	9.0625	1704	1.5	9.0625	194
1.5	9.1875	4	1.5	9.1875	741	1.5	9.1875	93
1.5	9.3125	3	1.5	9.3125	3318	1.5	9.3125	304
1.5	9.4375	25	1.5	9.4375	4809	1.5	9.4375	259
1.5	9.5625	47	1.5	9.5625	1748	1.5	9.5625	101
1.5	9.6875	32	1.5	9.6875	6848	1.5	9.6875	162
1.5	9.8125	22	1.5	9.8125	3940	1.5	9.8125	87
1.5	9.9375	1	1.5	9.9375	7918	1.5	9.9375	246
2	0.0625	72	2	0.0625	583	2	0.0625	415
2	0.1875	24	2	0.1875	675	2	0.1875	129
2	0.3125	12	2	0.3125	963	2	0.3125	48
2	0.4375	14	2	0.4375	989	2	0.4375	33
2	0.5625	24	2	0.5625	301	2	0.5625	14
2	0.6875	39	2	0.6875	352	2	0.6875	3
2	0.8125	21	2	0.8125	233	2	0.8125	40

2	0.9375	42	2	0.9375	757	2	0.9375	32
2	1.0625	1	2	1.0625	181	2	1.0625	17
2	1.1875	7	2	1.1875	956	2	1.1875	8
2	1.3125	7	2	1.3125	2642	2	1.3125	118
2	1.4375	11	2	1.4375	2064	2	1.4375	263
2	1.5625	22	2	1.5625	1022	2	1.5625	107
2	1.6875	10	2	1.6875	78	2	1.6875	26
2	1.8125	10	2	1.8125	82	2	1.8125	19
2	1.9375	15	2	1.9375	50	2	1.9375	89
2	2.0625	16	2	2.0625	283	2	2.0625	48
2	2.1875	4	2	2.1875	131	2	2.1875	12
2	2.3125	6	2	2.3125	178	2	2.3125	22
2	2.4375	40	2	2.4375	437	2	2.4375	138
2	2.5625	10	2	2.5625	631	2	2.5625	115
2	2.6875	3	2	2.6875	482	2	2.6875	176
2	2.8125	29	2	2.8125	165	2	2.8125	46
2	2.9375	6	2	2.9375	1086	2	2.9375	9
2	3.0625	7	2	3.0625	2806	2	3.0625	71
2	3.1875	42	2	3.1875	490	2	3.1875	309
2	3.3125	68	2	3.3125	334	2	3.3125	397
2	3.4375	20	2	3.4375	114	2	3.4375	33
2	3.5625	26	2	3.5625	201	2	3.5625	19
2	3.6875	21	2	3.6875	269	2	3.6875	25
2	3.8125	29	2	3.8125	1317	2	3.8125	10
2	3.9375	35	2	3.9375	2281	2	3.9375	54
2	4.0625	9	2	4.0625	220	2	4.0625	42
2	4.1875	5	2	4.1875	657	2	4.1875	89
2	4.3125	101	2	4.3125	195	2	4.3125	33
2	4.4375	279	2	4.4375	1368	2	4.4375	20
2	4.5625	81	2	4.5625	881	2	4.5625	56
2	4.6875	3	2	4.6875	256	2	4.6875	21
2	4.8125	3	2	4.8125	760	2	4.8125	19
2	4.9375	115	2	4.9375	227	2	4.9375	18
2	5.0625	299	2	5.0625	70	2	5.0625	30
2	5.1875	55	2	5.1875	485	2	5.1875	42
2	5.3125	76	2	5.3125	264	2	5.3125	211
2	5.4375	18	2	5.4375	143	2	5.4375	251
2	5.5625	113	2	5.5625	1127	2	5.5625	66
2	5.6875	93	2	5.6875	320	2	5.6875	130
2	5.8125	3	2	5.8125	162	2	5.8125	30
2	5.9375	10	2	5.9375	446	2	5.9375	13
2	6.0625	10	2	6.0625	326	2	6.0625	69
2	6.1875	78	2	6.1875	857	2	6.1875	76
2	6.3125	120	2	6.3125	3292	2	6.3125	24
2	6.4375	35	2	6.4375	2273	2	6.4375	8
2	6.5625	107	2	6.5625	301	2	6.5625	5
2	6.6875	26	2	6.6875	1950	2	6.6875	15

2	6.8125	25	2	6.8125	3653	2	6.8125	9
2	6.9375	26	2	6.9375	334	2	6.9375	8
2	7.0625	15	2	7.0625	472	2	7.0625	12
2	7.1875	27	2	7.1875	1474	2	7.1875	12
2	7.3125	6	2	7.3125	863	2	7.3125	13
2	7.4375	24	2	7.4375	21	2	7.4375	42
2	7.5625	34	2	7.5625	533	2	7.5625	45
2	7.6875	8	2	7.6875	3066	2	7.6875	6
2	7.8125	39	2	7.8125	843	2	7.8125	19
2	7.9375	13	2	7.9375	2536	2	7.9375	29
2	8.0625	50	2	8.0625	2276	2	8.0625	36
2	8.1875	316	2	8.1875	1685	2	8.1875	97
2	8.3125	191	2	8.3125	604	2	8.3125	54
2	8.4375	135	2	8.4375	1312	2	8.4375	7
2	8.5625	35	2	8.5625	2344	2	8.5625	23
2	8.6875	63	2	8.6875	3102	2	8.6875	58
2	8.8125	114	2	8.8125	757	2	8.8125	131
2	8.9375	73	2	8.9375	229	2	8.9375	80
2	9.0625	39	2	9.0625	746	2	9.0625	421
2	9.1875	35	2	9.1875	2164	2	9.1875	239
2	9.3125	20	2	9.3125	508	2	9.3125	22
2	9.4375	11	2	9.4375	206	2	9.4375	8
2	9.5625	41	2	9.5625	1374	2	9.5625	70
2	9.6875	48	2	9.6875	322	2	9.6875	73
2	9.8125	72	2	9.8125	125	2	9.8125	39
2	9.9375	14	2	9.9375	554	2	9.9375	208
2.5	0.0625	7	2.5	0.0625	5324	2.5	0.0625	190
2.5	0.1875	14	2.5	0.1875	4200	2.5	0.1875	55
2.5	0.3125	8	2.5	0.3125	4602	2.5	0.3125	8
2.5	0.4375	15	2.5	0.4375	4878	2.5	0.4375	17
2.5	0.5625	50	2.5	0.5625	5532	2.5	0.5625	122
2.5	0.6875	23	2.5	0.6875	912	2.5	0.6875	115
2.5	0.8125	10	2.5	0.8125	3706	2.5	0.8125	66
2.5	0.9375	39	2.5	0.9375	2925	2.5	0.9375	46
2.5	1.0625	14	2.5	1.0625	3405	2.5	1.0625	268
2.5	1.1875	7	2.5	1.1875	4719	2.5	1.1875	721
2.5	1.3125	19	2.5	1.3125	2006	2.5	1.3125	199
2.5	1.4375	16	2.5	1.4375	466	2.5	1.4375	25
2.5	1.5625	9	2.5	1.5625	606	2.5	1.5625	58
2.5	1.6875	15	2.5	1.6875	129	2.5	1.6875	14
2.5	1.8125	34	2.5	1.8125	2835	2.5	1.8125	55
2.5	1.9375	6	2.5	1.9375	5059	2.5	1.9375	151
2.5	2.0625	3	2.5	2.0625	203	2.5	2.0625	28
2.5	2.1875	3	2.5	2.1875	254	2.5	2.1875	159
2.5	2.3125	8	2.5	2.3125	628	2.5	2.3125	89
2.5	2.4375	6	2.5	2.4375	326	2.5	2.4375	154
2.5	2.5625	9	2.5	2.5625	5706	2.5	2.5625	11

2.5	2.6875	2	2.5	2.6875	6424	2.5	2.6875	79
2.5	2.8125	5	2.5	2.8125	662	2.5	2.8125	39
2.5	2.9375	46	2.5	2.9375	4473	2.5	2.9375	6
2.5	3.0625	137	2.5	3.0625	1800	2.5	3.0625	62
2.5	3.1875	186	2.5	3.1875	11189	2.5	3.1875	113
2.5	3.3125	91	2.5	3.3125	10591	2.5	3.3125	49
2.5	3.4375	59	2.5	3.4375	574	2.5	3.4375	122
2.5	3.5625	38	2.5	3.5625	555	2.5	3.5625	14
2.5	3.6875	123	2.5	3.6875	571	2.5	3.6875	8
2.5	3.8125	252	2.5	3.8125	1693	2.5	3.8125	116
2.5	3.9375	68	2.5	3.9375	1180	2.5	3.9375	236
2.5	4.0625	20	2.5	4.0625	169	2.5	4.0625	181
2.5	4.1875	10	2.5	4.1875	566	2.5	4.1875	404
2.5	4.3125	16	2.5	4.3125	1518	2.5	4.3125	56
2.5	4.4375	84	2.5	4.4375	3184	2.5	4.4375	199
2.5	4.5625	204	2.5	4.5625	2108	2.5	4.5625	57
2.5	4.6875	61	2.5	4.6875	294	2.5	4.6875	13
2.5	4.8125	6	2.5	4.8125	1324	2.5	4.8125	22
2.5	4.9375	52	2.5	4.9375	1237	2.5	4.9375	42
2.5	5.0625	32	2.5	5.0625	1377	2.5	5.0625	102
2.5	5.1875	41	2.5	5.1875	1927	2.5	5.1875	148
2.5	5.3125	47	2.5	5.3125	517	2.5	5.3125	90
2.5	5.4375	23	2.5	5.4375	752	2.5	5.4375	49
2.5	5.5625	44	2.5	5.5625	173	2.5	5.5625	32
2.5	5.6875	62	2.5	5.6875	113	2.5	5.6875	104
2.5	5.8125	5	2.5	5.8125	869	2.5	5.8125	49
2.5	5.9375	10	2.5	5.9375	2168	2.5	5.9375	46
2.5	6.0625	16	2.5	6.0625	247	2.5	6.0625	7
2.5	6.1875	51	2.5	6.1875	960	2.5	6.1875	12
2.5	6.3125	48	2.5	6.3125	1818	2.5	6.3125	32
2.5	6.4375	57	2.5	6.4375	276	2.5	6.4375	74
2.5	6.5625	69	2.5	6.5625	1524	2.5	6.5625	262
2.5	6.6875	2	2.5	6.6875	1492	2.5	6.6875	175
2.5	6.8125	6	2.5	6.8125	117	2.5	6.8125	30
2.5	6.9375	57	2.5	6.9375	101	2.5	6.9375	21
2.5	7.0625	32	2.5	7.0625	1200	2.5	7.0625	39
2.5	7.1875	40	2.5	7.1875	805	2.5	7.1875	237
2.5	7.3125	131	2.5	7.3125	146	2.5	7.3125	36
2.5	7.4375	12	2.5	7.4375	130	2.5	7.4375	19
2.5	7.5625	18	2.5	7.5625	187	2.5	7.5625	43
2.5	7.6875	2	2.5	7.6875	599	2.5	7.6875	34
2.5	7.8125	4	2.5	7.8125	789	2.5	7.8125	166
2.5	7.9375	9	2.5	7.9375	159	2.5	7.9375	129
2.5	8.0625	28	2.5	8.0625	438	2.5	8.0625	34
2.5	8.1875	6	2.5	8.1875	489	2.5	8.1875	26
2.5	8.3125	14	2.5	8.3125	18	2.5	8.3125	27
2.5	8.4375	11	2.5	8.4375	270	2.5	8.4375	16

2.5	8.5625	14	2.5	8.5625	1359	2.5	8.5625	20
2.5	8.6875	30	2.5	8.6875	2558	2.5	8.6875	52
2.5	8.8125	3	2.5	8.8125	1120	2.5	8.8125	12
2.5	8.9375	25	2.5	8.9375	472	2.5	8.9375	46
2.5	9.0625	29	2.5	9.0625	95	2.5	9.0625	159
2.5	9.1875	75	2.5	9.1875	1216	2.5	9.1875	1209
2.5	9.3125	29	2.5	9.3125	1329	2.5	9.3125	1030
2.5	9.4375	4	2.5	9.4375	129	2.5	9.4375	720
2.5	9.5625	8	2.5	9.5625	337	2.5	9.5625	190
2.5	9.6875	15	2.5	9.6875	133	2.5	9.6875	1194
2.5	9.8125	17	2.5	9.8125	1128	2.5	9.8125	3028
2.5	9.9375	20	2.5	9.9375	7061	2.5	9.9375	1610
3	0.0625	55	3	0.0625	4062	3	0.0625	151
3	0.1875	22	3	0.1875	1364	3	0.1875	348
3	0.3125	7	3	0.3125	469	3	0.3125	153
3	0.4375	4	3	0.4375	158	3	0.4375	14
3	0.5625	82	3	0.5625	1266	3	0.5625	24
3	0.6875	26	3	0.6875	3957	3	0.6875	10
3	0.8125	92	3	0.8125	3147	3	0.8125	45
3	0.9375	121	3	0.9375	1084	3	0.9375	46
3	1.0625	31	3	1.0625	6911	3	1.0625	46
3	1.1875	14	3	1.1875	9579	3	1.1875	351
3	1.3125	46	3	1.3125	3412	3	1.3125	498
3	1.4375	3	3	1.4375	175	3	1.4375	252
3	1.5625	22	3	1.5625	202	3	1.5625	537
3	1.6875	15	3	1.6875	436	3	1.6875	781
3	1.8125	6	3	1.8125	39	3	1.8125	274
3	1.9375	41	3	1.9375	33	3	1.9375	10
3	2.0625	23	3	2.0625	2678	3	2.0625	97
3	2.1875	66	3	2.1875	5231	3	2.1875	327
3	2.3125	52	3	2.3125	725	3	2.3125	52
3	2.4375	34	3	2.4375	1744	3	2.4375	49
3	2.5625	65	3	2.5625	645	3	2.5625	720
3	2.6875	144	3	2.6875	1272	3	2.6875	935
3	2.8125	150	3	2.8125	193	3	2.8125	275
3	2.9375	21	3	2.9375	1050	3	2.9375	26
3	3.0625	6	3	3.0625	359	3	3.0625	14
3	3.1875	5	3	3.1875	441	3	3.1875	8
3	3.3125	14	3	3.3125	233	3	3.3125	38
3	3.4375	21	3	3.4375	190	3	3.4375	81
3	3.5625	5	3	3.5625	358	3	3.5625	16
3	3.6875	23	3	3.6875	122	3	3.6875	32
3	3.8125	11	3	3.8125	258	3	3.8125	41
3	3.9375	17	3	3.9375	66	3	3.9375	56
3	4.0625	53	3	4.0625	13	3	4.0625	34
3	4.1875	59	3	4.1875	910	3	4.1875	174
3	4.3125	223	3	4.3125	2854	3	4.3125	258

3	4.4375	171	3	4.4375	1144	3	4.4375	35
3	4.5625	30	3	4.5625	424	3	4.5625	267
3	4.6875	0	3	4.6875	4460	3	4.6875	441
3	4.8125	24	3	4.8125	3273	3	4.8125	175
3	4.9375	139	3	4.9375	2209	3	4.9375	41
3	5.0625	40	3	5.0625	1319	3	5.0625	97
3	5.1875	1	3	5.1875	83	3	5.1875	55
3	5.3125	10	3	5.3125	1450	3	5.3125	79
3	5.4375	7	3	5.4375	3164	3	5.4375	75
3	5.5625	11	3	5.5625	3668	3	5.5625	137
3	5.6875	55	3	5.6875	667	3	5.6875	41
3	5.8125	6	3	5.8125	181	3	5.8125	46
3	5.9375	23	3	5.9375	109	3	5.9375	293
3	6.0625	111	3	6.0625	140	3	6.0625	80
3	6.1875	30	3	6.1875	1839	3	6.1875	102
3	6.3125	10	3	6.3125	804	3	6.3125	31
3	6.4375	111	3	6.4375	1389	3	6.4375	41
3	6.5625	59	3	6.5625	2752	3	6.5625	13
3	6.6875	61	3	6.6875	1153	3	6.6875	105
3	6.8125	24	3	6.8125	95	3	6.8125	165
3	6.9375	27	3	6.9375	669	3	6.9375	60
3	7.0625	110	3	7.0625	2551	3	7.0625	133
3	7.1875	174	3	7.1875	684	3	7.1875	233
3	7.3125	3	3	7.3125	97	3	7.3125	612
3	7.4375	2	3	7.4375	304	3	7.4375	1115
3	7.5625	58	3	7.5625	1745	3	7.5625	399
3	7.6875	51	3	7.6875	2426	3	7.6875	124
3	7.8125	10	3	7.8125	773	3	7.8125	185
3	7.9375	3	3	7.9375	163	3	7.9375	165
3	8.0625	19	3	8.0625	535	3	8.0625	251
3	8.1875	49	3	8.1875	197	3	8.1875	94
3	8.3125	6	3	8.3125	750	3	8.3125	10
3	8.4375	34	3	8.4375	310	3	8.4375	24
3	8.5625	69	3	8.5625	38	3	8.5625	15
3	8.6875	68	3	8.6875	316	3	8.6875	24
3	8.8125	67	3	8.8125	278	3	8.8125	46
3	8.9375	9	3	8.9375	135	3	8.9375	86
3	9.0625	32	3	9.0625	1014	3	9.0625	295
3	9.1875	97	3	9.1875	2404	3	9.1875	125
3	9.3125	68	3	9.3125	1966	3	9.3125	121
3	9.4375	16	3	9.4375	261	3	9.4375	154
3	9.5625	6	3	9.5625	858	3	9.5625	79
3	9.6875	1	3	9.6875	1196	3	9.6875	37
3	9.8125	1	3	9.8125	826	3	9.8125	56
3	9.9375	14	3	9.9375	102	3	9.9375	238
3.5	0.0625	65	3.5	0.0625	3254	3.5	0.0625	737
3.5	0.1875	44	3.5	0.1875	849	3.5	0.1875	206

3.5	0.3125	27	3.5	0.3125	1216	3.5	0.3125	112
3.5	0.4375	74	3.5	0.4375	1182	3.5	0.4375	58
3.5	0.5625	288	3.5	0.5625	1350	3.5	0.5625	112
3.5	0.6875	319	3.5	0.6875	6711	3.5	0.6875	281
3.5	0.8125	42	3.5	0.8125	1792	3.5	0.8125	54
3.5	0.9375	87	3.5	0.9375	187	3.5	0.9375	19
3.5	1.0625	31	3.5	1.0625	1233	3.5	1.0625	145
3.5	1.1875	89	3.5	1.1875	4084	3.5	1.1875	27
3.5	1.3125	61	3.5	1.3125	2053	3.5	1.3125	20
3.5	1.4375	3	3.5	1.4375	4768	3.5	1.4375	10
3.5	1.5625	5	3.5	1.5625	1105	3.5	1.5625	15
3.5	1.6875	36	3.5	1.6875	1185	3.5	1.6875	469
3.5	1.8125	86	3.5	1.8125	483	3.5	1.8125	398
3.5	1.9375	9	3.5	1.9375	1849	3.5	1.9375	184
3.5	2.0625	22	3.5	2.0625	1001	3.5	2.0625	126
3.5	2.1875	58	3.5	2.1875	3783	3.5	2.1875	91
3.5	2.3125	18	3.5	2.3125	3265	3.5	2.3125	258
3.5	2.4375	5	3.5	2.4375	972	3.5	2.4375	36
3.5	2.5625	6	3.5	2.5625	782	3.5	2.5625	261
3.5	2.6875	41	3.5	2.6875	398	3.5	2.6875	721
3.5	2.8125	104	3.5	2.8125	1466	3.5	2.8125	171
3.5	2.9375	59	3.5	2.9375	1464	3.5	2.9375	35
3.5	3.0625	87	3.5	3.0625	611	3.5	3.0625	9
3.5	3.1875	80	3.5	3.1875	161	3.5	3.1875	39
3.5	3.3125	32	3.5	3.3125	54	3.5	3.3125	37
3.5	3.4375	4	3.5	3.4375	339	3.5	3.4375	59
3.5	3.5625	5	3.5	3.5625	161	3.5	3.5625	283
3.5	3.6875	15	3.5	3.6875	940	3.5	3.6875	93
3.5	3.8125	39	3.5	3.8125	5142	3.5	3.8125	52
3.5	3.9375	16	3.5	3.9375	4772	3.5	3.9375	78
3.5	4.0625	55	3.5	4.0625	355	3.5	4.0625	307
3.5	4.1875	43	3.5	4.1875	1810	3.5	4.1875	79
3.5	4.3125	154	3.5	4.3125	6744	3.5	4.3125	17
3.5	4.4375	22	3.5	4.4375	6035	3.5	4.4375	44
3.5	4.5625	98	3.5	4.5625	1085	3.5	4.5625	103
3.5	4.6875	23	3.5	4.6875	1579	3.5	4.6875	258
3.5	4.8125	64	3.5	4.8125	151	3.5	4.8125	426
3.5	4.9375	80	3.5	4.9375	235	3.5	4.9375	131
3.5	5.0625	18	3.5	5.0625	383	3.5	5.0625	20
3.5	5.1875	26	3.5	5.1875	3916	3.5	5.1875	33
3.5	5.3125	12	3.5	5.3125	3572	3.5	5.3125	126
3.5	5.4375	9	3.5	5.4375	459	3.5	5.4375	37
3.5	5.5625	30	3.5	5.5625	556	3.5	5.5625	158
3.5	5.6875	2	3.5	5.6875	552	3.5	5.6875	82
3.5	5.8125	16	3.5	5.8125	3867	3.5	5.8125	193
3.5	5.9375	28	3.5	5.9375	5676	3.5	5.9375	13
3.5	6.0625	8	3.5	6.0625	376	3.5	6.0625	50

3.5	6.1875	10	3.5	6.1875	66	3.5	6.1875	197
3.5	6.3125	49	3.5	6.3125	312	3.5	6.3125	90
3.5	6.4375	7	3.5	6.4375	7027	3.5	6.4375	97
3.5	6.5625	6	3.5	6.5625	7460	3.5	6.5625	167
3.5	6.6875	11	3.5	6.6875	384	3.5	6.6875	12
3.5	6.8125	76	3.5	6.8125	237	3.5	6.8125	37
3.5	6.9375	102	3.5	6.9375	2029	3.5	6.9375	64
3.5	7.0625	18	3.5	7.0625	3215	3.5	7.0625	40
3.5	7.1875	9	3.5	7.1875	793	3.5	7.1875	61
3.5	7.3125	40	3.5	7.3125	453	3.5	7.3125	87
3.5	7.4375	21	3.5	7.4375	1300	3.5	7.4375	83
3.5	7.5625	1	3.5	7.5625	1349	3.5	7.5625	60
3.5	7.6875	28	3.5	7.6875	1610	3.5	7.6875	48
3.5	7.8125	8	3.5	7.8125	5176	3.5	7.8125	102
3.5	7.9375	13	3.5	7.9375	2359	3.5	7.9375	58
3.5	8.0625	10	3.5	8.0625	1455	3.5	8.0625	18
3.5	8.1875	28	3.5	8.1875	3012	3.5	8.1875	64
3.5	8.3125	22	3.5	8.3125	3244	3.5	8.3125	88
3.5	8.4375	6	3.5	8.4375	823	3.5	8.4375	24
3.5	8.5625	3	3.5	8.5625	468	3.5	8.5625	55
3.5	8.6875	27	3.5	8.6875	1180	3.5	8.6875	27
3.5	8.8125	23	3.5	8.8125	753	3.5	8.8125	7
3.5	8.9375	53	3.5	8.9375	829	3.5	8.9375	9
3.5	9.0625	76	3.5	9.0625	3474	3.5	9.0625	33
3.5	9.1875	24	3.5	9.1875	1660	3.5	9.1875	38
3.5	9.3125	5	3.5	9.3125	799	3.5	9.3125	49
3.5	9.4375	3	3.5	9.4375	527	3.5	9.4375	81
3.5	9.5625	5	3.5	9.5625	1756	3.5	9.5625	48
3.5	9.6875	9	3.5	9.6875	887	3.5	9.6875	67
3.5	9.8125	17	3.5	9.8125	5562	3.5	9.8125	89
3.5	9.9375	8	3.5	9.9375	15857	3.5	9.9375	423
4	0.0625	47	4	0.0625	4873	4	0.0625	115
4	0.1875	116	4	0.1875	677	4	0.1875	68
4	0.3125	17	4	0.3125	83	4	0.3125	126
4	0.4375	20	4	0.4375	1243	4	0.4375	17
4	0.5625	83	4	0.5625	2046	4	0.5625	26
4	0.6875	81	4	0.6875	321	4	0.6875	8
4	0.8125	2	4	0.8125	1553	4	0.8125	25
4	0.9375	7	4	0.9375	1201	4	0.9375	31
4	1.0625	4	4	1.0625	1487	4	1.0625	11
4	1.1875	12	4	1.1875	1352	4	1.1875	63
4	1.3125	48	4	1.3125	724	4	1.3125	20
4	1.4375	45	4	1.4375	45	4	1.4375	43
4	1.5625	45	4	1.5625	737	4	1.5625	103
4	1.6875	2	4	1.6875	3352	4	1.6875	213
4	1.8125	7	4	1.8125	3267	4	1.8125	134
4	1.9375	20	4	1.9375	1118	4	1.9375	31

4	2.0625	14	4	2.0625	243	4	2.0625	335
4	2.1875	26	4	2.1875	35	4	2.1875	631
4	2.3125	15	4	2.3125	1697	4	2.3125	320
4	2.4375	79	4	2.4375	1419	4	2.4375	52
4	2.5625	50	4	2.5625	534	4	2.5625	35
4	2.6875	85	4	2.6875	377	4	2.6875	298
4	2.8125	45	4	2.8125	1066	4	2.8125	117
4	2.9375	7	4	2.9375	733	4	2.9375	6
4	3.0625	4	4	3.0625	1814	4	3.0625	4
4	3.1875	7	4	3.1875	1450	4	3.1875	9
4	3.3125	48	4	3.3125	221	4	3.3125	65
4	3.4375	5	4	3.4375	303	4	3.4375	26
4	3.5625	20	4	3.5625	159	4	3.5625	14
4	3.6875	67	4	3.6875	186	4	3.6875	42
4	3.8125	55	4	3.8125	4092	4	3.8125	194
4	3.9375	269	4	3.9375	5673	4	3.9375	194
4	4.0625	121	4	4.0625	475	4	4.0625	18
4	4.1875	26	4	4.1875	133	4	4.1875	136
4	4.3125	22	4	4.3125	539	4	4.3125	255
4	4.4375	88	4	4.4375	422	4	4.4375	140
4	4.5625	27	4	4.5625	491	4	4.5625	40
4	4.6875	59	4	4.6875	1328	4	4.6875	2
4	4.8125	50	4	4.8125	330	4	4.8125	6
4	4.9375	23	4	4.9375	194	4	4.9375	16
4	5.0625	52	4	5.0625	43	4	5.0625	127
4	5.1875	30	4	5.1875	41	4	5.1875	84
4	5.3125	44	4	5.3125	26	4	5.3125	5
4	5.4375	20	4	5.4375	267	4	5.4375	41
4	5.5625	3	4	5.5625	1169	4	5.5625	23
4	5.6875	59	4	5.6875	516	4	5.6875	18
4	5.8125	217	4	5.8125	621	4	5.8125	33
4	5.9375	54	4	5.9375	296	4	5.9375	115
4	6.0625	96	4	6.0625	624	4	6.0625	134
4	6.1875	118	4	6.1875	879	4	6.1875	231
4	6.3125	30	4	6.3125	2308	4	6.3125	219
4	6.4375	98	4	6.4375	565	4	6.4375	112
4	6.5625	348	4	6.5625	292	4	6.5625	659
4	6.6875	113	4	6.6875	153	4	6.6875	663
4	6.8125	18	4	6.8125	65	4	6.8125	73
4	6.9375	5	4	6.9375	75	4	6.9375	10
4	7.0625	0	4	7.0625	614	4	7.0625	137
4	7.1875	4	4	7.1875	1300	4	7.1875	35
4	7.3125	21	4	7.3125	663	4	7.3125	170
4	7.4375	36	4	7.4375	175	4	7.4375	417
4	7.5625	25	4	7.5625	209	4	7.5625	230
4	7.6875	65	4	7.6875	219	4	7.6875	37
4	7.8125	29	4	7.8125	494	4	7.8125	171

4	7.9375	18	4	7.9375	531	4	7.9375	296
4	8.0625	21	4	8.0625	230	4	8.0625	428
4	8.1875	11	4	8.1875	627	4	8.1875	207
4	8.3125	15	4	8.3125	875	4	8.3125	70
4	8.4375	40	4	8.4375	716	4	8.4375	225
4	8.5625	89	4	8.5625	229	4	8.5625	264
4	8.6875	34	4	8.6875	127	4	8.6875	137
4	8.8125	17	4	8.8125	18	4	8.8125	2
4	8.9375	13	4	8.9375	47	4	8.9375	3
4	9.0625	21	4	9.0625	227	4	9.0625	9
4	9.1875	27	4	9.1875	461	4	9.1875	6
4	9.3125	14	4	9.3125	3524	4	9.3125	33
4	9.4375	102	4	9.4375	2760	4	9.4375	120
4	9.5625	27	4	9.5625	625	4	9.5625	28
4	9.6875	21	4	9.6875	29	4	9.6875	75
4	9.8125	25	4	9.8125	361	4	9.8125	28
4	9.9375	3	4	9.9375	746	4	9.9375	82
4.5	0.0625	128	4.5	0.0625	746	4.5	0.0625	73
4.5	0.1875	159	4.5	0.1875	407	4.5	0.1875	10
4.5	0.3125	60	4.5	0.3125	828	4.5	0.3125	21
4.5	0.4375	11	4.5	0.4375	686	4.5	0.4375	79
4.5	0.5625	41	4.5	0.5625	386	4.5	0.5625	29
4.5	0.6875	52	4.5	0.6875	659	4.5	0.6875	10
4.5	0.8125	55	4.5	0.8125	483	4.5	0.8125	20
4.5	0.9375	36	4.5	0.9375	49	4.5	0.9375	60
4.5	1.0625	25	4.5	1.0625	47	4.5	1.0625	115
4.5	1.1875	29	4.5	1.1875	95	4.5	1.1875	9
4.5	1.3125	155	4.5	1.3125	122	4.5	1.3125	7
4.5	1.4375	99	4.5	1.4375	1826	4.5	1.4375	38
4.5	1.5625	6	4.5	1.5625	3386	4.5	1.5625	395
4.5	1.6875	4	4.5	1.6875	472	4.5	1.6875	275
4.5	1.8125	36	4.5	1.8125	803	4.5	1.8125	32
4.5	1.9375	16	4.5	1.9375	3556	4.5	1.9375	100
4.5	2.0625	4	4.5	2.0625	1600	4.5	2.0625	48
4.5	2.1875	4	4.5	2.1875	2303	4.5	2.1875	208
4.5	2.3125	2	4.5	2.3125	7721	4.5	2.3125	142
4.5	2.4375	4	4.5	2.4375	5633	4.5	2.4375	73
4.5	2.5625	5	4.5	2.5625	1803	4.5	2.5625	61
4.5	2.6875	3	4.5	2.6875	1668	4.5	2.6875	19
4.5	2.8125	19	4.5	2.8125	1950	4.5	2.8125	17
4.5	2.9375	9	4.5	2.9375	503	4.5	2.9375	14
4.5	3.0625	4	4.5	3.0625	1147	4.5	3.0625	66
4.5	3.1875	10	4.5	3.1875	526	4.5	3.1875	35
4.5	3.3125	63	4.5	3.3125	165	4.5	3.3125	22
4.5	3.4375	13	4.5	3.4375	271	4.5	3.4375	144
4.5	3.5625	5	4.5	3.5625	241	4.5	3.5625	346
4.5	3.6875	16	4.5	3.6875	99	4.5	3.6875	66

4.5	3.8125	4	4.5	3.8125	206	4.5	3.8125	106
4.5	3.9375	13	4.5	3.9375	330	4.5	3.9375	43
4.5	4.0625	3	4.5	4.0625	462	4.5	4.0625	7
4.5	4.1875	11	4.5	4.1875	1001	4.5	4.1875	20
4.5	4.3125	8	4.5	4.3125	380	4.5	4.3125	175
4.5	4.4375	6	4.5	4.4375	1576	4.5	4.4375	46
4.5	4.5625	1	4.5	4.5625	2532	4.5	4.5625	121
4.5	4.6875	4	4.5	4.6875	1304	4.5	4.6875	109
4.5	4.8125	4	4.5	4.8125	754	4.5	4.8125	7
4.5	4.9375	64	4.5	4.9375	2327	4.5	4.9375	28
4.5	5.0625	8	4.5	5.0625	4176	4.5	5.0625	18
4.5	5.1875	5	4.5	5.1875	1757	4.5	5.1875	40
4.5	5.3125	23	4.5	5.3125	4389	4.5	5.3125	127
4.5	5.4375	2	4.5	5.4375	2390	4.5	5.4375	59
4.5	5.5625	9	4.5	5.5625	271	4.5	5.5625	113
4.5	5.6875	5	4.5	5.6875	1315	4.5	5.6875	52
4.5	5.8125	1	4.5	5.8125	1312	4.5	5.8125	30
4.5	5.9375	7	4.5	5.9375	608	4.5	5.9375	236
4.5	6.0625	5	4.5	6.0625	284	4.5	6.0625	235
4.5	6.1875	10	4.5	6.1875	376	4.5	6.1875	102
4.5	6.3125	7	4.5	6.3125	668	4.5	6.3125	261
4.5	6.4375	24	4.5	6.4375	456	4.5	6.4375	129
4.5	6.5625	4	4.5	6.5625	417	4.5	6.5625	105
4.5	6.6875	2	4.5	6.6875	182	4.5	6.6875	75
4.5	6.8125	15	4.5	6.8125	190	4.5	6.8125	74
4.5	6.9375	12	4.5	6.9375	1704	4.5	6.9375	71
4.5	7.0625	17	4.5	7.0625	175	4.5	7.0625	180
4.5	7.1875	16	4.5	7.1875	23	4.5	7.1875	58
4.5	7.3125	8	4.5	7.3125	1157	4.5	7.3125	39
4.5	7.4375	4	4.5	7.4375	2992	4.5	7.4375	89
4.5	7.5625	59	4.5	7.5625	836	4.5	7.5625	37
4.5	7.6875	83	4.5	7.6875	86	4.5	7.6875	82
4.5	7.8125	7	4.5	7.8125	103	4.5	7.8125	42
4.5	7.9375	1	4.5	7.9375	1089	4.5	7.9375	259
4.5	8.0625	14	4.5	8.0625	590	4.5	8.0625	79
4.5	8.1875	65	4.5	8.1875	908	4.5	8.1875	32
4.5	8.3125	93	4.5	8.3125	1122	4.5	8.3125	56
4.5	8.4375	250	4.5	8.4375	114	4.5	8.4375	46
4.5	8.5625	270	4.5	8.5625	265	4.5	8.5625	19
4.5	8.6875	22	4.5	8.6875	269	4.5	8.6875	52
4.5	8.8125	97	4.5	8.8125	147	4.5	8.8125	353
4.5	8.9375	69	4.5	8.9375	443	4.5	8.9375	154
4.5	9.0625	53	4.5	9.0625	1569	4.5	9.0625	460
4.5	9.1875	11	4.5	9.1875	3372	4.5	9.1875	320
4.5	9.3125	34	4.5	9.3125	787	4.5	9.3125	107
4.5	9.4375	21	4.5	9.4375	524	4.5	9.4375	125
4.5	9.5625	7	4.5	9.5625	613	4.5	9.5625	60

4.5	9.6875	7	4.5	9.6875	366	4.5	9.6875	253
4.5	9.8125	2	4.5	9.8125	4844	4.5	9.8125	93
4.5	9.9375	31	4.5	9.9375	7867	4.5	9.9375	25
5	0.0625	47	5	0.0625	1759	5	0.0625	6
5	0.1875	2	5	0.1875	1056	5	0.1875	51
5	0.3125	1	5	0.3125	4056	5	0.3125	166
5	0.4375	11	5	0.4375	7212	5	0.4375	86
5	0.5625	44	5	0.5625	4052	5	0.5625	64
5	0.6875	18	5	0.6875	2724	5	0.6875	170
5	0.8125	1	5	0.8125	1206	5	0.8125	79
5	0.9375	9	5	0.9375	35	5	0.9375	55
5	1.0625	24	5	1.0625	176	5	1.0625	27
5	1.1875	100	5	1.1875	917	5	1.1875	166
5	1.3125	158	5	1.3125	3062	5	1.3125	177
5	1.4375	13	5	1.4375	6223	5	1.4375	102
5	1.5625	46	5	1.5625	2426	5	1.5625	6
5	1.6875	25	5	1.6875	211	5	1.6875	64
5	1.8125	4	5	1.8125	267	5	1.8125	25
5	1.9375	6	5	1.9375	1913	5	1.9375	3
5	2.0625	0	5	2.0625	2322	5	2.0625	73
5	2.1875	15	5	2.1875	74	5	2.1875	61
5	2.3125	64	5	2.3125	563	5	2.3125	56
5	2.4375	46	5	2.4375	396	5	2.4375	22
5	2.5625	45	5	2.5625	1919	5	2.5625	127
5	2.6875	39	5	2.6875	974	5	2.6875	304
5	2.8125	2	5	2.8125	1460	5	2.8125	50
5	2.9375	41	5	2.9375	1063	5	2.9375	69
5	3.0625	91	5	3.0625	518	5	3.0625	101
5	3.1875	273	5	3.1875	10013	5	3.1875	22
5	3.3125	111	5	3.3125	14156	5	3.3125	26
5	3.4375	68	5	3.4375	2402	5	3.4375	41
5	3.5625	175	5	3.5625	35	5	3.5625	20
5	3.6875	98	5	3.6875	564	5	3.6875	13
5	3.8125	141	5	3.8125	494	5	3.8125	14
5	3.9375	57	5	3.9375	333	5	3.9375	15
5	4.0625	4	5	4.0625	834	5	4.0625	21
5	4.1875	25	5	4.1875	244	5	4.1875	6
5	4.3125	13	5	4.3125	114	5	4.3125	5
5	4.4375	1	5	4.4375	182	5	4.4375	17
5	4.5625	5	5	4.5625	117	5	4.5625	38
5	4.6875	33	5	4.6875	69	5	4.6875	58
5	4.8125	47	5	4.8125	251	5	4.8125	111
5	4.9375	3	5	4.9375	281	5	4.9375	99
5	5.0625	61	5	5.0625	1352	5	5.0625	233
5	5.1875	83	5	5.1875	838	5	5.1875	61
5	5.3125	23	5	5.3125	643	5	5.3125	15
5	5.4375	12	5	5.4375	4226	5	5.4375	11

5	5.5625	8	5	5.5625	2437	5	5.5625	15
5	5.6875	6	5	5.6875	853	5	5.6875	123
5	5.8125	28	5	5.8125	544	5	5.8125	310
5	5.9375	117	5	5.9375	147	5	5.9375	301
5	6.0625	26	5	6.0625	277	5	6.0625	398
5	6.1875	10	5	6.1875	389	5	6.1875	104
5	6.3125	12	5	6.3125	196	5	6.3125	152
5	6.4375	14	5	6.4375	528	5	6.4375	68
5	6.5625	9	5	6.5625	1266	5	6.5625	6
5	6.6875	15	5	6.6875	931	5	6.6875	102
5	6.8125	69	5	6.8125	4831	5	6.8125	94
5	6.9375	17	5	6.9375	1115	5	6.9375	7
5	7.0625	36	5	7.0625	260	5	7.0625	11
5	7.1875	7	5	7.1875	1049	5	7.1875	92
5	7.3125	27	5	7.3125	1051	5	7.3125	213
5	7.4375	6	5	7.4375	199	5	7.4375	50
5	7.5625	6	5	7.5625	1021	5	7.5625	50
5	7.6875	3	5	7.6875	454	5	7.6875	15
5	7.8125	5	5	7.8125	596	5	7.8125	104
5	7.9375	7	5	7.9375	103	5	7.9375	187
5	8.0625	8	5	8.0625	205	5	8.0625	734
5	8.1875	26	5	8.1875	835	5	8.1875	532
5	8.3125	24	5	8.3125	1337	5	8.3125	193
5	8.4375	17	5	8.4375	1012	5	8.4375	260
5	8.5625	3	5	8.5625	1923	5	8.5625	133
5	8.6875	4	5	8.6875	511	5	8.6875	69
5	8.8125	39	5	8.8125	637	5	8.8125	61
5	8.9375	23	5	8.9375	471	5	8.9375	25
5	9.0625	2	5	9.0625	259	5	9.0625	211
5	9.1875	3	5	9.1875	1170	5	9.1875	99
5	9.3125	3	5	9.3125	3644	5	9.3125	221
5	9.4375	1	5	9.4375	8644	5	9.4375	355
5	9.5625	1	5	9.5625	4708	5	9.5625	41
5	9.6875	6	5	9.6875	682	5	9.6875	310
5	9.8125	36	5	9.8125	1504	5	9.8125	534
5	9.9375	62	5	9.9375	364	5	9.9375	156
5.5	0.0625	113	5.5	0.0625	15223	5.5	0.0625	317
5.5	0.1875	3	5.5	0.1875	16098	5.5	0.1875	25
5.5	0.3125	0	5.5	0.3125	5199	5.5	0.3125	8
5.5	0.4375	5	5.5	0.4375	247	5.5	0.4375	35
5.5	0.5625	1	5.5	0.5625	1421	5.5	0.5625	66
5.5	0.6875	7	5.5	0.6875	3404	5.5	0.6875	69
5.5	0.8125	22	5.5	0.8125	5692	5.5	0.8125	679
5.5	0.9375	6	5.5	0.9375	5878	5.5	0.9375	322
5.5	1.0625	21	5.5	1.0625	2974	5.5	1.0625	9
5.5	1.1875	95	5.5	1.1875	822	5.5	1.1875	91
5.5	1.3125	19	5.5	1.3125	2506	5.5	1.3125	330

5.5	1.4375	2	5.5	1.4375	1413	5.5	1.4375	311
5.5	1.5625	8	5.5	1.5625	635	5.5	1.5625	71
5.5	1.6875	19	5.5	1.6875	1915	5.5	1.6875	65
5.5	1.8125	13	5.5	1.8125	1541	5.5	1.8125	20
5.5	1.9375	8	5.5	1.9375	898	5.5	1.9375	17
5.5	2.0625	23	5.5	2.0625	902	5.5	2.0625	17
5.5	2.1875	8	5.5	2.1875	3774	5.5	2.1875	11
5.5	2.3125	42	5.5	2.3125	2507	5.5	2.3125	16
5.5	2.4375	12	5.5	2.4375	322	5.5	2.4375	69
5.5	2.5625	32	5.5	2.5625	1264	5.5	2.5625	116
5.5	2.6875	110	5.5	2.6875	439	5.5	2.6875	15
5.5	2.8125	109	5.5	2.8125	558	5.5	2.8125	1
5.5	2.9375	42	5.5	2.9375	339	5.5	2.9375	24
5.5	3.0625	12	5.5	3.0625	457	5.5	3.0625	26
5.5	3.1875	55	5.5	3.1875	922	5.5	3.1875	32
5.5	3.3125	102	5.5	3.3125	1214	5.5	3.3125	96
5.5	3.4375	112	5.5	3.4375	7506	5.5	3.4375	123
5.5	3.5625	16	5.5	3.5625	5265	5.5	3.5625	104
5.5	3.6875	38	5.5	3.6875	490	5.5	3.6875	176
5.5	3.8125	32	5.5	3.8125	755	5.5	3.8125	175
5.5	3.9375	39	5.5	3.9375	2815	5.5	3.9375	101
5.5	4.0625	47	5.5	4.0625	1970	5.5	4.0625	144
5.5	4.1875	60	5.5	4.1875	363	5.5	4.1875	82
5.5	4.3125	32	5.5	4.3125	1215	5.5	4.3125	74
5.5	4.4375	14	5.5	4.4375	364	5.5	4.4375	63
5.5	4.5625	6	5.5	4.5625	932	5.5	4.5625	160
5.5	4.6875	37	5.5	4.6875	1188	5.5	4.6875	268
5.5	4.8125	20	5.5	4.8125	1646	5.5	4.8125	376
5.5	4.9375	12	5.5	4.9375	3145	5.5	4.9375	120
5.5	5.0625	3	5.5	5.0625	4126	5.5	5.0625	40
5.5	5.1875	19	5.5	5.1875	475	5.5	5.1875	51
5.5	5.3125	37	5.5	5.3125	1482	5.5	5.3125	44
5.5	5.4375	250	5.5	5.4375	1840	5.5	5.4375	69
5.5	5.5625	7	5.5	5.5625	3374	5.5	5.5625	233
5.5	5.6875	26	5.5	5.6875	4536	5.5	5.6875	220
5.5	5.8125	96	5.5	5.8125	1595	5.5	5.8125	125
5.5	5.9375	4	5.5	5.9375	186	5.5	5.9375	56
5.5	6.0625	41	5.5	6.0625	151	5.5	6.0625	14
5.5	6.1875	12	5.5	6.1875	162	5.5	6.1875	74
5.5	6.3125	1	5.5	6.3125	1017	5.5	6.3125	290
5.5	6.4375	1	5.5	6.4375	2657	5.5	6.4375	52
5.5	6.5625	1	5.5	6.5625	313	5.5	6.5625	222
5.5	6.6875	6	5.5	6.6875	185	5.5	6.6875	365
5.5	6.8125	2	5.5	6.8125	175	5.5	6.8125	81
5.5	6.9375	7	5.5	6.9375	154	5.5	6.9375	785
5.5	7.0625	21	5.5	7.0625	846	5.5	7.0625	1554
5.5	7.1875	7	5.5	7.1875	418	5.5	7.1875	225

5.5	7.3125	16	5.5	7.3125	404	5.5	7.3125	41
5.5	7.4375	30	5.5	7.4375	650	5.5	7.4375	151
5.5	7.5625	8	5.5	7.5625	1146	5.5	7.5625	265
5.5	7.6875	27	5.5	7.6875	488	5.5	7.6875	105
5.5	7.8125	13	5.5	7.8125	426	5.5	7.8125	526
5.5	7.9375	143	5.5	7.9375	270	5.5	7.9375	634
5.5	8.0625	17	5.5	8.0625	148	5.5	8.0625	129
5.5	8.1875	48	5.5	8.1875	210	5.5	8.1875	372
5.5	8.3125	39	5.5	8.3125	763	5.5	8.3125	109
5.5	8.4375	6	5.5	8.4375	178	5.5	8.4375	10
5.5	8.5625	0	5.5	8.5625	879	5.5	8.5625	21
5.5	8.6875	4	5.5	8.6875	1898	5.5	8.6875	44
5.5	8.8125	6	5.5	8.8125	1181	5.5	8.8125	7
5.5	8.9375	68	5.5	8.9375	483	5.5	8.9375	8
5.5	9.0625	129	5.5	9.0625	1722	5.5	9.0625	36
5.5	9.1875	124	5.5	9.1875	970	5.5	9.1875	782
5.5	9.3125	17	5.5	9.3125	899	5.5	9.3125	494
5.5	9.4375	51	5.5	9.4375	1453	5.5	9.4375	11
5.5	9.5625	78	5.5	9.5625	885	5.5	9.5625	150
5.5	9.6875	90	5.5	9.6875	3394	5.5	9.6875	766
5.5	9.8125	175	5.5	9.8125	1169	5.5	9.8125	187
5.5	9.9375	23	5.5	9.9375	2856	5.5	9.9375	5
6	0.0625	14	6	0.0625	8364	6	0.0625	1629
6	0.1875	55	6	0.1875	883	6	0.1875	1108
6	0.3125	33	6	0.3125	1374	6	0.3125	279
6	0.4375	46	6	0.4375	2055	6	0.4375	127
6	0.5625	67	6	0.5625	1414	6	0.5625	61
6	0.6875	11	6	0.6875	3534	6	0.6875	34
6	0.8125	41	6	0.8125	442	6	0.8125	290
6	0.9375	13	6	0.9375	89	6	0.9375	621
6	1.0625	8	6	1.0625	731	6	1.0625	188
6	1.1875	6	6	1.1875	538	6	1.1875	38
6	1.3125	5	6	1.3125	379	6	1.3125	107
6	1.4375	10	6	1.4375	836	6	1.4375	97
6	1.5625	45	6	1.5625	1578	6	1.5625	39
6	1.6875	26	6	1.6875	274	6	1.6875	449
6	1.8125	8	6	1.8125	282	6	1.8125	838
6	1.9375	48	6	1.9375	2260	6	1.9375	216
6	2.0625	39	6	2.0625	2668	6	2.0625	37
6	2.1875	11	6	2.1875	380	6	2.1875	56
6	2.3125	3	6	2.3125	182	6	2.3125	153
6	2.4375	4	6	2.4375	537	6	2.4375	35
6	2.5625	3	6	2.5625	917	6	2.5625	25
6	2.6875	9	6	2.6875	438	6	2.6875	19
6	2.8125	2	6	2.8125	304	6	2.8125	26
6	2.9375	47	6	2.9375	738	6	2.9375	108
6	3.0625	28	6	3.0625	759	6	3.0625	159

6	3.1875	72	6	3.1875	2126	6	3.1875	42
6	3.3125	4	6	3.3125	1672	6	3.3125	298
6	3.4375	52	6	3.4375	435	6	3.4375	227
6	3.5625	49	6	3.5625	1376	6	3.5625	148
6	3.6875	167	6	3.6875	3366	6	3.6875	97
6	3.8125	241	6	3.8125	2390	6	3.8125	55
6	3.9375	178	6	3.9375	516	6	3.9375	144
6	4.0625	91	6	4.0625	369	6	4.0625	152
6	4.1875	25	6	4.1875	230	6	4.1875	100
6	4.3125	11	6	4.3125	211	6	4.3125	7
6	4.4375	126	6	4.4375	121	6	4.4375	212
6	4.5625	42	6	4.5625	75	6	4.5625	1006
6	4.6875	16	6	4.6875	126	6	4.6875	841
6	4.8125	37	6	4.8125	436	6	4.8125	355
6	4.9375	131	6	4.9375	567	6	4.9375	2274
6	5.0625	11	6	5.0625	257	6	5.0625	1084
6	5.1875	3	6	5.1875	1596	6	5.1875	100
6	5.3125	4	6	5.3125	942	6	5.3125	46
6	5.4375	71	6	5.4375	3452	6	5.4375	196
6	5.5625	113	6	5.5625	2406	6	5.5625	424
6	5.6875	29	6	5.6875	1018	6	5.6875	35
6	5.8125	54	6	5.8125	110	6	5.8125	23
6	5.9375	30	6	5.9375	138	6	5.9375	9
6	6.0625	67	6	6.0625	558	6	6.0625	9
6	6.1875	68	6	6.1875	1693	6	6.1875	19
6	6.3125	99	6	6.3125	577	6	6.3125	41
6	6.4375	48	6	6.4375	803	6	6.4375	208
6	6.5625	4	6	6.5625	746	6	6.5625	46
6	6.6875	70	6	6.6875	237	6	6.6875	44
6	6.8125	85	6	6.8125	430	6	6.8125	23
6	6.9375	31	6	6.9375	3328	6	6.9375	7
6	7.0625	35	6	7.0625	4996	6	7.0625	6
6	7.1875	54	6	7.1875	845	6	7.1875	6
6	7.3125	50	6	7.3125	292	6	7.3125	16
6	7.4375	15	6	7.4375	2818	6	7.4375	156
6	7.5625	16	6	7.5625	5245	6	7.5625	1358
6	7.6875	51	6	7.6875	1743	6	7.6875	761
6	7.8125	15	6	7.8125	6171	6	7.8125	368
6	7.9375	11	6	7.9375	3649	6	7.9375	810
6	8.0625	24	6	8.0625	1418	6	8.0625	151
6	8.1875	11	6	8.1875	315	6	8.1875	33
6	8.3125	20	6	8.3125	811	6	8.3125	10
6	8.4375	124	6	8.4375	827	6	8.4375	119
6	8.5625	102	6	8.5625	787	6	8.5625	55
6	8.6875	32	6	8.6875	1864	6	8.6875	114
6	8.8125	15	6	8.8125	776	6	8.8125	89
6	8.9375	3	6	8.9375	1942	6	8.9375	369

6	9.0625	2	6	9.0625	620	6	9.0625	125
6	9.1875	69	6	9.1875	372	6	9.1875	17
6	9.3125	68	6	9.3125	5961	6	9.3125	139
6	9.4375	39	6	9.4375	4426	6	9.4375	149
6	9.5625	25	6	9.5625	663	6	9.5625	73
6	9.6875	32	6	9.6875	4417	6	9.6875	425
6	9.8125	51	6	9.8125	4098	6	9.8125	166
6	9.9375	1	6	9.9375	2484	6	9.9375	166
6.5	0.0625	18	6.5	0.0625	3522	6.5	0.0625	77
6.5	0.1875	23	6.5	0.1875	227	6.5	0.1875	177
6.5	0.3125	11	6.5	0.3125	504	6.5	0.3125	158
6.5	0.4375	1	6.5	0.4375	793	6.5	0.4375	45
6.5	0.5625	3	6.5	0.5625	777	6.5	0.5625	1
6.5	0.6875	9	6.5	0.6875	398	6.5	0.6875	17
6.5	0.8125	18	6.5	0.8125	210	6.5	0.8125	4
6.5	0.9375	23	6.5	0.9375	1133	6.5	0.9375	17
6.5	1.0625	41	6.5	1.0625	704	6.5	1.0625	30
6.5	1.1875	40	6.5	1.1875	260	6.5	1.1875	57
6.5	1.3125	12	6.5	1.3125	406	6.5	1.3125	44
6.5	1.4375	24	6.5	1.4375	434	6.5	1.4375	81
6.5	1.5625	156	6.5	1.5625	493	6.5	1.5625	18
6.5	1.6875	76	6.5	1.6875	1634	6.5	1.6875	12
6.5	1.8125	9	6.5	1.8125	2720	6.5	1.8125	5
6.5	1.9375	5	6.5	1.9375	374	6.5	1.9375	23
6.5	2.0625	9	6.5	2.0625	859	6.5	2.0625	10
6.5	2.1875	61	6.5	2.1875	1652	6.5	2.1875	32
6.5	2.3125	39	6.5	2.3125	446	6.5	2.3125	252
6.5	2.4375	13	6.5	2.4375	1063	6.5	2.4375	191
6.5	2.5625	13	6.5	2.5625	683	6.5	2.5625	690
6.5	2.6875	78	6.5	2.6875	3560	6.5	2.6875	251
6.5	2.8125	66	6.5	2.8125	5501	6.5	2.8125	148
6.5	2.9375	10	6.5	2.9375	1559	6.5	2.9375	247
6.5	3.0625	0	6.5	3.0625	83	6.5	3.0625	55
6.5	3.1875	0	6.5	3.1875	166	6.5	3.1875	20
6.5	3.3125	76	6.5	3.3125	1244	6.5	3.3125	8
6.5	3.4375	127	6.5	3.4375	845	6.5	3.4375	11
6.5	3.5625	16	6.5	3.5625	256	6.5	3.5625	9
6.5	3.6875	30	6.5	3.6875	180	6.5	3.6875	4
6.5	3.8125	10	6.5	3.8125	74	6.5	3.8125	12
6.5	3.9375	32	6.5	3.9375	619	6.5	3.9375	74
6.5	4.0625	30	6.5	4.0625	175	6.5	4.0625	4
6.5	4.1875	7	6.5	4.1875	306	6.5	4.1875	2
6.5	4.3125	14	6.5	4.3125	409	6.5	4.3125	14
6.5	4.4375	15	6.5	4.4375	983	6.5	4.4375	18
6.5	4.5625	36	6.5	4.5625	1519	6.5	4.5625	103
6.5	4.6875	9	6.5	4.6875	965	6.5	4.6875	379
6.5	4.8125	20	6.5	4.8125	588	6.5	4.8125	103

6.5	4.9375	7	6.5	4.9375	3444	6.5	4.9375	25
6.5	5.0625	3	6.5	5.0625	843	6.5	5.0625	468
6.5	5.1875	43	6.5	5.1875	49	6.5	5.1875	521
6.5	5.3125	35	6.5	5.3125	7	6.5	5.3125	115
6.5	5.4375	27	6.5	5.4375	124	6.5	5.4375	114
6.5	5.5625	6	6.5	5.5625	557	6.5	5.5625	93
6.5	5.6875	22	6.5	5.6875	362	6.5	5.6875	562
6.5	5.8125	29	6.5	5.8125	1982	6.5	5.8125	353
6.5	5.9375	29	6.5	5.9375	1891	6.5	5.9375	49
6.5	6.0625	13	6.5	6.0625	838	6.5	6.0625	13
6.5	6.1875	4	6.5	6.1875	3727	6.5	6.1875	35
6.5	6.3125	80	6.5	6.3125	2806	6.5	6.3125	165
6.5	6.4375	146	6.5	6.4375	580	6.5	6.4375	115
6.5	6.5625	40	6.5	6.5625	694	6.5	6.5625	24
6.5	6.6875	31	6.5	6.6875	2411	6.5	6.6875	43
6.5	6.8125	8	6.5	6.8125	555	6.5	6.8125	124
6.5	6.9375	11	6.5	6.9375	86	6.5	6.9375	310
6.5	7.0625	67	6.5	7.0625	166	6.5	7.0625	105
6.5	7.1875	67	6.5	7.1875	659	6.5	7.1875	221
6.5	7.3125	43	6.5	7.3125	991	6.5	7.3125	80
6.5	7.4375	21	6.5	7.4375	42	6.5	7.4375	75
6.5	7.5625	40	6.5	7.5625	27	6.5	7.5625	29
6.5	7.6875	174	6.5	7.6875	157	6.5	7.6875	41
6.5	7.8125	143	6.5	7.8125	270	6.5	7.8125	9
6.5	7.9375	92	6.5	7.9375	1233	6.5	7.9375	22
6.5	8.0625	9	6.5	8.0625	261	6.5	8.0625	31
6.5	8.1875	5	6.5	8.1875	134	6.5	8.1875	119
6.5	8.3125	12	6.5	8.3125	298	6.5	8.3125	18
6.5	8.4375	26	6.5	8.4375	1598	6.5	8.4375	32
6.5	8.5625	14	6.5	8.5625	685	6.5	8.5625	29
6.5	8.6875	1	6.5	8.6875	2750	6.5	8.6875	65
6.5	8.8125	5	6.5	8.8125	3719	6.5	8.8125	59
6.5	8.9375	4	6.5	8.9375	737	6.5	8.9375	246
6.5	9.0625	18	6.5	9.0625	2580	6.5	9.0625	32
6.5	9.1875	58	6.5	9.1875	1909	6.5	9.1875	9
6.5	9.3125	36	6.5	9.3125	525	6.5	9.3125	22
6.5	9.4375	9	6.5	9.4375	1381	6.5	9.4375	92
6.5	9.5625	18	6.5	9.5625	1032	6.5	9.5625	101
6.5	9.6875	11	6.5	9.6875	1360	6.5	9.6875	8
6.5	9.8125	19	6.5	9.8125	4607	6.5	9.8125	61
6.5	9.9375	23	6.5	9.9375	839	6.5	9.9375	147
7	0.0625	71	7	0.0625	932	7	0.0625	115
7	0.1875	29	7	0.1875	1006	7	0.1875	301
7	0.3125	10	7	0.3125	5105	7	0.3125	121
7	0.4375	9	7	0.4375	3254	7	0.4375	209
7	0.5625	12	7	0.5625	1000	7	0.5625	165
7	0.6875	7	7	0.6875	1727	7	0.6875	7

7	0.8125	3	7	0.8125	790	7	0.8125	5
7	0.9375	51	7	0.9375	1619	7	0.9375	3
7	1.0625	39	7	1.0625	903	7	1.0625	43
7	1.1875	10	7	1.1875	527	7	1.1875	64
7	1.3125	5	7	1.3125	205	7	1.3125	22
7	1.4375	18	7	1.4375	161	7	1.4375	23
7	1.5625	14	7	1.5625	150	7	1.5625	3
7	1.6875	32	7	1.6875	416	7	1.6875	44
7	1.8125	21	7	1.8125	313	7	1.8125	69
7	1.9375	8	7	1.9375	996	7	1.9375	99
7	2.0625	7	7	2.0625	675	7	2.0625	10
7	2.1875	17	7	2.1875	431	7	2.1875	29
7	2.3125	118	7	2.3125	855	7	2.3125	55
7	2.4375	211	7	2.4375	147	7	2.4375	230
7	2.5625	62	7	2.5625	109	7	2.5625	258
7	2.6875	82	7	2.6875	341	7	2.6875	19
7	2.8125	49	7	2.8125	1000	7	2.8125	22
7	2.9375	110	7	2.9375	410	7	2.9375	35
7	3.0625	19	7	3.0625	1702	7	3.0625	41
7	3.1875	1	7	3.1875	2022	7	3.1875	234
7	3.3125	16	7	3.3125	642	7	3.3125	52
7	3.4375	21	7	3.4375	2190	7	3.4375	377
7	3.5625	4	7	3.5625	1229	7	3.5625	313
7	3.6875	5	7	3.6875	78	7	3.6875	176
7	3.8125	4	7	3.8125	292	7	3.8125	65
7	3.9375	73	7	3.9375	682	7	3.9375	173
7	4.0625	61	7	4.0625	211	7	4.0625	323
7	4.1875	45	7	4.1875	1178	7	4.1875	366
7	4.3125	7	7	4.3125	749	7	4.3125	569
7	4.4375	17	7	4.4375	169	7	4.4375	372
7	4.5625	12	7	4.5625	323	7	4.5625	54
7	4.6875	14	7	4.6875	407	7	4.6875	207
7	4.8125	13	7	4.8125	4704	7	4.8125	26
7	4.9375	12	7	4.9375	5010	7	4.9375	73
7	5.0625	17	7	5.0625	1076	7	5.0625	111
7	5.1875	9	7	5.1875	1046	7	5.1875	117
7	5.3125	3	7	5.3125	354	7	5.3125	239
7	5.4375	4	7	5.4375	314	7	5.4375	38
7	5.5625	4	7	5.5625	274	7	5.5625	3
7	5.6875	11	7	5.6875	228	7	5.6875	8
7	5.8125	4	7	5.8125	985	7	5.8125	64
7	5.9375	4	7	5.9375	246	7	5.9375	539
7	6.0625	144	7	6.0625	4842	7	6.0625	518
7	6.1875	163	7	6.1875	2384	7	6.1875	215
7	6.3125	20	7	6.3125	767	7	6.3125	49
7	6.4375	80	7	6.4375	4775	7	6.4375	232
7	6.5625	25	7	6.5625	5278	7	6.5625	670

7	6.6875	22	7	6.6875	2026	7	6.6875	317
7	6.8125	5	7	6.8125	1052	7	6.8125	103
7	6.9375	13	7	6.9375	260	7	6.9375	44
7	7.0625	25	7	7.0625	470	7	7.0625	66
7	7.1875	16	7	7.1875	927	7	7.1875	68
7	7.3125	7	7	7.3125	582	7	7.3125	251
7	7.4375	2	7	7.4375	2555	7	7.4375	206
7	7.5625	4	7	7.5625	1104	7	7.5625	247
7	7.6875	13	7	7.6875	3096	7	7.6875	177
7	7.8125	10	7	7.8125	4816	7	7.8125	44
7	7.9375	60	7	7.9375	3388	7	7.9375	46
7	8.0625	129	7	8.0625	186	7	8.0625	102
7	8.1875	72	7	8.1875	58	7	8.1875	226
7	8.3125	54	7	8.3125	357	7	8.3125	454
7	8.4375	9	7	8.4375	920	7	8.4375	123
7	8.5625	9	7	8.5625	594	7	8.5625	32
7	8.6875	11	7	8.6875	85	7	8.6875	64
7	8.8125	2	7	8.8125	51	7	8.8125	9
7	8.9375	9	7	8.9375	1023	7	8.9375	186
7	9.0625	20	7	9.0625	1373	7	9.0625	368
7	9.1875	13	7	9.1875	477	7	9.1875	196
7	9.3125	7	7	9.3125	149	7	9.3125	459
7	9.4375	13	7	9.4375	1708	7	9.4375	76
7	9.5625	34	7	9.5625	688	7	9.5625	247
7	9.6875	61	7	9.6875	1430	7	9.6875	235
7	9.8125	40	7	9.8125	622	7	9.8125	64
7	9.9375	11	7	9.9375	488	7	9.9375	155
7.5	0.0625	43	7.5	0.0625	5275	7.5	0.0625	557
7.5	0.1875	2	7.5	0.1875	2471	7.5	0.1875	131
7.5	0.3125	15	7.5	0.3125	121	7.5	0.3125	15
7.5	0.4375	15	7.5	0.4375	83	7.5	0.4375	12
7.5	0.5625	2	7.5	0.5625	651	7.5	0.5625	8
7.5	0.6875	1	7.5	0.6875	1718	7.5	0.6875	60
7.5	0.8125	2	7.5	0.8125	756	7.5	0.8125	53
7.5	0.9375	3	7.5	0.9375	95	7.5	0.9375	37
7.5	1.0625	2	7.5	1.0625	583	7.5	1.0625	185
7.5	1.1875	8	7.5	1.1875	6943	7.5	1.1875	115
7.5	1.3125	15	7.5	1.3125	5130	7.5	1.3125	25
7.5	1.4375	10	7.5	1.4375	651	7.5	1.4375	48
7.5	1.5625	4	7.5	1.5625	66	7.5	1.5625	18
7.5	1.6875	42	7.5	1.6875	648	7.5	1.6875	18
7.5	1.8125	83	7.5	1.8125	3254	7.5	1.8125	117
7.5	1.9375	80	7.5	1.9375	444	7.5	1.9375	107
7.5	2.0625	7	7.5	2.0625	529	7.5	2.0625	67
7.5	2.1875	11	7.5	2.1875	557	7.5	2.1875	21
7.5	2.3125	11	7.5	2.3125	110	7.5	2.3125	26
7.5	2.4375	7	7.5	2.4375	204	7.5	2.4375	122

7.5	2.5625	11	7.5	2.5625	2188	7.5	2.5625	78
7.5	2.6875	6	7.5	2.6875	1161	7.5	2.6875	167
7.5	2.8125	4	7.5	2.8125	4162	7.5	2.8125	137
7.5	2.9375	2	7.5	2.9375	1998	7.5	2.9375	125
7.5	3.0625	2	7.5	3.0625	152	7.5	3.0625	362
7.5	3.1875	25	7.5	3.1875	1000	7.5	3.1875	362
7.5	3.3125	9	7.5	3.3125	1314	7.5	3.3125	52
7.5	3.4375	7	7.5	3.4375	3595	7.5	3.4375	6
7.5	3.5625	142	7.5	3.5625	4198	7.5	3.5625	7
7.5	3.6875	164	7.5	3.6875	574	7.5	3.6875	38
7.5	3.8125	64	7.5	3.8125	1035	7.5	3.8125	29
7.5	3.9375	3	7.5	3.9375	1151	7.5	3.9375	10
7.5	4.0625	52	7.5	4.0625	3386	7.5	4.0625	14
7.5	4.1875	161	7.5	4.1875	2494	7.5	4.1875	35
7.5	4.3125	92	7.5	4.3125	352	7.5	4.3125	279
7.5	4.4375	12	7.5	4.4375	170	7.5	4.4375	249
7.5	4.5625	37	7.5	4.5625	798	7.5	4.5625	128
7.5	4.6875	106	7.5	4.6875	484	7.5	4.6875	94
7.5	4.8125	80	7.5	4.8125	245	7.5	4.8125	200
7.5	4.9375	23	7.5	4.9375	2804	7.5	4.9375	205
7.5	5.0625	31	7.5	5.0625	2958	7.5	5.0625	51
7.5	5.1875	26	7.5	5.1875	3418	7.5	5.1875	88
7.5	5.3125	123	7.5	5.3125	897	7.5	5.3125	37
7.5	5.4375	124	7.5	5.4375	611	7.5	5.4375	70
7.5	5.5625	18	7.5	5.5625	620	7.5	5.5625	253
7.5	5.6875	16	7.5	5.6875	85	7.5	5.6875	101
7.5	5.8125	24	7.5	5.8125	208	7.5	5.8125	112
7.5	5.9375	22	7.5	5.9375	439	7.5	5.9375	314
7.5	6.0625	54	7.5	6.0625	58	7.5	6.0625	76
7.5	6.1875	56	7.5	6.1875	57	7.5	6.1875	301
7.5	6.3125	8	7.5	6.3125	53	7.5	6.3125	76
7.5	6.4375	96	7.5	6.4375	927	7.5	6.4375	89
7.5	6.5625	38	7.5	6.5625	851	7.5	6.5625	105
7.5	6.6875	98	7.5	6.6875	629	7.5	6.6875	1494
7.5	6.8125	12	7.5	6.8125	179	7.5	6.8125	1404
7.5	6.9375	23	7.5	6.9375	2	7.5	6.9375	151
7.5	7.0625	21	7.5	7.0625	31	7.5	7.0625	425
7.5	7.1875	70	7.5	7.1875	130	7.5	7.1875	1718
7.5	7.3125	44	7.5	7.3125	1342	7.5	7.3125	2502
7.5	7.4375	21	7.5	7.4375	1865	7.5	7.4375	1330
7.5	7.5625	163	7.5	7.5625	1378	7.5	7.5625	108
7.5	7.6875	46	7.5	7.6875	1570	7.5	7.6875	11
7.5	7.8125	19	7.5	7.8125	172	7.5	7.8125	9
7.5	7.9375	17	7.5	7.9375	504	7.5	7.9375	117
7.5	8.0625	53	7.5	8.0625	369	7.5	8.0625	71
7.5	8.1875	249	7.5	8.1875	449	7.5	8.1875	55
7.5	8.3125	113	7.5	8.3125	107	7.5	8.3125	26

7.5	8.4375	15	7.5	8.4375	213	7.5	8.4375	19
7.5	8.5625	19	7.5	8.5625	265	7.5	8.5625	52
7.5	8.6875	10	7.5	8.6875	758	7.5	8.6875	221
7.5	8.8125	5	7.5	8.8125	439	7.5	8.8125	585
7.5	8.9375	11	7.5	8.9375	1376	7.5	8.9375	273
7.5	9.0625	21	7.5	9.0625	183	7.5	9.0625	22
7.5	9.1875	108	7.5	9.1875	75	7.5	9.1875	38
7.5	9.3125	80	7.5	9.3125	602	7.5	9.3125	291
7.5	9.4375	27	7.5	9.4375	405	7.5	9.4375	239
7.5	9.5625	169	7.5	9.5625	429	7.5	9.5625	84
7.5	9.6875	152	7.5	9.6875	278	7.5	9.6875	173
7.5	9.8125	85	7.5	9.8125	1535	7.5	9.8125	211
7.5	9.9375	133	7.5	9.9375	763	7.5	9.9375	1568
8	0.0625	20	8	0.0625	6030	8	0.0625	1391
8	0.1875	138	8	0.1875	2728	8	0.1875	179
8	0.3125	42	8	0.3125	4371	8	0.3125	144
8	0.4375	11	8	0.4375	5824	8	0.4375	373
8	0.5625	10	8	0.5625	5775	8	0.5625	773
8	0.6875	1	8	0.6875	5375	8	0.6875	544
8	0.8125	19	8	0.8125	2618	8	0.8125	295
8	0.9375	15	8	0.9375	3772	8	0.9375	84
8	1.0625	97	8	1.0625	6837	8	1.0625	9
8	1.1875	51	8	1.1875	2234	8	1.1875	370
8	1.3125	52	8	1.3125	2068	8	1.3125	1353
8	1.4375	5	8	1.4375	1144	8	1.4375	537
8	1.5625	10	8	1.5625	298	8	1.5625	79
8	1.6875	13	8	1.6875	478	8	1.6875	43
8	1.8125	95	8	1.8125	634	8	1.8125	310
8	1.9375	35	8	1.9375	425	8	1.9375	547
8	2.0625	8	8	2.0625	1714	8	2.0625	108
8	2.1875	7	8	2.1875	618	8	2.1875	109
8	2.3125	19	8	2.3125	1697	8	2.3125	12
8	2.4375	34	8	2.4375	2684	8	2.4375	71
8	2.5625	20	8	2.5625	2736	8	2.5625	156
8	2.6875	33	8	2.6875	492	8	2.6875	41
8	2.8125	69	8	2.8125	61	8	2.8125	68
8	2.9375	31	8	2.9375	1566	8	2.9375	50
8	3.0625	30	8	3.0625	2173	8	3.0625	26
8	3.1875	27	8	3.1875	110	8	3.1875	22
8	3.3125	10	8	3.3125	85	8	3.3125	290
8	3.4375	2	8	3.4375	209	8	3.4375	254
8	3.5625	53	8	3.5625	793	8	3.5625	18
8	3.6875	15	8	3.6875	491	8	3.6875	62
8	3.8125	20	8	3.8125	1682	8	3.8125	93
8	3.9375	19	8	3.9375	3455	8	3.9375	15
8	4.0625	6	8	4.0625	2285	8	4.0625	35
8	4.1875	29	8	4.1875	282	8	4.1875	16

8	4.3125	104	8	4.3125	1649	8	4.3125	6
8	4.4375	12	8	4.4375	8215	8	4.4375	60
8	4.5625	7	8	4.5625	5331	8	4.5625	92
8	4.6875	5	8	4.6875	705	8	4.6875	59
8	4.8125	26	8	4.8125	536	8	4.8125	68
8	4.9375	31	8	4.9375	399	8	4.9375	240
8	5.0625	285	8	5.0625	450	8	5.0625	105
8	5.1875	29	8	5.1875	2057	8	5.1875	288
8	5.3125	180	8	5.3125	2205	8	5.3125	153
8	5.4375	104	8	5.4375	951	8	5.4375	27
8	5.5625	162	8	5.5625	85	8	5.5625	32
8	5.6875	24	8	5.6875	688	8	5.6875	28
8	5.8125	32	8	5.8125	2170	8	5.8125	270
8	5.9375	47	8	5.9375	2456	8	5.9375	101
8	6.0625	196	8	6.0625	2418	8	6.0625	177
8	6.1875	119	8	6.1875	276	8	6.1875	180
8	6.3125	3	8	6.3125	418	8	6.3125	51
8	6.4375	8	8	6.4375	933	8	6.4375	23
8	6.5625	65	8	6.5625	444	8	6.5625	139
8	6.6875	73	8	6.6875	3747	8	6.6875	176
8	6.8125	115	8	6.8125	6133	8	6.8125	91
8	6.9375	28	8	6.9375	1804	8	6.9375	17
8	7.0625	23	8	7.0625	3458	8.5	0.0625	84
8	7.1875	50	8	7.1875	2519	8.5	0.1875	89
8	7.3125	22	8	7.3125	436	8.5	0.3125	65
8	7.4375	30	8	7.4375	1570	8.5	0.4375	26
8	7.5625	34	8	7.5625	3362	8.5	0.5625	4
8	7.6875	7	8	7.6875	1662	8.5	0.6875	64
8	7.8125	24	8	7.8125	753	8.5	0.8125	171
8	7.9375	11	8	7.9375	2777	8.5	0.9375	94
8	8.0625	92	8	8.0625	1129	8.5	1.0625	132
8	8.1875	135	8	8.1875	399	8.5	1.1875	30
8	8.3125	151	8	8.3125	1734	8.5	1.3125	31
8	8.4375	242	8	8.4375	3329	8.5	1.4375	125
8	8.5625	165	8	8.5625	5159	8.5	1.5625	61
8	8.6875	53	8	8.6875	1278	8.5	1.6875	29
8	8.8125	33	8	8.8125	2251	8.5	1.8125	13
8	8.9375	55	8	8.9375	2279	8.5	1.9375	35
8	9.0625	55	8	9.0625	3792	8.5	2.0625	205
8	9.1875	12	8	9.1875	1147	8.5	2.1875	132
8	9.3125	2	8	9.3125	438	8.5	2.3125	48
8	9.4375	24	8	9.4375	385	8.5	2.4375	169
8	9.5625	57	8	9.5625	1654	8.5	2.5625	67
8	9.6875	16	8	9.6875	636	8.5	2.6875	452
8	9.8125	7	8	9.8125	6329	8.5	2.8125	157
8	9.9375	13	8	9.9375	7868	8.5	2.9375	31
8.5	0.0625	18	8.5	0.0625	4522	8.5	3.0625	77

8.5	0.1875	19	8.5	0.1875	369	8.5	3.1875	104
8.5	0.3125	7	8.5	0.3125	430	8.5	3.3125	28
8.5	0.4375	19	8.5	0.4375	717	8.5	3.4375	38
8.5	0.5625	125	8.5	0.5625	1095	8.5	3.5625	65
8.5	0.6875	108	8.5	0.6875	1140	8.5	3.6875	23
8.5	0.8125	72	8.5	0.8125	970	8.5	3.8125	23
8.5	0.9375	63	8.5	0.9375	248	8.5	3.9375	72
8.5	1.0625	29	8.5	1.0625	88	8.5	4.0625	37
8.5	1.1875	43	8.5	1.1875	869	8.5	4.1875	46
8.5	1.3125	15	8.5	1.3125	2249	8.5	4.3125	49
8.5	1.4375	0	8.5	1.4375	1588	8.5	4.4375	3
8.5	1.5625	17	8.5	1.5625	2231	8.5	4.5625	35
8.5	1.6875	75	8.5	1.6875	2782	8.5	4.6875	22
8.5	1.8125	6	8.5	1.8125	2759	8.5	4.8125	10
8.5	1.9375	26	8.5	1.9375	1179	8.5	4.9375	15
8.5	2.0625	26	8.5	2.0625	1205	8.5	5.0625	55
8.5	2.1875	15	8.5	2.1875	2348	8.5	5.1875	23
8.5	2.3125	23	8.5	2.3125	1014	8.5	5.3125	63
8.5	2.4375	21	8.5	2.4375	915	8.5	5.4375	205
8.5	2.5625	96	8.5	2.5625	287	8.5	5.5625	31
8.5	2.6875	15	8.5	2.6875	313	8.5	5.6875	48
8.5	2.8125	22	8.5	2.8125	215	8.5	5.8125	124
8.5	2.9375	5	8.5	2.9375	1468	8.5	5.9375	23
8.5	3.0625	0	8.5	3.0625	8228	8.5	6.0625	49
8.5	3.1875	5	8.5	3.1875	2792	8.5	6.1875	270
8.5	3.3125	17	8.5	3.3125	506	8.5	6.3125	126
8.5	3.4375	69	8.5	3.4375	1130	8.5	6.4375	95
8.5	3.5625	15	8.5	3.5625	2274	8.5	6.5625	19
8.5	3.6875	4	8.5	3.6875	365	8.5	6.6875	62
8.5	3.8125	20	8.5	3.8125	55	8.5	6.8125	374
8.5	3.9375	62	8.5	3.9375	1698	8.5	6.9375	183
8.5	4.0625	4	8.5	4.0625	857	9	0.0625	1365
8.5	4.1875	2	8.5	4.1875	2311	9	0.1875	170
8.5	4.3125	47	8.5	4.3125	226	9	0.3125	203
8.5	4.4375	164	8.5	4.4375	929	9	0.4375	51
8.5	4.5625	88	8.5	4.5625	1459	9	0.5625	19
8.5	4.6875	22	8.5	4.6875	3818	9	0.6875	11
8.5	4.8125	42	8.5	4.8125	2178	9	0.8125	15
8.5	4.9375	54	8.5	4.9375	368	9	0.9375	13
8.5	5.0625	153	8.5	5.0625	976	9	1.0625	179
8.5	5.1875	184	8.5	5.1875	2785	9	1.1875	214
8.5	5.3125	75	8.5	5.3125	1161	9	1.3125	29
8.5	5.4375	4	8.5	5.4375	1763	9	1.4375	225
8.5	5.5625	4	8.5	5.5625	3528	9	1.5625	534
8.5	5.6875	7	8.5	5.6875	1077	9	1.6875	112
8.5	5.8125	36	8.5	5.8125	612	9	1.8125	313
8.5	5.9375	34	8.5	5.9375	476	9	1.9375	154

8.5	6.0625	15	8.5	6.0625	175	9	2.0625	217
8.5	6.1875	98	8.5	6.1875	1246	9	2.1875	465
8.5	6.3125	158	8.5	6.3125	446	9	2.3125	82
8.5	6.4375	27	8.5	6.4375	129	9	2.4375	85
8.5	6.5625	11	8.5	6.5625	145	9	2.5625	125
8.5	6.6875	15	8.5	6.6875	2081	9	2.6875	112
8.5	6.8125	12	8.5	6.8125	1412	9	2.8125	817
8.5	6.9375	3	8.5	6.9375	339	9	2.9375	1061
8.5	7.0625	15	8.5	7.0625	1879	9	3.0625	141
8.5	7.1875	2	8.5	7.1875	1018	9	3.1875	72
8.5	7.3125	6	8.5	7.3125	1096	9	3.3125	523
8.5	7.4375	3	8.5	7.4375	2238	9	3.4375	1126
8.5	7.5625	9	8.5	7.5625	13279	9	3.5625	772
8.5	7.6875	6	8.5	7.6875	5463	9	3.6875	241
8.5	7.8125	8	8.5	7.8125	113	9	3.8125	548
8.5	7.9375	18	8.5	7.9375	39	9	3.9375	666
8.5	8.0625	26	8.5	8.0625	127	9	4.0625	113
8.5	8.1875	12	8.5	8.1875	809	9	4.1875	158
8.5	8.3125	1	8.5	8.3125	444	9	4.3125	38
8.5	8.4375	3	8.5	8.4375	162	9	4.4375	20
8.5	8.5625	3	8.5	8.5625	150	9	4.5625	75
8.5	8.6875	3	8.5	8.6875	1687	9	4.6875	19
8.5	8.8125	3	8.5	8.8125	6538	9	4.8125	56
8.5	8.9375	19	8.5	8.9375	4309	9	4.9375	74
8.5	9.0625	136	8.5	9.0625	556	9	5.0625	310
8.5	9.1875	34	8.5	9.1875	255	9	5.1875	158
8.5	9.3125	4	8.5	9.3125	283	9	5.3125	219
8.5	9.4375	28	8.5	9.4375	1201	9	5.4375	128
8.5	9.5625	7	8.5	9.5625	3628	9	5.5625	62
8.5	9.6875	4	8.5	9.6875	1318	9	5.6875	51
8.5	9.8125	9	8.5	9.8125	1682	9	5.8125	443
8.5	9.9375	12	8.5	9.9375	3178	9	5.9375	634
9	0.0625	67	9	0.0625	14409	9	6.0625	128
9	0.1875	20	9	0.1875	14810	9	6.1875	223
9	0.3125	4	9	0.3125	5344	9	6.3125	366
9	0.4375	115	9	0.4375	3359	9	6.4375	50
9	0.5625	255	9	0.5625	1328	9	6.5625	28
9	0.6875	15	9	0.6875	135	9	6.6875	65
9	0.8125	36	9	0.8125	34	9	6.8125	16
9	0.9375	2	9	0.9375	138	9	6.9375	151
9	1.0625	6	9	1.0625	409	9	7.0625	148
9	1.1875	5	9	1.1875	2466	9	7.1875	298
9	1.3125	3	9	1.3125	1762	9	7.3125	313
9	1.4375	4	9	1.4375	1196	9	7.4375	18
9	1.5625	11	9	1.5625	912	9	7.5625	13
9	1.6875	37	9	1.6875	1938	9	7.6875	32
9	1.8125	17	9	1.8125	4558	9	7.8125	29

9	1.9375	88	9	1.9375	6424	9	7.9375	618
9	2.0625	16	9	2.0625	1005	9	8.0625	852
9	2.1875	6	9	2.1875	3980	9	8.1875	76
9	2.3125	10	9	2.3125	1612	9	8.3125	84
9	2.4375	77	9	2.4375	2217	9	8.4375	104
9	2.5625	36	9	2.5625	1085	9	8.5625	457
9	2.6875	54	9	2.6875	971	9	8.6875	821
9	2.8125	89	9	2.8125	591	9	8.8125	587
9	2.9375	21	9	2.9375	1523	9	8.9375	133
9	3.0625	32	9	3.0625	460	9	9.0625	423
9	3.1875	25	9	3.1875	884	9	9.1875	159
9	3.3125	46	9	3.3125	506	9	9.3125	68
9	3.4375	120	9	3.4375	245	9	9.4375	144
9	3.5625	60	9	3.5625	146	9	9.5625	126
9	3.6875	1	9	3.6875	146	9	9.6875	895
9	3.8125	92	9	3.8125	51	9	9.8125	1037
9	3.9375	181	9	3.9375	869	9	9.9375	577
9	4.0625	95	9	4.0625	971	9.5	0.0625	80
9	4.1875	7	9	4.1875	199	9.5	0.1875	41
9	4.3125	43	9	4.3125	1089	9.5	0.3125	13
9	4.4375	75	9	4.4375	1740	9.5	0.4375	54
9	4.5625	54	9	4.5625	6931	9.5	0.5625	21
9	4.6875	18	9	4.6875	2222	9.5	0.6875	29
9	4.8125	52	9	4.8125	666	9.5	0.8125	15
9	4.9375	26	9	4.9375	554	9.5	0.9375	161
9	5.0625	8	9	5.0625	127	9.5	1.0625	132
9	5.1875	9	9	5.1875	1086	9.5	1.1875	124
9	5.3125	19	9	5.3125	970	9.5	1.3125	186
9	5.4375	69	9	5.4375	1606	9.5	1.4375	476
9	5.5625	37	9	5.5625	327	9.5	1.5625	642
9	5.6875	6	9	5.6875	384	9.5	1.6875	57
9	5.8125	21	9	5.8125	761	9.5	1.8125	12
9	5.9375	8	9	5.9375	2412	9.5	1.9375	20
9	6.0625	53	9	6.0625	646	9.5	2.0625	76
9	6.1875	47	9	6.1875	261	9.5	2.1875	70
9	6.3125	2	9	6.3125	721	9.5	2.3125	73
9	6.4375	3	9	6.4375	1951	9.5	2.4375	169
9	6.5625	4	9	6.5625	622	9.5	2.5625	451
9	6.6875	4	9	6.6875	148	9.5	2.6875	306
9	6.8125	52	9	6.8125	357	9.5	2.8125	1401
9	6.9375	116	9	6.9375	118	9.5	2.9375	1605
9	7.0625	14	9	7.0625	1412	9.5	3.0625	663
9	7.1875	59	9	7.1875	2986	9.5	3.1875	135
9	7.3125	20	9	7.3125	7200	9.5	3.3125	671
9	7.4375	75	9	7.4375	2089	9.5	3.4375	209
9	7.5625	91	9	7.5625	882	9.5	3.5625	44
9	7.6875	90	9	7.6875	790	9.5	3.6875	36

9	7.8125	126	9	7.8125	534	9.5	3.8125	46
9	7.9375	49	9	7.9375	1159	9.5	3.9375	314
9	8.0625	14	9	8.0625	742	9.5	4.0625	85
9	8.1875	111	9	8.1875	4012	9.5	4.1875	41
9	8.3125	91	9	8.3125	4444	9.5	4.3125	9
9	8.4375	51	9	8.4375	1465	9.5	4.4375	101
9	8.5625	40	9	8.5625	337	9.5	4.5625	115
9	8.6875	15	9	8.6875	1238	9.5	4.6875	46
9	8.8125	5	9	8.8125	934	9.5	4.8125	125
9	8.9375	6	9	8.9375	126	9.5	4.9375	222
9	9.0625	7	9	9.0625	129	9.5	5.0625	39
9	9.1875	52	9	9.1875	369	9.5	5.1875	78
9	9.3125	43	9	9.3125	561	9.5	5.3125	47
9	9.4375	24	9	9.4375	558	9.5	5.4375	105
9	9.5625	17	9	9.5625	1644	9.5	5.5625	157
9	9.6875	89	9	9.6875	1368	9.5	5.6875	16
9	9.8125	26	9	9.8125	2058	9.5	5.8125	7
9	9.9375	54	9	9.9375	2300	9.5	5.9375	151
9.5	0.0625	28	9.5	0.0625	6038	9.5	6.0625	378
9.5	0.1875	5	9.5	0.1875	3268	9.5	6.1875	74
9.5	0.3125	14	9.5	0.3125	842	9.5	6.3125	160
9.5	0.4375	3	9.5	0.4375	3094	9.5	6.4375	663
9.5	0.5625	4	9.5	0.5625	1129	9.5	6.5625	583
9.5	0.6875	0	9.5	0.6875	320	9.5	6.6875	94
9.5	0.8125	5	9.5	0.8125	1229	9.5	6.8125	52
9.5	0.9375	11	9.5	0.9375	602	9.5	6.9375	170
9.5	1.0625	20	9.5	1.0625	146	9.5	7.0625	175
9.5	1.1875	10	9.5	1.1875	610	9.5	7.1875	87
9.5	1.3125	6	9.5	1.3125	171	9.5	7.3125	39
9.5	1.4375	9	9.5	1.4375	406	9.5	7.4375	12
9.5	1.5625	6	9.5	1.5625	660	9.5	7.5625	14
9.5	1.6875	6	9.5	1.6875	1926	9.5	7.6875	6
9.5	1.8125	44	9.5	1.8125	1476	9.5	7.8125	40
9.5	1.9375	128	9.5	1.9375	862	9.5	7.9375	70
9.5	2.0625	54	9.5	2.0625	3109	9.5	8.0625	70
9.5	2.1875	5	9.5	2.1875	1333	9.5	8.1875	97
9.5	2.3125	22	9.5	2.3125	259	9.5	8.3125	376
9.5	2.4375	105	9.5	2.4375	389	9.5	8.4375	177
9.5	2.5625	56	9.5	2.5625	303	9.5	8.5625	618
9.5	2.6875	7	9.5	2.6875	1460	9.5	8.6875	356
9.5	2.8125	31	9.5	2.8125	5459	9.5	8.8125	1150
9.5	2.9375	31	9.5	2.9375	1197	9.5	8.9375	289
9.5	3.0625	3	9.5	3.0625	163	9.5	9.0625	350
9.5	3.1875	33	9.5	3.1875	1738	9.5	9.1875	86
9.5	3.3125	8	9.5	3.3125	10142	9.5	9.3125	25
9.5	3.4375	53	9.5	3.4375	9934	9.5	9.4375	8
9.5	3.5625	27	9.5	3.5625	4351	9.5	9.5625	20

9.5	3.6875	15	9.5	3.6875	7201	9.5	9.6875	24
9.5	3.8125	7	9.5	3.8125	9538	9.5	9.8125	73
9.5	3.9375	8	9.5	3.9375	2152	9.5	9.9375	82
9.5	4.0625	15	9.5	4.0625	893	10	0.0625	56
9.5	4.1875	9	9.5	4.1875	4254	10	0.1875	106
9.5	4.3125	4	9.5	4.3125	3090	10	0.3125	82
9.5	4.4375	4	9.5	4.4375	12287	10	0.4375	165
9.5	4.5625	14	9.5	4.5625	15930	10	0.5625	66
9.5	4.6875	41	9.5	4.6875	4636	10	0.6875	28
9.5	4.8125	46	9.5	4.8125	13024	10	0.8125	13
9.5	4.9375	5	9.5	4.9375	10393	10	0.9375	61
9.5	5.0625	30	9.5	5.0625	558	10	1.0625	33
9.5	5.1875	13	9.5	5.1875	892	10	1.1875	79
9.5	5.3125	11	9.5	5.3125	2160	10	1.3125	48
9.5	5.4375	12	9.5	5.4375	626	10	1.4375	35
9.5	5.5625	14	9.5	5.5625	1345	10	1.5625	6
9.5	5.6875	19	9.5	5.6875	3154	10	1.6875	71
9.5	5.8125	29	9.5	5.8125	818	10	1.8125	40
9.5	5.9375	1	9.5	5.9375	206	10	1.9375	26
9.5	6.0625	5	9.5	6.0625	310	10	2.0625	17
9.5	6.1875	7	9.5	6.1875	881	10	2.1875	12
9.5	6.3125	0	9.5	6.3125	346	10	2.3125	9
9.5	6.4375	5	9.5	6.4375	542	10	2.4375	131
9.5	6.5625	8	9.5	6.5625	151	10	2.5625	368
9.5	6.6875	2	9.5	6.6875	159	10	2.6875	91
9.5	6.8125	1	9.5	6.8125	214	10	2.8125	393
9.5	6.9375	17	9.5	6.9375	141	10	2.9375	375
9.5	7.0625	51	9.5	7.0625	2041	10	3.0625	16
9.5	7.1875	10	9.5	7.1875	2176	10	3.1875	25
9.5	7.3125	3	9.5	7.3125	125	10	3.3125	57
9.5	7.4375	40	9.5	7.4375	27	10	3.4375	99
9.5	7.5625	35	9.5	7.5625	77	10	3.5625	479
9.5	7.6875	40	9.5	7.6875	222	10	3.6875	80
9.5	7.8125	8	9.5	7.8125	959	10	3.8125	27
9.5	7.9375	0	9.5	7.9375	1865	10	3.9375	141
9.5	8.0625	5	9.5	8.0625	1096	10	4.0625	7
9.5	8.1875	21	9.5	8.1875	1311	10	4.1875	52
9.5	8.3125	17	9.5	8.3125	6273	10	4.3125	90
9.5	8.4375	3	9.5	8.4375	6389	10	4.4375	376
9.5	8.5625	3	9.5	8.5625	3308	10	4.5625	297
9.5	8.6875	8	9.5	8.6875	578	10	4.6875	96
9.5	8.8125	4	9.5	8.8125	3791	10	4.8125	150
9.5	8.9375	19	9.5	8.9375	4554	10	4.9375	16
9.5	9.0625	28	9.5	9.0625	933	10	5.0625	7
9.5	9.1875	39	9.5	9.1875	39	10	5.1875	42
9.5	9.3125	9	9.5	9.3125	121	10	5.3125	425
9.5	9.4375	18	9.5	9.4375	274	10	5.4375	456

9.5	9.5625	61	9.5	9.5625	820	10	5.5625	72
9.5	9.6875	15	9.5	9.6875	1618	10	5.6875	42
9.5	9.8125	37	9.5	9.8125	685	10	5.8125	44
9.5	9.9375	135	9.5	9.9375	932	10	5.9375	195
10	0.0625	98	10	0.0625	1035	10	6.0625	33
10	0.1875	109	10	0.1875	1198	10	6.1875	43
10	0.3125	16	10	0.3125	4161	10	6.3125	450
10	0.4375	6	10	0.4375	734	10	6.4375	168
10	0.5625	6	10	0.5625	970	10	6.5625	14
10	0.6875	17	10	0.6875	2031	10	6.6875	294
10	0.8125	56	10	0.8125	7050	10	6.8125	385
10	0.9375	10	10	0.9375	3571	10	6.9375	198
10	1.0625	7	10	1.0625	914	10	7.0625	153
10	1.1875	4	10	1.1875	173	10	7.1875	33
10	1.3125	43	10	1.3125	954	10	7.3125	78
10	1.4375	44	10	1.4375	1501	10	7.4375	36
10	1.5625	16	10	1.5625	217	10	7.5625	202
10	1.6875	15	10	1.6875	147	10	7.6875	93
10	1.8125	13	10	1.8125	253	10	7.8125	94
10	1.9375	40	10	1.9375	106	10	7.9375	126
10	2.0625	16	10	2.0625	261	10	8.0625	213
10	2.1875	8	10	2.1875	194	10	8.1875	107
10	2.3125	6	10	2.3125	296	10	8.3125	208
10	2.4375	11	10	2.4375	351	10	8.4375	32
10	2.5625	28	10	2.5625	429	10	8.5625	58
10	2.6875	5	10	2.6875	580	10	8.6875	496
10	2.8125	5	10	2.8125	849	10	8.8125	818
10	2.9375	19	10	2.9375	1193	10	8.9375	156
10	3.0625	13	10	3.0625	5573	10	9.0625	598
10	3.1875	41	10	3.1875	1725	10	9.1875	212
10	3.3125	3	10	3.3125	506	10	9.3125	323
10	3.4375	3	10	3.4375	2840	10	9.4375	82
10	3.5625	37	10	3.5625	3859	10	9.5625	39
10	3.6875	55	10	3.6875	1790	10	9.6875	14
10	3.8125	22	10	3.8125	12759	10	9.8125	20
10	3.9375	11	10	3.9375	12084	10	9.9375	85
10	4.0625	4	10	4.0625	16384			
10	4.1875	8	10	4.1875	9496			
10	4.3125	22	10	4.3125	372			
10	4.4375	80	10	4.4375	173			
10	4.5625	36	10	4.5625	390			
10	4.6875	3	10	4.6875	352			
10	4.8125	30	10	4.8125	3672			
10	4.9375	22	10	4.9375	3063			
10	5.0625	10	10	5.0625	5027			
10	5.1875	7	10	5.1875	1434			
10	5.3125	27	10	5.3125	835			

10	5.4375	13	10	5.4375	990
10	5.5625	2	10	5.5625	810
10	5.6875	3	10	5.6875	2222
10	5.8125	4	10	5.8125	2800
10	5.9375	27	10	5.9375	1348
10	6.0625	5	10	6.0625	794
10	6.1875	30	10	6.1875	1573
10	6.3125	7	10	6.3125	609
10	6.4375	2	10	6.4375	2068
10	6.5625	24	10	6.5625	3400
10	6.6875	12	10	6.6875	2242
10	6.8125	9	10	6.8125	426
10	6.9375	6	10	6.9375	313
10	7.0625	1	10	7.0625	408
10	7.1875	3	10	7.1875	248
10	7.3125	24	10	7.3125	30
10	7.4375	119	10	7.4375	6
10	7.5625	122	10	7.5625	173
10	7.6875	78	10	7.6875	220
10	7.8125	13	10	7.8125	747
10	7.9375	56	10	7.9375	318
10	8.0625	55	10	8.0625	732
10	8.1875	16	10	8.1875	925
10	8.3125	21	10	8.3125	263
10	8.4375	30	10	8.4375	173
10	8.5625	117	10	8.5625	750
10	8.6875	92	10	8.6875	376
10	8.8125	11	10	8.8125	75
10	8.9375	12	10	8.9375	89
10	9.0625	31	10	9.0625	47
10	9.1875	11	10	9.1875	1247
10	9.3125	7	10	9.3125	1827
10	9.4375	4	10	9.4375	497
10	9.5625	34	10	9.5625	831
10	9.6875	25	10	9.6875	330
10	9.8125	15	10	9.8125	58
10	9.9375	34	10	9.9375	142

Appendix C

Amoozemeter Lab

CCHP Data Sheet

Date: Location:
Soil and horizon:
Radius of hole (*r*): Depth from surface to hole bottom:
Distance from surface to reference level:
Total distance from reference level to hole bottom (*D*):
Desired depth of water in hole (*H*):
Desired distance to water level $d = D - H$:
Measured final value of d at steady state:
Final value of $H = D - d$:
Three-way valve position used: ___ 1-ON ___ 2-ON
Conversion factor: 20 cm^3 105 cm^3

Time	Change in time (min)	Water Level (mm)	Change in level (mm)	Q (cm^3/min)	K_{fs} (cm/min)
	XXXXXXXX		XXXXXXXX	XXXXXXX	XXXXXXX

Steady-state Q _____
Steady-state K_{fs} _____

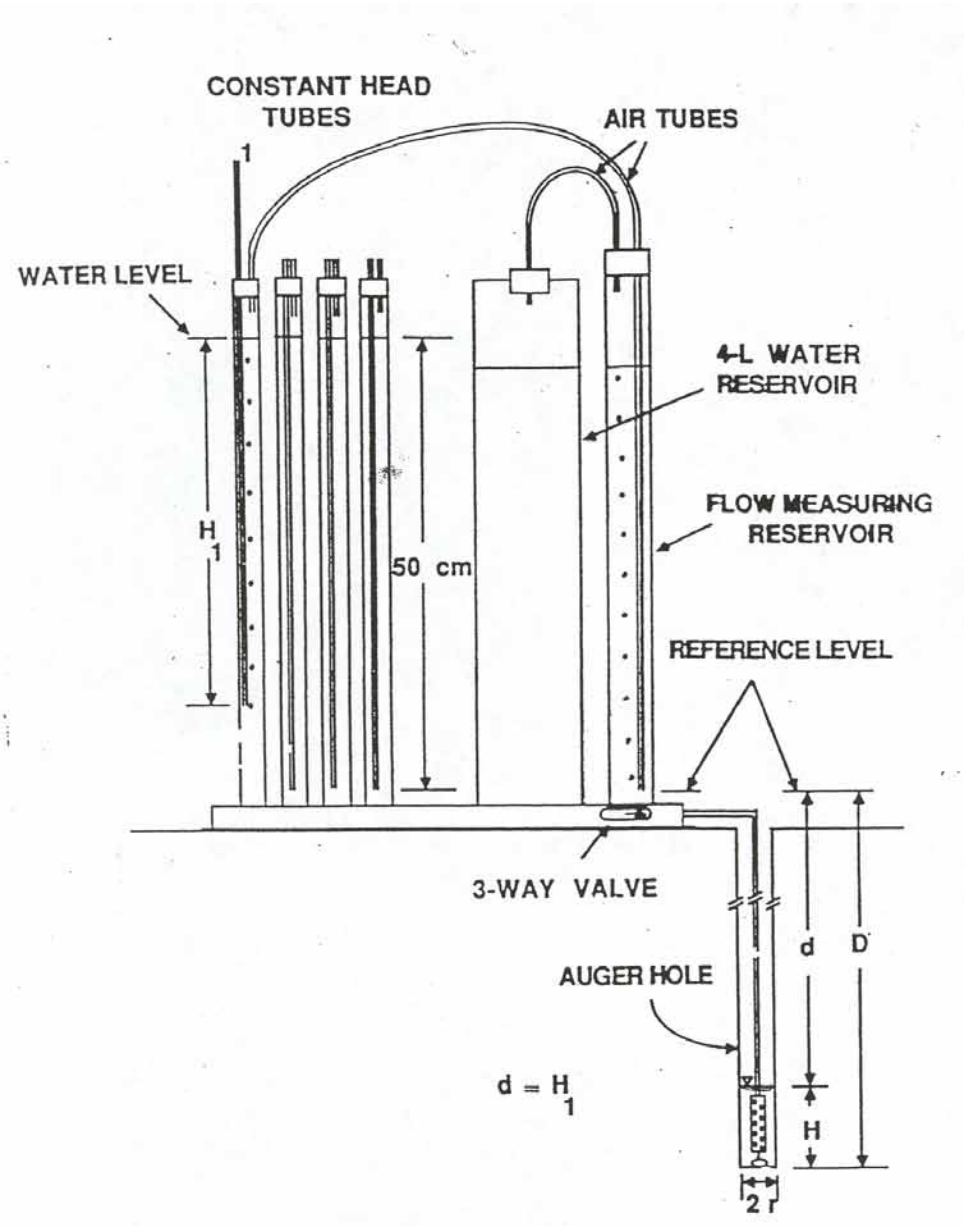
CONSTANT HEAD TUBES
1
AIR TUBES
WATER LEVEL
4-L WATER RESERVOIR
FLOW MEASURING RESERVOIR
H 1
50 cm
REFERENCE LEVEL
3-WAY VALVE
d
D
AUGER HOLE
d = H 1
H
2 r

Appendix D

Statistical Analyses

3/31/2011 2:59:26 PM

```
Welcome to Minitab, press F1 for help.
```

Descriptive Statistics: Tile Probe (cm), Knocking Pole (cm), Augur

Variable	N	N*	Mean	SE Mean	StDev	Minimum	Q1	Median
Tile Probe (cm)	35	1	19.31	1.32	7.79	9.00	13.00	17.00
Knocking Pole (cm)	24	12	40.04	4.26	20.89	10.00	25.00	39.00
Augur	24	12	13.21	1.42	6.96	4.50	8.63	11.50

Variable	Q3	Maximum
Tile Probe (cm)	24.00	41.00
Knocking Pole (cm)	51.50	84.00
Augur	17.75	33.00

Results for: Worksheet 2

Descriptive Statistics: Tile Probe (cm), Knocking Pole (cm), Augur

Variable	N	N*	Mean	SE Mean	StDev	Minimum	Q1	Median
Tile Probe (cm)	35	1	18.49	1.22	7.25	10.00	13.00	16.00
Knocking Pole (cm)	30	6	34.17	4.45	24.39	13.00	17.75	21.00
Augur	26	6	47.21	1.94	9.91	28.00	40.75	45.00

Variable	Q3	Maximum
Tile Probe (cm)	21.00	36.00
Knocking Pole (cm)	58.50	97.00
Augur	53.25	68.00

Results for: Worksheet 3

Descriptive Statistics: Tile Probe (cm), Knocking Pole (cm), Augur

Variable	N	N*	Mean	SE Mean	StDev	Minimum	Q1	Median
Tile Probe (cm)	33	3	46.67	2.67	15.37	27.00	36.50	42.00
Knocking Pole (cm)	21	15	65.10	5.10	23.36	1.00	56.00	65.00
Augur	24	12	74.40	3.25	15.91	44.50	61.75	76.00

Variable	Q3	Maximum
Tile Probe (cm)	56.50	88.00
Knocking Pole (cm)	78.00	103.00
Augur	86.75	102.00

Results for: Worksheet 1

Correlations: Tile Probe (cm), Knocking Pole (cm), Augur

	Tile Probe (cm)	Knocking Pole (c
Knocking Pole (c	-0.091	
	0.673	
Augur	-0.071	0.079
	0.741	0.712

```
Cell Contents: Pearson correlation
               P-Value
```

Summary for Tile Probe (cm)

Summary for Knocking Pole (cm)

Summary for Augur

Regression Analysis: Tile Probe (cm) versus Augur

```
The regression equation is
Tile Probe (cm) = 20.7 - 0.075 Augur


24 cases used, 12 cases contain missing values


Predictor     Coef  SE Coef      T      P
Constant    20.737    3.316   6.25  0.000
Augur      -0.0747   0.2231  -0.33  0.741


S = 7.44763   R-Sq = 0.5%   R-Sq(adj) = 0.0%


Analysis of Variance

Source          DF       SS     MS     F      P
Regression       1     6.22   6.22  0.11  0.741
Residual Error  22  1220.28  55.47
Total           23  1226.50


Unusual Observations

             Tile
            Probe
Obs  Augur   (cm)    Fit  SE Fit  Residual  St Resid
 32   33.0  19.00  18.27    4.67      0.73      0.13 X

X denotes an observation whose X value gives it large leverage.
```

Normplot of Residuals for Tile Probe (cm)

Residuals vs Fits for Tile Probe (cm)

Residual Histogram for Tile Probe (cm)

Residuals vs Order for Tile Probe (cm)

Regression Analysis: Knocking Pole (cm) versus Augur

```
The regression equation is
Knocking Pole (cm) = 36.9 + 0.238 Augur


24 cases used, 12 cases contain missing values


Predictor    Coef  SE Coef     T      P
```

```
Constant   36.896    9.479  3.89  0.001
Augur      0.2382   0.6378  0.37  0.712


S = 21.2878   R-Sq = 0.6%   R-Sq(adj) = 0.0%


Analysis of Variance

Source          DF       SS     MS     F      P
Regression       1     63.2   63.2  0.14  0.712
Residual Error  22   9969.8  453.2
Total           23  10033.0


Unusual Observations

             Knocking
Obs  Augur  Pole (cm)    Fit  SE Fit  Residual  St Resid
  3   13.0      84.00  39.99    4.35     44.01      2.11R
 32   33.0      43.00  44.76   13.35     -1.76     -0.11 X

R denotes an observation with a large standardized residual.
X denotes an observation whose X value gives it large leverage.
```

Normplot of Residuals for Knocking Pole (cm)

Residuals vs Fits for Knocking Pole (cm)

Residual Histogram for Knocking Pole (cm)

Results for: Worksheet 2

Regression Analysis: Tile Probe (cm) versus Augur

```
The regression equation is
Tile Probe (cm) = 14.9 + 0.055 Augur


26 cases used, 10 cases contain missing values


Predictor    Coef  SE Coef     T      P
Constant   14.874    6.639  2.24  0.035
Augur      0.0548   0.1377  0.40  0.694


S = 6.82242   R-Sq = 0.7%   R-Sq(adj) = 0.0%


Analysis of Variance

Source          DF       SS     MS     F      P
Regression       1     7.37   7.37  0.16  0.694
Residual Error  24  1117.09  46.55
Total           25  1124.46


Unusual Observations

             Tile
            Probe
```

```
Obs  Augur   (cm)    Fit  SE Fit  Residual  St Resid
 31   44.5  31.00  17.31    1.39     13.69      2.05R
 32   40.0  35.00  17.07    1.67     17.93      2.71R

R denotes an observation with a large standardized residual.
```

Normplot of Residuals for Tile Probe (cm)

Residuals vs Fits for Tile Probe (cm)

Residual Histogram for Tile Probe (cm)

Regression Analysis: Knocking Pole (cm) versus Augur

```
The regression equation is
Knocking Pole (cm) = 27.5 + 0.091 Augur


26 cases used, 10 cases contain missing values


Predictor    Coef  SE Coef     T      P
Constant    27.47    21.01  1.31  0.203
Augur      0.0910   0.4360  0.21  0.836


S = 21.5931   R-Sq = 0.2%   R-Sq(adj) = 0.0%


Analysis of Variance

Source          DF       SS     MS     F      P
Regression       1     20.3   20.3  0.04  0.836
Residual Error  24  11190.3  466.3
Total           25  11210.6


Unusual Observations

             Knocking
Obs  Augur  Pole (cm)    Fit  SE Fit  Residual  St Resid
 24   48.0      75.00  31.84    4.25     43.16      2.04R
 32   40.0      82.00  31.11    5.27     50.89      2.43R

R denotes an observation with a large standardized residual.
```

Normplot of Residuals for Knocking Pole (cm)

Residuals vs Fits for Knocking Pole (cm)

Residual Histogram for Knocking Pole (cm)

Results for: Worksheet 3

Regression Analysis: Tile Probe (cm) versus Augur

```
The regression equation is
```

```
Tile Probe (cm) = 5.2 + 0.571 Augur


24 cases used, 12 cases contain missing values


Predictor    Coef  SE Coef     T      P
Constant     5.21    11.81  0.44  0.664
Augur      0.5707   0.1554  3.67  0.001


S = 11.8560   R-Sq = 38.0%   R-Sq(adj) = 35.2%


Analysis of Variance

Source          DF      SS      MS      F      P
Regression       1  1896.9  1896.9  13.50  0.001
Residual Error  22  3092.4   140.6
Total           23  4989.3
```

Normplot of Residuals for Tile Probe (cm)

Residuals vs Fits for Tile Probe (cm)

Residual Histogram for Tile Probe (cm)

Regression Analysis: Knocking Pole (cm) versus Augur

```
The regression equation is
Knocking Pole (cm) = - 18.3 + 1.13 Augur


21 cases used, 15 cases contain missing values


Predictor    Coef  SE Coef      T      P
Constant   -18.32    13.67  -1.34  0.196
Augur      1.1312   0.1809   6.25  0.000


S = 13.7052   R-Sq = 67.3%   R-Sq(adj) = 65.6%


Analysis of Variance

Source          DF       SS      MS      F      P
Regression       1   7341.0  7341.0  39.08  0.000
Residual Error  19   3568.8   187.8
Total           20  10909.8


Unusual Observations

            Knocking
Obs  Augur  Pole (cm)    Fit  SE Fit  Residual  St Resid
 14     53       1.00  41.64    4.80    -40.64     -3.17R

R denotes an observation with a large standardized residual.
```

Normplot of Residuals for Knocking Pole (cm)

Residuals vs Fits for Knocking Pole (cm)

Residual Histogram for Knocking Pole (cm)

Results for: Worksheet 4

Descriptive Statistics: Tile Probe (cm), Knocking Pole (cm), Augur

Variable	N	N*	Mean	SE Mean	StDev	Minimum	Q1	Median
Tile Probe (cm)	103	5	27.80	1.65	16.78	9.00	15.00	21.00
Knocking Pole (cm)	75	33	44.71	3.02	26.20	1.00	20.00	40.00
Augur	74	34	45.00	3.18	27.33	4.50	17.75	45.00

Variable	Q3	Maximum
Tile Probe (cm)	37.00	88.00
Knocking Pole (cm)	65.00	103.00
Augur	64.50	102.00

Regression Analysis: Tile Probe (cm) versus Augur

The regression equation is
Tile Probe (cm) = 9.06 + 0.421 Augur

74 cases used, 34 cases contain missing values

Predictor	Coef	SE Coef	T	P
Constant	9.065	2.844	3.19	0.002
Augur	0.42079	0.05411	7.78	0.000

S = 12.6336   R-Sq = 45.6%   R-Sq(adj) = 44.9%

Analysis of Variance

Source	DF	SS	MS	F	P
Regression	1	9652.2	9652.2	60.47	0.000
Residual Error	72	11491.8	159.6		
Total	73	21144.0			

Unusual Observations

Obs	Augur	Tile Probe (cm)	Fit	SE Fit	Residual	St Resid
103	89	72.00	46.51	2.80	25.49	2.07R
106	96	80.00	49.46	3.13	30.54	2.49R

R denotes an observation with a large standardized residual.

Normplot of Residuals for Tile Probe (cm)

Residuals vs Fits for Tile Probe (cm)

Residual Histogram for Tile Probe (cm)

Regression Analysis: Knocking Pole (cm) versus Augur

```
The regression equation is
Knocking Pole (cm) = 25.5 + 0.434 Augur


71 cases used, 37 cases contain missing values


Predictor    Coef  SE Coef     T      P
Constant   25.529    5.190  4.92  0.000
Augur      0.4337   0.1015  4.27  0.000


S = 22.8986   R-Sq = 20.9%   R-Sq(adj) = 19.8%


Analysis of Variance

Source          DF       SS      MS      F      P
Regression       1   9571.5  9571.5  18.25  0.000
Residual Error  69  36179.8   524.3
Total           70  45751.3


Unusual Observations

            Knocking
Obs  Augur  Pole (cm)    Fit  SE Fit  Residual  St Resid
  3     13      84.00  31.17    4.12     52.83      2.35R
 86     53       1.00  48.52    2.88    -47.52     -2.09R

R denotes an observation with a large standardized residual.
```

Normplot of Residuals for Knocking Pole (cm)

Residuals vs Fits for Knocking Pole (cm)

Residual Histogram for Knocking Pole (cm)

4/1/2011 2:19:01 PM

Welcome to Minitab, press F1 for help.

Descriptive Statistics: bulk density (d=m/v), bd1, bd 2, bd3

Variable	N	N*	Mean	SE Mean	StDev	Minimum	Q1	Median
bulk density (d=m/v)	2	0	1.541	0.174	0.247	1.367	*	1.541
bd1	6	0	1.6239	0.0594	0.1455	1.4400	1.5043	1.6069
bd 2	6	0	1.6779	0.0515	0.1262	1.4290	1.6248	1.7104
bd3	5	0	1.5947	0.0674	0.1506	1.3702	1.4487	1.6297

Variable	Q3	Maximum
bulk density (d=m/v)	*	1.715
bd1	1.7452	1.8554
bd 2	1.7632	1.7652
bd3	1.7233	1.7505

Minitab Project Report

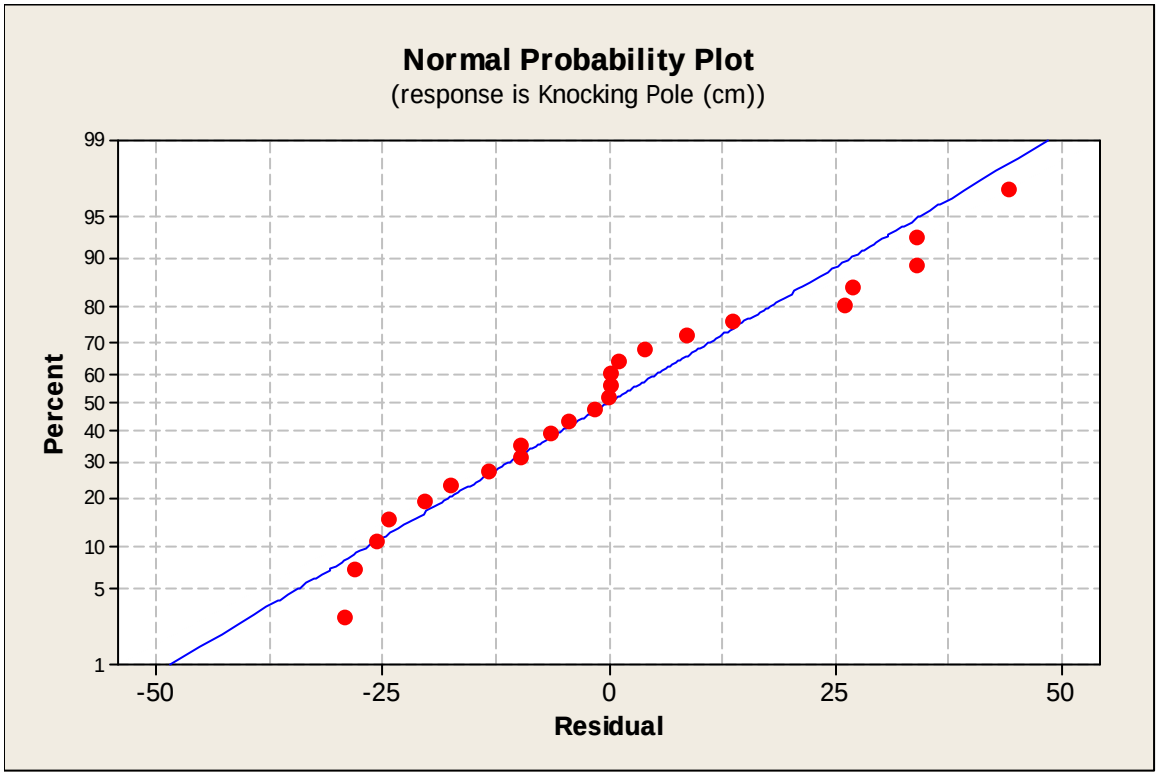

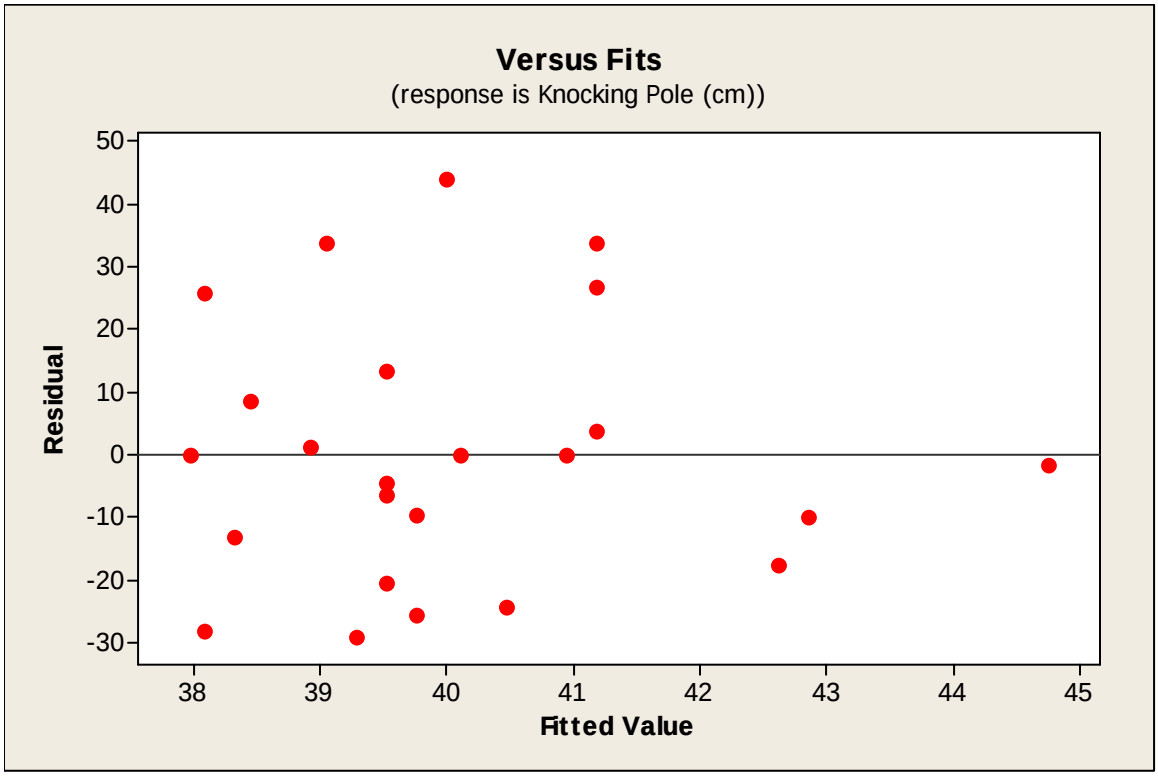

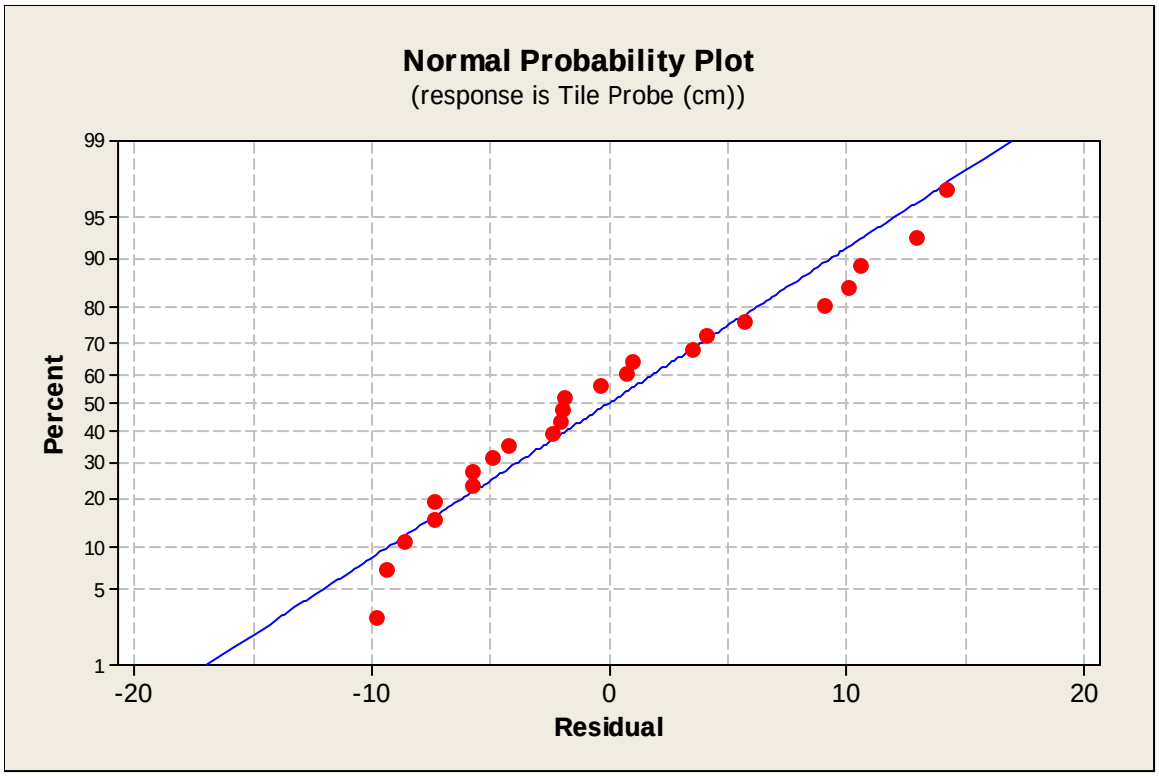
Normal Probability Plot
(response is Tile Probe (cm))
Percent
99
95
90
80
70
60
50
40
30
20
10
5
1
-20
-10
0
10
20
Residual

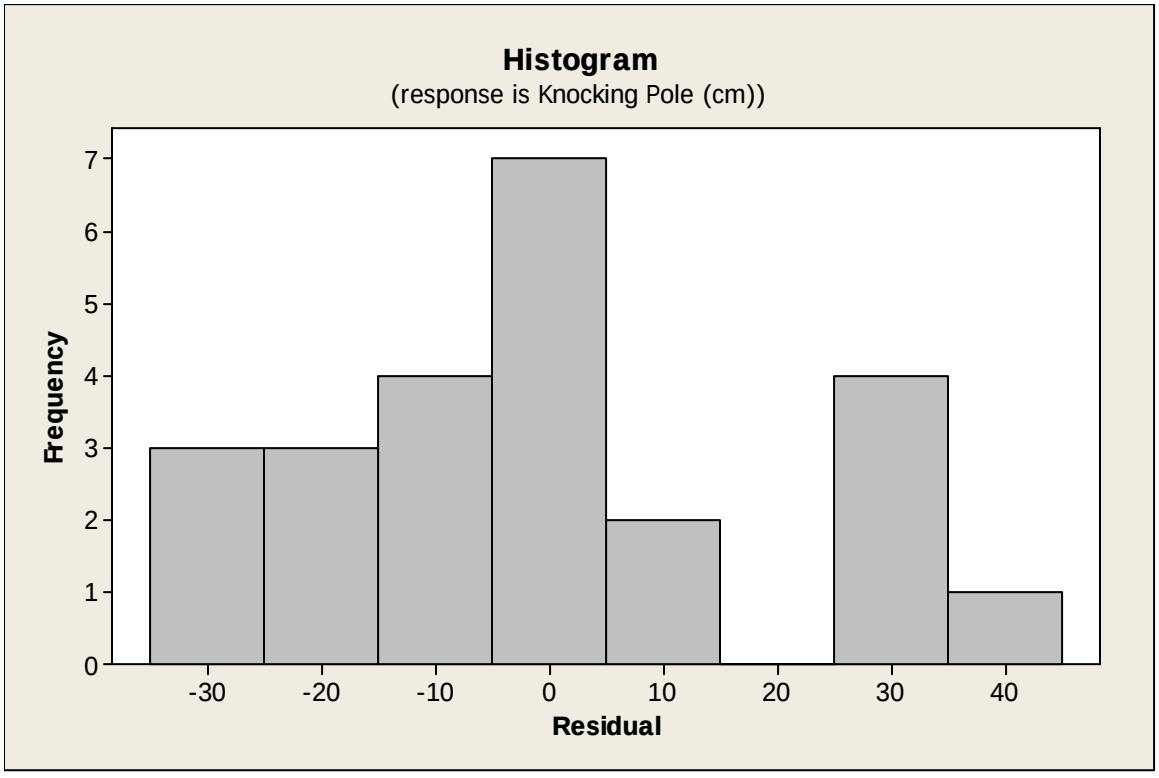
Histogram
(response is Knocking Pole (cm))
Frequency
7
6
5
4
3
2
1
0
-30
-20
-10
0
10
20
30
40
Residual

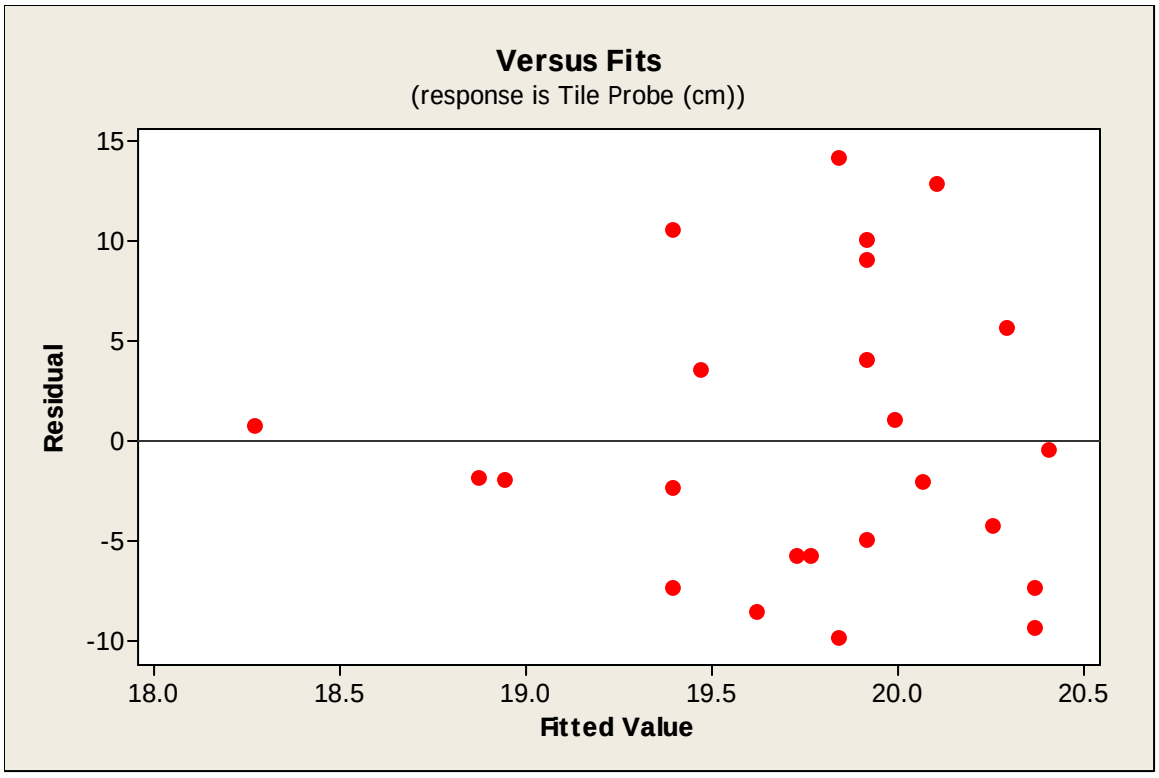
Versus Fits
(response is Tile Probe (cm))
Residual
Fitted Value
15
10
5
0
-5
-10
18.0
18.5
19.0
19.5
20.0
20.5

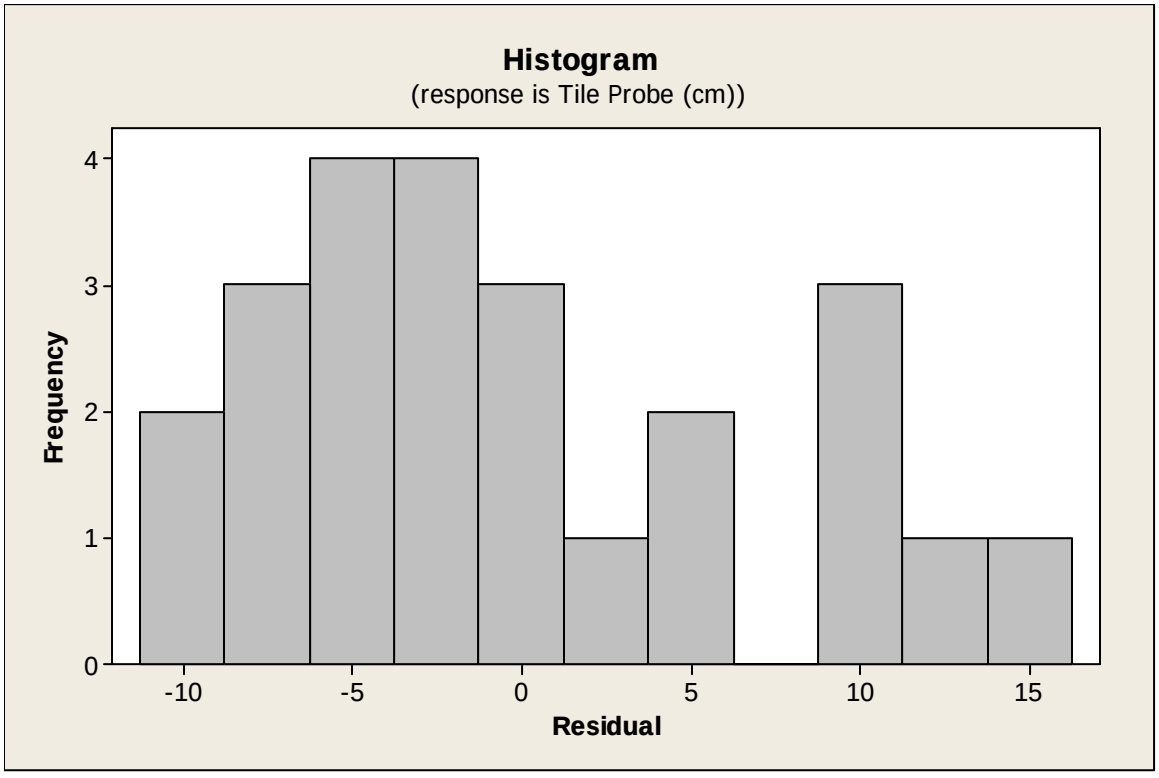
Histogram
(response is Tile Probe (cm))
Frequency
Residual
4
3
2
1
0
-10
-5
0
5
10
15

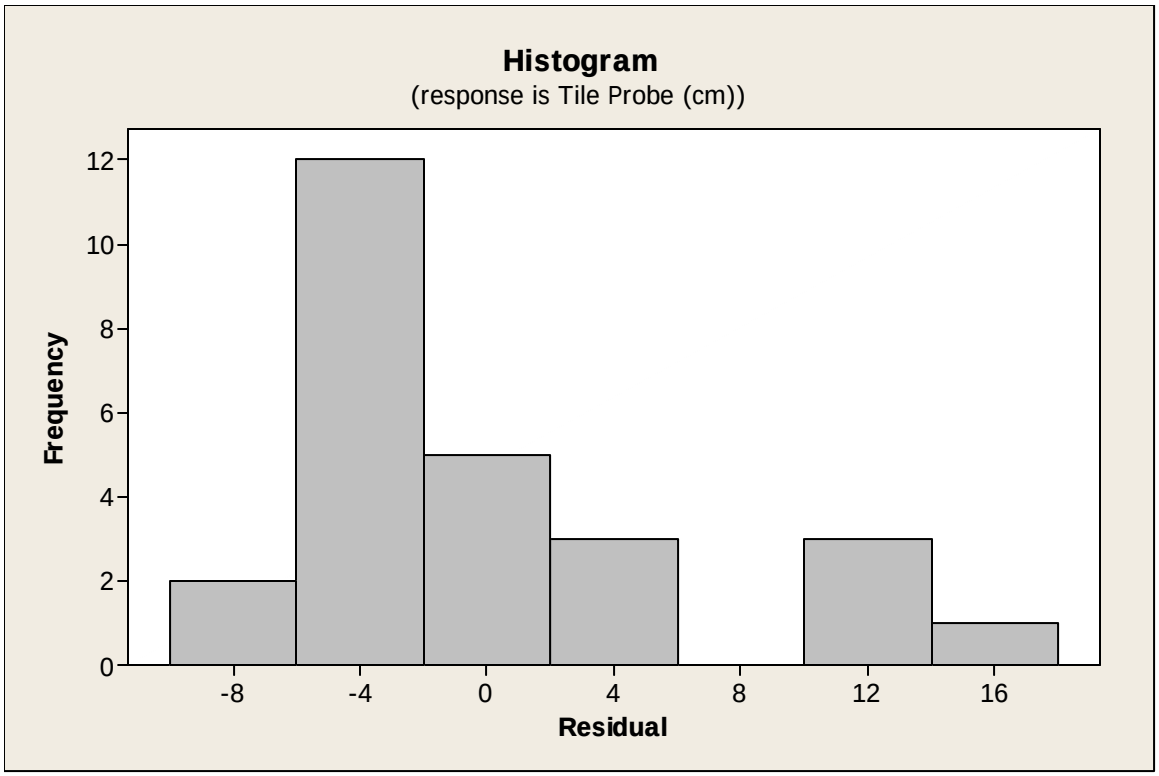
Histogram
(response is Tile Probe (cm))
Frequency
0
2
4
6
8
10
12
-8
-4
0
4
8
12
16
Residual

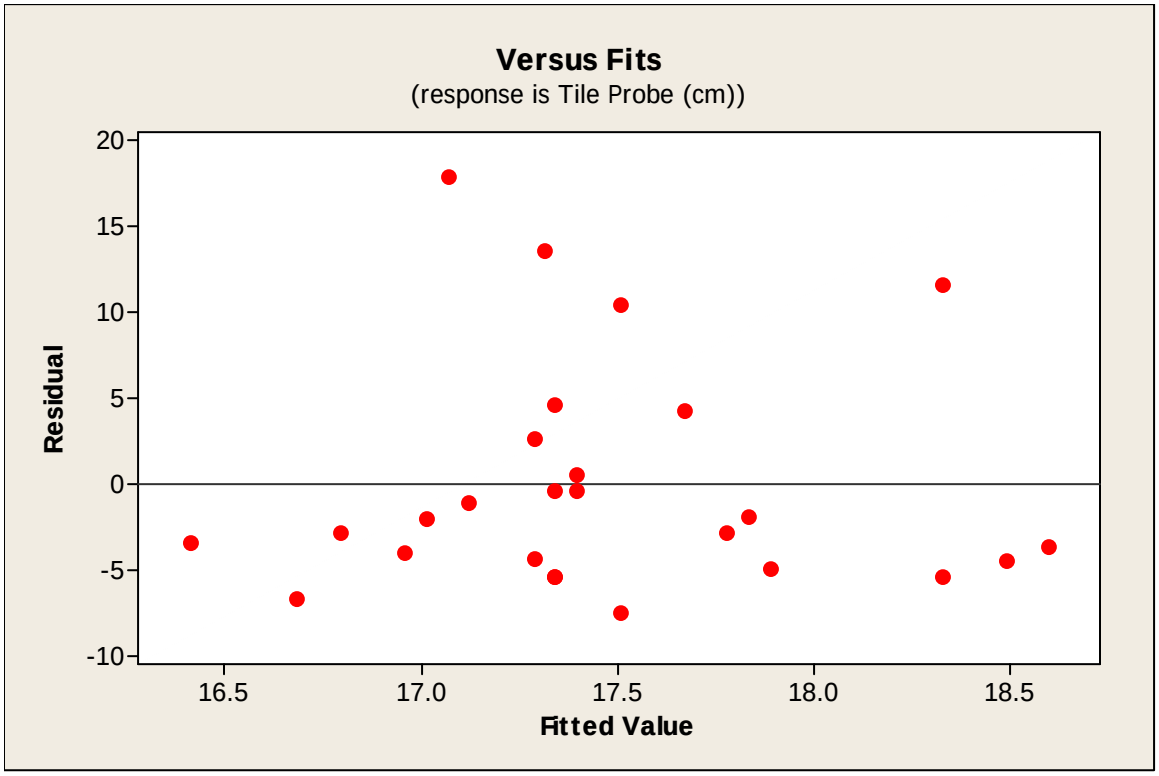
Versus Fits
(response is Tile Probe (cm))
Residual
20
15
10
5
0
-5
-10
16.5
17.0
17.5
18.0
18.5
Fitted Value

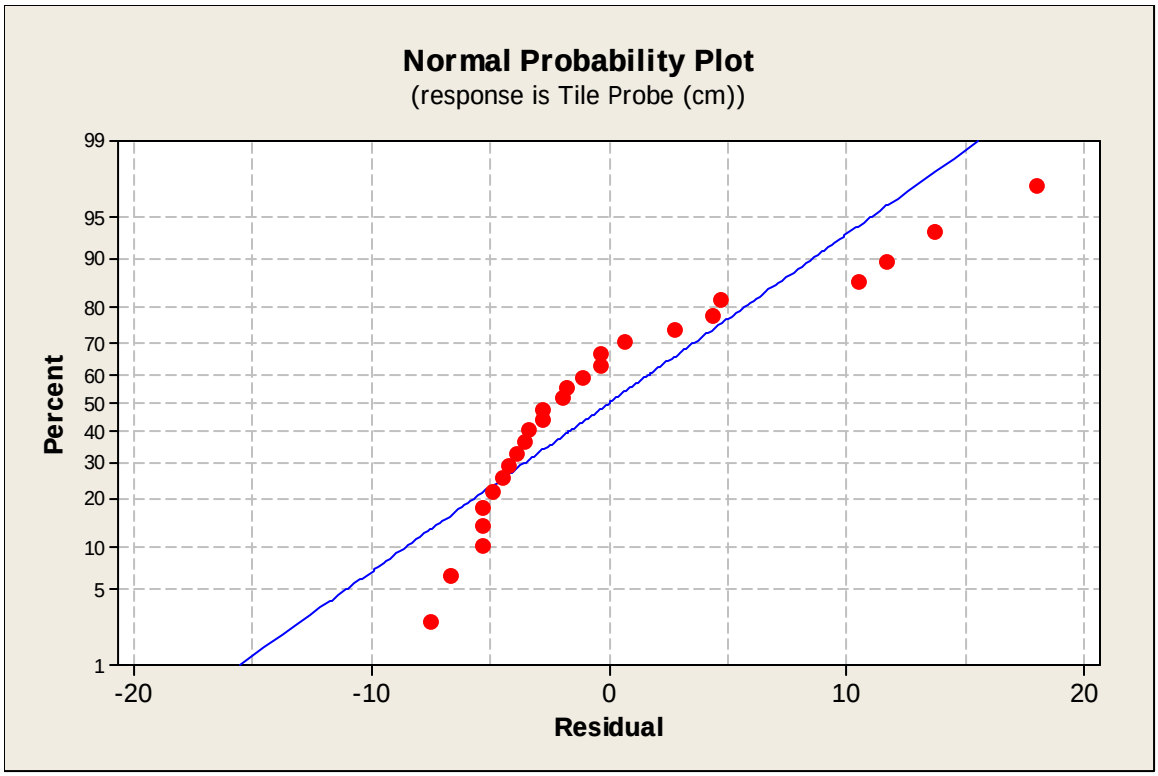
Normal Probability Plot
(response is Tile Probe (cm))
Percent
99
95
90
80
70
60
50
40
30
20
10
5
1
-20
-10
0
10
20
Residual

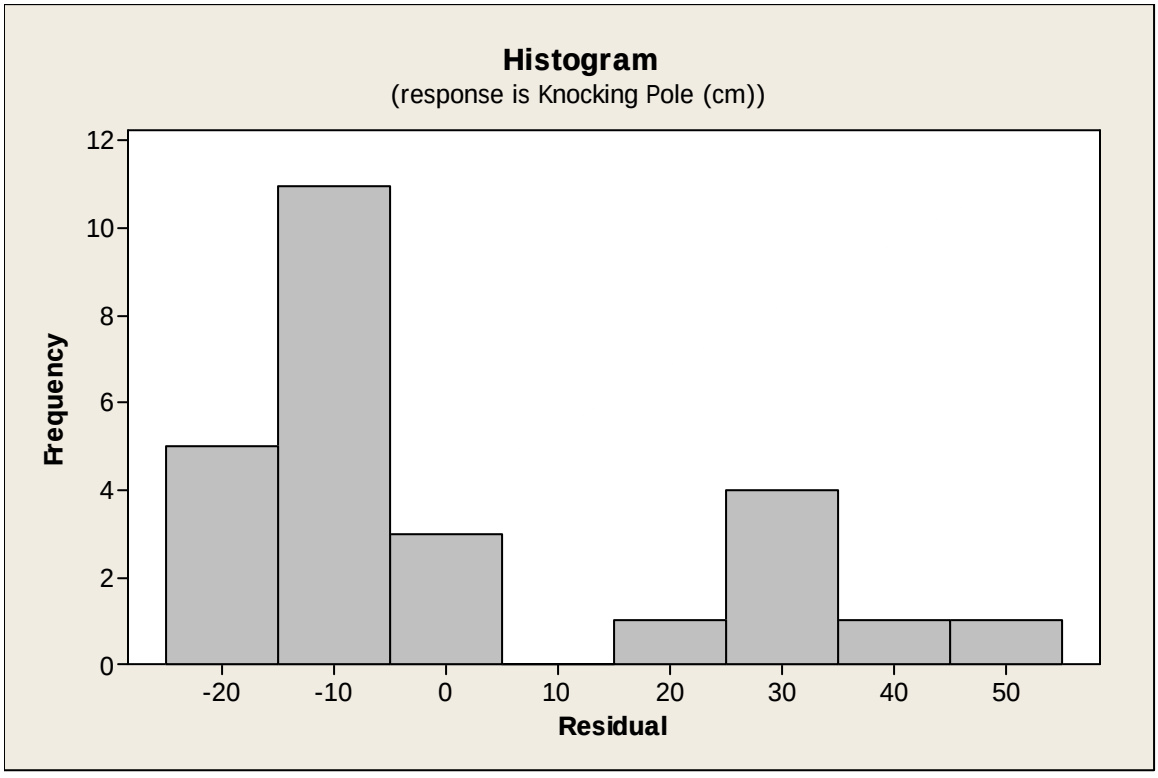
Histogram
(response is Knocking Pole (cm))
Frequency
12
10
8
6
4
2
0
-20
-10
0
10
20
30
40
50
Residual

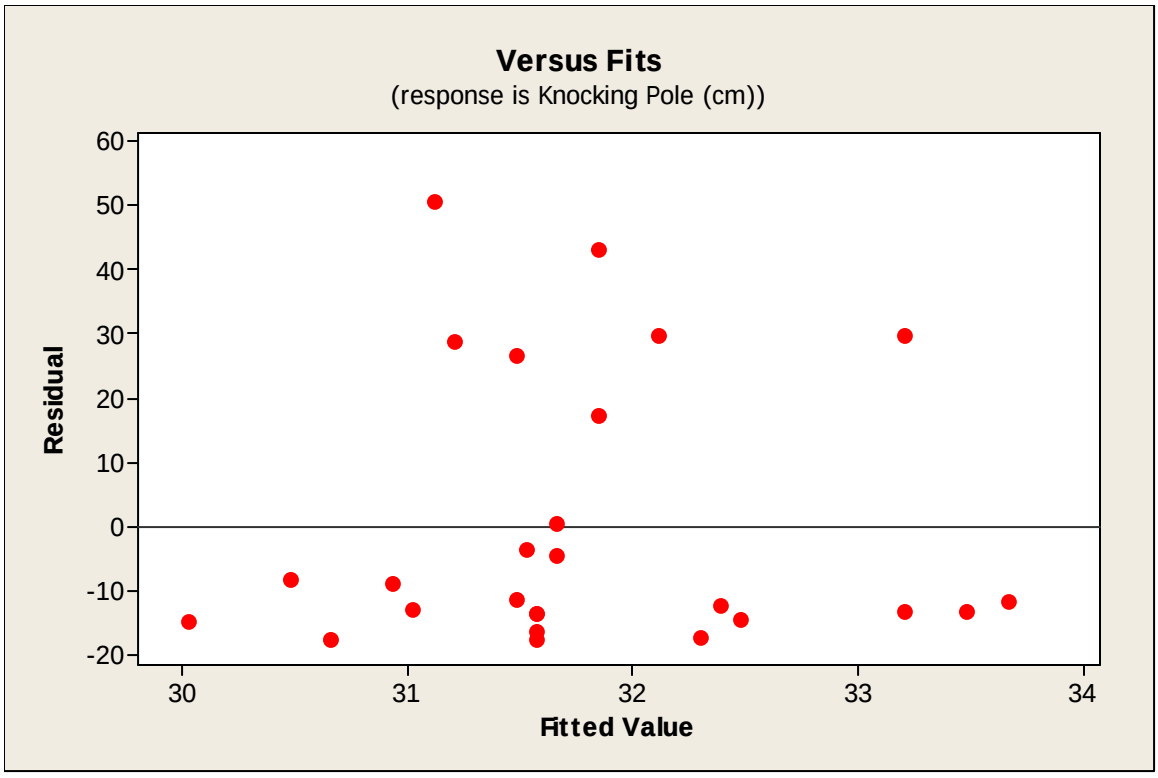
Versus Fits
(response is Knocking Pole (cm))
Residual
Fitted Value
60
50
40
30
20
10
0
-10
-20
30
31
32
33
34

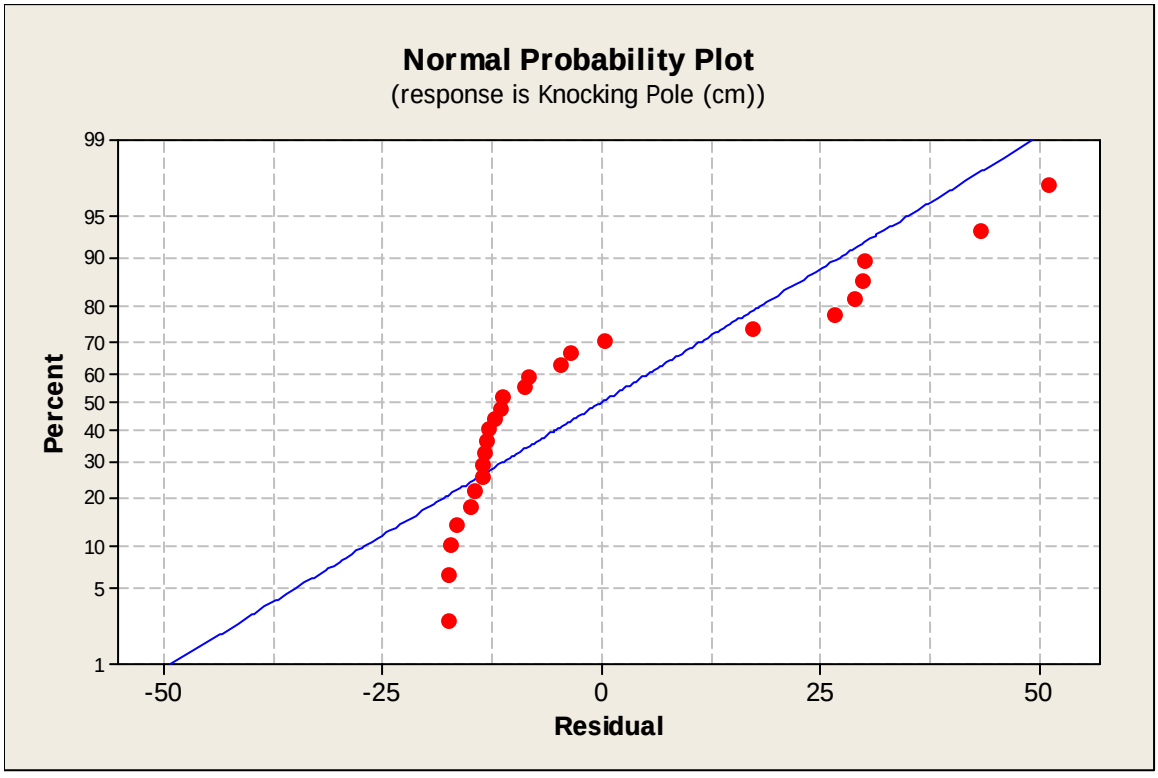
Normal Probability Plot
(response is Knocking Pole (cm))
Percent
Residual
99
95
90
80
70
60
50
40
30
20
10
5
1
-50
-25
0
25
50

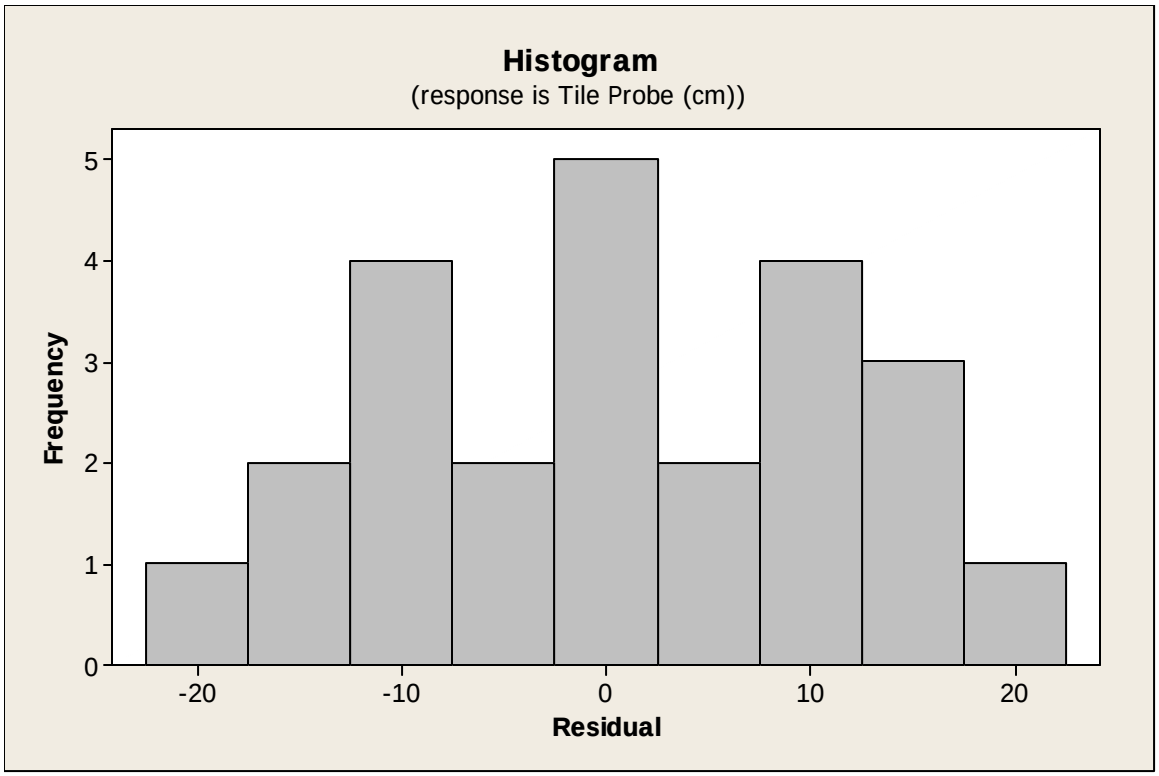
Histogram
(response is Tile Probe (cm))
Frequency
Residual
0
1
2
3
4
5
-20
-10
0
10
20

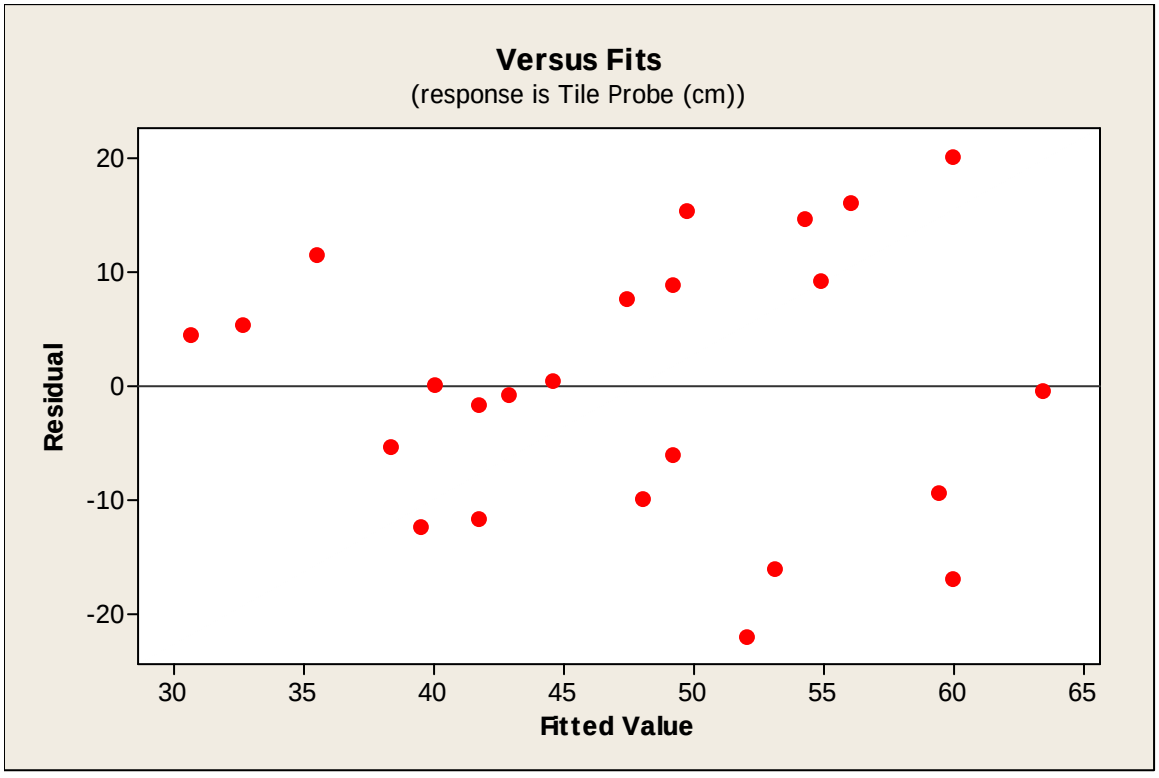
Versus Fits
(response is Tile Probe (cm))
Residual
Fitted Value
20
10
0
-10
-20
30
35
40
45
50
55
60
65

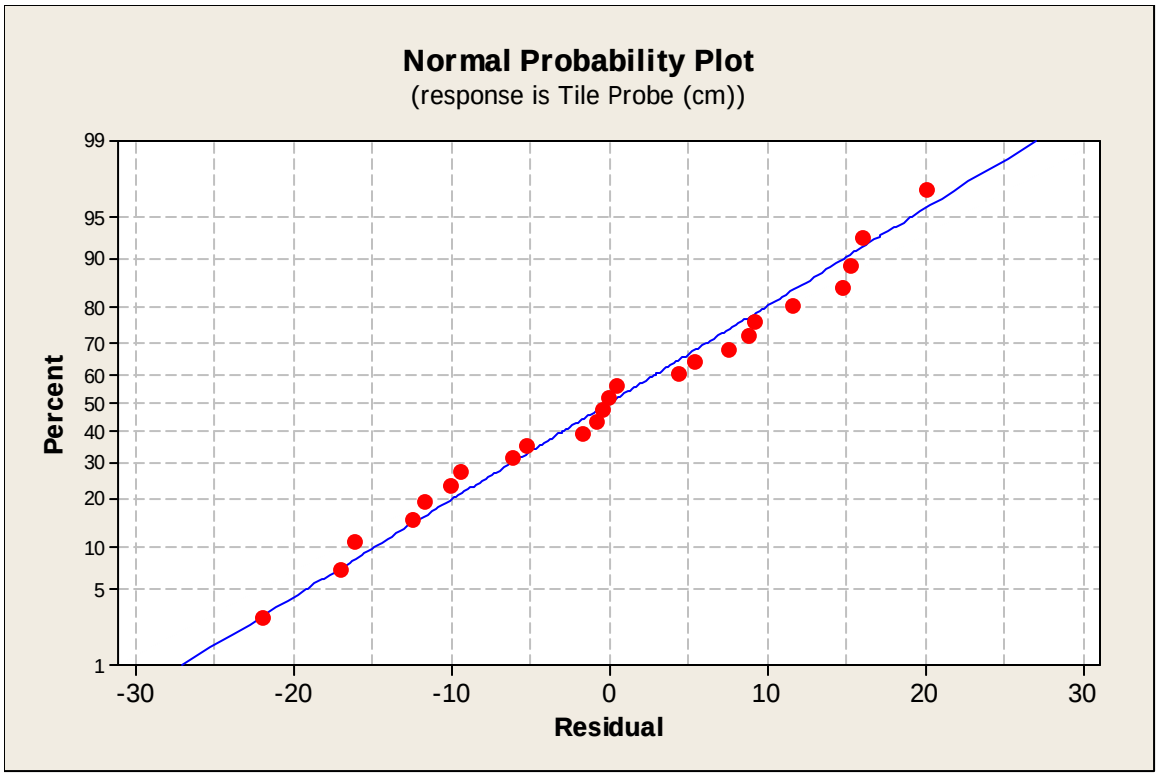
Normal Probability Plot
(response is Tile Probe (cm))
Percent
99
95
90
80
70
60
50
40
30
20
10
5
1
-30
-20
-10
0
10
20
30
Residual

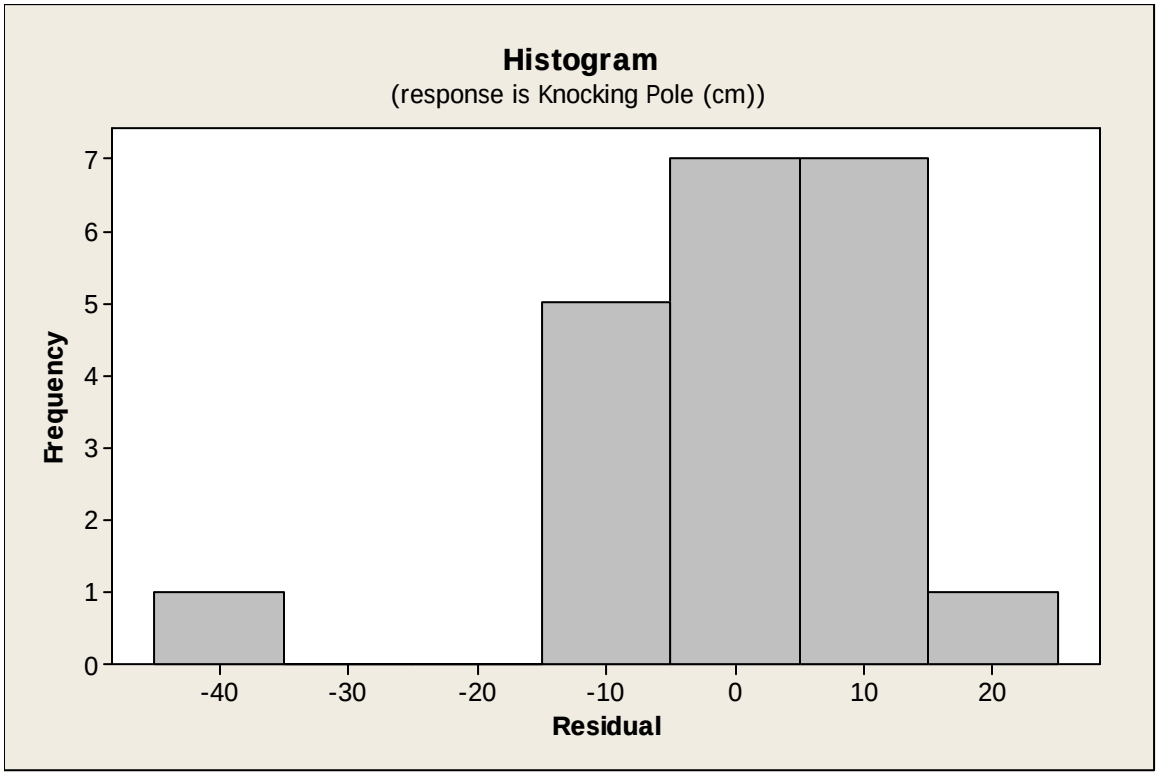
Histogram
(response is Knocking Pole (cm))
Frequency
7
6
5
4
3
2
1
0
-40
-30
-20
-10
0
10
20
Residual

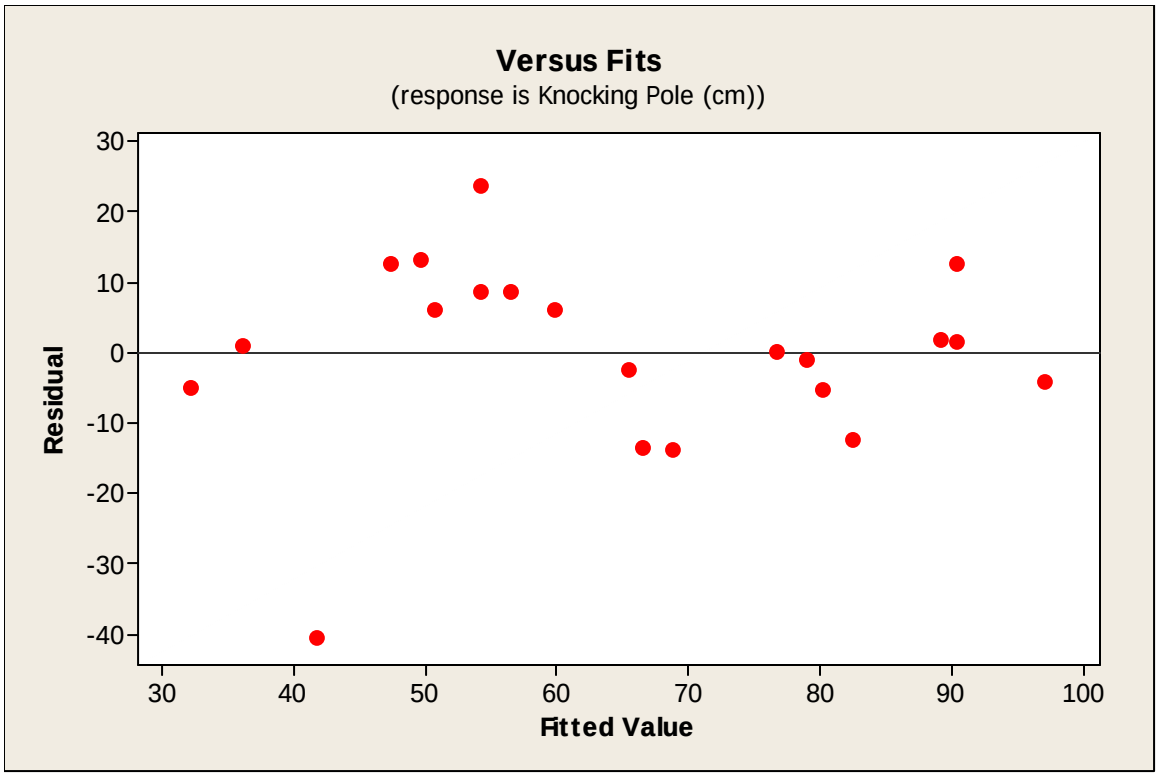
Versus Fits
(response is Knocking Pole (cm))
Residual
Fitted Value
30
20
10
0
-10
-20
-30
-40
30
40
50
60
70
80
90
100

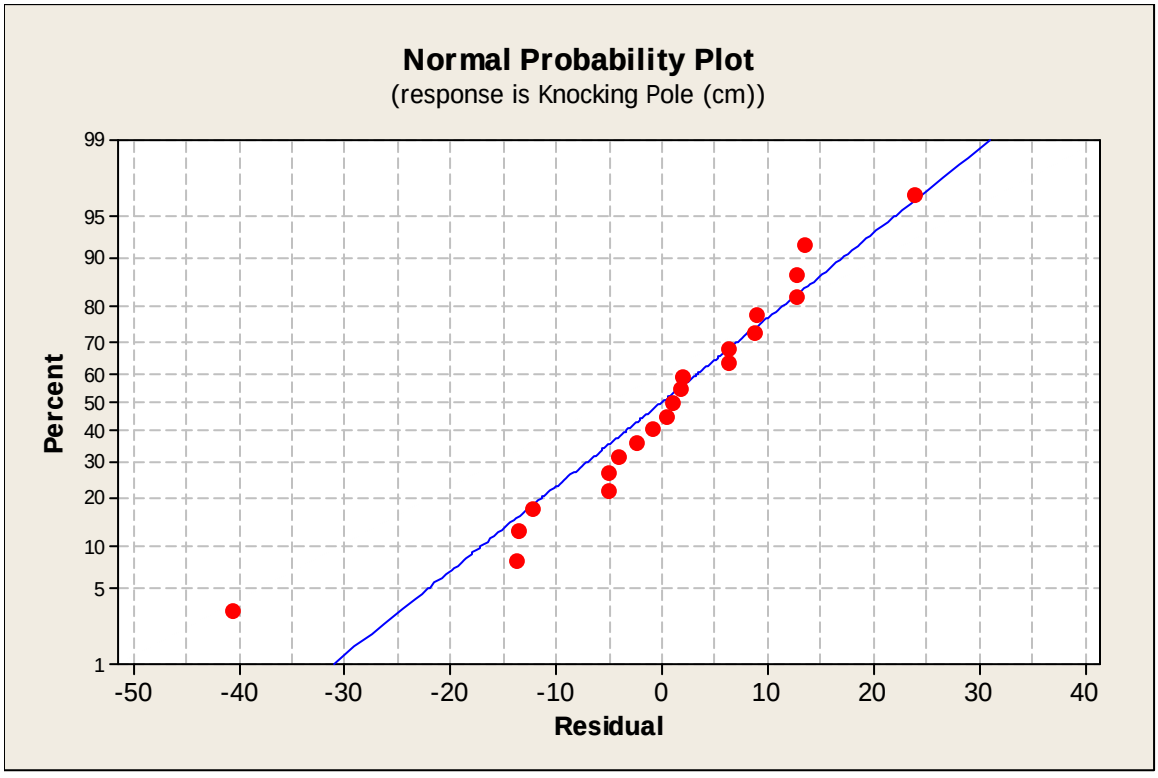
Normal Probability Plot
(response is Knocking Pole (cm))
Percent
Residual
99
95
90
80
70
60
50
40
30
20
10
5
1
-50
-40
-30
-20
-10
0
10
20
30
40

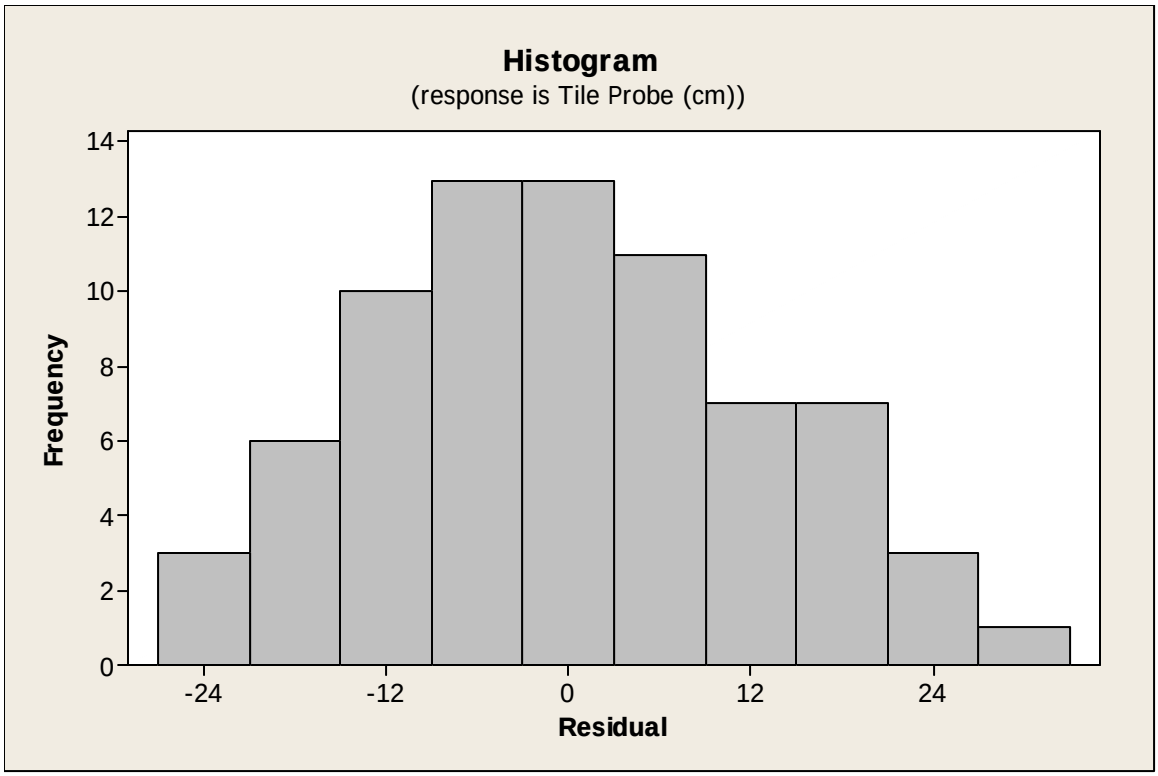
Histogram
(response is Tile Probe (cm))
Frequency
Residual
0
2
4
6
8
10
12
14
-24
-12
0
12
24

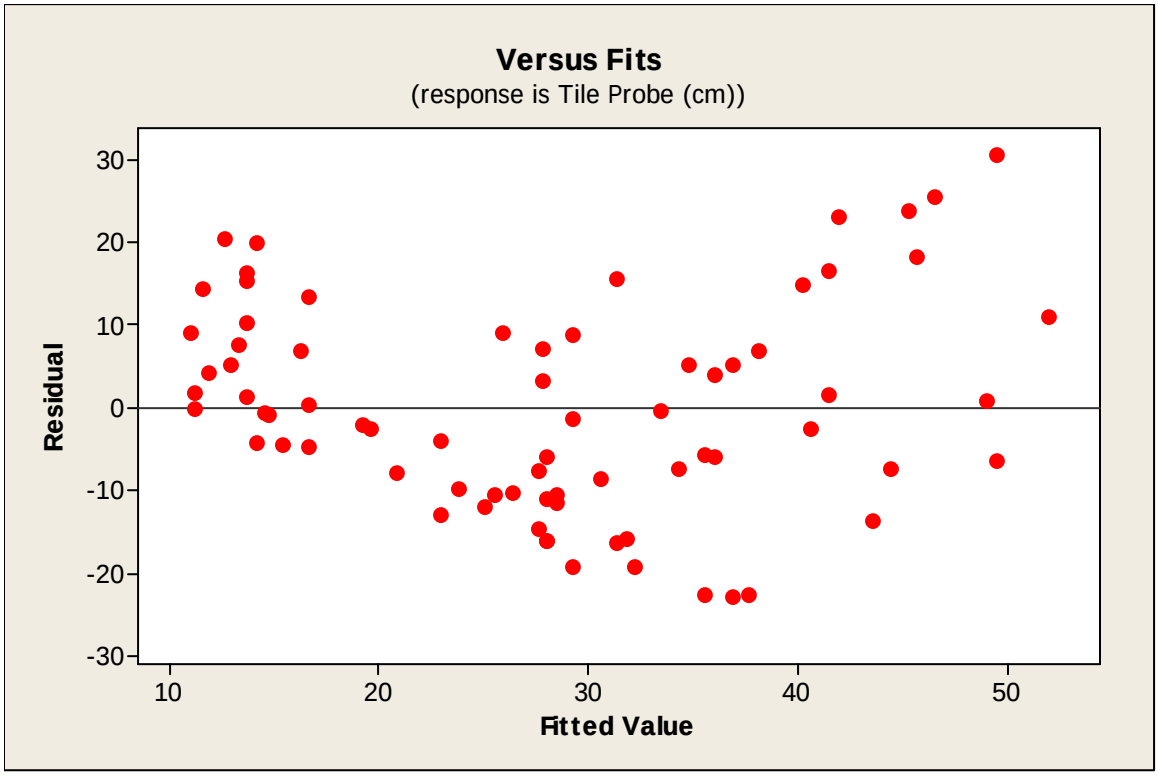
Versus Fits
(response is Tile Probe (cm))
Residual
Fitted Value
-30
-20
-10
0
10
20
30
10
20
30
40
50

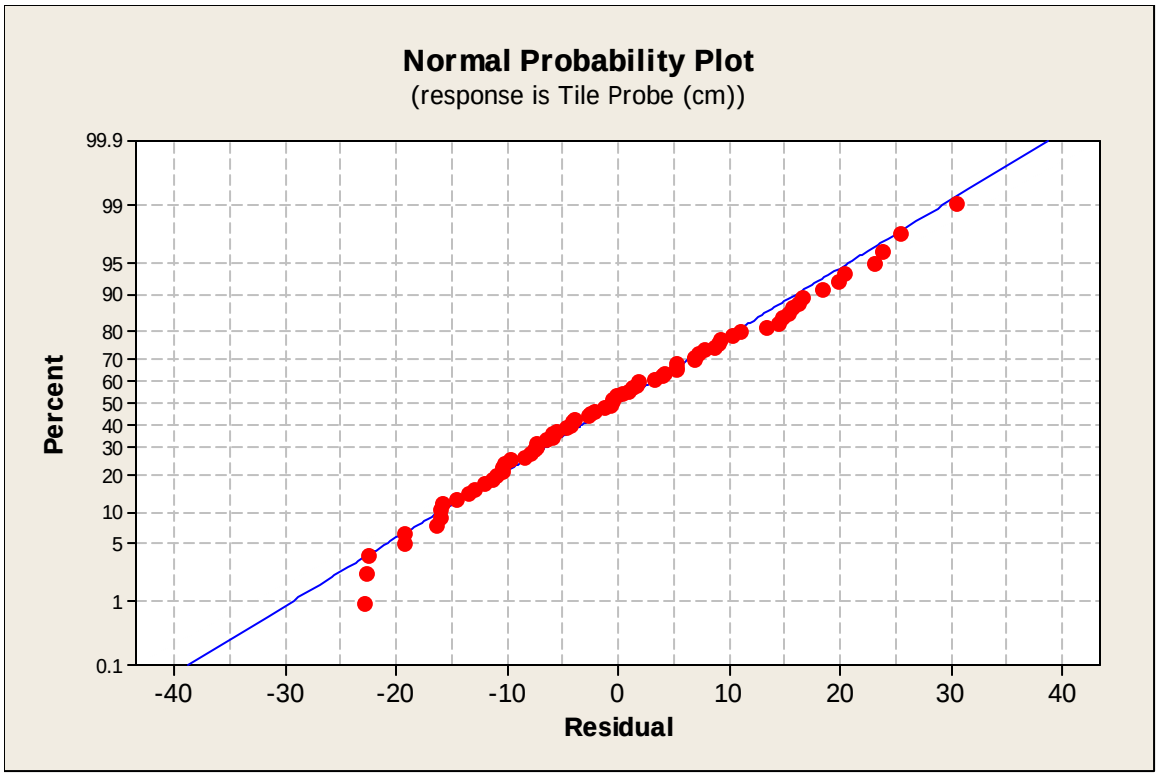
Normal Probability Plot
(response is Tile Probe (cm))
Percent
99.9
99
95
90
80
70
60
50
40
30
20
10
5
1
0.1
-40
-30
-20
-10
0
10
20
30
40
Residual

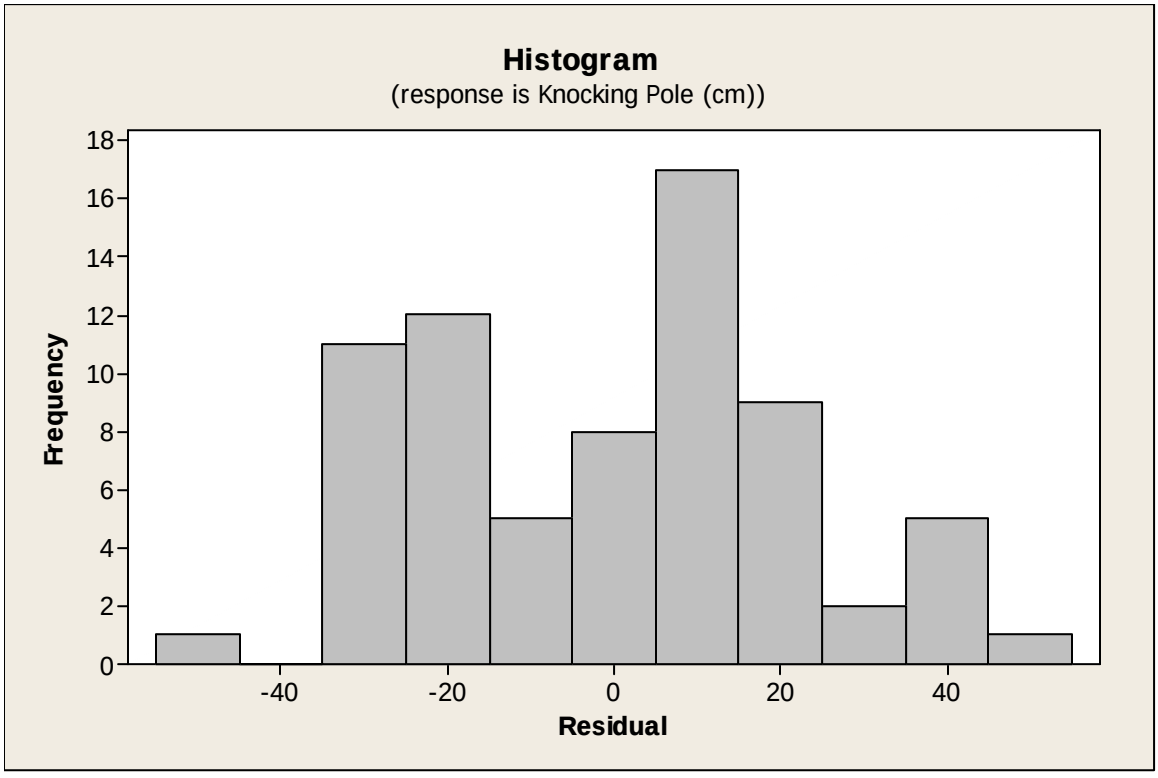
Histogram
(response is Knocking Pole (cm))
Frequency
18
16
14
12
10
8
6
4
2
0
-40
-20
0
20
40
Residual

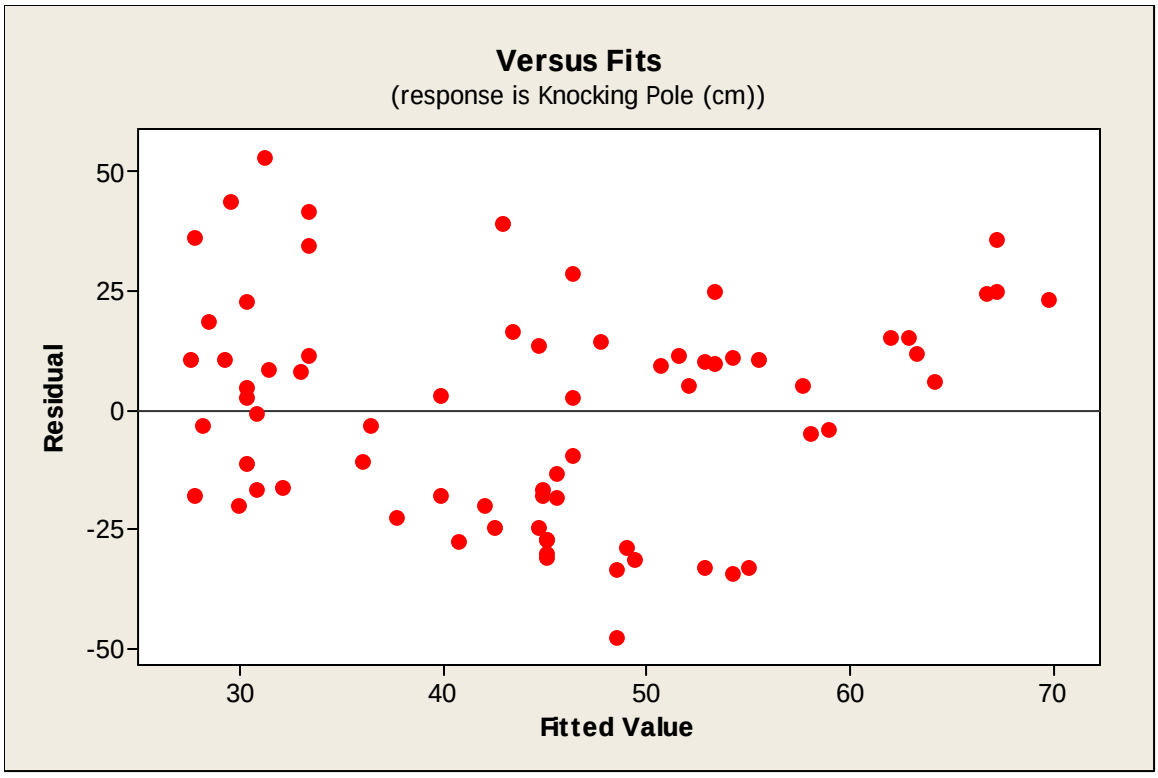
Versus Fits
(response is Knocking Pole (cm))
Residual
50
25
0
-25
-50
30
40
50
60
70
Fitted Value

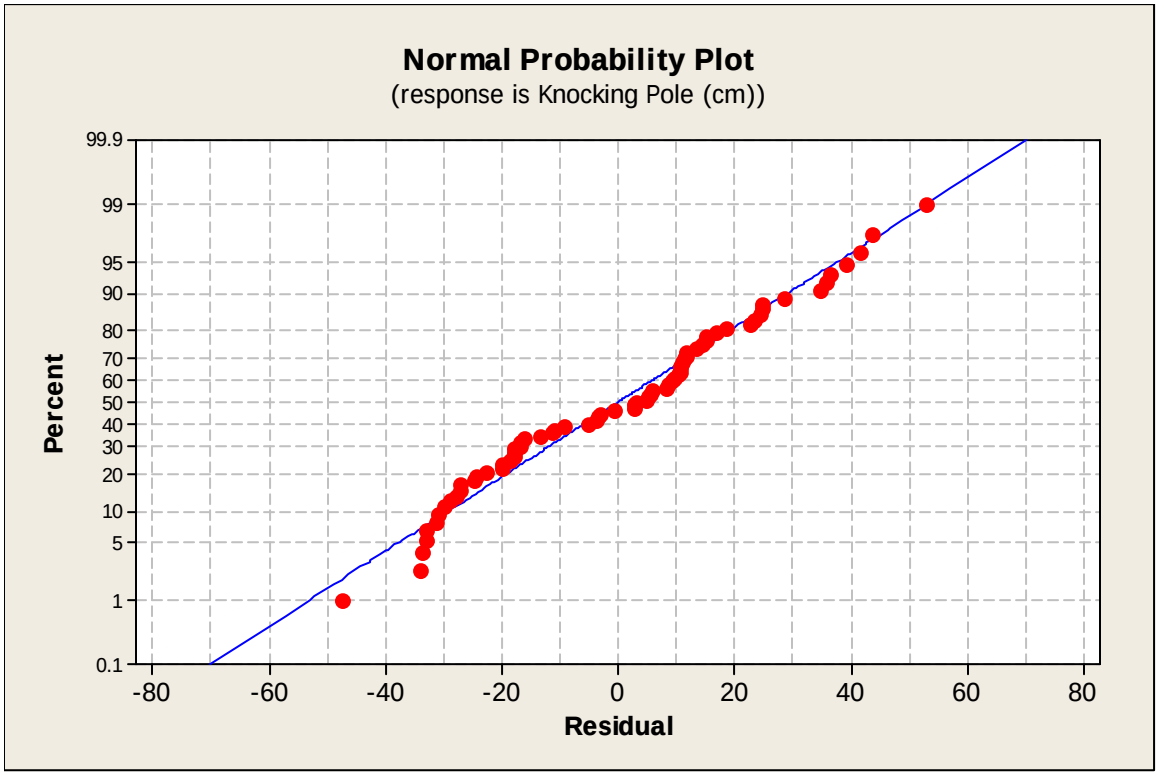
Normal Probability Plot
(response is Knocking Pole (cm))
Percent
99.9
99
95
90
80
70
60
50
40
30
20
10
5
1
0.1
-80
-60
-40
-20
0
20
40
60
80
Residual